Western Australia School of Mines: Minerals, Energy and Chemical Engineering

The extraction behaviour of zinc, lead and silver from ores and concentrates by glycine leaching processes

Mojtaba Saba

This thesis is presented for

The Degree of Doctor of Philosophy

of

Curtin University

September 2019

DECLARATION

To the best of my knowledge and belief this thesis contains no material previously published by any other person except where due acknowledgment has been made

This thesis contains no materials which has been accepted for the award of any other degree or diploma in any university.

Date: 17/09/19

X

Mojtaba Saba

ABSTRACT

Depletion of high-grade zinc recourses along with environmental restrictions and economic aspects have driven industries to promote direct leaching processes instead of using roasting, leaching, electrowinning process (RLE). However, several developments have been made on industrial scale for the related technologies in direct leaching processes, most of these technologies suffer from lack of efficiency and eco-friendliness. Many studies have been undertaken to reduce the footprints of this new processes. A most promising area is the use of organic acids which are considered as a promising reagent for leaching of zinc from its resources.

There are other valuable metals in zinc ores such as copper, lead, silver, and cadmium. Silver may be present as argentite (Ag_2S) but is probably more commonly present in association with antimony, copper and arsenic minerals such as pyrargyrite (Ag_3SbS_3), proustite (Ag_3AsS_3), freieslebenite ($(Pb, Ag)_8Sb_5S_{12}$), polybasite ($(Ag, Cu)_{16}(Sb, As)_2S_{11}$), and tetrahedrite ($(Cu, Fe)_{12}Sb_4S_{13}$) in which silver can partly replace copper. Small amounts of many of these minerals can be present in solid solution in galena. Furthermore, several isomorphic components of sphalerite do not form deposits of their own such as cadmium, indium, germanium, gallium, and thallium. Historically, copper and lead were viewed as the main by-products of the processing of zinc resources. More recently, as a result of resources depletion and increasing the mining cost, the recovery of a wider range of by-products from the zinc minerals may be feasible.

It is hypothesized that glycine, like the other complexing agents, may be able to accelerate the dissolution of zinc, even in the absence of strong oxidizing agents. Compared with other industrial zinc lixiviants, glycine has several advantages such as being environmentally safe, non-toxic, stable, enzymatically destructible, and readily metabolized in most living organisms. The particular attributes of glycine compared to the other lixiviants, make glycine a logical target lixiviant. A few articles have been published on the electrochemical behavior of zinc in glycinate electrolytes or the electrochemical behavior of sphalerite in acidic media. However, there are no published studies regarding anodic oxidation of sphalerite in alkaline glycine media.

This study tried to investigate some fundamental aspects of the direct leaching of sphalerite and the other zinc resources by considering the dissolution of other metal contents and their effects on the process such as silver, galena, and copper. Firstly, the electrochemical mechanism for zinc sulphide dissolution, lead sulphide dissolution and silver sulphide

dissolution in the alkaline glycine media was investigated based on cyclic voltammetry (CV) and chronoamperometry. Finding the thermodynamic data and drawing the Eh_pH diagrams for Metal-Sulphur-glycine-water play a crucial role to investigate the electrochemistry study. Subsequently, the electrochemical and dissolution mechanism aspects of sphalerite, galena, and silver sulphide in this system are addressed from a fundamental perspective.

Equilibrium potential–pH diagrams for the (zinc/Leaad/Silver)-sulfur-glycine-water system were derived at different total zinc and glycine concentrations. The diagrams illustrate that to optimally make use of the zinc-glycine complex formation area in alkaline media, a high concentration of glycine is needed. Under such conditions, the predominant zinc-glycine species is $ZnGly_3^-$. CV experiments revealed that the resulting voltammograms have three anodic peaks, namely: (1) zinc sulfide oxidation to soluble and insoluble species; (2) formation of $ZnGly_3^-$ from the produced $ZnGly_2$; and (3) oxidation of the produced zinc hydroxide at high negative potentials from the prior peaks. The cathodic peak includes the reduction of the produced zinc hydroxide.

Moreover, the effects of additives, namely potassium permanganate, cupric ions, sodium chloride, hydrogen peroxide, and lead nitrite, were investigated. The experiments showed that not only sodium chloride is the most effective additive in the process but also it has a positive impact on the dissolution of galena and silver in the process (in which above 90 wt.% of silver content in tested sphalerite concentrate can be extracted). With regard to modifying the pH, better results were obtained by using NaOH than by using $Ca(OH)_2$. Finally, the results obtained in this thesis can lead to the development of conceptual flowsheets for the industrial production of zinc and silver depending on their nature.

ACKNOWLEDGEMENTS

It is hard to find words to express my gratitude to my supervisors Prof. Jacques Eksteen and Dr. Elsayed Oraby for their wonderful contribution, guidance, patience, and untiring efforts during the last four years. Your advices and supports were instrumental in the successful completion of this project. It has been a great privilege to spend all these years at Curtin University. Special thanks to kind and supportive gold group members (Karen, Jim, Irlina, Tim, Rueben, Jeff, Greg, Deng, Alireza, Mpinga, Nirmala, and Liezl).

This research project was sponsored and financial supported by 2016 Curtin Strategic International Research Scholarship (CSIRS). I am so grateful for the financial support provide by Curtin University, Perth, Western Australia, Australia.

STATEMENT OF CONTRIBUTION OF OTHERS

The PhD candidate conceived, designed, performed the experiments, analysed and interpreted the experimental data and wrote all forming body of this thesis. The author of this dissertation is the first author in all listed papers. Professor Jacques Eksteen and Doctor Elsayed Oraby were responsible for editing and revising the manuscripts. Signed detailed statement is provided as appendix (A) at the end of this volume.

DEDICATION

I dedicated this work to my beautiful wife Melika and my beloved girls Zohreh and Maryam, my heroes Abbas and Mohsen and my dearly beloved brothers Morteza, Reza, Mamad, Jamshid, Ehsan, Aba, Naser, Milad, and Amir and my mentor Javad and Fereshteh for their spiritual and moral supports during the course of this doctoral journey. I appreciate it more than you know.

Love is from the infinite, and will remain so until eternity.

The seeker of love escapes the chains of birth and death.

Rumi

List of Contents

List of Figures

List of Tables

CHAPTER I: GENERAL INTRODUCTION AND OVERVIEW

In this Chapter, an introduction to the research work of the thesis has been summarised. It outlines the research background and demonstrates the motivation for pursuing the research work. The study objectives and interconnections between Chapters are clarified. The Chapter also briefly provides significant findings of the research study, which are of both scientific and fundamental interests. Recommendations for future research opportunities are listed as well.

1.1. Background

Nowadays, reducing environmental footprints in all industrial aspects has drawn attention. One of the most problematic industries is metal production. There have been lots of efforts to overcome such issues by alternating the conventional processes such as converting the pyrometallurgical procedure to a hydrometallurgical one or exchanging the reagents with more eco-friendlier reagents

Furthermore, there are other valuable metals in zinc ores such as copper, lead, silver, and cadmium. Silver may be present as argentite (Ag_2S) but is probably more commonly present in association with antimony, copper and arsenic minerals. Small amounts of many of these minerals can be present in solid solution in galena. Furthermore, several isomorphic components of sphalerite do not form deposits of their own such as cadmium, indium, germanium, gallium, and thallium. Historically, copper and lead were viewed as the main by-products of the processing of zinc resources (Sinclair 2005). More recently, as a result of resources depletion and increase the mining cost, the recovery of a broader range of by-products from the zinc minerals may be feasible (Sinclair 2009).

There are numerous recent investigations on the direct leaching of zinc which proposed: a new media such as application of organic and amino acids reagents (glycine for instance) (Hurşit et al. 2009; Ferella et al. 2010; Gilg et al. 2003; Eksteen and Oraby 2016). Glycine reagent, when used in the alkaline pH range, offers some unique advantages such as a high zinc glycinate stability constant, being environmental-benign, inherently recyclable, and have a high selectivity over iron, magnesium, silica and alumina co-dissolution. Eksteen and Oraby (2016) initially applied this approach to the extraction of gold, silver and copper (Eksteen and Oraby 2014); and they found that the leach and recovery approach can be extended to other chalcophile metals zinc, lead, nickel, cobalt, etc.

1.2. Objective

From the literature review, one of these processes that can be considered as a promising future in the zinc leaching industry is using glycine as a reagent in alkaline medium (Eksteen and Oraby 2015).

Glycine as simplest amino has been found as a perfect alternative reagent for many conventional metal extraction processes. It has been successfully tested for the extraction of copper form the primary and secondary resources and using as a complexing agent in the gold cyanidation that can be reduced the cyanide consumption by approximately five times. Because of its novelty, there was no reliable data available in the literature on direct leaching of zinc using the alkaline glycine procedure.

Therefore, fundamental studies such as thermodynamics and electrochemistry play a vital role in investigating the behaviour of zinc leaching using such media. Figure 1 illustrates the whole objectives of the research study used in this thesis based on the different zinc species. Thus, the first objective was to propose a mechanism for dissolution of zinc in the alkaline glycine media, thermodynamics and electrochemistry studies were tools for obtaining this target.
After proposing the reactions and mechanisms for dissolution of zinc and metals content in natural zinc resources (silver and galena), investigate the variables in the process was the second objective.
Finding the effects of independent parameters on the process by modelling and optimisation, and kinetics of the most effective parameters should have been applied to satisfy the second objective.

1.3. Significance of the study

This investigation tried to insight into the fundamental aspects of zinc sulphide dissolution behaviour in alkaline glycine media. Besides, the potential application of this new media (alkaline glycine media) to simultaneous leaching of zinc, silver, lead and copper has been introduced. Moreover, the effects of independent parameters and different dissolution procedures such as rotating disc dissolution, agitating reactor leaching, and bottle roll tests have been investigated. This investigation tried to deal with developing a new eco-friendly system for direct leaching of sphalerite without any pre-treatments (roasting for instance).

1.4. Delineation of the study

Comparing dissolution behaviour of all kind of zinc resources, including the primary and the secondary hardy achievable in the time frame of this study. However, in this study tried to investigate the most important resources from a fundamental viewpoint (e.g. pure minerals and synthetic one) and industrial aspect (e.g. sphalerite and zinc oxide). Furthermore, since the alkaline glycine procedure is new, there was no data available for developing the process, and it was hardly possible to draw a flowsheet for the process regarding the industrial point of view.

1.5. Thesis organisation

The dissertation is in full compliance with Curtin University copyright policies and specific guidelines for the thesis. The materials and methods for each part of the study are explained in the relevant chapters. The thesis is divided into eight interconnected Chapters as the following sequential and outlining development layout:

CHAPTER 1 provides an overall introduction. It summarised issues arising from the previous work, the overall objectives for this study and also delineates the research that was done. Chapter 1 pinpoints the gaps in fundamental research and hypotheses for future research.

CHAPTER 2 is a comprehensive review of all studies and recent developments on the direct leaching of zinc from its resources.
It covers the currents process and its new alternatives. Their process chemistry, flowsheet, and critical technical operating factors were compared.

CHAPTER 3 presents the materials, preparations and the methods used in this thesis — the applied analytical techniques in this study described in details in Chapter 3.

CHAPTER 4 is dealing with thermodynamics information for zinc, lead, and silver in alkaline glycine system. In this Chapter by using collected thermodynamics data, the distribution metal species diagram and the Pourbaix diagram for new leaching system (metal-glycine-sulphur-water) were produced.

CHAPTER 5 covers electrochemistry study for zinc, lead, and silver in the new alkaline glycine system. Cyclic voltammetry experiments were performed to find the possible reactions between zinc, lead, silver and glycine followed by proposing reactions for dissolution of the metals in the alkaline glycine media by using carbon-paste electrode. After that, the proposed reaction was confirmed by chronoamperometry experiments.

CHAPTER 6 is dealing with the dissolution responses of sphalerite, galena, and acanthite to the alkaline glycine media from a hydrometallurgical point of view. After screening the independent variables, the most effective parameters on the sphalerite dissolution was modelled and optimised along with cupric ion as an additive.

CHAPTER 7 investigates the kinetics controlling step of the reaction of zinc, silver, and copper under the optimum conditions found in Chapter 6. It was found that shrinking core model SCM has an excellent response to the kinetics of the zinc dissolution on the optimum condition at different temperatures.
CHAPTER 8 summarises the significant results obtained during this study and also outlines recommendations for future works.

1.6. Overall conclusions

This investigation offers an insight into the dissolution behaviour of zinc sulphide in the alkaline glycine process. As this process is nearly new, this study tried to focus on the fundamental studies to open the door for future research in this field by providing thermodynamic data, Eh-pH diagrams, related reactions, the effects of independent parameters and variables, proposing dissolution mechanism, empirical models, kinetics for zinc sulphide. The dissolution behaviour of the other sub reactions such as zinc oxide, lead sulphide, silver sulphide, and copper has been investigated and reported (the dissolution of zinc sulphide) as well.

CHAPTER 2: LITERATURE REVIEW

The chapter provides insight into the fundamental studies related to zinc resources such as thermodynamics, electrochemistry, and kinetics. The main objective of this chapter is to evaluate information across a wide range of publications related to direct leaching of different zinc resources. Generally, and depending on the characteristics of ores, three main process approaches are used to extract metal values from zinc ores and concentrates, namely pyrometallurgy, hydrometallurgy, and pyro-hydro processes. Optimum leaching conditions and the advantages and disadvantages of each process are summarized based on most of the previous research studies.

2.1. Chapter objective

This chapter is a comprehensive review of all studies and recent developments on the direct leaching of zinc from its resources. It covers the current process and its recent alternatives. This chapter describes the process chemistry, flowsheet, and key technical operating factors.

Normally, zinc resources contain other impurities and metals such as silver and lead. In other words, lead and silver are present in most zinc resources, and therefore two aspects of their dissolution behaviour can be considered in investigations: first, simultaneous leaching of lead and silver along with zinc in the alkaline glycine process, and second, the selective leaching of these elements from zinc resources.

2.2. Zinc deposits and minerals

Habashi (1997) reported that zinc deposits could be classified according to their economic importance as follows:

- Simic volcanogenic-sedimentary deposits
- Simic-hydrothermal or marine sedimentary deposits.
- Sialic lodes (impregnation and replacement deposits)

Zinc is a chalcophilic element that formed under the reducing conditions of the Earth's early atmosphere. Naturally, the main zinc source is sphalerite mineral (ZnS), which is often intergrown with pyrite and pyrrhotite (Habashi, 1997). In the conventional process for the production of metallic zinc, the sphalerite concentrate is subjected to the RLE process: roasting, followed by leaching in dilute H_2SO_4, and finally electrowinning (Gupta and Mukherjee, 1990). From an economic viewpoint, there are a few zinc minerals can be considered for the production of zinc. These include smithsonite, hydrozincite, hemimorphite, and willemite. Table 2.1 shows the most important zinc minerals for metallic zinc extraction (Lioyd and Showak, 2007; Habashi, 1997).

Table 2. 1. Most common zinc minerals (Habashi, 1997; Lioyd and Showak, 2007).

Mineral	Ideal Formula	Wt.% Zn
Sphalerite, zinc blend, wurtzite	ZnS	67.09
Hemimorphite, calamine	$Zn_4Si_2O_7(OH)_2.2H_2O$	54.3
Smithsonite Calamine	$ZnCO_3$	52.14
Hydrozincite	$Zn_5(OH)_6(CO_3)_2$	57.7
Zincite	ZnO	80.03
Willemite	Zn_2SiO_4	58.68
Farnklinite	$(Zn,Fe, Mn)(Fe,Mn)_2O_4$	15-20
Sauconite	$Na_{0.3}(Zn,Mg)_3(Si,Al)_4.(OH)_2.nH_2O$	~35

There are other valuable metals in zinc ores such as copper, lead, silver, and cadmium. Silver may be present as argentite (Ag_2S) but is probably more commonly present in association with antimony, copper, and arsenic minerals such as pyrargyrite (Ag_3SbS_3), proustite (Ag_3AsS_3), freieslebenite ($(Pb, Ag)_8Sb_5S_{12}$), polybasite ($(Ag, Cu)_{16}(Sb, As)_2S_{11}$), and tetrahedrite ($(Cu, Fe)_{12}Sb_4S_{13}$), in which silver can partly replace copper. Small amounts of many of these minerals can be present in solid solution in galena (PbS). Furthermore, several isomorphic components of sphalerite do not form deposits of their own, such as cadmium, indium, germanium, gallium, and thallium. Historically, copper and lead were viewed as the main by-products of the processing of zinc resources (Sinclair, 2005). More recently, as a result of resource depletion and increasing mining costs, the recovery of a wider range of byproducts from zinc minerals may be feasible. In the past, for instance, lead ores were mined for the production of lead and silver. Today, this method of lead production is uncommon, and most lead concentrates are produced in conjunction with zinc concentrates from lead-zinc ores (Sinclair, 2009).

Metallic silver is produced as a byproduct of gold production by cyanidation or zinc/lead production by pyrometallurgical procedures (Jiang et al., 2015; Aparajith et al., 2010; Chang et al., 2018; Luna and Lapidus 2000). Nowadays, three main factors, namely the environmental impact of cyanidation and pyrometallurgy procedures, the depletion of easy-to-treat silver resources, and an increasing silver price, have led to the development of alternative leaching systems for silver production (Xiao et al., 2018; Lorenzo-Tallafigo et al., 2019; Behnejadi and Moghaddam, 2014; Jadhav and Hocheng, 2013; Urzúa-Abarcaa et al., 2018; Puente-Siller et al., 2013; Deutsch and Dreisinger, 2013; Balaz et al., 2003; Lewis, 1982). Almost all silver minerals are compounds of silver with sulfur, and argentite (Ag2S) is the most common silver compound associated with other sulfidic minerals, mainly galena (PbS) (Habashi, 1997). Today, because of resource depletion and increases in mining costs, there is a positive attitude towards the recovery of both metals from zinc-lead minerals (Sinclair, 2005, 2009).

On the other hand, the formation of lead sulfate prohibits the recovery of lead from bacterial and ferric sulfate leaching via traditional solvent extraction/electrowinning routes and creates an environmental hazard resulting from the greater solubility of lead sulfate compared to galena'. Furthermore, processing of low-grade ores with mixed mineralogy is difficult to carry out through traditional flotation and smelting cycle. As a result of these issues, there is a driving force to use the hydrometallurgy process in the production of lead and zinc, even with the elimination of the roasting stage. This struggle has led to the creation of a new hydrometallurgy process without roasting, called direct leaching. Several different direct

leaching procedures have been published to address the issues, one of which is the use of alkaline glycine media (Tanda et al., 2017; Silva, 2004).

2.3. Zinc extraction processes

Nowadays, the hydrometallurgical process produces over 90% of zinc and the rest of of it is produced through the pyrometallurgical process ("Asianmetal," 2020). The most common zinc smelting process is the Imperial Smelting Process which utilises a lead splash condenser, and is based on the carbothermic reduction of zinc oxides (which can be obtained by roasting sulfide concentrates). Zinc roasting itself can take place in continuous fluid bed roasters or moving grate roasters.

2.3.1. Pyrometallurgical process

The most common route for zinc processing by pyrometallurgical processing is shown in Figure 2.1, which consists of four high-level operations, namely (Vignes, 2011; Constantineau et al., 2011):

1. Fluidized bed reactors for roasting-sintering of the zinc sulfide concentrates: The operation targets complete conversion of the sulfide into an oxide (Equations 2.1 and 2.2):

$$2ZnS + 3O_2 \rightarrow 2ZnO + SO_2 \quad (2.1)$$

$$2SO_2 + O_2 \rightarrow 2O_3 \quad (2.2)$$

2. Reduction of the zinc oxide by the imperial smelting process: In this process, sulfide concentrates of both zinc and lead are mixed for treatment and thus zinc and lead to be produced. Moreover, the other elements such as copper, bismuth, silver, arsenic, and antimony (if present) are concentrated in lead bullion. After that, by spraying liquid lead, which flows countercurrently in the condenser, the zinc fumes condense. Finally, at the exit of the condenser, lead enriched in zinc is cooled down to 450 ˚C.

3. Separation by liquation: In this stage, three products are obtained: refined zinc with a concentration of lead equal to 0.9%, lead with 5–6% zinc, and zinc matte of $FeZn_{13}$ crystals.

4. Refining by distillation: Zinc (99.995%) enriched in low-volatility elements (Fe, Cu, Pb) and purified cadmium (99.997%) are recovered at the exit of the columns. The product zinc enriched in low-volatility elements is treated again by a new cycle.

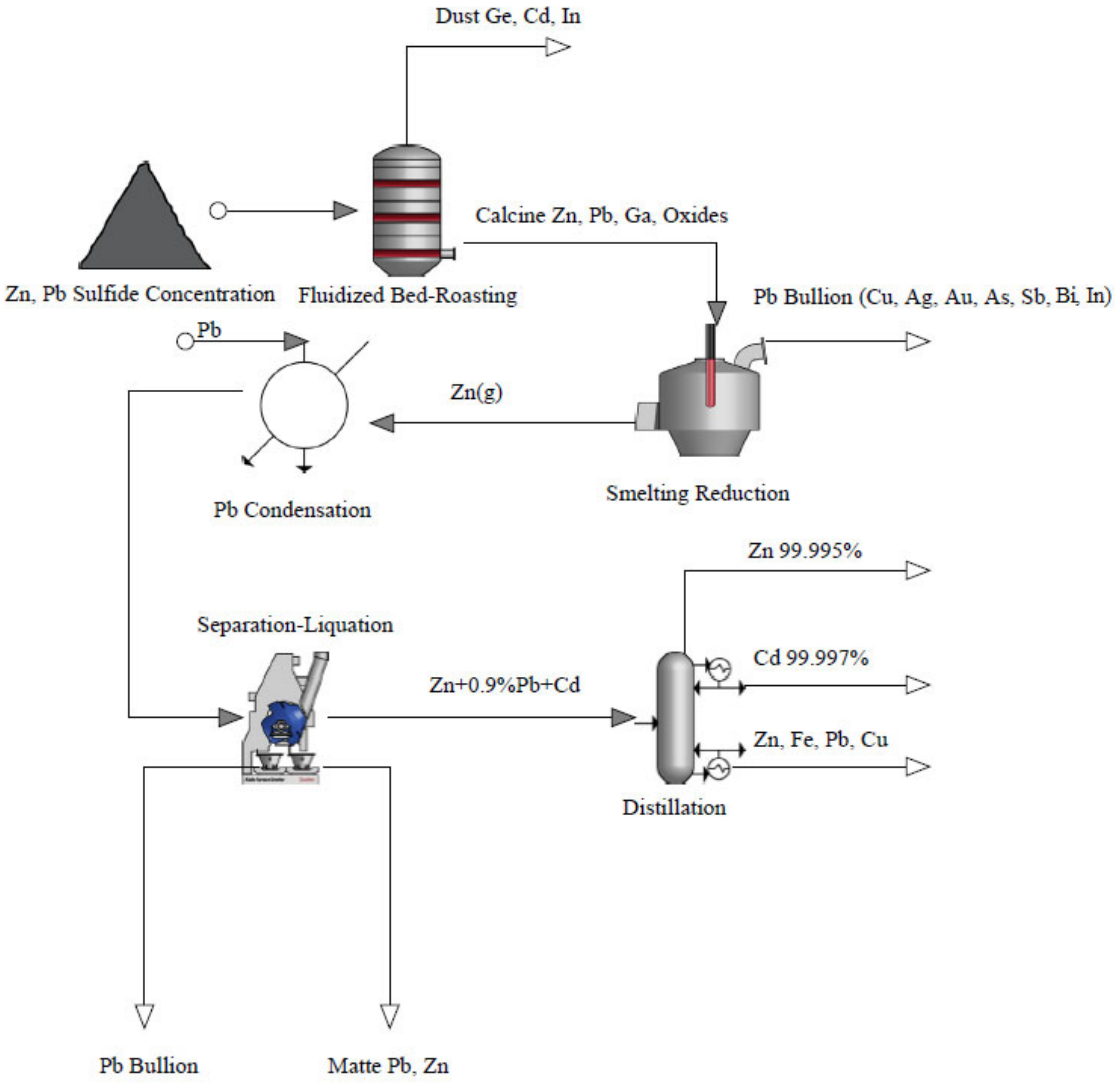

Figure 2. 1. Pyrometallurgical process of zinc extraction (Vignes, 2011).

2.3.2. Hydrometallurgical processes

The first patent concerning zinc production via electrolysis was submitted by Luckow of Danz in 1880 (Abkhoshk et al., 2014). About 35 years later, Anaconda Electrolytic Zinc of Australia pioneered the production of zinc by this method (West-sells, 1992). Currently, this process dominates in the production of more than 80% of zinc metal throughout the world (Balarini et al., 2008). Generally, there are three distinct steps in this process: roasting, leaching (with purification), and electrowinning (RLE) (Gupta, 2003).

In the first stage, the zinc sulfide concentrate is roasted to give acid-soluble zinc oxide (calcine). In this stage, sulfur dioxide (SO_2) is produced through the reaction of the sulfur contained in the concentrate and air at above 900 °C. Consequently, in a recovery unit, this produces SO_2 which is converted to sulfuric acid. The calcine obtained by high-temperature roasting of the sulfide concentrate contains predominantly zinc oxide, about 4% zinc sulfate, and minor content of zinc ferrite spinel mineral (Gupta and Mukherjee, 1990).

In the second stage, zinc oxide is dissolved in diluted sulfuric acid (H_2SO_4), producing a zinc sulfate solution. At this stage, the impurities present in the zinc concentrate such as Co, Cd, Ni, Cu, Fe, As, Sn, Se, Ge, Sb, Cl, and F enter the solution simultaneously. Table 2.2 shows the effects of impurities on the zinc electrowinning process (Lioyd and Showak, 2007). Since the presence of impurities, even in trace amounts, can have detrimental effects on zinc production, purification of the electrolyte is vital in the RLE process. Zinc electrowinning is strongly affected by the presence of these impurities in the electrolyte, and therefore adequate purification of zinc electrolyte is essential before electrowinning (Behnajady et al., 2014; Behnajady and Moghaddam, 2015).

2.3.2.1. Purification

Chemicals

From the perspective of the chemical process, the purification step can be divided into two stages. The first stage of the purification is to precipitate the hydrous iron oxides, silica, alumina, and tin, which carry along with As, Sb, and Ge in the neutral leaching step. However, lead and silver sulfates co-precipitate, while the corrosion of anodes brings about the introduction of lead into the electrolyte, copper from bus-bar corrosion, and aluminium from the cathodes (Lioyd and Showak, 2007). Iron removal is a decisive factor in the co-removal of impurities such as arsenic, germanium, and antimony (Souza et al., 2009; Raghavan et al., 1998; Claassen et al., 2002).

There are four commercialized iron precipitation processes: the jarosite, goethite, paragoethite, and haematite processes. All these processes work based on precipitating the iron compounds before settling by adding a base to the system. In each case, iron is dissolved from the leach residue, and then the solution is subjected to iron precipitation by one of the processes mentioned above (Ozberk et al., 1995). In addition, the use of flocculating agents

Table 2. 2. Effect of impurities on electrowinning parameters.

			Effect			
Impurity	**Reported range**	**Class[a]**	**Current efficiency**	**Resolution**	**Deposit**	**Other**
Gr	0.005-0.2	4	Lowers	High	Spongy	Worse with cobalt
Te	<0.001	4	Lowers	High	Uneven	Worse with cobalt
Se	<0.002	4	Lowers	High	Uneven	
Ar	0.003-0.02	4	Lowers	High	Corrugated	Worse with cobalt
Sb	0.01-0.03	4	Lowers	High	Beady, poor adhesion	Worse with cobalt or germanium
Cu	0.05-0.2	4	Lowers	Yes		
Ni	<0.01-0.5	3	Lowers	Mild	Holes	
Co	0.03-2.0	3	Lowers	Mild	Holes	Reduces lead deposition
Sn	<0.02	3	Lowers	Yes	Filmy	
Fe	0.2-25	3	Lowers			May reduce anode corrosion
Cd	0.01-5	2				Deposits with zinc
Pb	1	2				Deposits with zinc
Tl	0.5-5					Increases lead deposition, deposits
Al	10	1				Increases electrolyte resistivity
Mg	6.5-12 g/l	1				Increases electrolyte resistivity
Mn	3.3.5 g/l	1				Oxide forms on the anode, lower corrosion, may insulate the anode
Cl	20-100					corrodes lead anodes
F	2					Corrodes electrodes, causes sticking of zinc to the cathode

[a] Class 1. Higher reduction potential than zinc. Will not deposit on cathode but will affect conductivity. 2. Lower reduction potential than zinc. Hydrogen overvoltage above 0.65 V. Deposits with zinc but does not affect zinc deposition. 3. Reduction potential between zinc and hydrogen. May deposit and redissolve, affecting current efficiency. Causes local lowering of hydrogen overvoltage, making pits, holes, etc. 4. Reduction potential below hydrogen. Hydrogen overvoltage below 0.65 V. deposits and cause hydrogen evolution. Tends to form hydrides (Lioyd and Showak, 2007).

to address the jarosite precipitation and silica gel problem has been studied by several researchers (Espiari et al., 2006). Bodas (1996) also studied the effect of different parameters on flocculating agents and reported the amount of different flocculating agents required for the coagulation of silicic acid (Table 2.3).

Table 2. 3. Flocculating agents required for the coagulation of silicic acid (Bodas, 1996).

Flocculating agent	Quantity required (kg/kg of ore)
$Al_2(SO_4)_3$	0.258-0.46
Limestone	0.041
Calcinated lime	0.05-0.11
$Ca(OH)_2$	0.101
NaOH	0.70
Na_2Co_3	0.058
Calcine	0.048
Magnafloc	0.0005

This stage includes using zinc powder for precipitating impurities such as Cu, Cd, Ni, Co and Ti through cementation. For this purpose, approximately five per cent of the zinc is recycled, and further zinc is added over the stoichiometric requirement. Adding copper sulfate can accelerate the cementation reaction by forming zinc-copper couples which activate zinc dust. (Raghavan et al., 1999; Casaroli et al., 2005). Nevertheless, antimony is less toxic compared with arsenic and its hydride. Figure 2.2 shows the reverse antimony procedure for separation of cadmium and cobalt (Friedrich et al., 2001; Lioyd and Showak, 2007). Furthermore, it is reported that cobalt can be removed by precipitation by α-Nitroso-β-naphtol (Weiss et al., 1961).

To summarise, the purification processes highly depend on ore compositions. During the purification process, aeration can resolubilise the impurities. The problem is that alkali metals such as Mg, Cl, and F are just removed by stripping the zinc from a portion of the electrolyte and discharging the solution. Consequently, investigation of new purification processes resulted in solvent extraction methods.

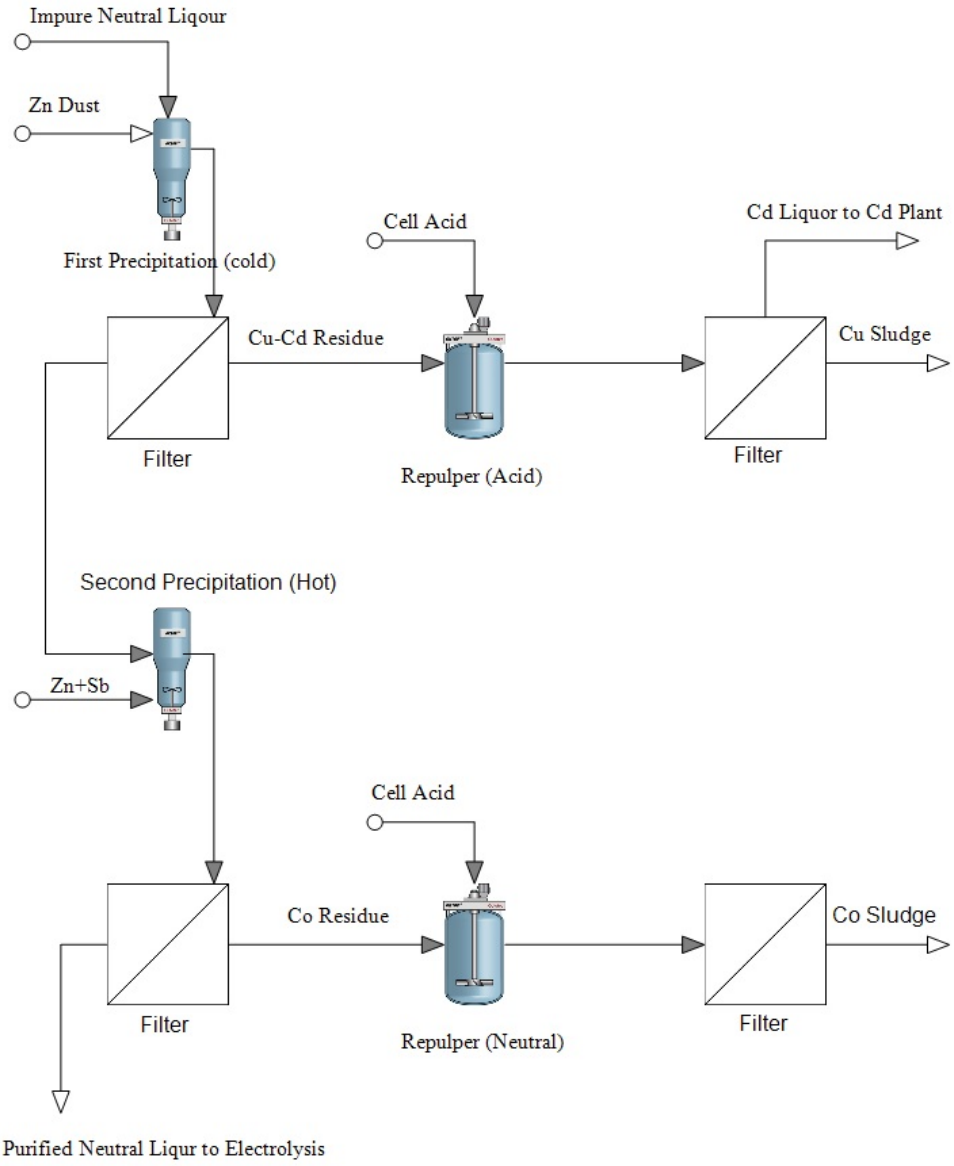

Figure 2. 2. Reverse solution purification (Friedrich et al., 2001).

Solvent extraction

Solvent extraction is an essential and useful process to simultaneously concentrate and purify the solution for the subsequent electrowinning step. From a zinc extraction point of view, metal can be extracted selectively into an organic extractant such as di(2-ethylhexyl) phosphoric acid (DEHPA) in diluent such as kerosene to purify and concentrate the pregnant leach solution (Díaz and Martín, 1994). The next stage is stripping of zinc from the organic phase using a barren solution of zinc electrowinning. In the past, this process was used to treat zinc secondary materials (for instance, electronic arc furnace fly ash). Nowadays, solvent extraction can be used to concentrate weak zinc solutions such as the leaching solution obtained from treating low grade oxide ores (Cole and Sole, 2002; Xie et al., 2008).

Table 2.4 summarizes Zn^{2+} extractants according to their media. Deep and Carvalho (2008) suggested that zinc solvent extraction can be divided into three categories by medium, namely sulfuric, chloride, and phosphoric media. From Table 2.4, it is clear that DEHPA is one of the best extractants for Zn^{2+} in terms of selectivity and stability at low pH (1-1.5). However, DEHPA forms a strong organic complex with Fe^{3+} which complicates stripping, and requires the use of concentrated hydrochloric acid for stripping. To address this issue, DEHPA can be used for extracting Zn^{2+} and Fe^{3+} at low pH (1-1.5), followed by the selective stripping of Zn^{2+} using sulfuric acid. There are some stripping routes for removing of the Fe^{3+} from the loaded DEHPA phase including Fe^{3+} reduction to Fe^{2+} in the organic phase, the galvanic stripping of Fe^{3+}, stripping Fe^{3+} by 6 N nitric acid from DEHPA (in kerosene), and the mixing of the extractant with other reagents, such as tri- n-butyl phosphate (TBP), tri-n-octyl phosphine oxide (TOPO), CYANEX 923, and amines (Deep and Carvalho, 2008). The extraction behaviour of Zn^{2+} using different extractants and the pH-dependency of zinc extraction is shown in Figure 2.3 (Cole and Sole, 2003). However, attitudes have recently changed towards solvent extraction in zinc production, and there are several successful industrial applications such as the ZINCEX and ZINCLOR processes (Díaz and Martín, 1994; Nogueira et al., 1982; Nogueira et al., 1979).

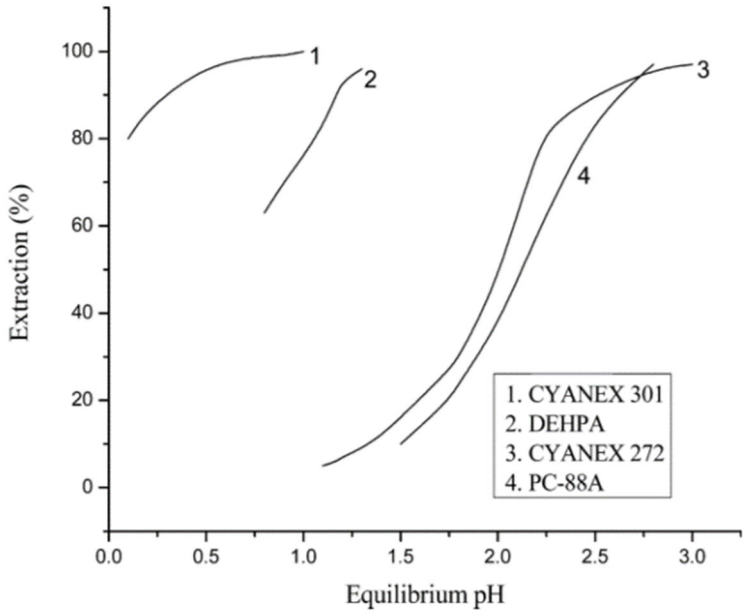

Figure 2. 3. Extraction behaviour of Zn^{2+} in DEHPA, PC-88A, CYANEX 272 and i. CYANEX 301 extractants (V_{aq}/V_{org}=1) as a function of equilibrium pH (Cole and Sole 2003).

Table 2. 4. Zinc solvent extractants in different media (Deep and Carvalho, 2008).

Media	Name	Formula	Reference
Sulphuric	DEHPA	Di-(2-ethylhexyl)phosphoric acid	(Rice and Smith 1975)
	PC-88A	2-ethylhexyl phosphonic acid mono-2-ethyl hexyl ester	(Cole and Sole 2003)
	CYANEX 301	bis-(2,4,4-trimethyl pentyl) dithiophosphinic acid	(Darvishi et al. 2011)
	CYANEX 272	bis-(2,4,4-trimethylpentyl) phosphinic acid	(Devi et al., 1997)
Chloric	DEHPA	Di-(2-ethylhexyl)phosphoric acid	(Rice and Smith 1975)
	N1923	primary amine with the following formula: R1R2CHNH2, the total number of carbon atoms is 19–23	(Jia et al., 2003)
	CYANEX 302	bis-(2,4,4-trimethyl pentyl) monothiophosphinic acid	(Alguacil, Cobo, and Caravaca 1992)
	CYANEX 272	bis-(2,4,4-trimethylpentyl) phosphinic acid	(Ali et al., 2006)
	CYNEX 293	93% pure mixture of four trialkylphosphine oxides: R3P5O, R9R2P5O, R2R9P5O, and R39P5O, where R and R9 represent n-octyl and n-hexyl hydrocarbon chains	(Tian et al. 2011)
	KELEX 100	7-(4-Ethyl-1-methylocty)-8-hydroxyquinoline	(Jakubiak and Szymanowski 1998)
	Aliquat 336	tricaprylmethylammonium chloride	(Wassink et al., 2000)
	TBP	tri-n-butyl phosphate	(Rice and Smith 1975)
	DBBP	dibutylbutyl phosphonate	(Grzeszczyk and Regel-Rosocka 2007)
	ACORGA ZNX50	0% wt. of the active substances consisting of unreacted dimethyl bibenzimidazole, dimethyl 1-mono(tridecyloxycarbonyl)-2,2'-bibenzimidazole and dimethyl 1,1'-bis(tridecyloxycarbonyl(22,2'-bibenzimidazole dissolved in Cl0-Cl5 hydrocarbons	(Cooper et al. 1992a)
Phosphoric	DEHPA	Di-(2-ethylhexyl)phosphoric acid	(Mellah and Benachour 2006)
	CYANEX 301	bis-(2,4,4-trimethyl pentyl) dithiophosphinic acid	(Riveros and Dutrizac 1997)

2.4. Direct leaching of zinc resources

In this process, without any roasting (pre-oxidation process), zinc ores are leached. The distinct advantages of the direct leaching process compared with the RLE process include the following (Crundwell, 1988; Filippou, 2004; Abkhoshk et al., 2014):

- The process can be used for small-scale operations without high investment in a roasting and sulfuric acid plant
- Low investment cost
- Low energy consumption
- High Zn recovery
- Absence of sulfur dioxide and explosion risk

On the other hand, there are also disadvantages such as lack of recovery of the exothermal heat from the roasting stage and the requirement for disposal of sulfur residues for environmental reasons. Nevertheless, different research studies have been published concerning the recovery of elemental sulfur from zinc leach residues by flotation (Li et al., 2014).

Furthermore, sphalerite in oxidative acidic media (Covadonga and Hourn, 2008; Santos et al., 2010) dissolves through a redox electrochemical reaction. Thus, ZnS acts as a mixed electrode since sphalerite is a semiconductor. The main electrochemical reactions of the oxidative leaching are as follows:

- Cathodic reactions: A list of oxidizing agents and their corresponding equilibrium redox potentials is given in Table 5. The primary oxidizing reagent used in zinc extraction can be considered as oxygen, ferric ion (Fe^{3+}), cupric ion (Cu^{2+}), chlorine, and nitric acid.

- Anodic reactions: Two reactions with the dissolution of sulfide and formation of either elemental sulfur (S°) or ion SO_4^{2-} in different ratios can occur as shown by Equations (2.3) and (2.4) (Vignes, 2013):

$$MS_x(S) \rightarrow M^{2+} + xS^0(S) + 2e \quad (2.3)$$

$$MS_x(S) + 4xH_2O \rightarrow M^{2+} + xSO_4^{2-} + 8xH^+ + (6x + 2)e \quad (2.4)$$

To carry out the dissolution, the redox potential of the reduction reaction of the oxidizing specimens should be higher than that of the dissolution reaction of the sulfide (E*Rc > E*Ra). According to the Eh–pH diagram of the S-H_2O system shown in Figure 2.4, it can be seen that oxidative leaching of the sulfides should occur with the formation of HSO_4^- and SO_4^{2-} ions. However, from the kinetic point of view, the oxidation rate of elemental sulfur (S°) into SO_4^{2-} ion at low temperatures is slow since sulfur is metastable at low temperature within a wide range of pH and potential. At 25 °C, the stability limit of sulfur is equal to a potential of 0.87 V at pH 0.0 and approximately 0 V at pH 10.0 (Mu et al., 2010).

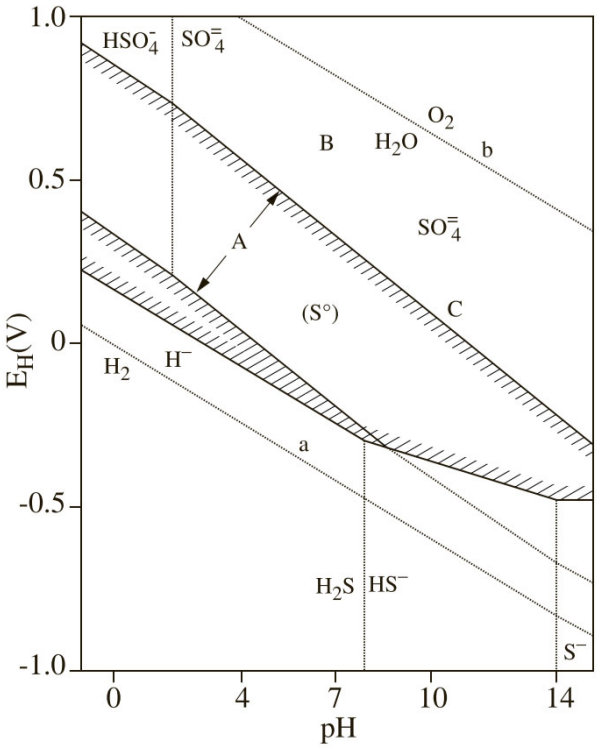

Figure 2. 4. The Eh-pH diagram for the S-H_2O (Demopoulos, 1999).

2.4.1. Direct leaching with sulfuric acid

Today, sulfuric acid leaching of zinc ores is considered the most practical and available processes (Abkhoshk et al., 2014). The insolubility of lead in sulfuric acid media allows easy separation of lead from zinc. In some cases, forming silica gel brings serious problems in the solid/liquid separation step (Fugleberg et al., 2009; Frenay, 1985). However, sulfuric acid is inappropriate for the processing of carbonate and rich magnesium-bearing zinc ores: for the former, the consumption of acid is too high and for the latter, magnesium removal from the leach solution is too complex (Safari et al., 2009; Espiari et al., 2006). The direct leaching process of zinc ores with sulfuric acid is represented by Equations (2.5) to (2.8) for sphalerite, smithsonite, willemite, and hemimorphite, respectively (Xu et al., 2013; Abkhoshk et al., 2014):

$$ZnS + H_2SO_4 \rightarrow ZnSO_4 + H_2S_{(aq)} \quad (2.5)$$

$$ZnCO_3 + H_2SO_4 \rightarrow ZnSO_4 + H_2O + CO_2 \quad (2.6)$$

$$Zn_2SiO_4 + 2H_2SO_4 \rightarrow 2ZnSO_4 + Si(OH)_4 \quad (2.7)$$

$$Zn_4Si_2O_7(OH)_2 \,.H_2O + 4H_2SO_4 \rightarrow 4ZnSO_4 + Si_2O(OH)_6 + 3H_2O \quad (2.8)$$

Generally, the hydrometallurgy process of zinc is carried out by oxygen in a sulfuric medium. There are two main routes for processing zinc concentrate: one is a high-pressure process at high temperature (i.e. 150 °C) and high oxygen pressure (i.e. 11 bars of oxygen); the other is an atmospheric leaching process at 95 °C.

The presence of a species as an agent for oxygen transfer is vital since even at high temperature and pressure, zinc sulfide leaching by oxygen in a sulfuric medium is extremely slow. Therefore, the ferric ion acts as an oxygen transfer agent. Furthermore, during the process, Fe^{3+} is regenerated by oxygen, and elemental sulfur is the main product. Research findings confirm that cupric ion plays a crucial role in the oxidation of ferrous to ferric ions and its presence at about 1 g/l is desired in the leaching step (Filippou, 2004).

2.4.1.1. Direct pressure leaching (DPL)

According to a study by Doyle et al. (1978), the development of direct pressure leaching (DPL) commenced in the late 1950s. However, the first commercial plant was built in Cominco's zinc refinery at Trail, British Columbia, Canada in the 1980s (Jankola, 1995). In this process, the zinc production is independent of the sulfuric acid consumption since zinc sulfide is directly leached and produced the elemental sulfur. Furthermore, the leach residue can be treated to recover valuable metals such as lead and silver. In the DPL process, the sulfidic sulfur is oxidized to elemental sulfur instead of SO_2. Therefore, SO_2 pollution is completely avoided. Under DPL conditions, the leaching reaction of sphalerite may be described as shown in Equation (2.9) (Doyle et al., 1978):

$$ZnS + H_2SO_4 + \frac{1}{2}O_2 \rightarrow ZnSO_4 + H_2O + S^0 \quad (2.9)$$

In this reaction, dissolved iron can be viewed as an oxygen carrier to boost the rate of the reaction. To predict the oxidation rate under DPL conditions, it is critical to understand the ferrous oxidation reaction (Dreisinger and Peters, 1989; Markus et al., 2004). Normally, there is sufficient acid-soluble iron in zinc concentrates to meet the process's need for iron ions. Since zinc concentrates contain iron and the iron minerals are leached during pressure leaching, the behaviour of iron in the autoclave is monitored by the acid content in the leach solution.

The DPL process for zinc concentrates is divided into two different systems according to the acid concentration: (1) a low-acidity leach and (2) a high-acidity leach (Buban et al., 2000). Figure 2.5 shows the two-stage Sherritt zinc pressure leaching process for the HBM&S refinery (Ozberk et al., 1995). Under conditions of low oxygen availability, low temperature,

and high acid concentration, the oxidation of pyrite may lead to the production of elemental sulfur as shown in Equation (2.10) (Buban et al., 2000):

$$FeS_2 + H_2SO_4 + \frac{1}{2}O_2 \rightarrow FeSO_4 + H_2O + 2S^0 \quad (2.10)$$

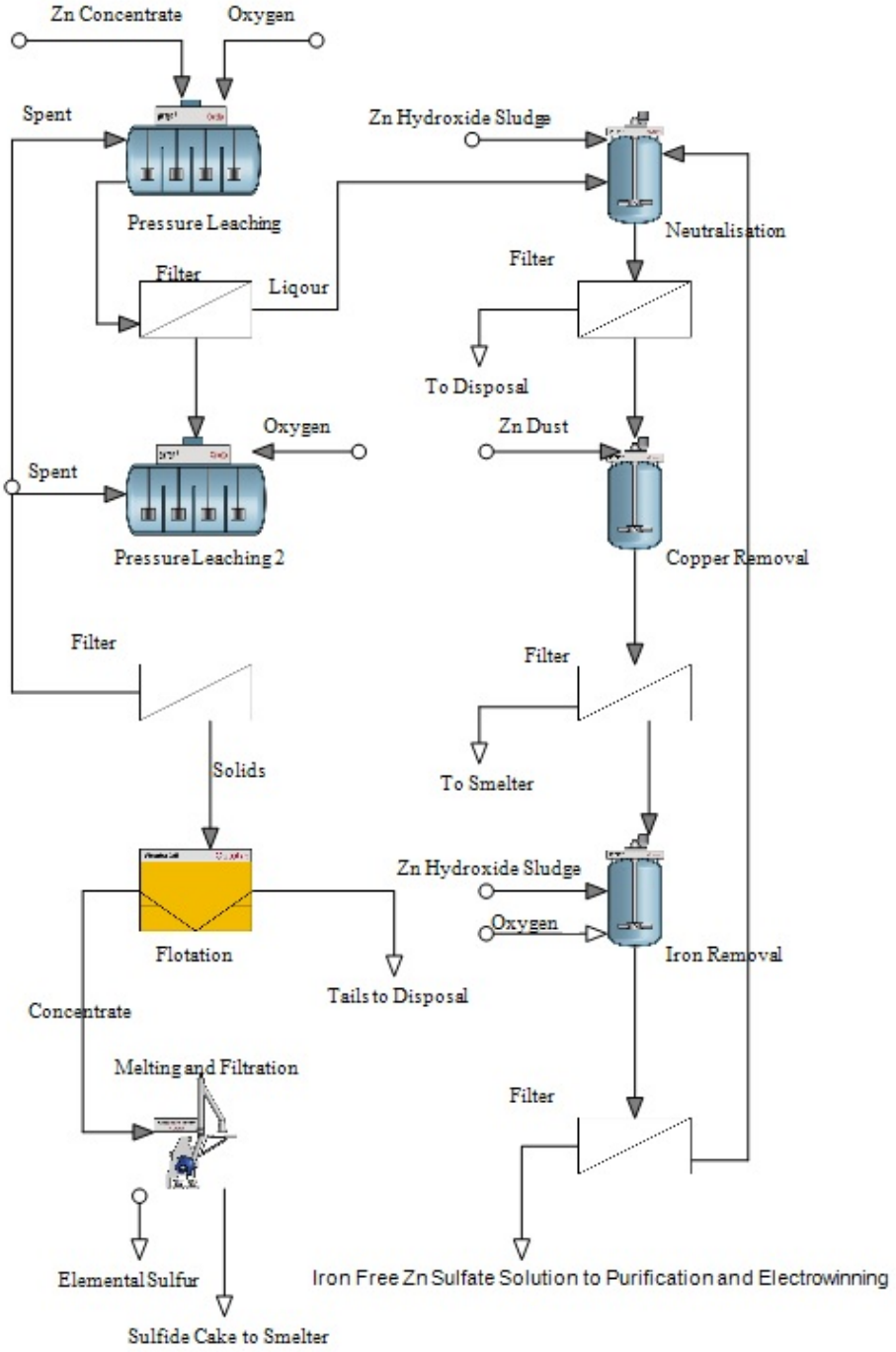

Figure 2. 5. The two-stage sherrite zinc pressure leach process for HBM&S refinery (OZBERK et al. 1995).

During the DPL process, a significant proportion of the lead components in the zinc concentrates are converted to lead jarosite ($Pb_{0.5}Fe_3(SO_4)_2(OH)_6$) in the leach residue instead of lead sulfate ($PbSO_4$) (Buban et al., 2000). Consequently, by forming the lead jarosite in the presence of dissolved zinc, a large proportion of the divalent base metals enter the jarosite lattice; zinc replaces Fe^{3+}, with charge neutrality being maintained by increasing the concentration of Pb^{2+}. In addition, beaverite [Pb(Cu, Zn)-$Fe_2(SO_4)_2(OH)_6$] can be obtained in the structure and composition only under extreme co-precipitation conditions. Research findings confirm that the order of incorporation of co-precipitated with lead jarosite is: $Fe^{3+} >> Cu^{2+} > Zn^{2+} > Co^{2+} \sim Ni^{2+} \sim Mn^{2+}$. It was also reported that neither acid concentration nor reaction time nor temperature has a significant effect on the proportion of zinc co-precipitation (in the range between 130 and 180 °C) (Canterford et al., 1985; Dutrizac and Dinardo, 1983; Dutrizac et al., 1980).

One of the main challenges of the DPL process is that it is performed at a temperature above the sulfur melting point (115 °C). Consequently, the liquid sulfur spreads rapidly throughout the surface of unreacted mineral particles, which results in a decrease in the rate of metal dissolution (Kawulka et al., 1973). However, if the leaching is performed in the presence of an appropriate surfactant, the liquid sulfur produced is broken down on the particle surface. This can provide the leaching reagent with a fresh mineral surface and increases the leaching rate (Owusu et al., 1992). Numerous research studies have identified suitable surfactants as dispersants for liquid sulfur. Owusu investigated the role of several surfactants such as lignin sulfonic acid, coco amido hydroxyl sulfobetaine (CAHSB), tallow amido hydroxyl sulfobetaine (TAHSB), coco amido betaine (CAB), naphthalene sulfonic acid-formaldehyde condensates, and orthophenylene diamine (OPD) in the liquid sulfur-aqueous zinc-sulfate–zinc-sulfide mineral system (Owusu, 1993). The appropriate additives for this purpose include lignins, lignosulfonates, tannin compounds, particularly quebracho, and alkylaryl sulfonates (Lochmann and Pedĺik, 1995; Owusu et al., 1995).

Xie and co-workers (2007) suggested that in the DPL process of high iron sphalerite concentrates, when the agitation rate is greater than 600 r/min, diffusion is not the control step of the leaching reaction but rather the reaction is controlled by the surface chemical reaction. Moreover, they reported that the activation energy for the process is 55.04 kJ/mol (Xie et al., 2007).

Some empirical models for optimization of the process were also developed (Guler, 2016). The effect of leaching parameters such as temperature, liquid properties, mixing conditions, particle size, solid/liquid ratio, and additive dosage on the DPL process of the zinc sulfide concentrate were studied (Gu et al. 2010). It was shown that the temperature is the most

decisive factor in zinc dissolution behaviour in the DPL process of zinc sulfide concentrates (Lampinen et al., 2015). Another model using Markov Chain Monte Carlo (MCMC) methods has been developed by Lampinen and co-workers (2015), and the activation energy at 70–110 °C was also calculated to be 112 kJ/mol.

Recently, besides zinc sulfide concentrate and sphalerite, the leaching behaviour of zinc silicate ores (hemimorphite and smithsonite) in pressure leaching has drawn some attention (Xu et al., 2012). The DPL process was carried out for zinc silicate ore to determine the effect of parameters such as sulfuric acid concentration, particle size, pressure, temperature, and reaction time on the dissolution of zinc and silica (Li et al., 2010). They reported that the primary mineral in leaching residue is quartz and small amounts of unreacted oxide minerals such as Fe, Pb, and Al are associated with quartz. It was also shown that, as a result of electrostatic attraction, electropositive $Fe(OH)_3$ colloids electronegative and silica gel aggregate and co-precipitate if the pH at the end of the process is 4.8–5.0 (He et al., 2011; He et al., 2010).

Mechanism of pressurized leaching processes

The dissolution of sphalerite can be performed by both direct and indirect oxidation. In direct leaching, oxidization of sphalerite is performed by either ferric iron in solution or by a coupling electropositive mineral through a galvanic cell reaction. In the process, sulfur is produced in the solid state on the mineral surface since the temperature is lower than the sulfur melting point. Thus, there is significant elemental sulfur in the mineral residue. Equations (2.11)–(2.13) show the reactions of electrochemical oxidation of sphalerite (Mackiw and Veltman, 1967; Pawlek, 1969):

$$ZnS \rightarrow Zn^{2+} + 2e + S^0 \quad (2.11)$$

$$H_2SO_4 + 2FeSO_4 + \frac{1}{2}O_2 \rightarrow Fe_2(SO_4)_3 + H_2O \quad (2.12)$$

$$ZnS + Fe_2(SO_4)_3 \rightarrow ZnSO_4 + 2FeSO_4 + S^0 \quad (2.13)$$

In the indirect process, the dissolution of sphalerite takes place, and then the H_2S produced is transferred from the sphalerite surface into the solution and further oxidized into elemental sulfur by either dissolved oxygen or ferric iron. However, at temperatures lower than 150 °C, the oxidization of H_2S is mainly through the reaction with oxygen. Equation (2.1) and the following Equations (2.14) and (2.15) show the reaction of sphalerite in the indirect process (Corriou et al., 1988):

$$H_2S_{(aq)} + \frac{1}{2}O_2 \rightarrow H_2O + S^0 \quad (2.14)$$

$$H_2S_{(aq)} + Fe_2(SO_4)_3 \rightarrow H_2SO_4 + 2FeSO_4 + S^0 \quad (2.15)$$

Xu and co-workers (2013) reported that there is no elemental sulfur layer on the mineral surface and proposed the dissolution of sphalerite through the indirect oxidation reactions.

2.4.1.2. Atmospheric direct leaching (ADL)

In the 1990s, Fugleberg and Jarvinen developed the atmospheric direct leaching (ADL) process for zinc sulfide concentrate (Fugleberg and Jarvinen, 1992, 1994, 1998). The ADL process is similar to low-temperature pressure leaching since it is operated under oxygen-rich conditions. In this process, the zinc concentrates are oxidized in sulfuric acid media in the presence of an iron couple (Fe^{3+}/Fe^{2+}) as an intermediate between the dissolved oxygen and the mineral according to Eeactions (2.10) and (2.14). The ADL process reactors was developed by Outokumpu and has been practised at an industrial scale. In 2008, Zhuzhou Smelter Group, Outotec, carried out an ADL process for sulfidic zinc concentrate (Haakana et al., 2008; Saxén, 2008; Lahtinen et al., 2008). In other work, Haakana and co-workers (2007) developed the direct leaching of zinc sulfide concentrates at pilot scale and semi-batch experiment and using copper ion as a catalysing agent for leaching rate. Similarly to the chemistry of the DPL process, ADL converts the sulfide to elemental sulfur instead of sulfur dioxide.

This process is conducted in a single stage where zinc is leached and the iron is precipitated as jarosite/goethite at the same time. To achieve this goal, the sulfuric acid concentration should be maintained between 10 and 30 g/l in the leach solution by the addition of sulfuric acid and spent electrolyte. In addition, through the removal of the elemental sulfur and untouched sulfide minerals from the lead-rich fraction, an appropriate lead concentrate for lead production can be obtained from the leach residue (Filippou, 2004; Haakana et al., 2008; Karimi et al., 2017).

The general leaching reaction of sphalerite in the ADL process is shown in Equation (2.11). Iron ions play a vital role in ADL. Therefore, the required high iron concentration is provided by recycling of iron precipitates. In other words, this process is carried out by reaction of the spent electrolyte and the iron oxide residue, which contains sulfuric acid, and ferric iron is dissolved as a function of the iron oxide species as shown in Equations (2.16), (2.17), and (2.18) (Buban et al., 2000; Vignes, 2013):

$$2FeO.OH + 3H_2SO_4 \rightarrow Fe_2(SO_4)_3 + 4H_2O \quad (2.16)$$

$$Fe_2O_3.xH_2O + 3H_2SO_4 \rightarrow Fe_2(SO_4)_3 + (x+3)H_2O \quad (2.17)$$

$$2FeOHSO_4 + H_2SO_4 \rightarrow Fe_2(SO_4)_3 + 2H_2O \quad (2.18)$$

The ADL variables such as pressure, temperature, liquid properties, and mixing conditions were investigated to study mass transfer by Kaskiala (2005). It was reported that pressure and mixing have positive effects on the process and also that increasing the temperature has a direct effect on oxygen consumption in the solution (Kaskiala, 2005). A study by Xu and co-workers (2013) shows that application of the shrinking core model (SCM) to the description of leaching behaviour of sphalerite in the ADL process with the calculated apparent activation energy of 44.28 ± 4.28 kJ/mol confirms that the chemical reaction is the controlling step in ADL.

2.4.1.3. Modified nitrosyl process

A modified nitrosyl process involving atmospheric leaching of complex sulfide concentrate (zinc and copper sulfides) using sulfuric acid was patented by O'Brien and Peters. This process was carried out by leaching of the mixed sulfides in sulfuric acid media (55–75% H_2SO_4), while the solid/liquid ratio was 30% for a leaching time of 1 h at 125–135 °C (O'Brien and Peters, 1998). During the leaching, zinc sulfate is introduced to the solution and H_2S gas is produced. Furthermore, copper sulfides dissolve to some extent; however, due to the presence of the H_2S, copper ions reprecipitate in sulfide form. The H_2S off-gas is converted to elemental sulfur in a separate unit. After the leaching stage, the high acid concentration in the solution results in the precipitation of zinc as zinc sulfate monohydrate ($ZnSO_4.H_2O$) crystals (Filippou, 2004). Zinc is subsequently dissolved from the leach residue using diluted sulfuric acid and forms a zinc sulfate solution which can be treated by conventional electrolysis. Finally, to boost the recovery of copper, the residue is treated further in a mixed HNO_3-H_2SO_4 media.

2.4.1.4. Outokumpu nonsulfidic process

This process was developed by Outokumpu (Fugleberg and Jarvinen, 1996). In this process, the silicate zinc feed is leached at a pH of approximately 3 and a temperature of nearly 80 °C. Under these operational conditions, silicates and zinc ferrite remain unreacted and do not pose filtering issues. After the leaching step, the solution is subjected to electrolysis, whereas the remaining zinc in the silicate residue is recovered from the off-gas of a Waelz kiln. During the treatment of residue in the Waelz kiln, the collected zinc fumes from the off-gases are returned to the leaching step. The Waelz kiln slag is produced by combining silica and iron and forming an iron silicate slag (Filippou, 2004).

2.4.1.5. Oxidative leaching at low temperature

According to Table 2.5, nitric acid is the third most powerful oxidant among the acidic media. Therefore, coupling leaching of sulfide zinc concentrate by a mixture of sulfuric acid (as the

base medium) and nitric acid (as an oxidant) has attracted profound interest. Generally, oxidation of metal sulfides using nitric acid can be conducted through two possible reactions. In the first one, the oxidizing agent is the NO_3^- ion and is reduced to NO or NO_2 during the reaction. In the other, the oxidant is oxygen derived from nitric acid decomposition. The overall reaction in the leaching process is shown in Equation (2.19) (Habashi, 1999):

$$2ZnS + O_2 + 2H_2SO_4 \xrightarrow{HNO_3} ZnSO_4 + 2S^0 + 2H2O \quad (2.19)$$

Table 2. 5. The equilibrium redox potentials of the corresponding reactions (Vignes, 2013).

Oxidizing agent	Reaction	(pH 0) H_2 (ref)
Cu^{2+}	Cu^{2+} / Cu^{+}	0.153 V
Fe^{3+}	$Fe^{3+} + e \rightarrow Fe^{2+}$	0.77 V
HNO_3	$NO_3^- + 4H^+ + e \rightarrow NO_{(g)} + 2H_2O$	0.957 V
MnO_2	$MnO_2 + 4H^+ + 2e \rightarrow Mn^{2+} + 2H_2O$	1.2 V
HNO_2	$NO_2^- + 2H^+ + e \rightarrow NO_{(g)} + H_2O$	1.202 V
O_2(g)	$½\ O_{2\,(aq)} + H^+ + 2e \rightarrow H_2O$	1.230 V
$K_2Cr_2O_7$	$Cr_2O_7^{2-} + 14H^+ + 6e \rightarrow 2\ Cr_{3+} + 7\ H_2O$	1.33 V
Cl_2(g)	$Cl_2(g) + 2\ e \rightarrow 2\ Cl^-$	1.358 V
NO^+	$NO^+ + e \rightarrow NO(g)$	1.450 V
$NaClO_3$	$ClO_3^- + 6\ H^+ + 6e \rightarrow Cl^- + 4\ H_2O$	1.450 V
$KMnO_4$	$MnO_4^- + 8\ H^+ + 5e \rightarrow Mn^{2+} + 4\ H_2O$	1.49 V
H_2O_2	$H2O2 + 2\ H^+ + 2e \rightarrow 2\ H_2O$	1.77 V
H_2SO_5	$SO_5^{2-} + 2\ H^+ + 2e \rightarrow SO_4^{2-} + H_2O$	1.81 V
$K_2S_2O_8$	$S_2O_8^{2-} + 2e \rightarrow 2SO_4^{2-}$	2 V
O_3	$O_3 + 2\ H^+ + 2e \rightarrow O_2 + H_2O$	2.07 V

In 1996, O'Brien proposed the nitrosyl process. In this process, complex sulfide concentrates are treated in a mixed concentrated of nitric acid and sulfuric acid solutions. The main parameters of the process are the molar ratio of nitric acid to copper in the feed (1.0–1.5 mol HNO_3 per mol Cu) and a sulfuric acid concentration of 40–65%. The concentrate is then heated to a temperature ranging between 110 and 170 °C for a leaching time of 1 h.

Consequently, two products are obtained as precipitates. The one consists of hydrated zinc-copper-ferric sulfates and the other contains elemental sulfur. After that, the precipitated hydrated zinc-copper-ferric sulfates are leached in a diluted acid solution and converted to a copper/zinc solution. After removal of copper from the leached solution, the raffinate is neutralized with lime to pH 4–5. At this pH, iron is removed from the solution by precipitation

(as $Fe(OH)_3$) and zinc is recovered by solvent extraction with D2EHPA or Cyanex 302 (O'Brien, 1996).

Peng and co-workers studied the coupling process (by H_2SO_4–HNO_3) in a sphalerite concentrate under pressure. The mechanism of coupling leaching, the solid-to-liquid ratio, and the temperature of the leaching process were separately determined. The results showed that zinc recovery of up to 99.6% could be obtained at 85 °C and an oxygen pressure of 0.1 MPa with a solid-to-liquid ratio of 10% in a leaching solution containing 2.0 mol/l H_2SO_4 and 0.2 mol/l HNO_3 after 3 h (Peng et al., 2005a). The kinetic investigation indicated that the rate-controlling step of the process was the diffusion through the product layer. Technically, the leaching rate was controlled by diffusion of the reagent through the precipitated sulfur layer on the surface of the particle (Sokić et al., 2012). To address this issue, studies showed that by using tetrachloroethylene (C_2Cl_4) as the extracting agent for the elemental sulfur, the overall extraction rate could be achieved in the shorter leaching time. Tetrachloroethylene was chosen as the solvent for sulfur for two reasons: first, because sulfur has high solubility in it, and second, because it has good stability in the leaching pulp. During the leaching process, tetrachloroethylene extracts the produced elemental sulfur in Reaction (2.21). The reaction that occurs in this extraction is shown in Equation (2.20) (Peng et al., 2005b):

$$\tau S^0 + C_2Cl_4 = \tau S^0.C_2Cl_4 \qquad (2.20)$$

Ferric sulfate leaching

In this process, the initial sphalerite dissolution rate was found to be directly proportional to the ferric ion concentration in the solution at a temperature of 80 to 100 °C. This was interpreted as an indicative rate control by solution diffusion. The dissolution rate is independent of the initial concentrations of zinc and ferrous ions in the solution (Kuzminkh and Yakhontova, 1950). Kuzminkh and Yakhontova (1950) also reported that at a constant concentration of ferric sulfate, the dissolution rate decreased with increasing acid strength. They found that the rate of zinc extraction increased with increasing ferric concentration to a maximum at three times the stoichiometric requirement; after that, an additional ferric ion was found not to affect the rate (Gupta and Mukherjee, 1990). The leaching rate is proportional to the surface area of the sphalerite and increases as the amount of sphalerite decreases. However, it does not have a significant effect on the leaching process. In fact, the temperature is the most effective parameter during the leaching process. It has been shown that the leaching rate increases with increasing temperature. The relatively high value of the apparent activation energy (i.e. 44 kJ/mol) indicates that zinc dissolution is a chemically controlled reaction (Dutrizac, 2006). This study caused controversy regarding the rate controlling model of the process. After that, Souza and co-workers (2007) showed that the leaching process of

sphalerite in ferric sulfate media includes two stages. The initial stage follows a chemical control mechanism, while controlled diffusion is the kinetic mechanism of the final stage of leaching. The process is carried out according to Equations (2.21) and (2.22) (Souza et al., 2007):

$$ZnS + 2Fe^{3+} \rightarrow Zn^{2+} + 2Fe^{2+} + S^0 \quad (2.21)$$

$$2FeSO_4(aq) + SO_2(g) + O_2 \rightarrow Fe_2(SO_4)_3(aq) \quad (2.22)$$

The reproduction of ferric sulfate can be carried out by oxygen either simultaneously with the leaching stage or in a separate stage. The simultaneous stage allows the use of fewer reactors. However, to reach a high rate of sphalerite oxidation, the temperature should be approximately the solution boiling point. Therefore, the separate stage offers good chemical control of the process since the maximum regeneration rate of ferric sulfate occurred at about 80 °C (Ghosh and Ghosh, 2014).

The effect of process parameters including the concentration of sulfuric acid and ferric ions, temperature, solid-to-liquid ratio, reaction time, and particle size on the process for different kinds of feeding materials was investigated by different studies (Santos et al., 2010; Dehghan et al., 2008). Shibayama and co-workers (2001) leached a sphalerite concentrate at 100 °C for leaching time in the range of 3 to 6 h, which resulted in 94% extraction of zinc. A copper-zinc sulfide ore was treated by ferric sulfate solutions (Buttinelli et al., 1992). The study showed that complete recovery was only reached at a high temperature of about 140 °C, even in the presence of a solvent for elemental sulfur such as C_2C1_4.

MIM Albion process

This process was developed in 1994 by Xstrata PLC and patented worldwide. The process is carried out by ultrafine grinding followed by ferric sulfate oxidative leaching. The process is conducted in agitated tanks at atmospheric pressure, and lignosol is applied to avoid frothing in the reactor (Hourn et al., 1996; Hourn et al., 1999). Research findings confirm that ultrafine grinding increases the available surface area and consequently enhances the leaching rate.

Dowa process

This process is based on a combination of grinding and leaching of sphalerite under either atmospheric or elevated pressure (Kanno et al., 2002). In this process, grinding is combined with leaching in sulfuric acid solution along with ferric sulfate as an additive under an atmospheric pressure condition. The sulfur product from the zinc sulfide particles is removed by grinding. This action leads to an increase in the rate of solution (dissolution of more than 95% of the zinc in less than 1 h). The regeneration of ferric ions with oxygen can be carried

out under atmospheric pressure conditions in a stirred reactor or under high-pressure conditions in a pipe reactor. To avoid the formation of jarosite, the sulfuric acid concentration in the solution should be kept above 40 g/l. So far, this process has only been carried out at laboratory scale (Filippou, 2004).

2.4.1.6. Low-grade zinc silicate leaching by sulfuric acid

Recently, due to the enforcement of strict laws in the zinc production industry to compel businesses to decrease sulfur emissions, in spite of the shortage of zinc silicate ores, they are considered as an alternative to zinc sulfide (De Wet and Singleton, 2008). Skorpion Zinc Mine can be considered as the first industrial application of sulfuric acid leaching of zinc silicate ores. This process includes three stages: leaching with sulfuric acid, concentration and purification by solvent extraction (modified ZINCEX,) and electrowinning (Alberts and Dorfling, 2013; Díaz and Martín, 1994; Nogueira et al., 1982; Nogueira et al., 1979).

Abdel-Aal (2000) determined the impact of variable parameters such as ore particle size, temperature, and acid concentration on the rate of the leaching process. The results showed that by using a particle size distribution between 53 and 75 μm, a temperature of 70 °C, a sulfuric acid concentration of 10%, and a leaching time of 180 min, about 94% of the zinc was leached, while the solid-to-liquid ratio remained constant at 1:20 g/ml. Furthermore, diffusion through the product layer was determined as the rate controlling process during the reaction. This result was confirmed by the calculated activation energy, which was approximately 13.39 kJ/mol.

2.4.2. Direct leaching with hydrochloric acid

Muir and co-workers (1976) reported that it was possible to extract lead, zinc, and silver from McArthur River zinc-lead sulfide concentrate using both HCl and HCl-O_2 leaching. This leaching reaction proceeded with vigorous evolution of H_2S and formation of froth. When leaching was carried out along with slow O_2/air bubbling through the slurry, elemental sulfur was generated as shown in Equation (2.23) (Muir et al., 1976):

$$2MS + 4HCl + O_2 \rightarrow 2MCl_2 + 2S^0 + 2H_2O \qquad (2.23)$$

where M denotes zinc, lead, or silver. However, some H_2S gas always formed whenever a high pulp density, high total chloride ion concentration (> 6 M), and air in place of O_2 were used. A pyritic zinc-lead sulfide concentrate was leached by Mizoguchi and Habashi (1981) with 1–2 N HCl at 120 °C using an O_2 pressure of 100 kPa. In pyritic ores, the grain size of the individual minerals may be extremely fine (a few microns) and the mutual grain boundaries of the minerals show a high degree of locking. It was found that more than 97%

of the Zn and 95% of the Cu were leached, while 83% of the Pb remained in the residue as $PbCl_2$ and $PbSO_4$ (Jansz, 1984). A conceptual flowsheet for the leaching of a pyritic zinc-lead sulfide concentrate in 7 mol/l HCl is shown in Figure 2.6.

Baba and co-workers (2010) investigated the effect of different parameters such as particle size, stirring speed, hydrochloric acid concentration, temperature, and solid-to-liquid ratio on the dissolution kinetics of a sphalerite ore in hydrochloric acid. They reported that increasing hydrochloric acid concentration and temperature have positive effects on zinc dissolution, whereas that of decreases with particle size and solid-to-liquid ratio. Moreover, by data fitting of the kinetics analysis on the SCM, the rate-determining step for the reaction was reported to be a surface chemical reaction (Baba and Adekola, 2010).

2.4.2.1. Ferric chloride leaching

The vast majority of sphalerite dissolution studies have focused on the application of strong oxidants, particularly Fe^{3+} as ferric chloride (Santos et al. 2007; Dehghan et al. 2009; Lochmann and Pedĺik 1995; Leclerc et al. 2003; Santos et al. 2010). It has been shown that sphalerite is readily soluble in acidic ferric chloride solutions. By using $FeCl_3$ lixiviant containing 94 g/l Fe^{3+}, 60 g/l Fe^{2+}, and 5 g/l HCl, about 100% zinc extraction has been achieved at 95–106 °C and a pulp density of 10% in a leaching time of 6 h. The research findings showed that reaching 85% zinc extraction required a 150% excess over stoichiometric $FeCl_3$ and the process had to be conducted at the boiling point of the leachant. Furthermore, to extract over 98% of the Zn from sphalerite ore at 106 °C, one gram of the concentrate requires 2.7 g of a solution containing 100 g/l Fe^{3+} and 50 g/l Fe^{2+} (Gupta and Mukherjee, 1990). The reaction order, kinetic model, and activation energy for a vast range of $FeCl_3$ concentrations in a temperature range from 25 to 100 °C have been studied by several researchers (Jin et al. 1983; Aydogan et al., 2005). For instance, it was reported that for a solution containing 0.1 to 1 M of $FeCl_3$ and a temperature range between 44 and 90 °C, the reaction was of the first order with respect to Fe^{3+} concentration and the activation energy was 49.79 kJ/mol (Demopoulos, 1977).

2.4.2.2. Noranda zinc-oxide process

To produce pure zinc sulfide, low-grade zinc sulfide leaching in hydrochloric acid can be carried out (Molleman et al., 1998). In this process, the pH should be increased to 1.0 to precipitate zinc sulfide from zinc-iron chloride solutions by adding a base such as sodium hydroxide (NaOH). The changing of NaOH with magnesium oxide (MgO) was proposed by Van Weert and van Sandwijk (1999). Therefore, MgO converts to soluble magnesium chloride during the neutralization, and after precipitation of zinc, the magnesium chloride

solution can be hydrolysed to MgO and HCl gas. As a result, both the reagent and the neutralizing agent are recovered. Also, it has been claimed that the precipitation of zinc oxide compared with zinc sulfide has some advantages: the product is sulfur free and it is also thermodynamically feasible under certain conditions (Allen et al., 2002).

2.4.2.3. Oxidative hydrochloric leaching by using pyrolusite

In this process, there is a galvanic interaction between zinc sulfide and pyrolusite (MnO_2). During contact between these two species, the leaching rate of the least noble species (zinc) by oxygen is accelerated relative to pyrolusite (the noblest one). In other words, according to the galvanic interaction effect, the oxygen reduction on the surface of the pyrolusite leads to an increase in the dissolution rate of zinc sulfide (Vignes, 2013).

Some researchers have conducted experiments using pyrolusite for atmospheric zinc sulfate leaching (Pande et al. 1982; Madhuchhanda et al., 2000a; Madhuchhanda et al., 2000b). The dissolution is carried out through three major reactions:

- Cyclic action of the Fe^{3+}/Fe^{2+} redox couple
- Galvanic interaction between ZnS and MnO_2
- The action of Cl_2 gas generated from the MnO_2-HCl reaction on ZnS, as described by Equation (2.24 (Madhuchhanda et al. 2003):

  $$MnO_2 + 4HCl \rightarrow MnCl_2 + 2H_2O + Cl_2 \uparrow \quad (2.24)$$

All three reactions play crucial roles in the leaching process at lower hydrochloric acid concentrations, whereas Reaction (2.24) is dominant at higher hydrochloric acid concentrations. One of the important issues that this process is dealing with, posing a substantial decline in current efficiency due to the build-up of manganese in the electrolyte (Filippou, 2004).

Figure 2. 6. Flowsheet for the leaching of a pyritic zinc-lead sulphide concentrate in 7 mol/l HCl (Jansz 1984).

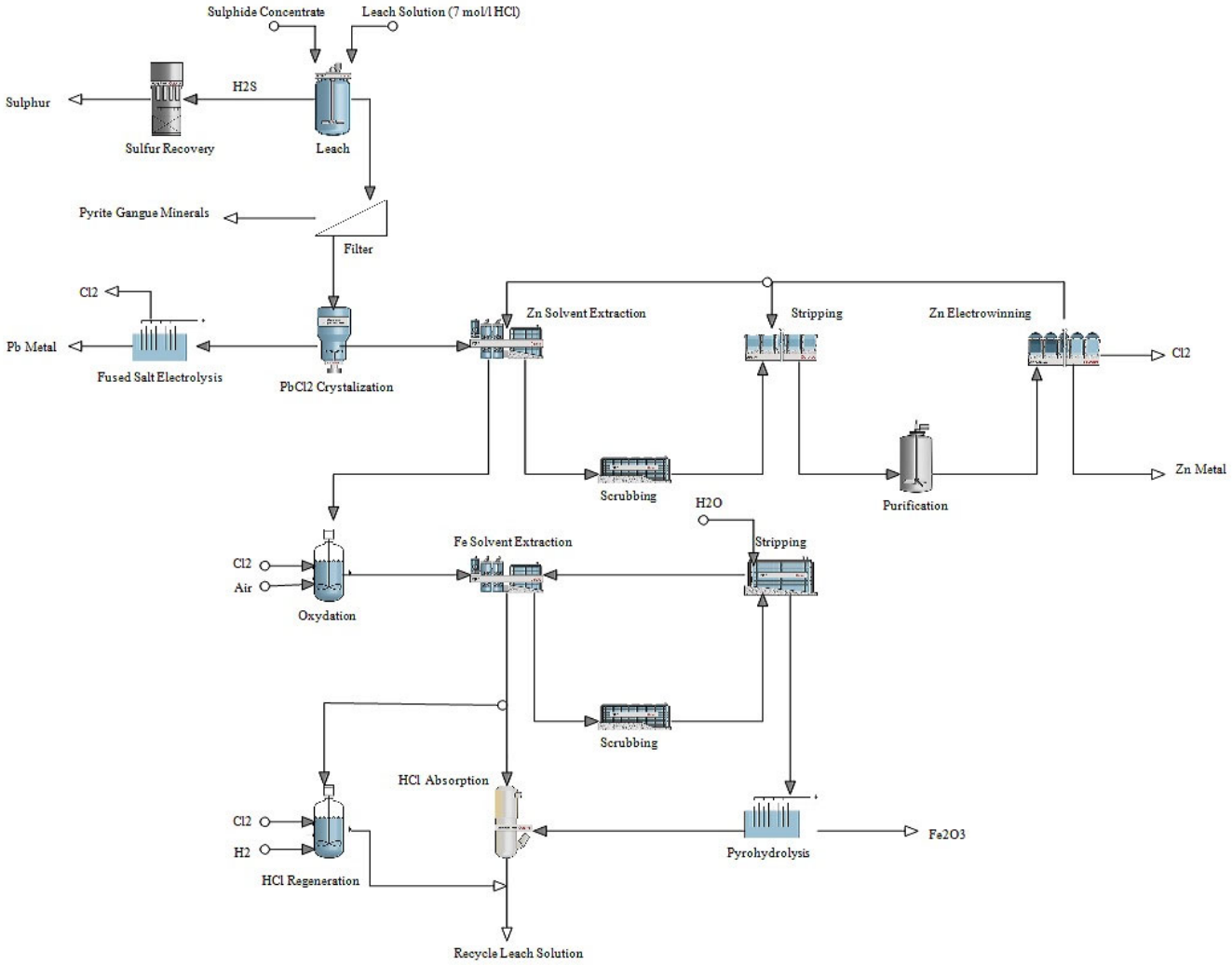

2.4.2.4. Oxidative hydrochloric leaching by sodium chlorate

In this process, it was shown that increases in the sodium chlorate concentration, hydrochloric acid concentration, and reaction temperature have positive impacts on the dissolution rate, while this decreases with increasing particle size. In addition, stirring speeds above 400 rpm did not affect zinc extraction substantially (Uçar, 2009). The kinetic study indicated that by using the SCM, the zinc dissolution was caused by a surface chemical reaction, which was confirmed by the calculated activation energy of 41.1 kJ/mol. Uçar reported that the reaction orders of the sphalerite dissolution for sodium chlorate and hydrochloric acid concentrations were 1.5 and 2.0 respectively (Uçar, 2009).

2.4.2.5. Oxidative leaching by H_2O_2 as an oxidant

In investigations of the role of H_2O_2 in zinc leaching, most researchers considered H_2O_2 as an oxidant for sphalerite leaching process (Tkáčová et al., 1993; Santos et al., 2010). Pecina and co-workers (2008) assessed the influence of various parameters on zinc-lead sulfide concentrate leaching. Despite the layer of elemental sulfur on the particles, the oxidative leaching of sphalerite is controlled by a surface reaction control step with an activation energy of 50 kJ/mol (Pecina et al., 2008). Increases in the sulfuric acid and hydrogen peroxide concentrations have a positive impact on sphalerite dissolution, and the reaction orders for the sulfuric acid and hydrogen peroxide concentrations are 0.35 and 0.48, respectively. It was shown that stirring speed does not affect the dissolution process (Aydogan, 2006). The leaching process was carried out on a complex sulfide concentrate while the variable parameters were kept constant at 40% solids, 0.55 g hydrochloric acid, and 0.26 g hydrogen peroxide per gram of concentrate. Under this leaching condition, extraction rates of approximately 97% for zinc, 40% for lead, 80% for silver, and well under 12% for iron were achieved after a leaching time of 6 h at atmospheric pressure (Vazarlis 1987).

2.4.2.6. Chlorine-oxygen leaching

The kinetics of sphalerite leaching along with pyrite by water saturated in chlorine have been investigated by Ekinci and co-workers (1998). Increasing the temperature, gas flow rate, and stirring speed has positive effects on the sphalerite leaching rate while increasing the particle size has a detrimental effect on the leaching process. The rate controlling mechanism for the dissolution of sphalerite was determined to be the controlled diffusion through the product layer. The chemistry of this process for sphalerite can be described as shown in Equations (2.25)–(2.27) (Smyres and Garnahan, 1985):

$$Cl_2 + H_2O \rightarrow HCl + HOCl \qquad (2.25)$$

$$ZnS + HCl + \frac{1}{2}O_2 \rightarrow ZnCl_2 + S^0 + H_2O \quad (2.26)$$

$$ZnS + 4HOCl \rightarrow ZnSO_4 + HCl \quad (2.27)$$

Although chlorine-oxygen leaching of sphalerite can occur without copper being present, the leaching rate is faster with copper. Thus, the secondary leaching reactions that probably occurred include Reactions (2.28 and 2.29) (Demarthe et al., 1979):

$$ZnS + 2CuCl_2 \rightarrow ZnCl_2 + 2CuCl + S^0 \quad (2.28)$$

$$ZnS + 2FeCl_3 \rightarrow ZnCl_2 + 2CuCl + S^0 \quad (2.29)$$

$CuCl_2$ and $FeCl_3$ are formed by aqueous oxidation of copper- and iron-bearing sulfide minerals in the feed. Under ideal conditions, chlorine-oxygen leaching solubilizes all of the valuable base metals and iron remains in the leach residue. Chloride control is required to ensure that enough chloride is present to satisfy the counter-ion needs of the zinc, copper, cadmium, and lead and to ensure that insufficient chloride remains to complex the iron, which is rather precipitated from solution as goethite. When the final pH after the reaction is almost 1.7, the solution is iron-free (Smyres and Garnahan, 1985). Sulfate ions should be removed from the solution to minimize the losses of valuable metal by precipitation of a basic sulfate mineral such as beaverite. This can be accomplished by adding BaS, $CaCl_2$, or $BaCl_2$ to the reactor to form insoluble sulfates as shown in Equations (2.30) and (2.31) (Smyres and Garnahan, 1985):

$$BaS + 2HCl + \frac{1}{2}O_2 \rightarrow BaCl_2 + H_2O + S^0 \quad (2.30)$$

$$BaCl_2 \; or \; CaCl_2 + SO_4^{2-} \rightarrow 2Cl^- + BaSO_4 \; or \; CaSO_4 \quad (2.31)$$

If a chloride salt is added, the chloride makes up for losses to the leach residue. The conceptual flowsheet for this process is shown in Figure 2.7.

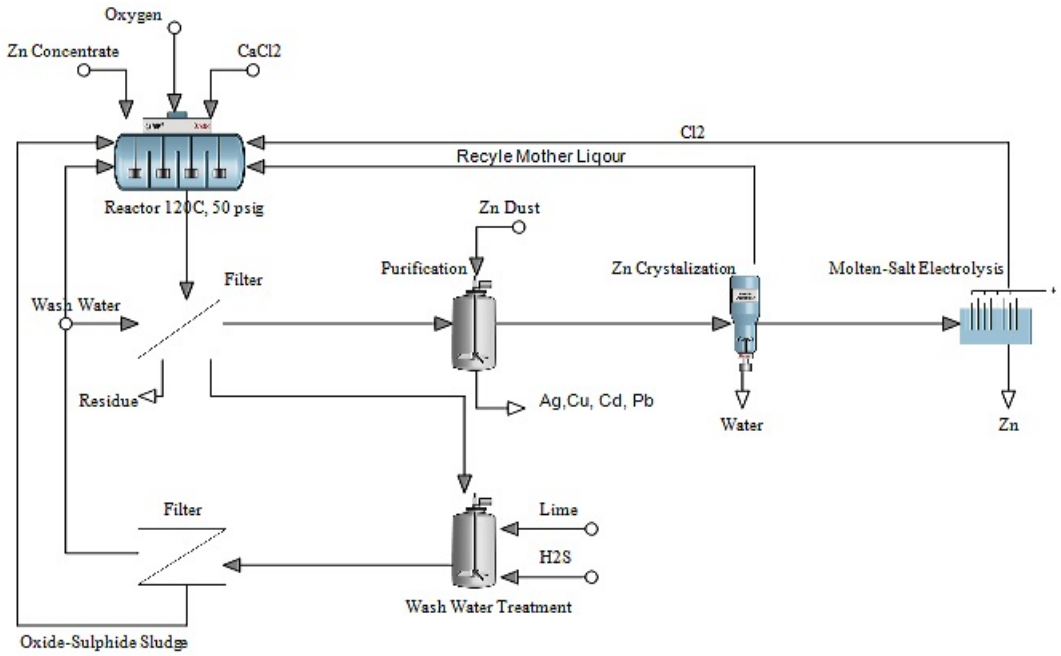

Figure 2. 7. Block diagram of low-grade zinc concentrate leaching by chlorine-oxygen (Smyres and Garnahan 1985).

2.4.3. Leaching with perchloric acid

In this process, a sphalerite ore with 0.45 wt.% iron content and a particle size between 38 and 75 µm is leached in O_2-purged perchloric acid medium at different temperatures from 25 to 85 °C in a range of reaction times up to 144 h (Weisener et al., 2003). In these conditions, two leaching rates were observed: an initial rapid leaching rate following by a slower leaching rate. The formation of polysulfide layers on the surface caused a decrease in zinc dissolution in the initial rapid leaching stage. Therefore, the thickness of the polysulfide layers increases in the rapid leaching step (initial rate) and then reaches a steady state in the slow leaching period. It was proposed that the rate-controlling step is either Zn^{2+} diffusion through the sulfur-enriched surface layer or diffusion of H_3O^+ from the interface of the solution to the unreacted zinc sulfide. The elemental sulfur does not have a decreasing effect on the kinetics and is not considered as a determination parameter for the rate control mechanism during perchloric acid leaching (Weisener et al., 2003).

2.4.4. Alkaline leaching

High acid consumption and a low zinc leaching rate are the main issues that raise substantial concern regarding zinc ores which have high contents of iron, calcium, magnesium, chloride, and carbonate. Alkaline leaching is generally more selective compared with acidic leaching for the following reasons (Abkhoshk et al., 2014):

- Many problematic impurities such as Fe_2O_3, SiO_2, CaO, and MgO are not soluble in the solution as a result of the high pH of the medium (pH 6–7).
- Purification of the barren solution is simpler compared with acid leaching.
- Treating high alkaline gangue-bearing ores with alkaline solutions does not result in excessive consumption of the leaching reagent or conventional filtration problems related to the silica gel issue.

However, lower recoveries, the formation of iron hydroxide layers, and the oxygen demand can be considered as drawbacks of alkaline leaching systems. The following sections cover the most common alkaline leaching systems in detail.

2.4.4.1. Ammonia leaching

Research findings confirm that ammonia leaching (NH_3) of sphalerite is affected by process parameters such as the ammonia concentration, temperature, particle size, and partial pressure of oxygen (Tromans, 2000). It was reported that beyond 450 min, the solution pH and agitation speed did not significantly affect the leaching rate (Ghosh et al., 2002). Ghosh and co-workers (2003) also studied the influence of Cu^{2+} as a catalyst of the leaching process. They reported that the use of Cu^{2+} along with oxygen has a synergistic effect on the dissolution rate during ammonia leaching of sphalerite. In the process using Cu^{2+} as an additive, it was established that increasing the temperature, ammonia concentration, and Cu^{2+} concentration and the use of finer particles size have positive effects on the leaching rate. The leaching rate increases with partial oxygen pressures of up to 5 atmospheres, after which the partial pressure of oxygen does not influence the rate. In addition, in a range of studies, pH did not affect the leaching rate. The catalytic action of the cupric ion was related to the redox couple Cu^{2+}/Cu^{+}, where cupric ammine $[Cu(NH3)_4^{2+}]$ oxidizes sphalerite and then the reduced cuprous ammine $[Cu(NH_3)^{2+}]$ is subsequently oxidized by dissolved oxygen (Ghosh et al., 2003). While alkaline ammonia may be considered in enclosed agitated tanks or autoclaves, it is not suitable for heap and vat leaching approaches due to its volatility and occupational health challenges. Given the declining grades of ores, this is considered as a distinct disadvantage of ammonia leaching and has prevented its application for different resources.

2.4.4.2. Ammonium chloride leaching

In this process, as a result of the relatively high pH, marginal contamination by metal species occurs in the barren solution (in particular, the barren solution is iron free). As a result of the high complexation abilities of both ammonia and chloride ions, several minerals such as zinc oxide, lead oxide, copper oxide, and silver can be easily dissolved by using ammonium

chloride (Yin et al., 2010). The leaching process occurs (especially for zinc oxide minerals such as hemimorphite or smithsonite) according to Reactions (2.32)–(2.35) (Ju et al., 2005):

$$NH_4Cl \rightarrow NH_3(aq) + Cl^- + H^+ \quad (2.32)$$

$$ZnCO_3(S) + 2H^+ \rightarrow Zn^{2+} + CO_2 \uparrow + H_2O \quad (2.33)$$

$$Zn^{2+} + i(NH_3)(aq) \rightarrow Zn(NH_3)_i^{2+} \quad (2.34)$$

$$Zn(NH_3)_2^{2+} + 2Cl^- \rightarrow Zn(NH_3)_2Cl_2(ag) \quad (2.35)$$

where i =1, 2,3,4.

Wang et al. (2008) proposed the rate controlling steps for a new particle surface following a mixed control model which included a chemical reaction rate limiting step along with a diffusion rate limiting step through the inert particle pores (Wang et al., 2008). Rao and co-workers (2015) used nitrilotriacetic acid (NTA) as an alternative complexing agent in this process and reported that the addition of NTA plays a synergistic role in the dissolution process. Their results indicated that the zinc leaching depends strongly on the stability constant of zinc complexes (zinc ions and ligand). In other words, zinc extraction can be facilitated by improving the stability constant of zinc complexes (Rao et al., 2015).

One of the commercial applications of this process is the CENIM-LNETI process, which has been developed on the basis of the oxidation leaching of the sulfides in an ammonium chloride solution which forms ammonia, copper, and zinc ammine complexes in an iron-free solution. The flowsheet of the CENIM-LNETI process for the treatment of sulfidic bulk concentrates is shown in Figure 2.8. In this process, the oxidation of sulfide minerals is carried out by the cupric ion, and oxygen is responsible for the re-oxidation produced cuprous ion. In these reactions, in the case of pure sphalerite, 1.5 mol of ammonia is required for each mol of solubilized zinc and the elemental sulfur to sulfate ratio obtained at 3. However, the production of ammonia is moderately reduced if the mineral contains iron in its structure. Since the produced elemental sulfur is stable under the leaching conditions, the only driving force for reducing the amount of ammonia produced for each mole of solubilized metal is the

attack by the pyrite, which leads to the release of acid in the medium (Limpo et al., 1992; Amer et al., 1995).

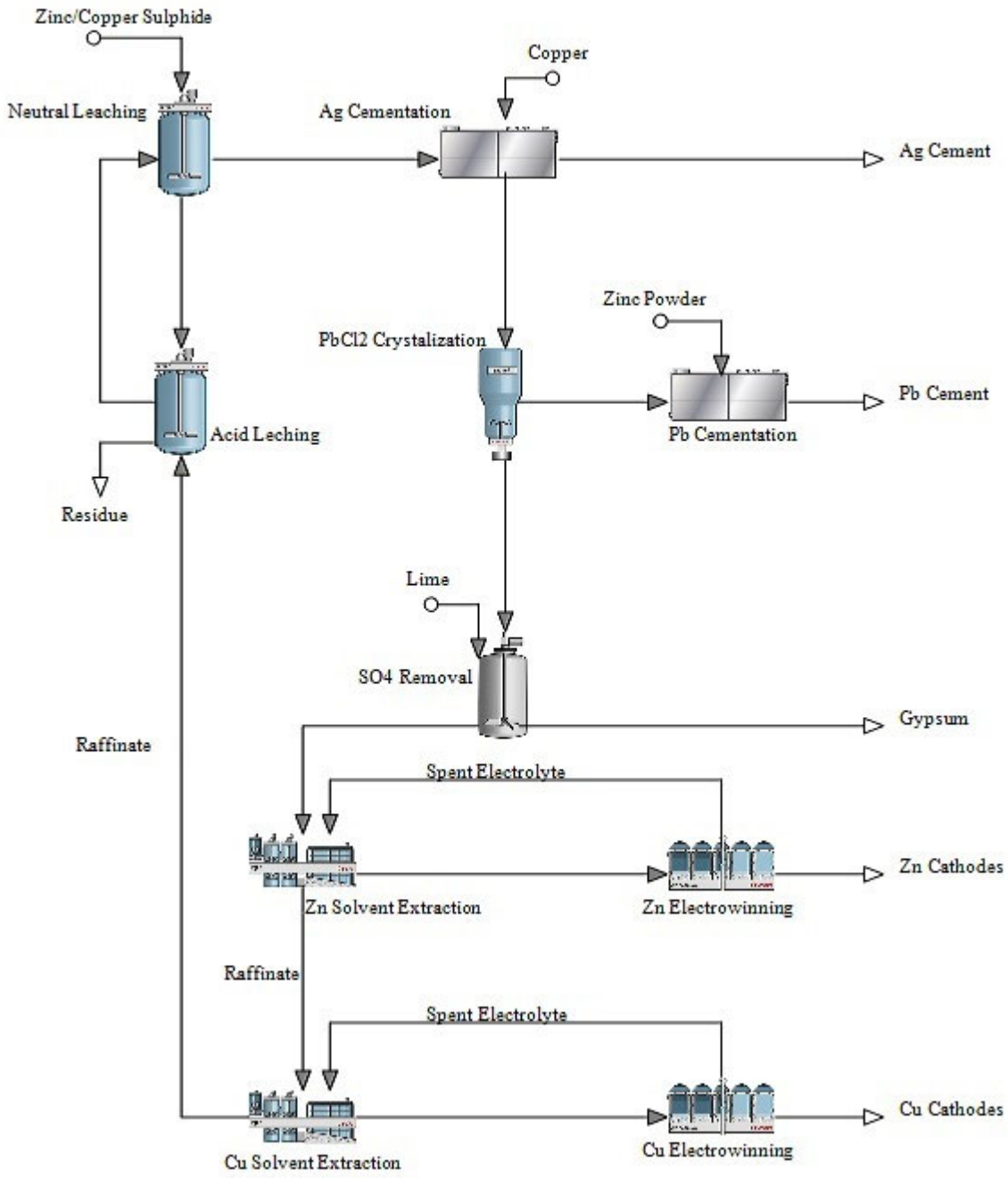

Figure 2. 8. The flowsheet of CENIM-LNETI process for the treatment of sulphidic bulk concentrates (Filippou 2004).

2.4.4.3. Ammonium carbonate leaching

This oxidative couple process was used for the industrial extraction of zinc many years before the application of this process to copper and nickel extraction. The two main processes based on zinc ammonium carbonate leaching include the Schnabel process and the Buka zinc process. Harvey (2006) reviewed the Schnabel process in a separate review paper. On the other hand, the Buka zinc process was expanded for the Lady Loretta zinc deposit in Australia, which is a fine-grained Pb-Zn-Ag deposit. This process can be divided into three stages: ore fuming, followed by ammonia-ammonium carbonate leaching of the zinc fumes, and finally the production of zinc oxide by calcination of a basic zinc carbonate precipitate (Buckett et al., 1998).

2.4.4.4. Caustic soda leaching

Since caustic soda is unable to react with carbonaceous materials and iron compounds, caustic soda leaching is sometimes found to be attractive compared to sulfuric acid for the processing of different zinc ores. However, a high caustic soda concentration in the leach solution needs to be maintained to boost the zinc leaching efficiency. The other issues affecting this process are liquid/solid separations and washing stemming from the high viscosity. Moreover, caustic soda in the solution can react with carbon dioxide in the air, and this reaction results in the consumption of reagents and causes the re-precipitation of zinc (Santos et al. 2010). Frenay (1985) investigated the caustic soda leaching process with five different zinc oxide ores and reported that smithsonite is completely leached but the process is unable to dissolve hemimorphite. The effect of variable parameters on refractory hemimorphite leaching was studied by Chen and co-workers (2009). The results indicated that leaching rates of approximately 73, 45, 11, and 5% could be achieved for zinc, aluminium, lead, and cadmium, respectively, while the iron leaching rate was less than 1% under leaching conditions of an ore particle size of 65–76 μm, sodium hydroxide concentration of 5 mol/l, solid-to-liquid ratio of 1:10, and reaction temperature of 85 °C for 2 h. It can be considered that a chemically controlled process was the controlling step of the process since the calculated activation energy was 45.7 kJ/mol (Chen et al., 2009).

A zinc recovery process from sphalerite in alkaline solution using a chemical conversion with lead carbonate ($PbCO_3$) was developed by Chenglong and co-workers (2008). Lead carbonate in alkaline solution was shown to be able to convert the sulfur content in sphalerite into galena, while the zinc was converted into sodium zincate ($Na_2Zn(OH)_4$). After that, the lead content of deposited galena in the leach residues could be recovered again as lead carbonate in the sodium carbonate solution (Na_2CO_3). It was found that over 90% of the zinc was extracted from zinc sulfide under a leaching condition of a sodium hydroxide concentration of 6 mol/L

with lead carbonate as an additive and a reaction temperature of 90 °C. Meanwhile, over 95% of the deposited galena in the leach residues was recovered into lead carbonate through leaching residues in a sodium carbonate solution with air bubbles at a temperature of 80 °C. In a separate work, they studied the effect of mechanochemical leaching (mechanical activation and leaching in one stage) of this mentioned process. They found that it was more effective compared with separate mechanical activation and subsequent chemical leaching (Chenglong et al., 2008).

2.4.5. Mechanical activation for treatment of zinc ores

Tkáčová and co-workers (1993) investigated the preferential leaching of a complex zinc sulfide concentrate using mechanical activation. They reported that the reaction of hydrogen peroxide with galena produces insoluble products separated from soluble sulfate. Moreover, the selective separation of zinc and copper sulfates in the solution can be carried out with a multi-step leaching process; this separation can be attributed to the differences in activity of sphalerite and chalcopyrite by mechanical activation. They found that the selective extraction of zinc increases with the reaction surface due to the grinding (Tkáčová et al., 1993). In another work, the effects of variable process parameters such as mechanical activation, leaching time, CaO dosage, liquid-to-solid ratio, reaction temperature, and NaOH concentration on leaching of a refractory zinc silicate in an alkaline medium including caustic soda and burnt lime were investigated (Zhao et al., 2009). Adding CaO leads to inhabitation of silica dissolution, while the zinc extraction rate remains stable. Furthermore, it was reported that preferential galena leaching is possible when the reaction temperature is kept stable at a lower temperature. Moreover, the addition of sulfuric acid to the leaching solution results in preferential sphalerite leaching from galena (Mandre and Sharma, 1993).

This process can be considered as a pre-treatment stage for the extraction of zinc by creating new surfaces and structural defects in the crystal lattices of minerals. In other words, the energy provided by milling results in some disorders in the mineral structure by fracturing the crystalline network. Mechanochemistry is a branch of this process in which mechanical activation is carried out with simultaneous leaching of ores. In other words, the energy supplied by milling resulted in structural disorders by distorting the crystalline network (Baláž, 2003; Baláž and Ebert, 1991). Tiechui and co-workers (2010) studied the mechanical activation effect on hemimorphite leaching in caustic soda and ammonium chlorate media. From the perspective of zinc recovery, increasing the milling time enhances the rate and yield of alkaline leaching of hemimorphite, and also the mechanochemical process showed improvement in zinc extraction compared to dry milling (Tiechui et al., 2010). A comparison between leaching behaviour of inactivated and mechanically activated sphalerites was

investigated by Chen and co-workers (2002). The results of thermogravimetry (TG) showed that leaching of mechanically activated sphalerite is significantly better than that of inactivated sphalerite (Chen et al., 2002).

2.4.6. Bacterial leaching

Recently, biological mineral processing for extraction of zinc has attracted much attention. The use of bacterial leaching for copper, uranium, and refractory gold using both heap and tank leaching processes has become widespread and has led to research to develop this process for zinc extraction (Giaveno et al., 2007; Shi et al., 2006; Nilsson et al., 1996; Da Silva, 2004). This process can be achieved by either bioleaching processes or integrated leaching processes. The integrated leaching processes include either a bioleaching step followed by the chemical step or bio-oxidation followed by bioleaching, which can be conducted simultaneously or in separate stages (Giaveno et al., 2007; Pistorio et al., 1995). A comparison between the bioleaching behaviour of three zinc sulfide ores, namely sphalerite, marmatite, and synthetic sphalerite, with *Acidithiobacillus ferrooxidans* and a moderately thermoacidophilic iron-oxidizing bacterium (MLY) was conducted by Shi and co-workers (2006). Their research findings confirm that marmatite has the highest dissolution rate amongst the minerals due to the difference in physicochemical properties. In other words, compared with synthetic zinc sulfide, the dissolution of zinc sulfides is facilitated by galvanic interaction with the iron portion which comes from pyrite in the concentrate.

Moreover, a greater iron content in the mineral structure of marmatite was released and oxidized to ferric ions by bacterial strains in the bioleaching process. This phenomenon resulted in an increase in the redox potential in the leach solution and accelerated the dissolution of marmatite. Researchers from Lulea˚ University of Technology, Sweden (Nilsson et al., 1996; Sandström and Petersson, 1997) have developed a bioleaching process for complex sulfide ores. The process uses extremely thermophilic archaea (*Sulfolobus acidocaldarius* type) instead of moderately thermophilic bacteria (*Thiobacillus caldus*). These bacteria can be used at higher temperatures (up to 65 °C) and higher pulp densities (15–20% wt.). However, discarding of the impurities is one of the biggest issues in this process (Nilsson et al., 1996; Sandström and Petersson, 1997).

From a kinetics perspective, several studies have been published (Da Silva, 2004). The mineral properties and concentration of ferric and ferrous ions can affect the reaction kinetics of zinc sulfides. Furthermore, in the case of insufficient bacterial oxidation of the sulfur layer, a diffusion controlled mechanism becomes essential, particularly in the marmatite leaching process (Chaudhury and Das, 1987). As mentioned before, researchers have reported an improvement of the leaching rate during the simultaneous leaching of metal oxides and metal

sulfides. Kai and co-workers (2000) investigated the influence of the presence of *Thiobacillus ferrooxidans* on the simultaneous leaching of zinc sulfide and manganese dioxide. They reported that in the leaching system containing ZnS and MgO, the dissolution rates were improved by the iron-oxidizing bacterium (*T. ferrooxidans*). The bacterial oxidation of zinc sulfide and elemental sulfur on the surface of the mineral can be considered as an effective parameter for this improvement. In addition, the sulfur removal might also enhance the galvanic reaction rate (Kai et al., 2000).

2.4.6.1. MIM bioleaching process

This process was developed for high-halogen bearing zinc concentrates (Steemson et al., 1994). This process is conducted at a pH of around 1.5 using a mixed bacterial population (i.e. *T. ferrooxidans*, *Leptospirillum ferrooxidans*, *Thiobacillus thiooxidans*, *Sulfobacillus* strains, *T. caldus*, *Acidiphilium cryptum, Acidiphilium organovorum*, and other heterotrophic microorganisms) in a stirred-tank reactor while the temperature remains stable at 40–45 °C and the residence time is 3 days and the total extraction of zinc was 96%. The reactor is aerated with 2% v/v recovered carbon dioxide gas from the following neutralization step during the bioleaching process. The inventors claimed that the process could tolerate a copper content of up to 5% in the solid feed without an extra copper extraction cycle (Steemson et al., 1997; Steemson et al., 1994).

2.4.6.2. Integrated processes included bioleaching

Bioleaching and chemical leaching as an integrated process in the zinc industry was investigated by De Souza and co-workers (2007). There were two bioleaching reactors in this proposed process; in the first one, Fe^{3+} was produced with a concentration above 20 g/l. This solution was used for oxidizing the sphalerite in the second bioleaching reactor. After that stage, the residue of the second bioreactor was fed to the chemical leaching stage. The effects of total iron and acidity on zinc extraction in the chemical leaching stage were investigated. It was reported that a cupric concentration of over 12 g/l had a slight effect on zinc extraction and increasing the acidity led to increases in the zinc extraction when the experiments were carried out with sulfuric acid with a concentration of up to 181 g/l (De Souza et al. 2007). Ghosh and co-workers (2004) examined alternative chemical processes for the second stage of the integrated process such as direct sulfuric acid leaching, oxidizing roasting followed by acid leaching, ammonia pressure leaching, and ferric chloride leaching. They reported that the addition of lignin sulfonate as a surfactant agent in the solution substantially increased the overall extraction. However, the acid concentration had a significant positive effect on the leaching process, while increasing the temperature did not have a significant effect on the extraction (Ghosh et al., 2004).

The IBES (or BRISA) process was developed based on two separate stages: firstly, oxidative leaching of sulfides with ferric ions, and secondly the regeneration of the ferric ions by bacterial oxidation of the ferrous ions. The purpose of the division of the process into two stages is to optimize each of them separately to boost the extraction efficiency. Figure 2.9 shows the high-level process flowsheet. In this process, the biooxidation stage is carried out with *T. ferrooxidans* bacteria in a flooded packed-bed reactor at a solution pH of 1.2 while the oxidation reaction temperature is maintained at 30 °C (Carranza and Iglesias, 1998; Romero et al., 1998; Palencia et al., 2002; Palencia et al., 1998). In a different research study, the effects of particle size, solution pH, pulp density, and temperature on zinc extraction by combined sequential biooxidation and acidic brine leaching from complex sulfide ores containing sphalerite, pyrite, and galena were reported. It was shown that the use of an acidic brine solution could dissolve over 98% of the lead from the residues after a leaching time of 90 min at 60 °C (Liao and Deng, 2004).

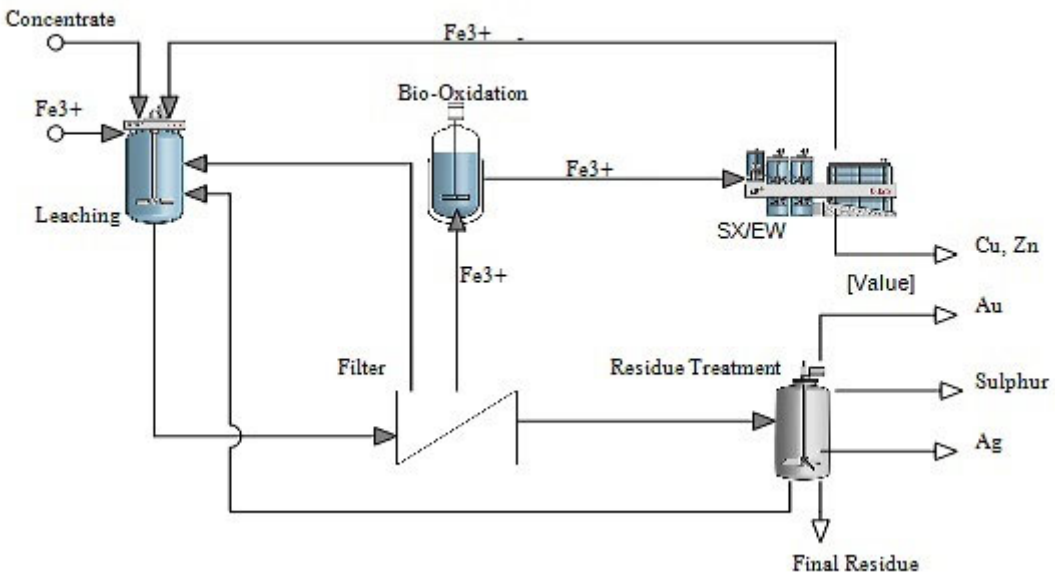

Figure 2. 9. Block diagram of the IBES process (Carranza and Iglesias, 1998).

2.4.6.3. GeoBiotic/GEOCOAT process

This technology is mainly used for the extraction of base metals from ores or concentrates in an engineered bio-heap leaching process. This process combines a heap leaching stage with stirred-tank reactors, which allows low capital and operating costs along with a high extraction rate. In this process, raw materials are coated onto a carrier rock which is barren or contains sulfide or oxide mineral values. After that, the coated materials are stacked on an impervious

pad for biooxidation (Harvey et al., 2002). Soleimani and co-workers (2011) coated a concentrate with a low-grade sphalerite ore. Zinc extraction rates of 97 and 78% were achieved from concentrate and low-grade support, respectively. Moreover, it was found that if leaching of the coated concentrate is not complete, leaching of the carrier will not proceed substantially (Soleimani et al., 2011).

2.4.6.4. HydroZinc process

This process was developed for the leaching of zinc from low-grade zinc sulfide ore by the Canadian zinc producer Teck Cominco, Ltd., Toronto, Ontario, Canada (formerly Cominco, Ltd.). The main advantages of this process are derived from the electrowinning of zinc from the manganese-free electrolyte. In this process, heap leaching can be conducted with a vast range of microorganisms such as mesophiles, thermophiles, or extreme thermophiles at average heap temperatures ranging from approximately 35 °C to just over 60 °C (Harlamovs et al., 2003). During leaching by the HydroZinc process, sufficient aeration from the heap bottom plays a vital role in the extraction of zinc (at least 5 l/m^2.min of heap surface). Furthermore, to prevent precipitation of iron in lower regions of the leaching heap, the process needs an adequately high sulfuric acid content in the solution (Petersen and Dixon, 2007). However, this process seems to be appropriate for volcanogenic massive sulfides and sedimentary exhalative deposits, whereas it is not suitable for carbonate replacement deposits.

2.4.7. Microwave-assisted leaching

The application of microwaves in hydrometallurgy processes has been studied by several researchers over the past two decades. Microwave irradiation causes selective heating and reduction of energy consumption. In most cases, the microwave causes microcracks and surface alteration along the sulfide mineral -gangue mineral grain boundary due to differential expansion rates. It can accelerate the metal extraction rate by reducing the overall reaction time (Xia and Picklesi, 2000; Al-Harahsheh and Kingman, 2004). Peng and Liu (1992) studied the influence of microwaves on the sphalerite leaching kinetics in a solution of 1.0 M $FeCl_3$ and 0.1 M HCl at 95 °C. The maximum extraction of zinc was about 52% under conventional leaching conditions, while that of reached 90% (Peng and Liu, 1997). However, it was shown that sphalerite is a poor absorber of microwave energy compared with the other sulfide minerals (Walkiewicz et al., 1988).

Regarding zinc silicate ores, decreasing the iron and silica dissolution and increasing the extraction of zinc are the most important concerns which should be addressed. A rapid leaching approach succeeded in reducing the silica dissolution, but iron dissolution increased, which is not preferred. In addition, microwave irradiation can facilitate the dehydration of

silica by dehydration of zinc sulfate hydrate, which can accelerate the silica filtration rate (Hua et al., 2002).

2.5. Recent developments

Table 6 presents a summary of existing technologies in the direct leaching of zinc from metal sulfide ores and concentrates. As can be seen from the table, the particle size of materials plays a vital role in direct leaching processes and a fine or ultrafine particle size can be considered. The other striking feature of this table is the time of reaction which almost exceeds the leaching time in a normal RLE process. Apart from the leaching approaches presented above, there are numerous recent investigations on the direct leaching of zinc which proposed new media such as the application of organic and amino acid reagents (e.g. glycine) (Hurşit et al., 2009; Ferella et al., 2010; Gilg et al., 2003; Eksteen and Oraby, 2016) or a new solution to one of the issues mentioned above, such as ultrasound-assisted leaching (Doche et al., 2003; Al-Merey et al., 2002). A vast number of these applications are in the early stages of investigation and require additional research before they can be applied for commercial purposes. One of these processes that can be considered to have a promising future in the zinc leaching industry is the use of glycine as a reagent in alkaline medium (Eksteen and Oraby, 2016). The reagent, when used in the alkaline pH range, offers some unique advantages such as being environmentally benign and having a high zinc glycinate stability constant, inherent recyclability, and a high selectivity over iron, magnesium, silica and alumina co-dissolution. Eksteen and Oraby (2016) initially applied this approach to the extraction of gold, silver, and copper (Eksteen and Oraby, 2014) and found that the leach and recovery approach can be extended to other chalcophile metals such as zinc, lead, nickel, cobalt, and so on.

Table 2. 6. Summary of existing technologies in the direct leaching of zinc from metal sulphide ores and concentrates.

Media	Process	Particle size (µm)	Leaching temperature (°C)	Pressure	Special Condition	S product	Leaching time,	Extraction	References
H2SO4	DPL	P80 10-50	150-210	11 bar of oxygen	- Fe^{3+} considered as the oxygen transfer agent - Needs surfactant	S^0	1-2hr	>99 %	1,2,3,4
	ADL	P50 10-46	70-80	Atm.	- In the presence of Iron couple Fe^{3+}/Fe^{2+} - Needs a special reactors - Copper ion as a catalyst	S^0	2-3hr	67-95 %	5, 6, 7,
	Modified Nitrosyl	P75 50	125-135	Atm.	Uses nitric acid	H2S	1hr	NA	8, 9
	Outokumpu Nonsulfidic		80		pH=3	S^0		98 %	10
	Ferric sulphate leaching	-	80-100	Atm.	Uses concentrate of Ferric sulphate	S^0	2-6hr	60-90 %	11,12, 13, 14
	MIM Albion	3-10	100	Atm.	- Uses Lignosol to avoid frothing - Uses ferric ion	S^0	10hr	>97 %	15, 16
	Dowa	-	-	Atm.	Grinding simultaneously Use ferric sulphate	S^0	1hr	>95 %	17, 9
HCl	Noranda zinc-oxide	-	85-100	100 kpa	Uses oxygen	S^0	7hr	78 %	18, 19
	Ferric chloride	-	The boiling point of leachant	Atm.	Uses $FeCl_3$ as the oxidant	S^0	6hr	99 %	20, 21, 22, 23, 24
	Oxidative leaching	P100 43	95	Atm.	Uses H_2O_2 as an oxidant	S^0	6hr	65 %	25, 26, 27
Perchloric	Perchloric acid	38-75	85	Atm.	Purging O_2		144hr	NA	28
Alkaline	Ammonia	53-45	130	5 atm	Cu^{2+} as an catalyst	SO42-	3hr	70 -90 %	29, 30, 31
	CENIM-LNETI	-	105	100kpa	Cu^{2+} as an catalyst	SO42	2hr	>95 %	32, 33
	Buka	<20	varies	Atm.	3 different stages	SO2	½hr	70-75 %	34
	Caustic soda	65-76	90	Atm.	Uses lead carbonate	PbS	2day	73 %	35
	Ammonia & ammonium chlorate	--	30	Atm.	Uses mechano chemical activation	SO42-	7day	85-90 %	36, 37, 38
Bioleaching	MIM bioleaching	16-18	40-45	Atm.	Uses a mixed bacterial population	consumed	72day	96 %	39, 40
	IBES	-	30	Atm.	Uses two integrate stages: one is oxidative leaching by Fe^{3+}, and two is bacterial oxidation of Fe^{2+}	consumed	90day	60-90 %	41, 42, 43, 44
	GeoCoat	<75	ambient	Atm.	Uses coated carrier rocks	consumed	100day	>99 %	45, 46
	HydroZinc	Top size 12.7	35-65	Atm.	Needs sufficient aeration from the heap bottom	consumed	240day	30-50 %	47, 48

References: 1 - Doyle et al., 1978; 2 - Jankola, 1995; 3 – Ozberk et al., 1995; 4 – Li et al., 2010; 5- Haakana et al, 2008; 6 - Saxén, 2008; 7 - Lahtinen et al, 2008; 8 - O'Brien and Peters, 1998; 9 - Filippou, 2004; 10 - Fugleberg and Jarvinen, 1996; 11 - Shibayama et al., 2001; 12 - Kuzminkh and Yakhontova, 1950; 13 - Souza et al., 2007; 14 - Santos et al., 2010; 15 – Hourn et al., 1999; 16 – Hourn et al., 1996; 17 - Kanno et al., 2002; 18 - Aleen et al. 2002; 19 - Weert and sandwijk 1999;20 - Santos et al., 2007; 21 - Dehghan et al., 2009; 22 - Lochmann and Pedĺik, 1995; 23 - Leclerc et al., 2003; 24 - Santos et al., 2010; 25 - Vazarlis, 1987; 26 - Santos et al., 2010; 27 - Aydogan, 2006; 28 - Weisener et al., 2003; 29 - Tromans, 2000; 30 - Ghosh et al., 2002; 31 - Ghosh et al., 2003; 32 – Limpo et al., 1992; 33 – Amer et al., 1995; 34 - Buckett et al., 1998; 35 - Chenglong et al., 2008; 36 - Tiechui et al., 2010; 37 - Baláž, 2003; 38 - Chen et al., 2002; 39 - Steemson et al., 1997; 40 - Steemson et al., 1994; 41 - Carranza and Iglesias, 1998; 42 - Romero et al., 1998; 43 - Palencia et al., 2002; 44 - Palencia et al., 1998; 45 - Harvey et al., 2002; 46 - Soleimani et al., 2011; 47 - Harlamovs et al., 2003; 48 - Petersen and Dixon, 2007

2.6. Alkaline glycine process

Glycine is the simplest amino acid and is produced cheaply in bulk on an industrial scale. Glycine has been used as a complexing agent in the electrodeposition of a wide range of alloys such as Zn–Ni and Zn–Co–Cu alloys (Rodriguez-Torres et al., 2000; Mohamed et al., 2012). Because of its complexing ability, glycine can enhance the solubility of a vast range of metal ions in aqueous solutions (Tanda, 2017). The complexing behaviour of glycine is similar to that of other kinds of complexing agents such as ammonia, cyanide, and ethylenediamine (Aksu and Doyle, 2001).

It is hypothesized that glycine, like the other complexing agents, may be able to accelerate the dissolution of zinc, even in the absence of strong oxidizing agents. Compared with other industrial zinc lixiviants, glycine has several advantages such as being environmentally safe, non-toxic, stable, enzymatically destructible, and readily metabolized in most living organisms (Oraby and Eksteen, 2014). The particular attributes of glycine compared to the other lixiviants make glycine a logical target lixiviant (Oraby and Ekstee, 2015b). A few articles have been published on the electrochemical behaviour of zinc in glycinate electrolytes or the electrochemical behaviour of sphalerite in acidic media (Ballesteros et al., 2011; Srinivasan and Venkatakrishna Iyer, 2000; Ahlberg and Ásbjörnsson, 1994; Nava et al., 2004). However, there are no published studies regarding anodic oxidation of sphalerite in alkaline glycine media.

2.4. Summary

SECTION 2 has revealed that the current direct leaching processes for sphalerite are inefficient or have some environmental impacts and the need for further research on ways to effectively extract zinc from different resources in a benign manner is necessitated. Attributes of different lixiviants have also been investigated. Stability of glycine (as the simplest amino acid) over a wide range of pH has shown great capabilities for the selective leaching of zinc and other metals. With a continuous decline in zinc ore grades, different hydrometallurgical processes such as dump, heap and vat leaching applicable to such ores have been explored and may see increasing use in the future.

CHAPTER 3: MATERIALS AND METHODS

A wide range of materials and methods have been used in this thesis. Therefore, this chapter aim to describe the materials, preparations, procedures, and analytical techniques that were applied in this study. Furthermore, this Chapter describes the fundamentals of different techniques used to collect the needed data in the subsequent Chapters.

3.1. Chapter objective

This chapter attempts to cover the materials, chemical and processes used in this thesis. In this Chapter, all techniques that used in this research study has been investigated and introduced from a hydrometallurgical point of view.

3.2. Materials and chemicals

All chemicals and reagents used in this research study were of analytical grade. All solutions were prepared using deionized water. Table 3.1 shows the list of chemicals and materials used in all of the experiments described in the thesis.

Table 3. 1. List of chemicals and reagents used in this study.

Reagent	Chemical Formula	Application	Purity
Glycine	H_2NCH_2COOH	Main reagent	Analytical grade (AR)
Sodium Hydroxide	NaOH	pH modifier	AR
Lime	$Ca(OH)_2$	pH modifier	AR
Hydrogen peroxide	H_2O_2	Oxidising agent	AR
Graphite	C	Sample preparation	AR
Paraffin	C_nH_{2n+2}	Sample preparation	AR
Sodium chloride	NaCl	Additive agent	AR
Potassium permanganate	$KMnO_4$	Oxidising agent	AR
Lead nitrate	$Pb(NO_3)_2$	Additive agent	AR
Oxygen	O_2	Oxidising agent	Industrial grade
Air		Oxidising agent	Atmospheric
Nitrogen	N_2	Neutralising agent	Industrial grade
Copper sulphate	$CuSO_4$	Additive agent	AR

3.3. Minerals and ore samples

In this thesis, synthetic silver sulfide (from Sigma-Aldrich) has been used for the electrochemical investigation of acanthite. A galena sample from Borieva mine, Madan area field in Bulgaria, Russia was used for the electrochemical investigations. The chemical analysis of the sample is given in Table 3.2. Since sphalerite naturally includes significant concentrations of cationic impurities, with iron being the most common substituent (marmatite is observed when iron is present at a level of 10% or more), instead of using

synthetic sphalerite, high-purity natural sphalerite was used for the electrochemical study of sphalerite. A sphalerite sample with 6.2% Fe from Dalnegorsk in Russia was used in this research. A chemical analysis of the sphalerite sample is given in Table 3.2. Furthermore, Table 3.2 shows an elemental analysis of sphalerite concentrate and zinc oxide residue used in this study.

Table 3. 2. Elemental analysis of different mineral and ore specimens sources used in this study.

Elements (wt.%)	Zn	S	Fe	Pb	Cu	Ag*	Application
Sphalerite Mineral	52.2	33.6	6.2	0.02	0.028	50.1	Electrochemistry
Sphalerite Conc.	56.1	30.9	4.03	2.16	.387	40.6	Leaching
Zinc oxide	11.02	>10.0	1.39	0.586	.2	17.8	Optimisation
Galena mineral	4.09	14.7	0.22	80.9	0.029	ND	Electrochemistry

***In ppm**

3.4. Procedure

3.4.1. Electrochemical experiments

3.4.1.1. Carbon Paste Electrode (CPE)

There are several reasons of choosing a CPE as a working electrode in the electrochemical experiments of this research, including the following (Ahlberg and Ásbjörnsson, 1994; Kiss et al., 1991):

- It has been established that the electrochemical behaviour of the CPE can represent the conditions under which real leaching processes are conducted.
- The carbon paste does not influence the electrochemical nature of sulfide minerals.
- Due to the poor conductivity of sphalerite, it is not possible to use pure sphalerite as a working electrode.
- One of the most critical issues in electrochemical studies is reproducibility, which can be addressed by the use of a CPE.

For these reasons, as well as having both good selectivity and sensitivity without the need for particular pre-treatment steps before experiments, voltammetric techniques using a CPE have been found to be appropriate (Almeida and Giannetti, 2002).

The (mineral)-carbon paste working electrode was prepared by thoroughly hand-mixing a 40: 30: 30 wt% ratio of graphite: specific specimen (e.g. sphalerite, galena, and acanthite): paraffin oil. To achieve this, 4 g of graphite powder (Sigma-Aldrich, mean diameter < 20 μm, 100% C), 3 g of high-purity mineral, and 3.53 mL of paraffin oil (Merck, density of 0.85 g/mL at 20 °C) were combined using a mortar and pestle until a uniformly wetted paste was obtained (Shi et al., 2006). The paste was pressed into the electrode cavity until the surface was flush with the edges. The excess paste was trimmed with a small spatula and then smoothed with a filter paper to produce a reproducible working surface.

3.4.1.2. Dissolution setup

A rotator (AFMSRCE), and a potentiostat (AFTP), both from Pine Instruments, a five-compartment glass cell, a platinum wire counter electrode, and an Ag/AgCl reference electrode in 3 mol/L KCl were used for the electrochemical cell setup. Solutions were prepared by dissolving the required mass of glycine in distilled water, and the pH was adjusted with sodium hydroxide. Before the commencement of each experiment, the solutions were thoroughly deoxygenated by purging with high-purity nitrogen for 30 min. The pH measurement was carried out with a TPS WP-90 field meter. The sphalerite sample was investigated by the cyclic voltammetry (CV) technique in the potential range from –1 to 1 V (Ag/AgCl) in alkaline glycine media.

3.4.2. Leaching tests

3.4.2.1. Rotating disc dissolution tests

Preparing the rotating disc

For acanthite, a synthetic silver sulfide powder (P80 = 16 μm) was pressed under a pressure of 15 MPa with a protective manual powder press (Protech Technology, China) to form a 5-mm-thick disc with a diameter of 12 mm. No sintering process was applied to avoid the decomposition of the sample. The disc had a density of 7.2 g/mL, which was about 99% of the theoretical value of argentite density (7.3 g/mL). The disc was coated with epoxy resin, and one flat surface was left exposed. The surface was polished and rinsed with deionized water and ethanol to remove any grease and scrape on the surface (Xie and Dreisinger, 2007).

A sphalerite sample with 6.2% Fe with P80 = 60 μm from Dalnegorsk in Russia was used for the rotating disc leaching tests of sphalerite. The sphalerite sample was pressed under a pressure of 15 MPa with a protective manual powder press (Protech Technology, China) to form a 5-mm-thick disc with a diameter of 12 mm. No sintering process was applied to avoid the decomposition of the sample. The disc was coated with epoxy resin, and one flat surface

was left exposed. The surface was polished and rinsed with deionized water and ethanol to remove any grease and scrape on the surface (Xie and Dreisinger, 2007).

Leaching setup

For the leaching study, rotating disc experiments were carried out in a 0.5-L stirred water jacketed reactor to maintain the desired leaching temperature and a reflux condenser to avoid any solution losses. Before the commencement of each experiment, the solutions were thoroughly deoxygenated by purging high-purity nitrogen for 30 min. The pH of the glycine solutions was modified by NaOH, and the mixture was stirred at 500 rpm. Dissolved oxygen (DO), pH, and Eh were recorded by pH meter (TPS, 90 series) during the experiments. Sub-samples were drawn at regular interval times (10, 20, 30, and 40 min) and freshly analysed for silver by atomic absorption spectrometry (AAS, Agilent 55 AA atomic absorption spectrometer). After sampling, a fresh solution was added in an amount equivalent to the sampled solution to keep the solution volume constant. The leaching time was chosen to the maximum metal extractions to (1) prevent the formation of cracks on the disc surface; (2) maintain the reaction under steady-state conditions; and (3) minimize the change in the leach pH (Xie and Dreisinger, 2009; Deutsch and Dreisinger, 2013a). Furthermore, during the experiments, the sparging tube of nitrogen was maintained 5 mm above the surface of the solution with 0.15 lpm flow rate. Afterwards, the leach residue was analysed by fire assay. A schematic of this setup is shown in Figure 3.1.

3.4.2.2. Agitated reactor experiments

All the leaching experiments were carried out in a 0.5-L stirred tank reactor with a water jacket to maintain the desired temperature and a reflux condenser to avoid any solution losses. Before the commencement of each experiment, the pH of the glycine solutions was modified by NaOH, and the mixture was stirred at 500 rpm. DO, pH, and Eh were recorded by pH meter (TPS, 90 series) during the experiments. Subsamples were drawn at regular intervals and freshly analysed for zinc, silver, and lead by AAS (Agilent, 55 AA atomic absorption spectrometer). After sampling, a fresh solution was added in an amount equivalent to the sampled solution to keep the solution volume constant. The optimum leaching time was chosen to prevent the formation of cracks on the surface of the disc, to maintain the reaction under quasi steady-state conditions, and to minimize changes in the pH of the solution. If the leach time became too long changes in the solution chemistry will become noticeable and influence the outcome (Xie and Dreisinger, 2009; Deutsch and Dreisinger, 2013a).

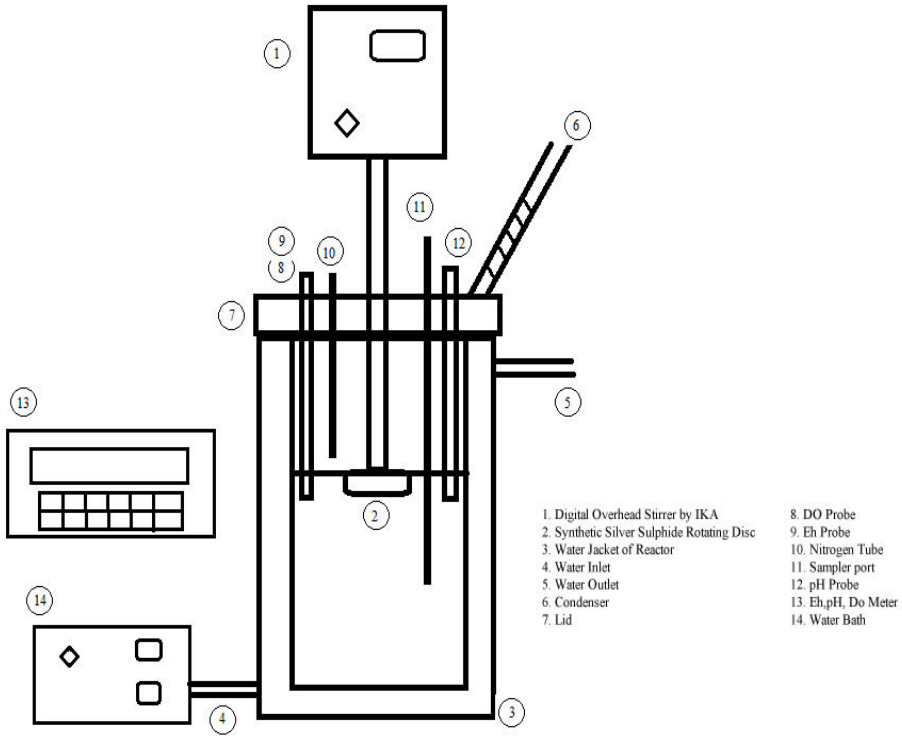

Figure 3. 1. Schematic set up the rotating disc experiments.

3.5. Modelling and design of experiments

Three designs of experiments were used to screen the parameters and to develop a numerical model to obtain the optimum condition for the leaching process. Duplication of the centre points was used to determine the experimental error (Mirazimi et al., 2015). The experiments were carried out in a random order to minimize the effect of systematic errors. Tables 3.3 - 3.6 summarize the different parameters and designs used in this study.

As can be seen from Tables 3.3 and 3.4, Taguchi design was chosen for screening the additives and for the bottle roll experiments. As shown in Table 3.3, the independent variables A, B, C, D, E, F, and G represent the glycine concentration, pH modifier, lead nitrate, sodium chloride, potassium permanganate, hydrogen peroxide, and pH of the solution, respectively. In Table 3.4, A, B, and C represent the pH, glycine to total metals (Zn, Ag, and Pb) molar ratio, and cupric ion concentration.

For modelling and optimization, RSM by I-Optimal experimental design was used. The I-Optimal algorithm chooses runs that minimize the integral of the prediction variance across the factor space. To determine the effects of the independent variables on the zinc and silver glycine leaching processes, I-Optimal designs consisting of 25 and 24 runs were carried out, respectively (Tables 3.5 and 3.6).

Table 3. 3. Summary design, Experimental range of the factors for rotating disc experiments.

Build Information					
Study Type	Factorial				
Design Type	Taguchi (L8)				
Design Model	Main effects				
Runs	8				
Factors					
Factor	Name	Unit	Levels	Minimum	Maximum
A	Glycine	mole	2	3	4
B	Modifier		2	NaOH	Ca(OH)2
C	$Pb(NO_3)_2$	g/t	2	0	200
D	NaCl	g/l	2	0	300
E	$KMnO_4$	g/l	2	0	2
F	H_2O_2	mole	2	0	0.04
G	pH		2	9	10.5

Table 3. 4. Summary design, Experimental range of the factors for Bottle role tests.

Build Information						
Study Type	Factorial					
Design Type	Taguchi (L9)					
Design Model	Main effects					
Runs	9					
Factor	Name	Unit	Levels	Level A	Level B	Level C
A	pH		3	9	10	11
B	Gly/Total Metal	mole	3	3	7	15
C	NaCl	mole	3	0	0.5	1
D	Cu++	ppm	3	0	10	20

Table 3. 5. Summary design, Experimental range of the factors for sphalerite leaching experiments.

Build Information						
Study Type	Response Surface					
Design Type	I-Optimal					
Design Model	Quadratic					
Runs	24					
Factor	Name	Unit	Type	Minimum	Maximum	Level C
A	pH		Numeric	9	11	11
B	Gly/Total Metal	g	Numeric	1.97	5.25	15
C	Cu++	g	Numeric	0.039	0.393	1

Table 3. 6. Summary design, Experimental range of the factors for silver sulphide Rotating disc experiments.

Build Information					
Study Type	Response Surface				
Design Type	I-Optimal				
Design Model	Quadratic				
Runs	25				
Factor	Name	Unit	Type	Minimum	Maximum
A	Glycine	mole	Numeric	0	2
B	NaCl	mole	2	0	3
C	pH		2	9	11.5

The I-Optimal criteria are recommended to build response surface designs where the goal is to optimize the factor settings, requiring greater precision in the estimated model (Myers and Montgomery, 1995). This method can be more useful than conventional response surface methods such as the central composite design method since it demands fewer experiments and can also tackle categorical factors included in the design of experiments (Azriel, 2014; Coetzer and Haines, 2017). Design-Expert 10 software (State-Ease Inc., Minneapolis, MN, USA) was used for the analysis of variance (ANOVA) and regression and graphical analyses.

The quadratic model of the optimization process has been used to explain the relationship between the given factors, as indicated in Equation (3.1).

$$y = \beta_0 + \Sigma\beta_i x_i + \Sigma\beta_{ii} x_i^2 + \Sigma\Sigma\beta_{ij} x_i x_j \quad (3.1)$$

where β_0, βi, βii, and β_{ij} are the constant, linear, square, and interaction regression coefficients, respectively, and x_i and x_j indicate the independent variables. By using Equation (3.1), the zinc sulfide alkaline glycine leaching process was modulated and evaluated. After that, the magnitude of the interaction between the independent variables and the response was obtained via the ANOVA. The correlation of fit for the polynomial model was expressed using the values from the normal regression (R^2) and the adjusted regression (R^2_{adj}) coefficients.

3.6. Kinetics modelling

The SCM for spherical particle shape was used for the dissolution reactions of the sphalerite and other metals during the alkaline glycine process. The SCM is based of following assumptions:

- The shape of particle is spherical and its diameter remains constant
- Constant concentration of solid reactant in the unreacted core
- the effective diffusivity of components is constant

The SCM for particles of unchanging size consists of the following steps (Nazemi et al., 2011):

Step 1: Diffusion of the leachant through the liquid film surrounding the particle.

Step 2: Diffusion of the leachant through the product layer at the surface of the unreacted core.

Step 3: Chemical reaction of the leachant at the surface of the core.

Normally, one of the steps mentioned above is significantly slower than the others. Hence, the leaching rate can be characterised by this controlling step (Levenspiel, 1999). In the conventional method, the contolling step will be chosen by the testing the formula of each step against experimental data to find the best fitting results. The disadvantage of determining the leaching rate through this method is that checking all formulas separately (Espiari et al., 2006; Mulak et al., 2005; Momade and Momade, 1999; Souza et al., 2007). Furthermore, this method is unable to determining cases where more than one of the steps mentioned above are involved in the overall rate equation or when the correlation coefficients for the diagrams are too close to distinguish the prevalent mechanism. To address such issues, all three steps can be combined together to determine the leaching kinetics by the SCM. In this method, the simultaneous actions of these three steps, which act in series, are taken into acount as follows (Levenspiel, 1999):

$$t = \tau_F X + \tau_P\left(1 - 3\left(1 - X\right)^{\frac{2}{3}} + 2(1 - X)\right) + \tau_R(1 - (1 - X)^{\frac{1}{3}}) \qquad (3.2)$$

The contributon of each of the steps mentioned above in the leaching kinetics can be identified by fitting the experimental data to Equation (3.2) and evaluating the constants of this equation, τ_F, τ_P, and τ_R. To prevent negative values for constantsovercome, it is proposed to perform a constrained least squares technique to determine the constants of Equation (3.2). This technique can be formulated as:

$$\varphi = \sum_i [\tau_F X_i + \tau_P(1 - 3(1 - X_i)^{\frac{2}{3}} + 2(1 - X_i)) + \tau_R(1 - (1 - X_i)^{\frac{1}{3}}) - t_i]^2 \quad (3.3)$$

$$\text{Min } \varphi \qquad (3.4)$$

Subject to τ_F, τ_P and τ_R>0 (Nazemi, et al., 2011).

Equation (3.4) is an optimization problem that can be solved by any optimization technique by which τ_F, τ_P, and τ_R can be evaluated. Furthermore, the leaching process with fine particles may result in two stages with different slopes, which can be described as changing in the kinetics model. Therefore, Equation (3.3) cannot be directly applied to the data in the second

stage since the boundary condition for this stage (zero recovery at t = 0) is different from that of Equation (3.3). Moreover, the metal recovery at the beginning of the second leaching stage (t_1) is not zero ($X_1 \neq 0$). In such a case, the following generalized formula should be used instead (Aarabi-Karsagani et al., 2010):

$$t - t_1 = \tau_F(X - X_1) + \tau_P(1 - 3(\frac{1-X}{1-X_1})^{\frac{2}{3}} + 2(1 - (1 - X_1)^{\frac{1}{3}} + 2\Bigg(1 - \Bigg(1 - X_1)^{\frac{1}{3}}(X - X_1)\Bigg)\Bigg) + \tau_R(1 - (\frac{1-X}{1-X_1})^{\frac{1}{3}}) \quad (3.5)$$

In this study, the RSM was used to determine the operating conditions for maximizing the dissolution of zinc, lead, silver, and copper in the alkaline glycine process. Based on the methods described above, the SCM and improved SCM equations were listed in Table (3.7).

Table 3. 7. The shrinking core model equations used in the kinetics modelling.

Controlling Regimes in the SCM	Single Stage	Improved for the Second Stage
Liquid Film Diffusion control	$\frac{t}{\tau_F} = 1 - (1 - X)^{2/3}$ $\tau_F = \frac{\rho R_0^2}{2bD_C}$	$\frac{t - t_1}{\tau_F} = 1 - (\frac{1 - X}{1 - X_1})^{2/3}$ $\tau_F = \frac{\rho R_0^2 (1 - X_1)^{2/3}}{2bD_C}$
Reaction control	$\frac{t}{\tau_R} = 1 - (1 - X)^{1/3}$ $\tau_R = \frac{\rho R_0}{bk_a c}$	$\frac{t - t_1}{\tau_R} = 1 - (\frac{1 - X}{1 - X_1})^{1/3}$ $\tau_R = \frac{\rho R_0 (1 - X_1)^{1/3}}{bk_a c}$
Solid Product diffusion control	$\frac{t}{\tau_P} = 1 - 3(1 - X)^{\frac{2}{3}} + 2(1 - X)$ $\tau_P = \frac{\rho R_0^2}{6bD_C}$	$\frac{t - t_1}{\tau_P} = 1 - 3(\frac{1 - X}{1 - X_1})^{\frac{2}{3}} + 2(1 - (1 - X_1)^{\frac{1}{3}}(X - X_1))$ $\tau_P = \frac{\rho R_0^2 (1 - X_1)^{2/3}}{6bD_C}$

3.7. Software

In order to achieve the targets, different software packages were used in this study, including:

- Chemical equilibrium software Hydra and Medusa, Inorganic Chemistry Department, Royal Institute of Technology, Stockholm, Sweden, www.inorg.kth.se/medusa.
- MATLAB, The MathWorks, Inc., www.mathworks.com
- HSC Chemistry, version 8, Outotec, www.outotec.com
- Design Expert, version 10, www.statease.com

CHAPTER 4: THERMODYNAMICS OF ZINC, LEAD AND SILVER GLYCIATE

The chapter covers the fundamental study of zinc, silver, and lead sulfides dissolution in alkaline glycine media from a thermodynamic viewpoint.

4.1. Chapter objective

This chapter describes the thermodynamic data collected or predicted by HSC Chemistry software to produce Eh–pH diagrams. This thermodynamic information either collected from resources or predicted by HSC Chemistry software was used for the distribution species diagrams and the potential–pH diagrams for new leaching systems including:

- Zinc-glycine-sulfur-water
- Silver-glycine-sulfur-water
- Lead-glycine-sulfur-water

This chapter involves the study of thermodynamics regarding to find the stability of zinc, silver, and lead in this novel alkaline glycine system followed by determing the quantities of required glycine for the reactions.

4.2. Thermodynamic analysis

4.2.1. Zinc sulfide-glycine system

Ortiz-Aparicio and co-workers (2007) have drawn a Pourbaix diagram for the system of Zn-glycine assuming that no mixed hydroxyl-glycine-metal complexes are present. However, the mixed glycine-metal complexes along with zinc-sulfide species play a vital role in the leaching system to find both the stability of the compounds in the working conditions and the quantities of the required glycine. Thus, to describe the complexes formed, in the current study, expanded Pourbaix diagrams for the Zn-S-glycine-water system were derived from the thermodynamic data based on the method described in the literature using Van't Hoff and Nernst equations (Ballesteros, 2010; Vernik, 2011; Thompson et al., 2011; Rojas-Hernández et al., 1993).

Depending on the pH value, glycine can exist in aqueous solutions in three different forms, namely $^{+}H_3NCH_2COOH$ (glycinium cation), $^{+}H_3NCH_2COO^{-}$ (glycine zwitterion), and $H_2NCH_2COO^{-}$ (glycinate anion). These species are denoted as H_2Gly^{+}, HGly, and Gly^{-}, respectively. The equilibria between these may be depicted as (Miceli and Stuehr, 1972):

$$^{+}H_3NCH_2COOH \overset{k_{a1}}{\Longleftrightarrow} {}^{+}H_3NCH_2COO^{-} \overset{k_{a2}}{\Longleftrightarrow} H_2NCH_2COO^{-} \quad (4.1)$$

which are characterized by the equilibrium constants (Ballesteros et al., 2011):

$$k_{a1} = \frac{[HGly][H^+]}{[H_2Gly^+]} \quad (4.2)$$

$$k_{a2} = \frac{[Gly^-][H^+]}{[HGly]} \quad (4.3)$$

The pK values of glycine are: pK_{a1} = 2.35 and pK_{a2} = 9.97 at 25 °C.

The formation of zinc–glycinate complexes, including $Zn(Gly)^{+}$, $Zn(Gly)_2$, and $Zn(Gly)_3^{-}$, strongly depends on the concentrations of zinc and glycine as well as the solution pH. Moreover, to achieve significant concentrations of higher zinc–glycine complexes, increasing the total glycine concentration and the pH is essential. The concentration of the complexes, therefore, is related to the Zn^{2+} concentration as shown in the following reaction (Ballesteros et al., 2011):

$$Zn^{2+} + iGly^{-} \leftrightarrow ZnGly_i^{(2-i)} \quad (4.4)$$

The thermodynamic information for the formation of species in the Zn-S-glycine-water system has been collected from different resources (Aksu and Doyle, 2001; Ballesteros et al., 2011; Miceli and Stuehr, 1972; Kiss et al., 1991). By considering all thermodynamically meaningful reactions between the species in the Zn-S-glycine-water system and using the collected thermodynamic information, each equilibrium line on the Pourbaix diagram of the studied system has been plotted to support the interpretation of the observations from the leach and electrochemical studies.

4.2.2. Silver and lead sulfides systems

The thermodynamic data for the formation of species in the (Pb/Ag)-S-glycine-water systems has been collected from the resources (Kiss et al., 1991). Considering all thermodynamically meaningful reactions between the species in the (Pb/Ag)-S-glycine-water system and using the collected data, each equilibrium line on the Eh–pH diagram of the studied system has been plotted via HSC Chemistry 10 software.

4.3. Pourbaix Diagrams

4.3.1. Zinc-glycine-sulfur-water system

Figure 4.1 illustrates the potential–pH diagram of the Zn-S-glycine-H_2O system at ambient temperature in 10^{-6} M of zinc concentrate and 0.1 M of glycine. As can be seen from the data shown in Figure 1, to maximize the zinc-glycine complexibility in the alkaline media, a high concentration of glycine is needed. This result confirms the research findings of Miceli and Stuehr (1972). Under the studied conditions, the predominant zinc-glycine species was found to be $ZnGly_3^{-}$. Figure 4.2 illustrates the distribution of zinc-glycine species in the current study. As shown in Figure 4.2, from pH 8 to 12, the predominant zinc species is the $ZnGly_3^{-}$ complex. In this region, the main impurity (Fe) remains uncomplexed. These results led to the selection of pH 10 as the working pH, unless specified, for the whole set of experiments.

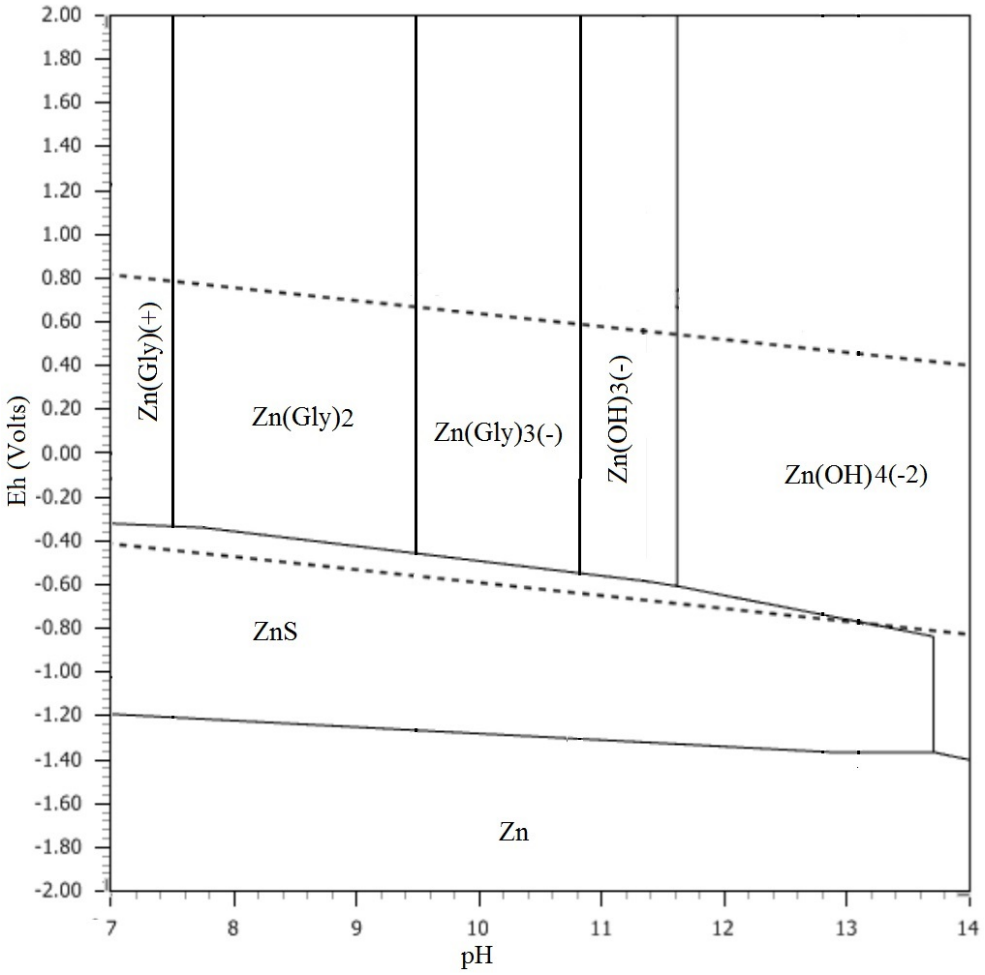

Figure 4. 1. Eh-pH diagrams for Zn-S-Gly-H2O systems at ambient temperature in 10-6 M of zinc concentrates and 0.1 M of glycine.

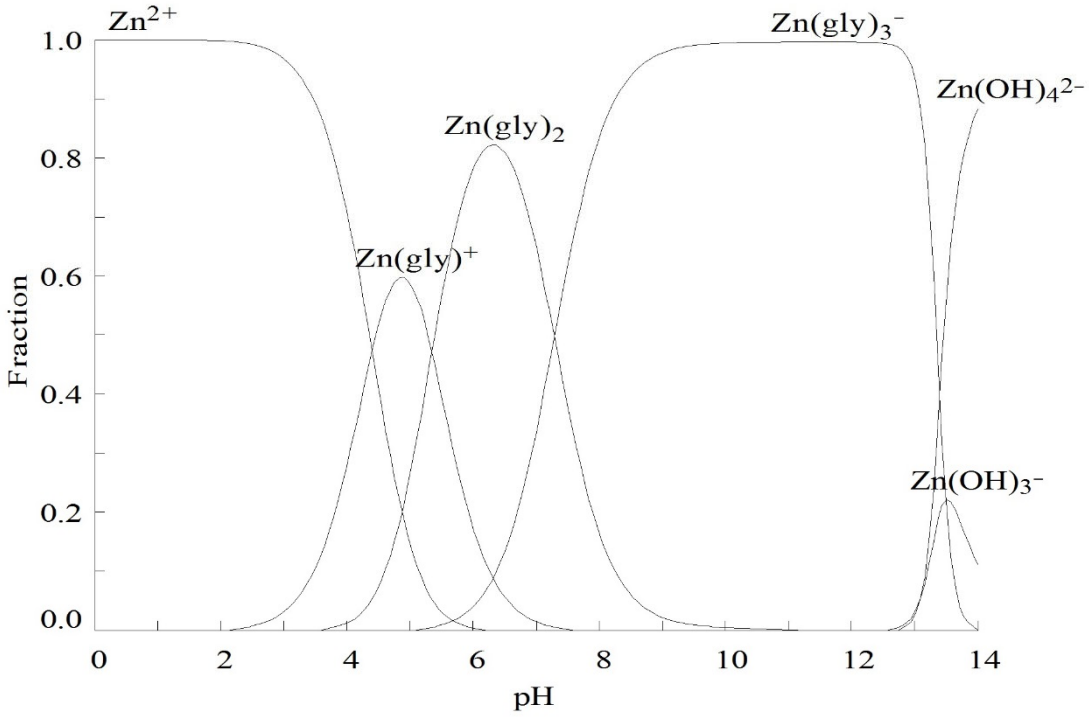

Figure 4. 2. Distribution zinc species diagrams for zinc-glycine complexes at Eh=0.5, temperature 25°C, zinc concentration of 10-6 M, and glycine concentration of 0.1 M.

4.3.2. Silver-glycine-sulfur-water system

Figure 4.3 illustrates the potential–pH diagrams for the Ag-S-glycine-H_2O system at glycine and silver concentrations of 1 M and 10^{-6} M respectively. As can be seen from Figure 4.3, the most significant area of stability of $Ag(Gly)_2^-$ complex is located from pH 7 to 13 and the second species of $Ag(HGly)^+$ complex is located in the pH range between 3 and 6. It was shown that Ag(Gly) complex has a narrow area of stability at pH 6.5. This diagram illustrates that the maximum silver-glycine complexibility occurs under alkaline conditions. Therefore, under the studied conditions, the predominant silver-glycine species was found to be $Ag(Gly)_2^-$. Figure 4.4 illustrates the fraction of silver-glycine species in the current study. As shown in Figure 4.4, from pH 9 to 11, the predominant zinc species is the $AgGly_2^-$ complex. In this region, the main impurities, such as iron, remain uncomplexed. These results led to the

selection of pH 10 as the working pH, unless specified, for the whole series of experiments

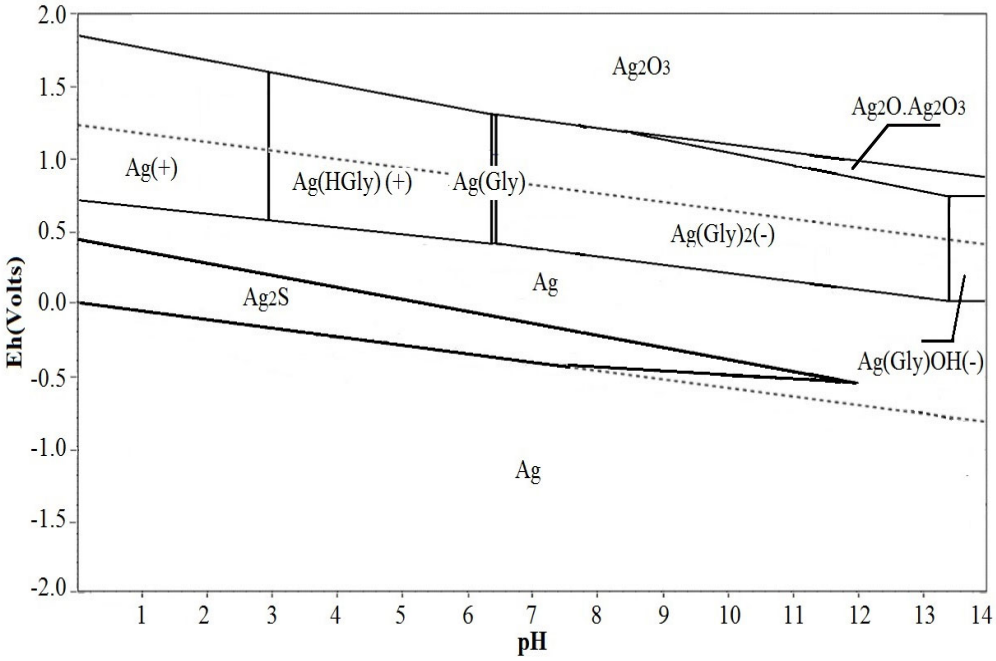

Figure 4. 3. The Pourbaix diagram of Ag-S-Glycine-H2O systems with 10-6M Ag and 1M glycine at 25◦C.

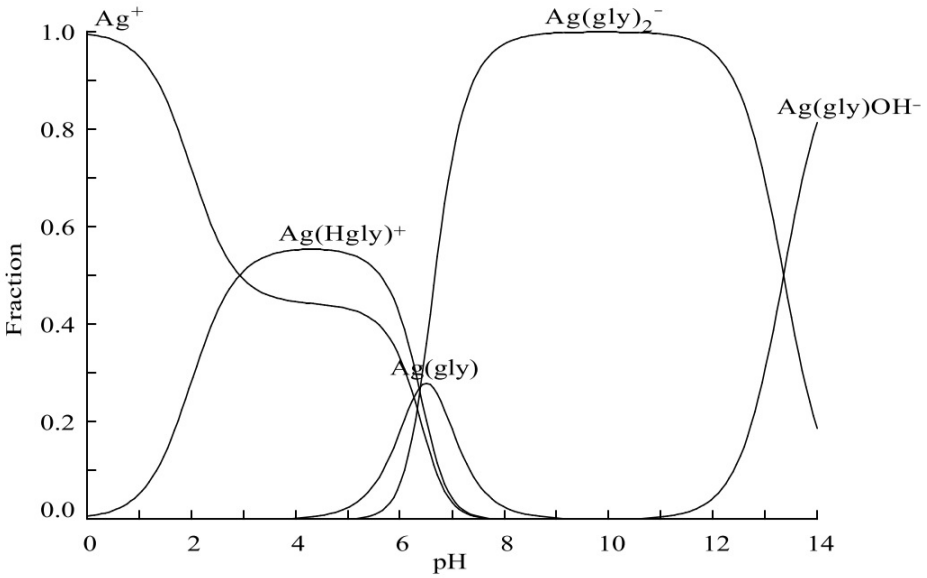

Figure 4. 4. The fractions of silver-glycine species with 10-6M Ag and 1M glycine at 25◦C.

4.3.3. Lead-glycine-sulfur-water system

Figure 4.5 describes the potential–pH diagrams for the Pb-S-glycine-H_2O system at 25 ºC when the concentration of glycine is 1 M and the lead concentration is 10^{-6} M in the solution. As can be seen from Figure 4.5, the most significant area of stability belongs to $Pb(Gly)_2$ complex (from pH 7 to just over pH 11), followed by $Pb(HGly)_2^{2+}$ complex and $Pb(HGly)(Gly)^{+}$, respectively. According to Figure 4, unlike the silver-glycine complexes, the lead-glycinate complexes are found under a wide range of pH values from acidic (about pH 2) to alkaline (pH 11). Figure 4.5 depicts the fractions of lead-glycine species under the mentioned condition. In Figure 4.6, compared with Figure 4.4, there are multi-species at each pH, and the final solution will contain more than one kind of lead-glycine species. Therefore, to remove the impurities such as iron from the final solution and to compare the electrochemical behaviours of lead and silver, pH 10 has been selected as the working pH for the electrochemical study of the dissolution of lead sulfide in alkaline glycine media. At the selected pH, it has been considered that all of the produced lead-glycine species is $Pb(Gly)_2$ complex without any partial formation of Pb(Gly)OH complex.

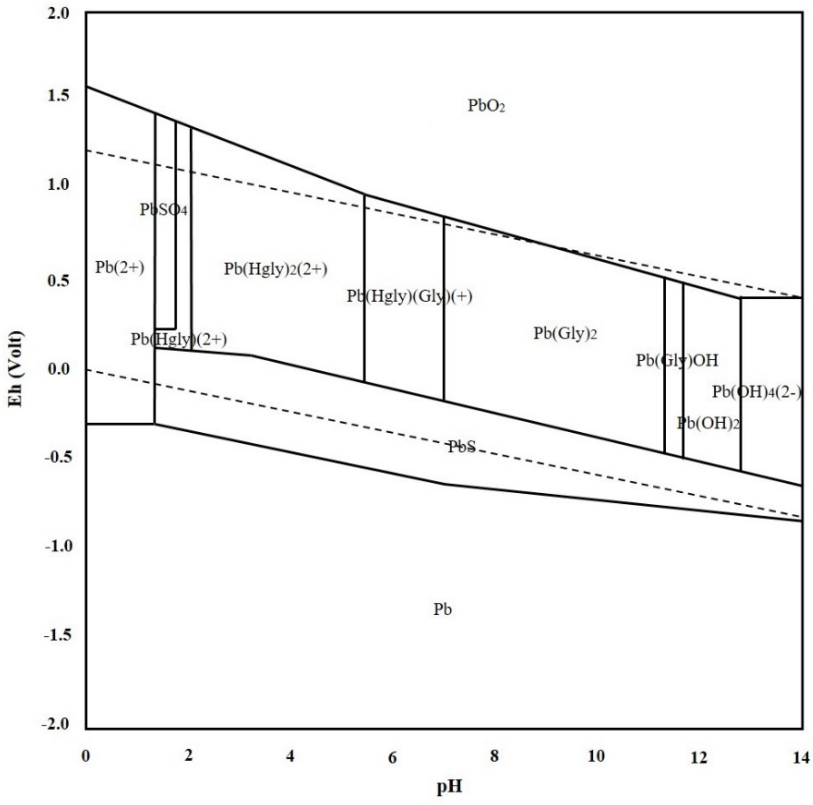

Figure 4. 5. The Pourbaix diagram of Pb-S-Glycine-H2O systems with 10-6M Pb and 1M glycine at 25◦C.

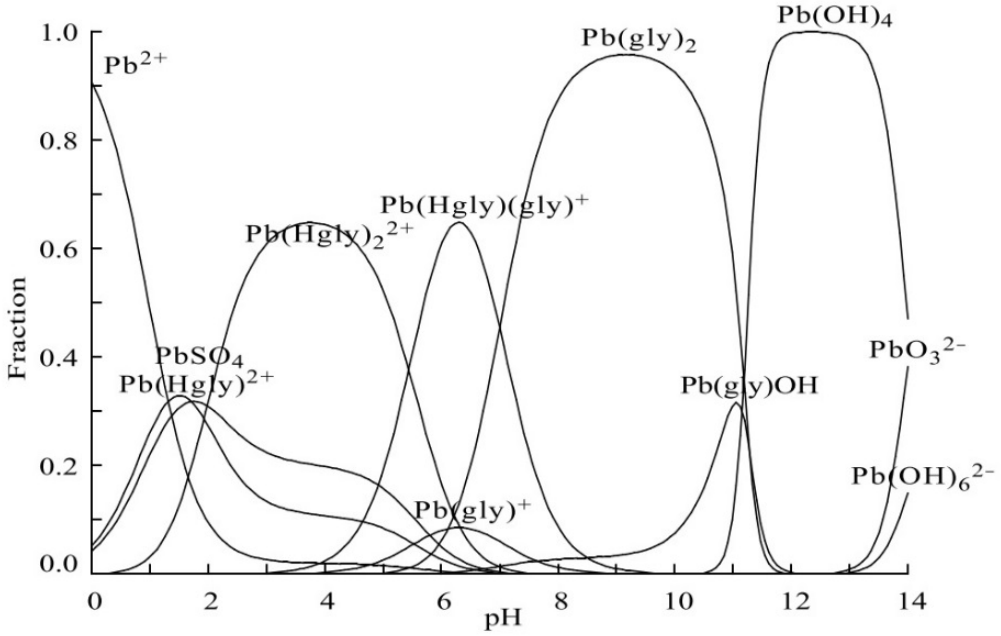

Figure 4. 6. The fraction of Lead-glycine species with 10-6M Pb and 1M glycine at 25◦C.

4.4. Summary

Equilibrium Pourbaix diagram for the zinc-sulfur-glycine-water system was derived. The diagram illustrates that to optimally make use of the zinc-glycine complex formation area in alkaline media, a high concentration of glycine is needed. Under such conditions, the predominant zinc-glycine species is $ZnGly_3^-$.

Equilibrium Pourbaix diagrams for the silver-sulfur-glycine-water and lead-sulfur-glycine-water systems were derived from thermodynamic data. The diagrams illustrate that the predominant metal-glycine species at pH 10 are $AgGly_2^-$ and $PbGly_2$.

CHAPTER 5: ELECTORCHEMISTRY

Chapter 5 depicts the fundamental study of zinc, lead, and silver sulfides dissolution in the alkaline glycine solutions. To achieve this objective, the appropriate dissolution reactions between zinc, lead, and silver with glycine were proposed by applying cyclic voltammetry and chronoamperometry experiences.

5.1. Chapter objective

The main objective of this chapter is to determine an electrochemical mechanism for zinc sulfide, lead sulfide, and silver sulfide dissolution in alkaline glycine media. Chapter 4 summarized the thermodynamic aspects of the metal species-S-glycine-H_2O system based on Eh–pH diagrams and its implications from an electrochemical perspective. Subsequently, in this chapter, the electrochemical and dissolution mechanism aspects of sphalerite, acanthite, and galena in this system based on CV and chronoamperometry are addressed from a fundamental perspective.

with the electrochemistry of solid compounds, their qualitative and quantitative identification is possible. On the other hand, electrochemical investigation via carbon paste electrodes (CPEs) is useful in kinetic and thermodynamic studies (Cisneros-Gonzalez et al., 2000; Cisneros-Gonzalez et al. 1999). Galena is a semiconductor, and its semiconductivity is due to free charge carriers, for which three sources may be distinguished: (l) deviation from stoichiometry, (2) trace elements in solid solution, and (3) thermal excitation across the energy gap. The energy gap of galena is 0.4 eV.

A few articles have reported on the electrochemical behaviour of sphalerite, galena, and acanthite (Ballesteros et al., 2011; Nava et al., 2004; Srinivasan and Iyer, 2000; Ahlberg and Broo, 1996), but there are no published studies regarding anodic oxidation of lead and silver sulfides in alkaline glycine media. On the other hand, study of the electrochemical behaviour of these minerals is of interest as it has provided additional insight into the mechanisms which the leaching studies have been unable to provide.

5.2. Cyclic voltammetry (CV)

5.2.1. Zinc sulfide in alkaline glycine solutions

The hydrophobic properties of the CPE prevent the penetration of supporting electrolyte towards the interior of the electrode. Therefore, the electrochemical reactions are limited to the surface of the electrode. In this study, the open circuit potential (OCP) was found to vary with time, which was probably due to the natural reactions required to reach an equilibrium between the electrode and the electrolyte. The OCP was measured, upon reaching steady state after 500 s, as –188.8 mV versus Ag/AgCl.

Figure 5.1 illustrates the voltammograms obtained from the CV of a stationary working electrode analysis to study the electrochemical leaching behaviour of sphalerite in alkaline

glycine media. The solid line refers to when the potential scan was started in the anodic direction and the dashed line refers to when it was started in the cathodic direction. The grey line presents the observed voltammogram from a CPE electrode without sphalerite to distinguish between possible reactions of glycine on the electrode. As quartz and pyrite are inert in the working potential region, this result can be anticipated (Ahlberg and Ásbjörnsson, 1994). As shown in Figure 5.1, the voltammogram for the CPE (the grey line) shows one small anodic peak (A^*) and one small cathodic peak (C^*). These peaks are not related to the decomposition of glycine since these reactions need a higher overpotential than the peaks that appeared at alkaline pH (Ogura et al., 1998; Chen et al., 2013). These peaks can be attributed to the conversion of glycine anion to glycine zwitterion as follows:

$$H_2NCH_2COOH + OH^- = H_2NCH_2COO^- + H_2O \quad (5.1)$$

$$H_2NCH_2COO^- + H_2O = {}^+H_3NCH_2COO^- + OH^- \quad (5.2)$$

At high alkaline pH (pH ≥ 10), anionin glycine (glycinate) is the dominant species of glycine, as shown by Equation (5.1). On the other hand, according to Figure 4.1, at this pH, there is an insignificant proportion of glycine zwitterion (Ballesteros et al., 2011). Therefore, these minor oxidation–reduction reactions appearing on the grey voltammogram can be considered as the conversion of glycinate anion to glycine zwitterion.

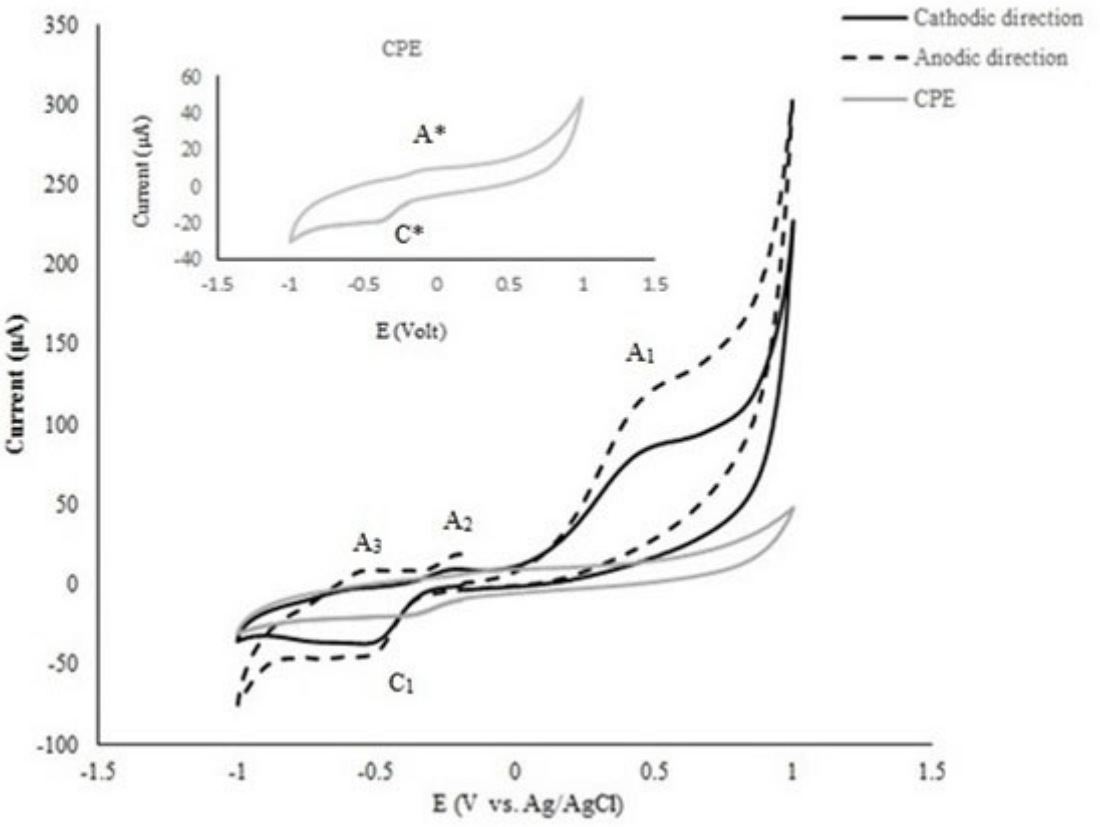

Figure 5. 1. Cyclic voltammogram for the oxidation and reduction of sphalerite-CPE in 1 M glycine at pH 10, at temperature of 25°C, and sweep rate of 20 mVs-1.

While peak A_1 is considered as the oxidation of zinc sulfide, peak A_2 can be considered for complexation and oxidation reaction of zinc species with anionic glycine. Peak A_3 appeared when the scan was initiated in the positive direction and only appeared when the scan potential was inverted at negative inversion potential, whereas peak C_1 was related to the reduction of products formed in oxidation reactions. These proposed reactions are discussed in detail below.

The complex nature of the reactions is evident from Figure 5.2, which shows that changing the sweep rate changes the intensity and position of the peaks. In other words, by using different sweep rates, the thickness of the diffusion layer changes dramatically. In the case of slow sweep rates, the diffusion layer is very thick, while at faster sweep rates the diffusion layer is relatively thin (Brownson and Banks, 2014). Figure 5.2 illustrates the voltammograms for the sphalerite-CPE electrode using different sweep rates from 2 to 100 mVs^{-1}. As can be seen from this figure, the peaks encourage greater electrochemical irreversibility by applying fast sweep rates. The results indicate that the dissolution mechanism is not a simple reversible

mechanism and therefore determination of the kinetic and thermodynamic parameters of the process needs further investigation.

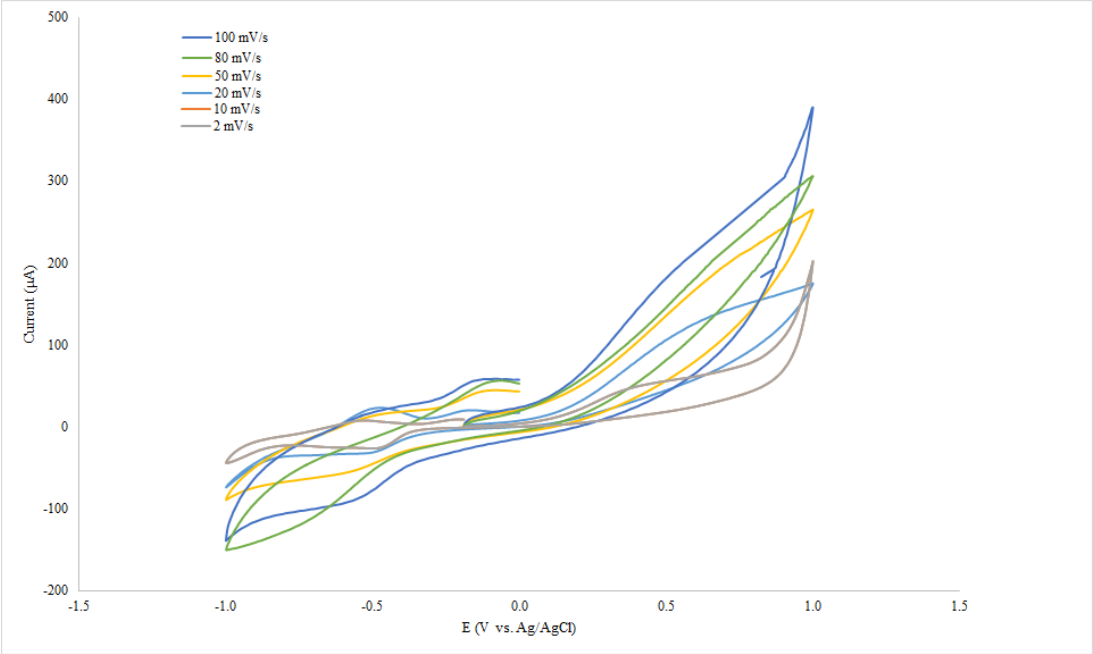

Figure 5. 2. Scan rate variation effect on the intensity and position of the peaks of the stationary sphalerite-CPE in 1M glycine at temperature 25°C, pH 10.

5.2.1.1. Oxidation reactions

The effect of cycling on the voltammogram of sphalerite-CPE in 1 M glycine under the constant working condition is shown in Figure 5.3. Furthermore, to determine the oxidation process at peak A_1, a series of additional experiments were performed by changing the anodic switching potential (Eλ+). The switching potential was changed from $0.350 \leq E\lambda+ \leq 0.650$ V in increments of 0.15 V. Eλ- was kept constant at −0.65 V to eliminate the reactions associated with the peak (C_1) [Figure 5.4 (unstirred) and Figure 5.5 (stirred)].

Figure 5.4 shows three voltammograms at different $E_{\lambda+}$. The anodic current associated with the process at peak A_1 grows as a function of $E_{\lambda+}$, in the same way as the current at peak C_1. It can be seen from this figure that progressing the oxidation process at peak A_1 results in the production of some insoluble species on the electrode surface, and therefore these product species form a layer on the electrode. On the other hand, as shown in Figure 5.5, while the cathodic peak disappeared during stirring, increasing $E_{\lambda+}$ brings about an increasing current at peak A_1, the same as in Figure 5.4. However, the currents associated with peak A_1 (with stirring of the solution) were kept the same as without stirring, while those associated with peak C_1 were increased by stirring the solution. Moreover, Figure 5.5 shows that by stirring

the solution, peak A_2 was unchanged while peak C_1 was eliminated. This result seems to indicate that the oxidation process at peak A_2 is not related to the surface of the electrode.

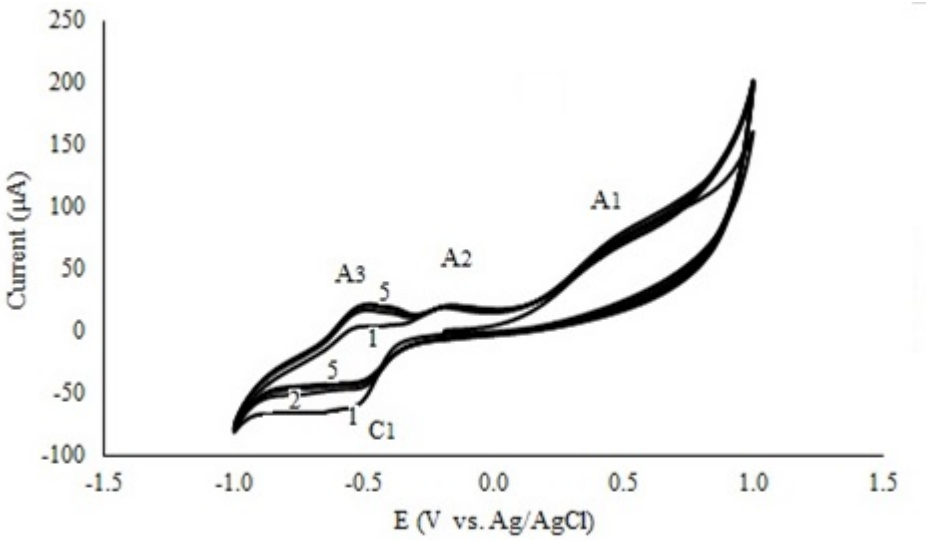

Figure 5. 3. Effect of cycling on the voltammogram of sphalerite-CPE in 1 M glycine at temperature 25°C, pH 10, and sweep rate 20 mVs-1.

The above shows that the reduced species at peak C_1 have been produced at peak A_1. By stirring the solution, these species at C_1 were eliminated (Figure 5.5). The associated charge of the reduction processes at C_1 is notably lower than that at peak A_1. This indicates that the redox processes for the dissolution of sphalerite are complex. These results lead to the suggestion of a pathway for the oxidation process at peak A_1 according to Equations (5.3) and (5.4):

$$ZnS + 10OH^- \rightarrow Zn(OH)_{2(aq)} + SO_4^{2-} + 4H_2O + 8e^- \quad (5.3)$$

$$ZnS + 10OH^- \rightarrow Zn(OH)_{2(C)} + SO_4^{2-} + 4H_2O + 8e^- \quad (5.4)$$

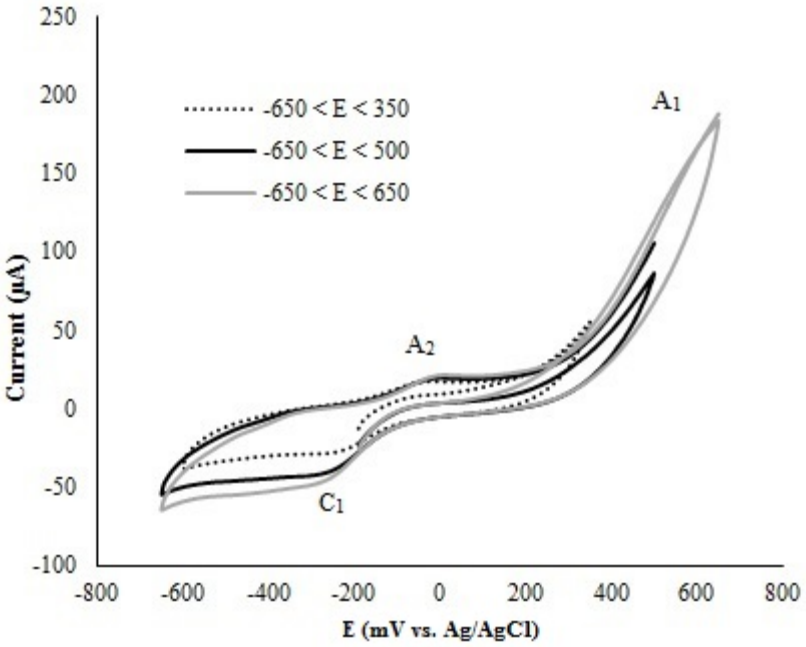

Figure 5. 4. Cyclic voltammogram for the oxidation process at peak A1 of sphalerite-CPE in 1 M glycine at pH 10, at temperature 25°C, and anodic sweep rate of 20 mVs-1 at different Eλ+.

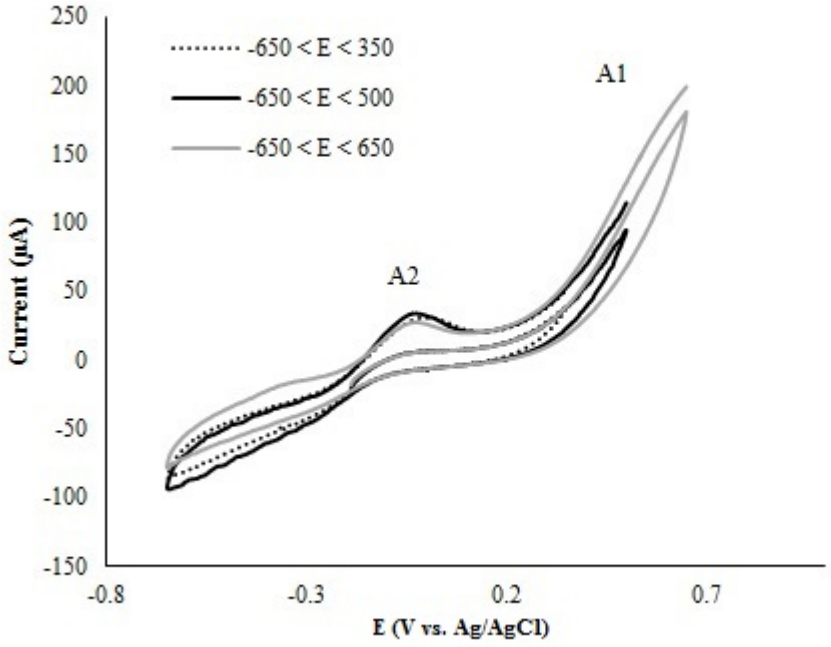

Figure 5. 5. Cyclic voltammogram for the oxidation process at peak A1 of sphalerite-CPE in 1 M glycine at pH 10, at temperature 25°C, and sweep rate of 20 mVs-1 at different Eλ+ with stirring rate of 650 rpm.

At peak A_1, at lower potentials, oxidation of sphalerite has been carried out via Equation (5.3); by increasing the introduced potential, a small amount of insoluble zinc hydroxide (as a

subreaction) was produced (Equation (5.4)). Therefore, the formation of these products on the surface of the electrode results in an increase in the cathodic current at peak C_1. These insoluble hydroxide species may have been removed from the electrode surface by stirring. On the other hand, research findings have confirmed that in direct leaching of sulfide minerals, the reduction of sulfate species in solution is limited by slow kinetics and the formation of sulfate ions is considered to be irreversible for all practical purposes (Marsden and House, 2006; Peters, 1976).

For peak A_3, this peak only appeared when the scan potential was inverted at negative inversion potential. Therefore, this oxidation peak only appears when the reaction at peak A_1 has already run to completion according to Equation (5.5):

$$Zn(OH)_{2_{(aq)}} + 2Gly^- = Zn(Gly)_2 + 2OH^- \quad (5.5)$$

The structure [$Zn(Gly)_2$] is an intermediate product at the working pH. Therefore, this intermediate product involves a chemical reaction at peak A_2 to produce a stable oxidation form.

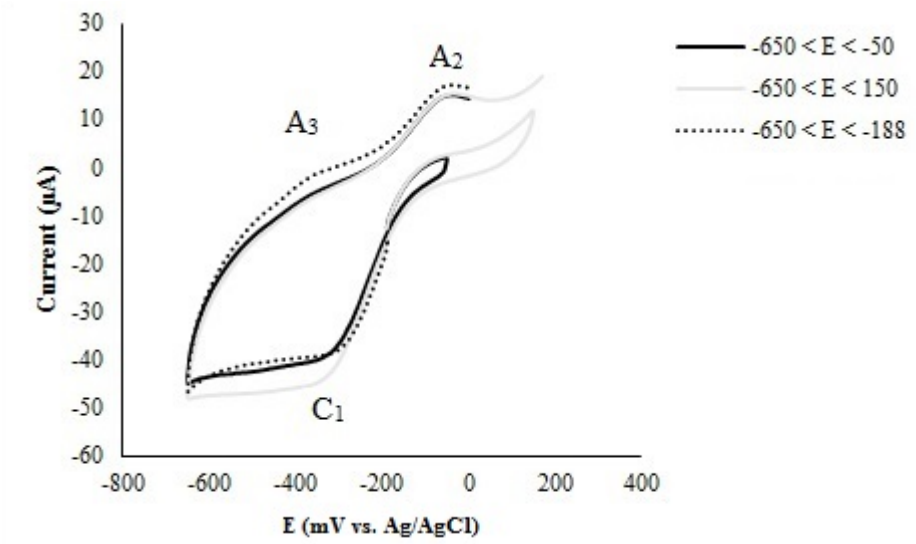

Figure 5. 6. Cyclic voltammogram for the oxidation process at peak A2 of sphalerite-CPE in 1 M glycine at pH 10, at temperature of 25°C, and anodic sweep rate of 20 mVs-1 at different Eλ+.

Figure 5.6 illustrates three voltammograms at different values of $E_{\lambda+}$. Having an OCP at about –189 mV shows a minor oxidation reaction which had already started after running the experiment. Figure 8 shows that the currents associated with peaks A_2 and C_1 remained

roughly the same when $-0.188 \leq E_{\lambda+} \leq -0.050$ V. The author proposed an oxidation reaction for peak A_2 as follows:

$$Zn(Gly)_2 \overset{k_f}{\Leftrightarrow} Zn(Gly)_{2'} + Gly^- = Zn(gly)_3^- \quad (5.6)$$

This observation is consistent with the results of other researchers (Miceli and Stuehr, 1972), who proposed a five-step reaction to produce $Zn(Gly)_3^-$ in alkaline media.

As can be seen from Figure 5.7, the current associated with peak A_2 remained roughly the same. This behaviour can be attributed to a change in the state of zinc glycinate species in the process. These results are consistent with Equation (5.6).

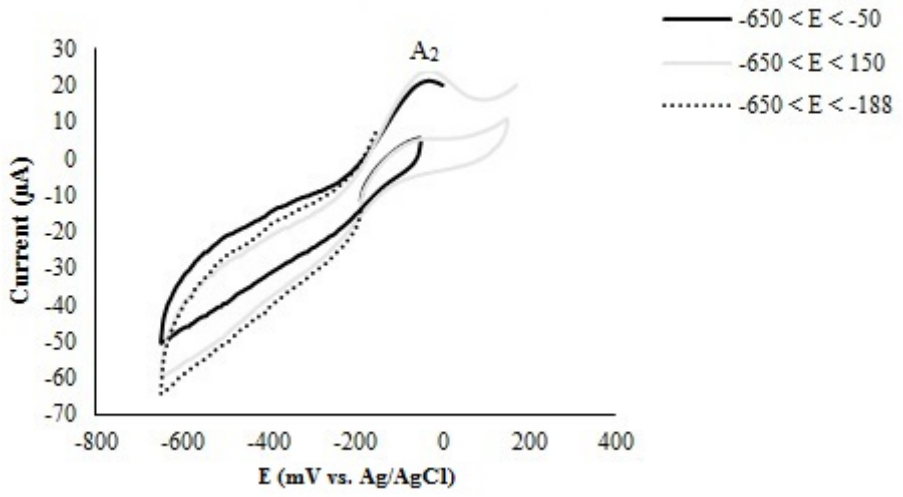

Figure 5. 7. Cyclic voltammogram for the oxidation process at peak A2 of sphalerite-CPE in 1 M glycine at pH 10, at temperature 25°C, and sweep rate of 20 mVs-1 at different Eλ+ with stirring rate of 650 rpm.

5.2.1.2. Reduction reaction

In order to characterize the sphalerite reduction process, a voltammetric study was performed by scanning in the negative direction at different values of negative switching potential, $E_{\lambda-}$, ranging between $-0.400 < E_{\lambda-} < -0.600$ V with increments of 0.1 V (Figure 5.8 for the unstirred solution and Figure 11 for the stirred one).

In general, according to Figure 5.9, increasing $E_{\lambda-}$ results in a shift towards higher associated currents. Furthermore, a cathodic peak was observed at well over –400 mV. A pre-wave (peak A_3) was observed after inverting the scan direction. The pattern is not shaped like a peak, and therefore there is no adsorption mechanism here. On the other hand, the cathodic current associated with the reduction process experienced a marginal decrease between –400 and –

500 mV after which it remained roughly constant. In this figure, as in the previous figures, the current intensity at peak A_2 does not change significantly.

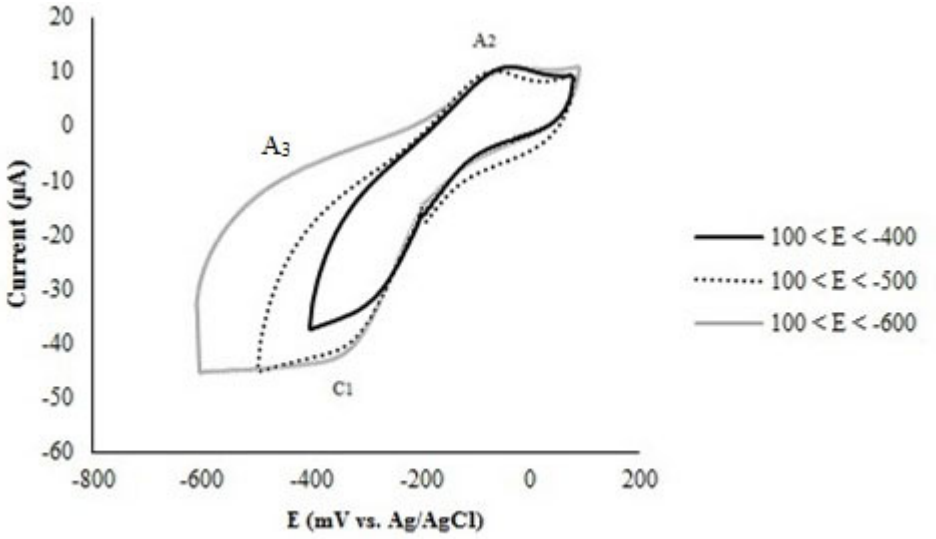

Figure 5. 8. Cyclic voltammogram for the reduction process at peak C1 of sphalerite-CPE in 1 M glycine at pH 10, at temperature of 25°C, and sweep rate of 20 mVs-1 at different Eλ+.

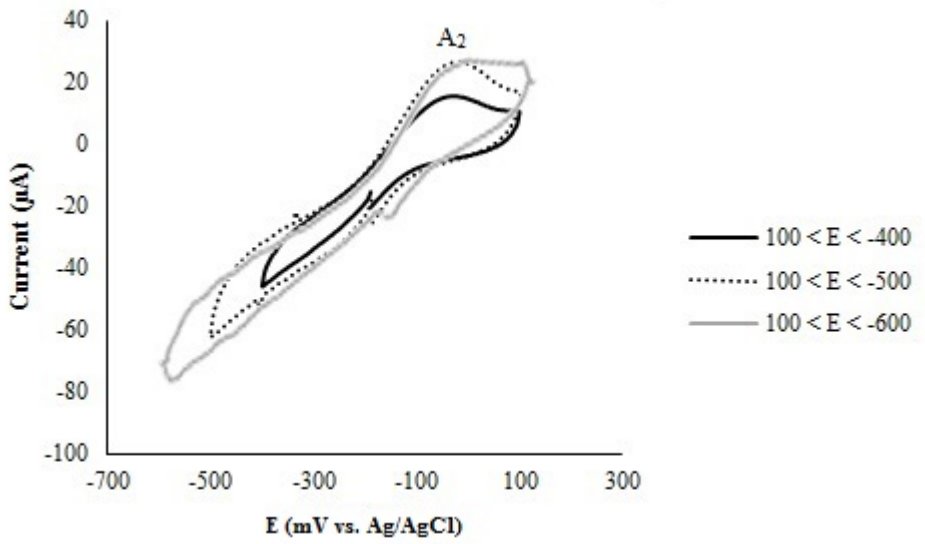

Figure 5. 9. Cyclic voltammogram for the reduction process at peak C1 of sphalerite-CPE in 1 M glycine at pH 10, at temperature 25°C, and sweep rate of 20 mVs-1 at different Eλ+ with stirring rate of 650 rpm.

Furthermore, peak A_3 is becoming more apparent in decreasing the $E_{\lambda-}$ when the scan is inverted. Moreover, in Figure 5.9, it can be seen that peak C_1 disappeared whereas the pre-wave (A_3) was not detected after inverting the scan. This confirms that the products at peak

C_1 are soluble and diminish their concentration at the interface as a result of stirring, which impedes their detection at peak C_1. As a result of this electrochemical behaviour and considering the abovementioned thermodynamic analysis, the author suggests that the following reaction can explain the reduction process at peak C_1 concerning the products at peak A_1:

$$Zn(OH)_2 + 2e^- = Zn + 2OH^- \quad (5.7)$$

If the reaction attributed to peak C_1 were related to the reduction of the sulfate produced at peak A_1, the electrode surface would be expected to be covered either wholly or partially by sulfur, and thus the area of the electrode exposed in the subsequent cycle would be less. Hence, the peak current should be less than that in the first cycle. In practice, it can be seen from Figure 5 that the current increased in subsequent cycles, which confirms the previous assumption that the reaction at peak C_1 is not related to sulfate reduction but is related to the reduction of the products produced at peaks A_1 and A_2.

Integrating the area under the curve for the oxidation processes of sphalerite leads to charges of 8.447 mC at peak A_1 and 5.990 mC at peak A'_1. Furthermore, since the value of the cathodic process charge is only −1.429 mC, the significant difference between the current and charge of the oxidation process in the negative direction voltammogram is not related to the oxidation of products formed during reduction at peak C'_1 (Nava et al., 2002). On the other hand, having a significant difference between the cathodic and anodic charges associated with the peaks shown in Figure 3 suggests that besides sphalerite oxidation reactions, the process may encounter other subreactions (Cisneros-Gonzalez, 2000), which will be discussed in a future study.

5.2.2. Silver sulfide in alkaline glycine solutions

The OCP was measured, upon reaching a steady state after 500 s, to be 61 mV versus Ag/AgCl.

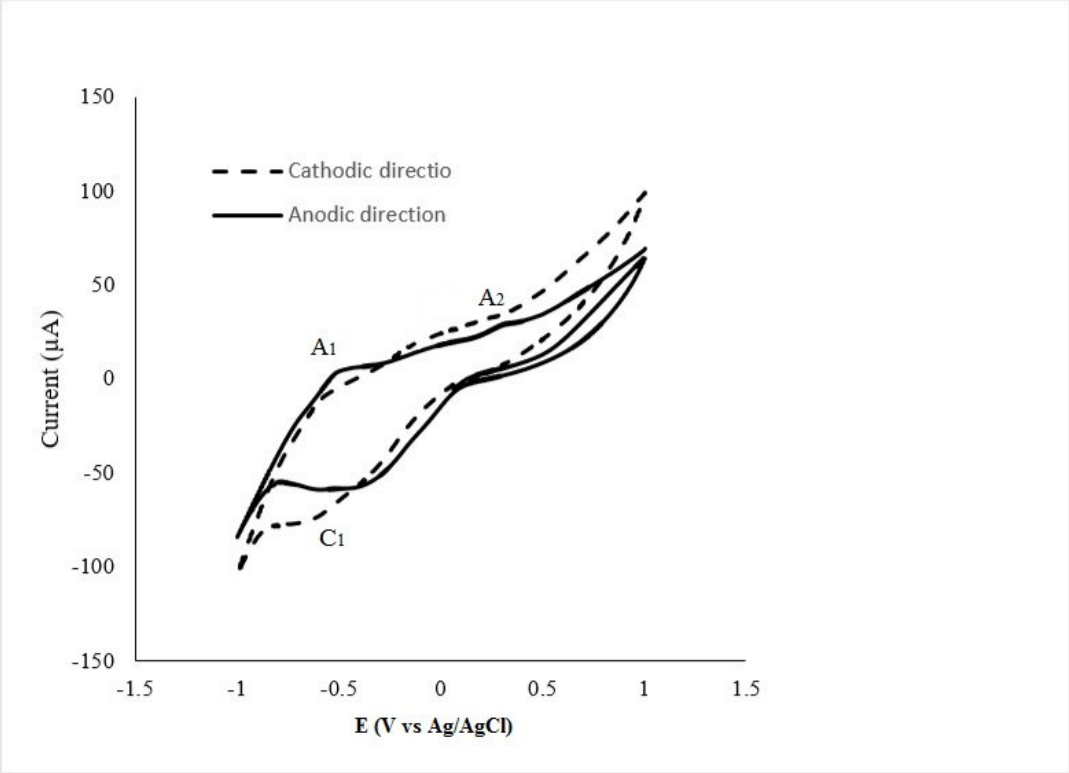

Figure 5. 10. Cyclic voltammogram for the oxidation and reduction of silver sulfide-CPE in 1 M glycine at pH 10, at temperature 25°C, and sweep rate of 20 mVs-1.

Figure 5.10 illustrates the voltammograms obtained from the CV of a stationary working electrode analysis to study the electrochemical leaching behaviour of silver sulfide in alkaline glycine media. The solid line depicts when the potential scan was started in the anodic direction and the dashed line depicts the cathodic direction. As the influence of silver ions on the electrochemical quartz and pyrite is inert in the working potential region, this result is not extraordinary (Ahlberg and Asbjornsson, 1994). As shown in Figure 5.10, the voltammograms show two anodic peaks and one cathodic peak in which A_1 is related to the oxidation of silver sulfide, C_1 is related to the reduction of silver sulfide, and peak A_2 is related to the oxidation of the production of peaks A_1 and C_1, respectively, as discussed in detail below. Peak A_1 at lower anodic overpotential can be attributed to the oxidation of silver sulfide according to Equation (5.8):

$$Ag_2S \rightarrow 2Ag^+ + S^0 + 2e^- \quad (5.8)$$

while peak C_1 is related to the reduction of silver sulfide according to Equation (5.9):

$$Ag_2S + H_2O + 2e^- \rightarrow 2Ag + HS^- + OH^- \quad (5.9)$$

As shown in Figure 5.10, in the anodic sweep direction, peak A_2 does not exist at first sweep in the anodic direction and appears after the cathodic sweep has been completed and the reactions at peaks C_1 and A_1 have taken place.

The formation of the silver-glycine complex occurs at peak A_2. This complexation of the metallic silver produced by the cathodic reaction (C_1) stems from two steps, including a redox reaction follows by a chemical reaction [Equations (5.10) and (5.11)]. The Ag(Gly) species is an intermediate product at this pH and is not stable in this area according to Figures 4.3 and 4.4. Therefore, peak A_2 represents a reaction to produce a stable oxidation form according to Equation (5.10):

$$Ag + Gly^- = Ag(Gly) + e^- \quad (5.10)$$

$$Ag(Gly) + Gly^- = Ag(Gly)_2^- \quad (5.11)$$

$$Ag + 2Gly^- = Ag(Gly)_2^- + e^- \quad (5.12)$$

This behaviour can be considered as an electrochemical reaction. Thus, a two-step reaction to produce $Ag(Gly)_2^-$ in alkaline media has been proposed.

According to the abovementioned proposed reactions for each peak, if a multi-cycle CV test is done, the area of current associated with the process should be developed. This hypothesis is consistent with the results of Figure 5.11. The other striking feature of Figure 5.10 is that the current increased in subsequent cycles, which shows that no passivation layer formed on the surface of the silver sulfide CPE.

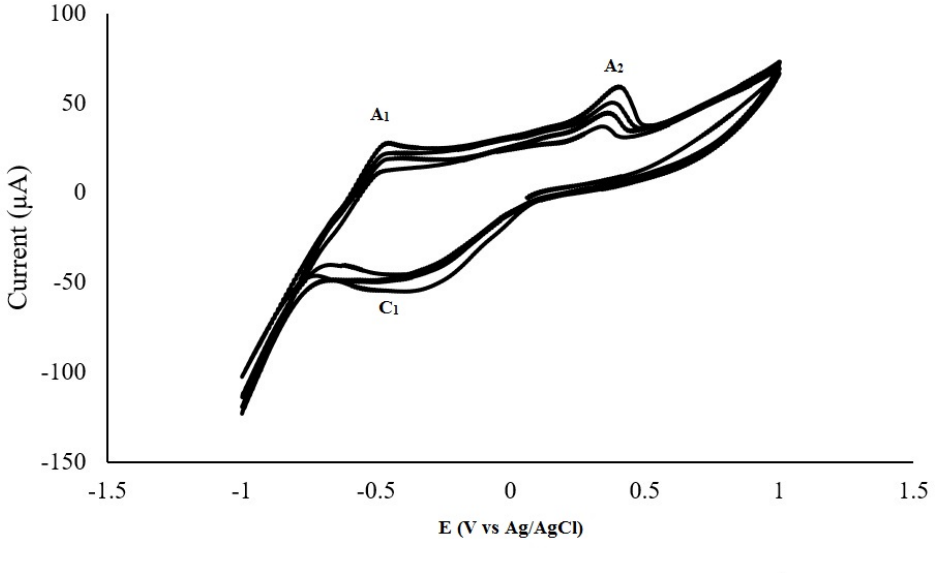

Figure 5. 11. Effect of cycling on the voltammogram of silver sulfide-CPE in 1 M glycine at temperature 25°C, pH 10, and sweep rate 20 mVs-1.

5.2.3. Lead-glycine cyclic voltammetry

Figure 5.12 shows the voltammograms from the CV of a stationary working electrode analysis to study the electrochemical leaching behaviour of galena in alkaline glycine media. The solid line depicts the anodic current scanning and the dashed line depicts the cathodic direction. The measured OCP, upon reaching steady state after 500 s, was –75 mV versus Ag/AgCl. As shown in Figure 5.12, the voltammograms show four anodic peaks and two cathodic peaks. The most striking feature of Figure 5.12 is that most of the oxidative peaks (A_4, A_3, and even A_2) only appeared when the scanning was initiated in a positive direction. On the other hand, there is an activation behaviour (higher current in the reverse scan than in the forward scan) in the anodic current direction. Thus, to describe this specific behaviour of the sample in alkaline glycine media, more experiments have been carried out. Figure 5.13 illustrates the multi-cycle CV test for galena carbon paste electrode (G-CPE).

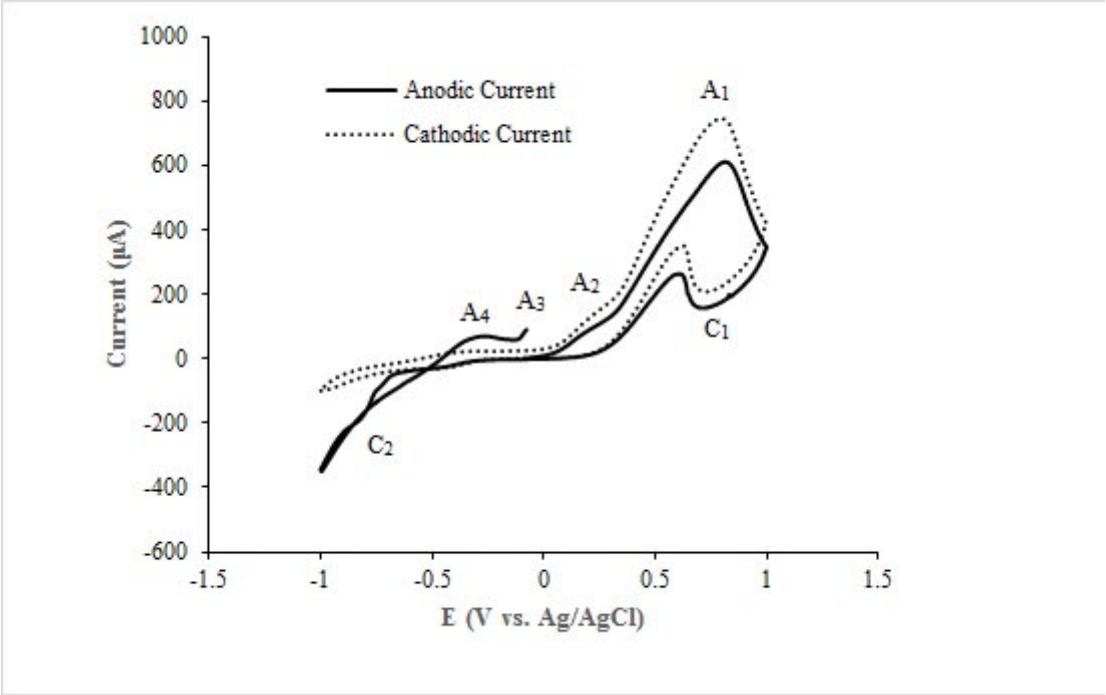

Figure 5. 12. Cyclic voltammogram for the oxidation and reduction of G-CPE in 1 M glycine at pH 10, at temperature 25°C, and sweep rate of 20 mVs-1.

As can be seen from Figure 5.13, the products of the oxidation reaction at peak A_1 are reduced in the reaction at peak C_1.

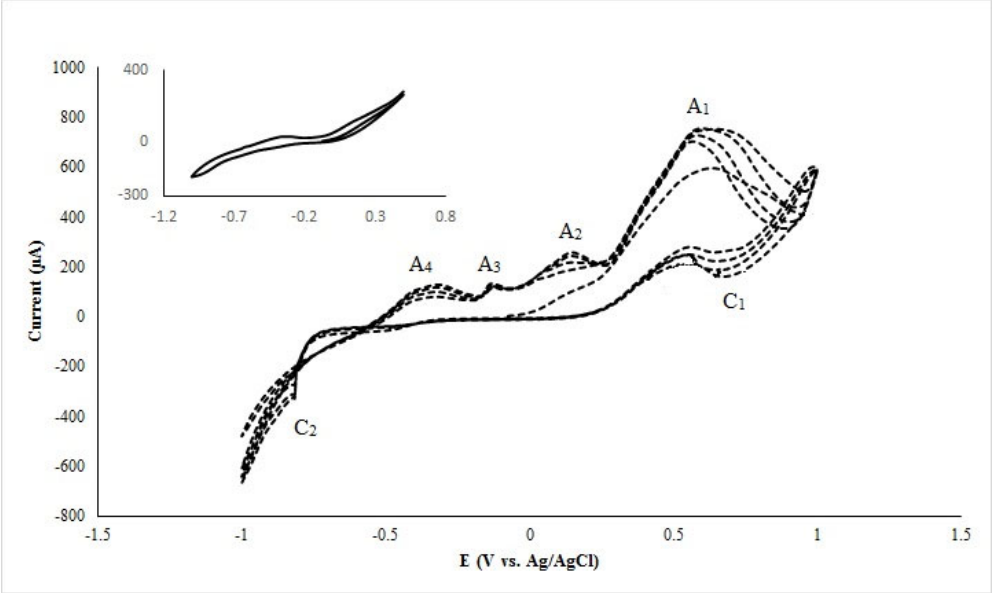

Figure 5. 13. Effect of cycling on the voltammogram of G-CPE in 1 M glycine at temperature 25°C, pH 10, and sweep rate 20 mVs^{-1}.

However, this reaction is not able to consume all the oxidation products of peak A_1. There are some reasons for this hypothesis that the products of A_1 are not consumed by a kind of chemical reaction before reaching peak C_1. Firstly, the distinct difference between the charge associated with peaks A_1 and C_1 indicates that the quantity of the reactions is not equal. On the other hand, as can be seen from Figure 5.12 (the top-left corner chart), removing peak A_1 had a negative effect on the rest of the reactions and process. Hence, as a result of the observation of these behaviours, the following reactions can be proposed for peaks A_1 and C_1 according to the mentioned Eh–pH diagram (Figure 4.5):

$$PbS + 12OH^- = Pb(OH)_4 + SO_4^{2-} + 4H_2O + 12e^- \quad (5.13)$$

$$Pb(OH)_4 + SO_4^{2-} + 4H_2O + 10e^- = PbS + 12OH^- \quad (5.14)$$

The production of peak A_1 [lead (IV) hydroxide] can be considered as an oxidant for the rest of the process and plays a vital role in performing the rest of the direct leaching of the G-CPE. Furthermore, research findings confirmed that in direct leaching of sulfide minerals, sulfur does not readily oxidize to sulfate despite the high oxidizing potential. Also, the reduction of sulfate species in solution is limited by slow kinetics, and the formation of sulfate ions is considered to be irreversible for all practical purposes; therefore, some thiosulfate and a variety of other thionates are formed over a wide range of Eh–pH conditions, especially in alkaline media (Mardsen and House, 2006; Peters, 1976).

The other striking feature of Figure 5.13 is that the current remained approximately the same in subsequent cycles, which may imply that after the maximum capacity of each product can

be achieved under the experimental conditions. The position of the peak A_2 indicates that this peak relates to the oxidation of galena to lead (II) hydroxide as follows:

$$2PbS + 10OH^- = Pb(OH)_2 + SO_4^{2-} + 4H_2O + 8e^- \quad (5.15)$$

Peak A_3 only appeared after the reductive reaction at peak C_2; also, peak A_3 has a unique character in that the associated current and potential remained stable. From this evidence, the following reaction can be proposed for peaks C_2 and A_3, respectively:

$$PbS + H_2O + 2e^- = Pb + HS^- + OH^- \quad (5.16)$$

$$Pb + 2Gly^- = Pb(Gly)_2 + 2e^- \quad (5.17)$$

The above-proposed mechanism shows that glycine is unable to oxidize galena directly, and productions of peak C_2 can meet the needs of peak A_3. Again, at peak C_2, sulfur is converted to a new species according to the Eh of the reaction. Finally, peak A_4 at relatively lower anodic overpotential can be attributed to direct oxidation of galena as follows:

$$PbS = Pb^{2+} + S^0 + 2e^- \quad (5.18)$$

5.3. Chronoamperometry

5.3.1. Zinc sulfide in alkaline glycine solutions

The typical current transient obtained from chronoamperometric experiments on the sphalerite-CPE for a series of anodic potentials from –550 to 700 mV versus an Ag/AgCl reference electrode is shown in Figure 5.14.

It can be seen from this figure that the current rises as a function of the applied potential. The change in the oxidation mechanisms is the most striking feature of the results shown in Figure 5.14. At the low potentials of –550 and –450 mV, the current drops dramatically from its initial value, passes through a minimum, and rises marginally to a semi-steady state value. This behaviour of sphalerite seems to indicate that initially, unstable passive layers may form and prevent the charge transfer, after which partial dissolution of the passive layers leads to the formation of cracks. These cracks allow the electrolyte to access the mineral surface. In the final stage of the reaction, the formation and dissolution rates of the oxidation products are virtually equivalent. This behaviour corresponds with the proposed reaction for oxidation of sphalerite at peak A_1 [Equations (5.3) and (5.4)].

Between –175 and –100 mV, the mechanism changes and appears to involve a chemically controlled reaction which eventually reaches a steady state. Above an anodic potential of 500

mV, another mechanism is involved. At such anodic potentials, the current increases rapidly to values of more than 100 µA in less than 10 s and approaches a maximum.

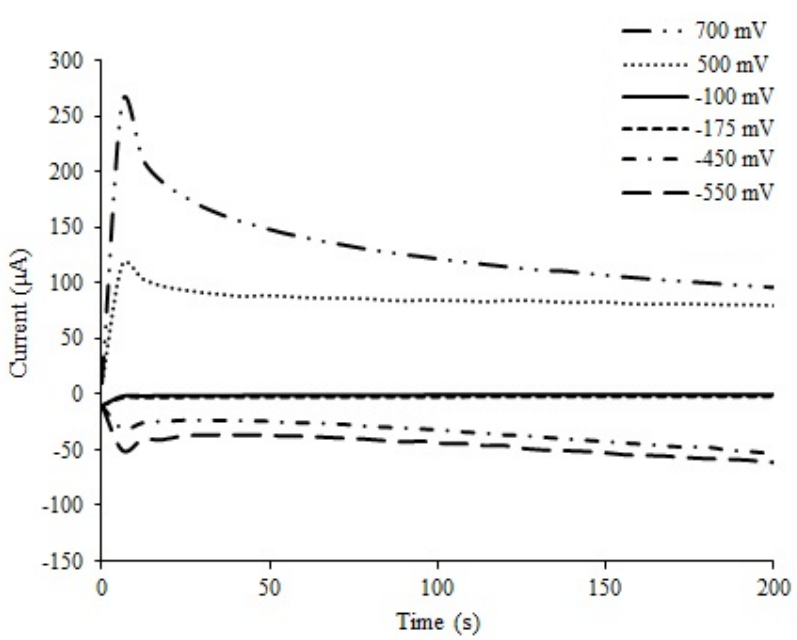

Figure 5. 14. Chronoamperometry curves of sphalerite-CPE at pH 10. (V vs. Ag/AgCl reference electrode).

After that, the current decreases rapidly from the maximum value, indicating the formation of a thin passive layer, and continues to decrease at a gradually slowing rate (Azizkarimi, 2014). Based on this result, it is proposed that the oxidation reaction proceeds for the oxidation products of peak A_2, and direct oxidation of the sphalerite occurs at high anodic potential A_1. Ultimately, the rate of formation of passive oxide layers on the mineral exceeds that of glycine diffusion from the diffusion layer to the surface, thus effecting a diffusion-controlled process.

Figure 5.15 shows the influence of the applied anodic potential on the total anodic transferred charge and the dissolved zinc ions from the sphalerite-CPE at time = 200 s. As can be seen from this figure, three regions of potential can be identified. The first region is in the interval –600 mV < E_{anod} < –400 mV versus Ag/AgCl, where the changes of charge are fluctuating around 70 mC. After that, the transferred charge falls dramatically to about 20 mC. The second region corresponds to the interval of –400 mV < E_{anod} < 300 mV, where the transferred charge stays at roughly the same level of just under 20 mC.

The third region is located between 300 mV < E_{anod} < 700 mV and shows that the charge increases marginally, indicating the potential region where the direct dissolution of sphalerite probably occurs. The slopes corresponding to the anodic charges versus the imposed anodic potential can be attributed to the changes occurring in the mechanism of sphalerite dissolution

in alkaline glycine media. As shown in this figure, the zinc content in solution co-occurring with the first anodic peak A_1 corresponds to the sphalerite dissolution mechanism in alkaline glycine media proposed in Reactions (7) and (8) agrees with the proposed electrochemical process for the ZnS oxidation.

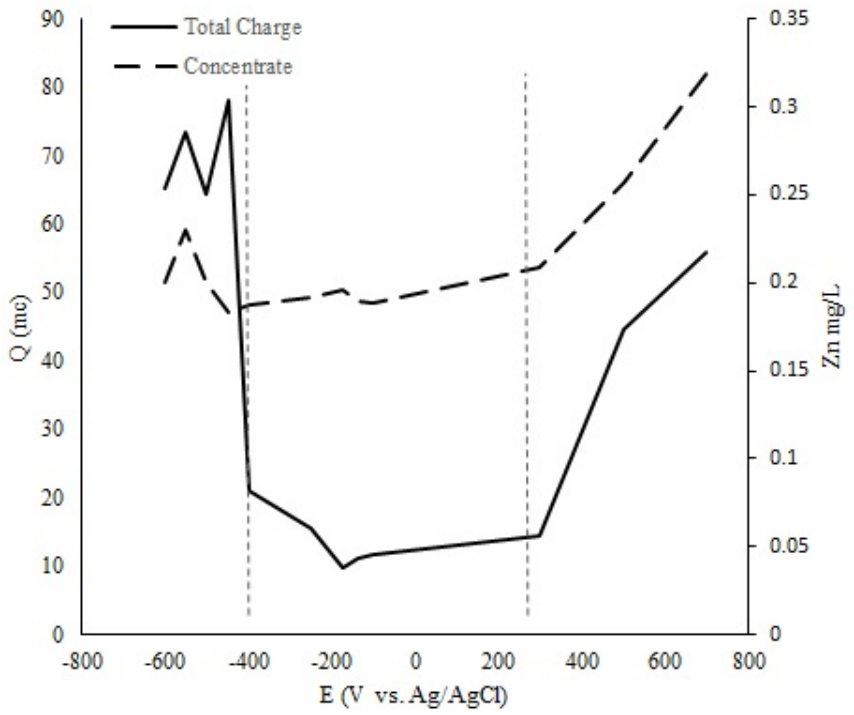

Figure 5. 15. The influence of applied anodic potential with total anodic transferred charge (mC) and the dissolved zinc ions from the sphalerite-CPE at time = 200 s.

5.3.2. Lead sulfide in alkaline glycine solutions

The typical current transient obtained from chronoamperometry experiments on the G-CPE for a series of anodic potentials from –450 to 700 mV versus an Ag/AgCl reference electrode is shown in Figure 5.16. It can be seen from Figure 5.16 that the current rises as a function of the applied potential. However, a change in the oxidation mechanisms is the most striking feature of Figure 5.16. At the low potentials of –200 and –450 mV, the current drops slightly from its initial value and reaches a semi-steady state value. This behaviour of galena seems to indicate that in the first stage, unstable passive layers may form and prevent the charge transfer, after which the formation and dissolution rates of the oxidation products become almost the same.

This behaviour corresponds with the proposed reaction for the oxidation of galena at peak A_4 [Equation (5.17)]. Between –160 and –80 mV, the mechanism has changed, and it seems to face a chemically controlled reaction which reaches a steady state after a while. Between 100

and 175 mV, the oxidation process shows the same behaviour as is seen in the range of –200 to –450 mV. Nonetheless, in this range, the rate of decrease is much bigger than in the former range. Finally, above the anodic potential of 250 mV, the other mechanism is involved. At such anodic potentials, the current increases rapidly to values of more than 200 μA in less than 10 s and approaches a maximum. After that, the current decreases rapidly from the maximum value, indicating the formation of a thin passive layer, and then continues to decrease at a gradually slowing rate (Chen et al., 2013). Based on this result, it can be proposed that the oxidation proceeds for the oxidation products of the peaks (A_4 and A_2) and the direct oxidation of the galena at the high anodic potential. After a while, the rate of formation of passive oxide layers on the mineral exceeds that of the diffusion from the diffusion layer to the surface and brings about a diffusion-controlled process.

Figures 5.17 shows the influence of the applied anodic potential with the total anodic transferred charge (mC) and the dissolved lead ions from the G-CPE and silver at 200 s. As can be seen from Figure 5.17, four regions of potential can be identified. The first region is in the interval –400 mV < E_{anod} < –80 mV versus Ag/AgCl, where the changes of charge are fluctuating around 10 mC. After that the transferred charged rises over twice as high as in the first region and reaches approximately 40 mC (–80 mV < E_{anod} < 250 mV); the third region is located between 250 mV < E_{anod} < 563 mV and shows that the charge increases significantly, indicating the potential region where the direct dissolution of sphalerite probably occurs; in the last region, above 563 mV, the transferred charge decreases dramatically as a result of the formation of a passive layer on the electrode's surface; however, after a while, the associated charge begins to increase due to the formation of cracks on the passivation layer.

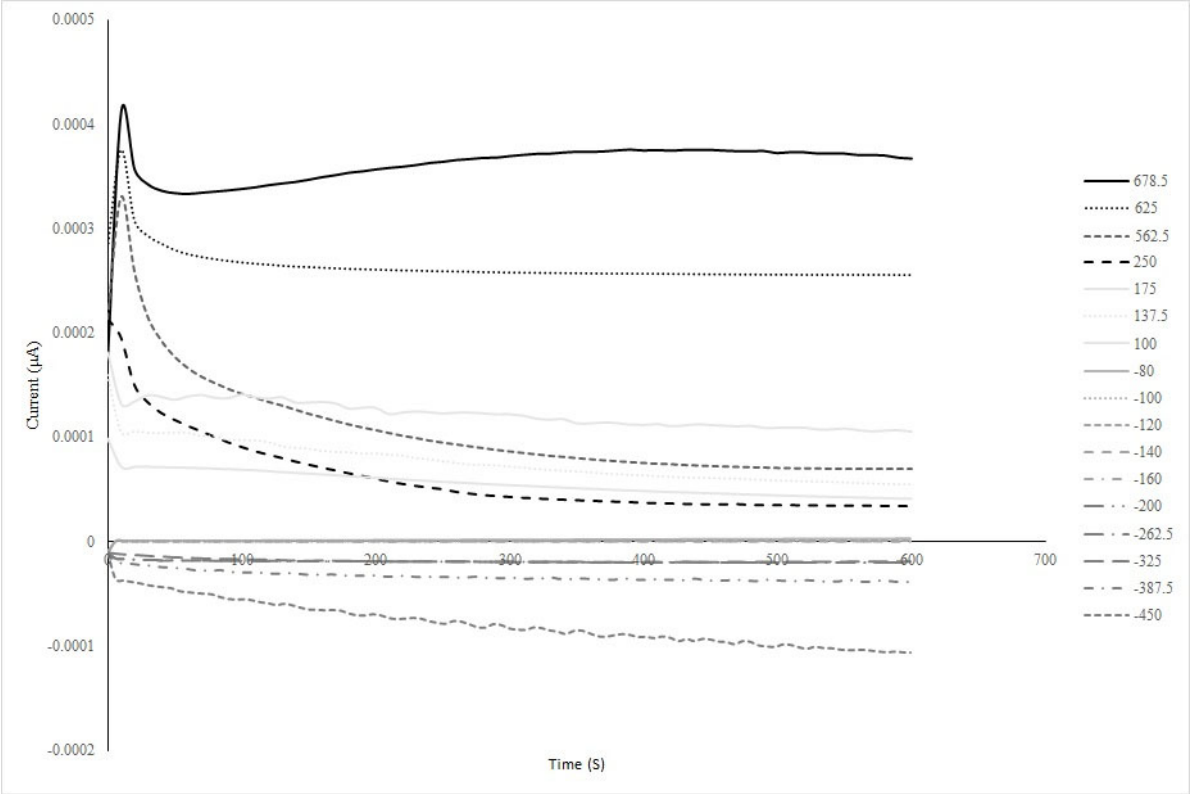

Figure 5. 16. Chronoamperometry curves of G-CPE at pH 10. (V vs. Ag/AgCl reference electrode).

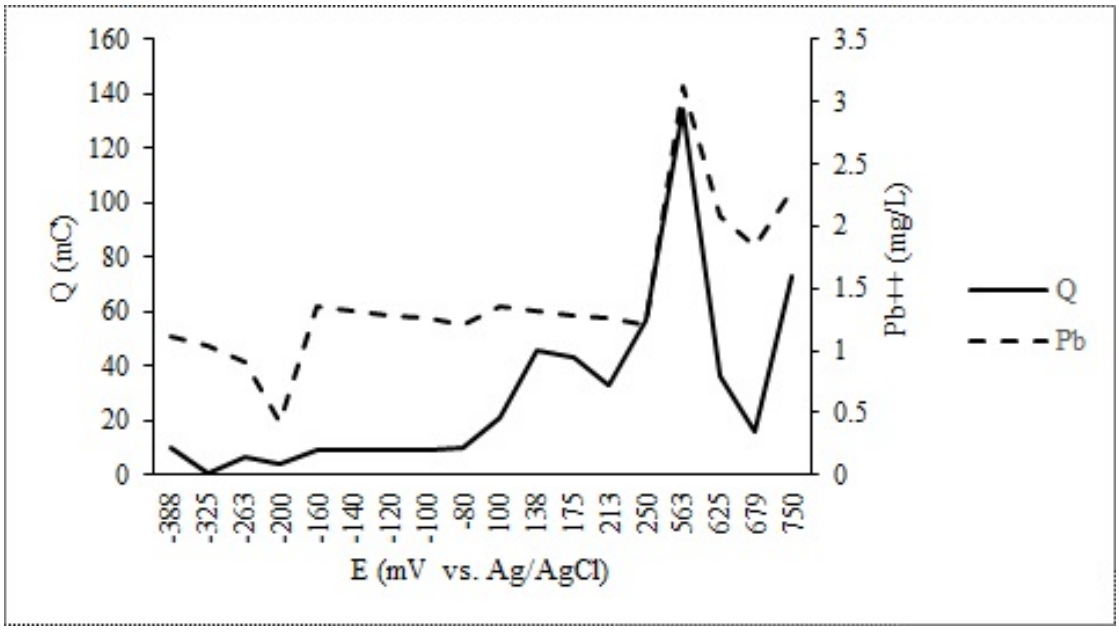

Figure 5. 17. The influence of applied anodic potential with total anodic transferred charge (mC) and the dissolved lead ions from the G-CPE at time = 200 s.

5.3.3. Silver sulfide in alkaline glycine solutions

It can be seen from Figure 5.18 that, as in Figure 5.16, the current rises as a function of the applied potential. At low potentials in the range of –600 to –415 mV, the current drops dramatically from its initial value, passes through a minimum, and then rises marginally to a semi-steady state value. This behaviour of silver sulfide seems to indicate that in the first stage, unstable passive layers may form and prevent the charge transfer, after which the dissolution of the passive layers leads to the formation of some cracks in the layers. These cracks allow easy access of the electrolyte to fresh materials. The final stage can be considered as occurring when the formation and dissolution rates of the oxidation products become almost the same. After that, above the anodic potential of 200 mV, the other mechanism is involved. At such anodic potentials, the current increases rapidly to values of more than 40 μA, and after that, the current decreases erratically and continues to decrease at a gradually slowing rate. Based on this result, it can be proposed that the oxidation proceeds for the oxidation of the produced silver at high anodic potential by glycine. After a while, the rate of formation of passive oxide layers on the mineral exceeds that of glycine diffusion from the diffusion layer to the surface and brings about a diffusion-controlled process.

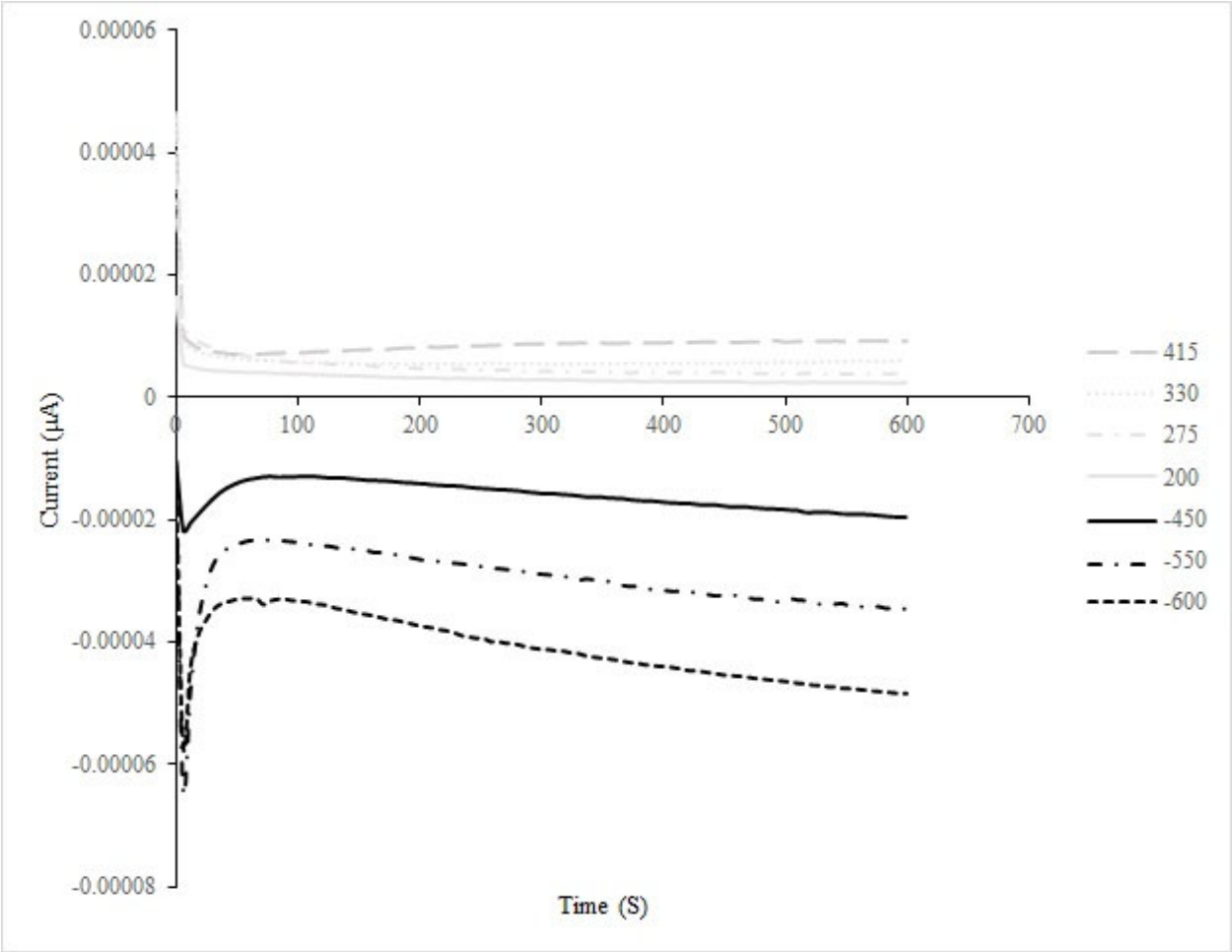

Figure 5. 18. Chronoamperometry curves of A-CPE at pH 10. (V vs. Ag/AgCl reference electrode).

Figure 5.19 shows the influence of the applied anodic potential with the total anodic transferred charge (mC) and the dissolved silver ions from the silver sulfide-CPE at 600 s. As shown in Figure 5.19, three regions of potential can be identified. The first region is related to the reaction at peak A_1 in the interval –600 mV < E_{anod} < –400mV versus Ag/AgCl, where the charge increases marginally, indicating the potential region where the direct dissolution of silver sulfide probably occurs the changes of charge are fluctuating around 70 mC. After that the transferred charge falls dramatically to about 20 mC. The second region corresponds to the interval of –450 mV < E_{anod} < 200 mV where the transferred charge has the same behaviour as in the first region and should be related to the process at peak C_1. The charge in the last region remains at roughly the same level of just under 20 mC. From the dashed line illustrating the dissolution of silver in the solution, it can be concluded that the rate of complexation is too slow although the silver content in the solution increases slightly.

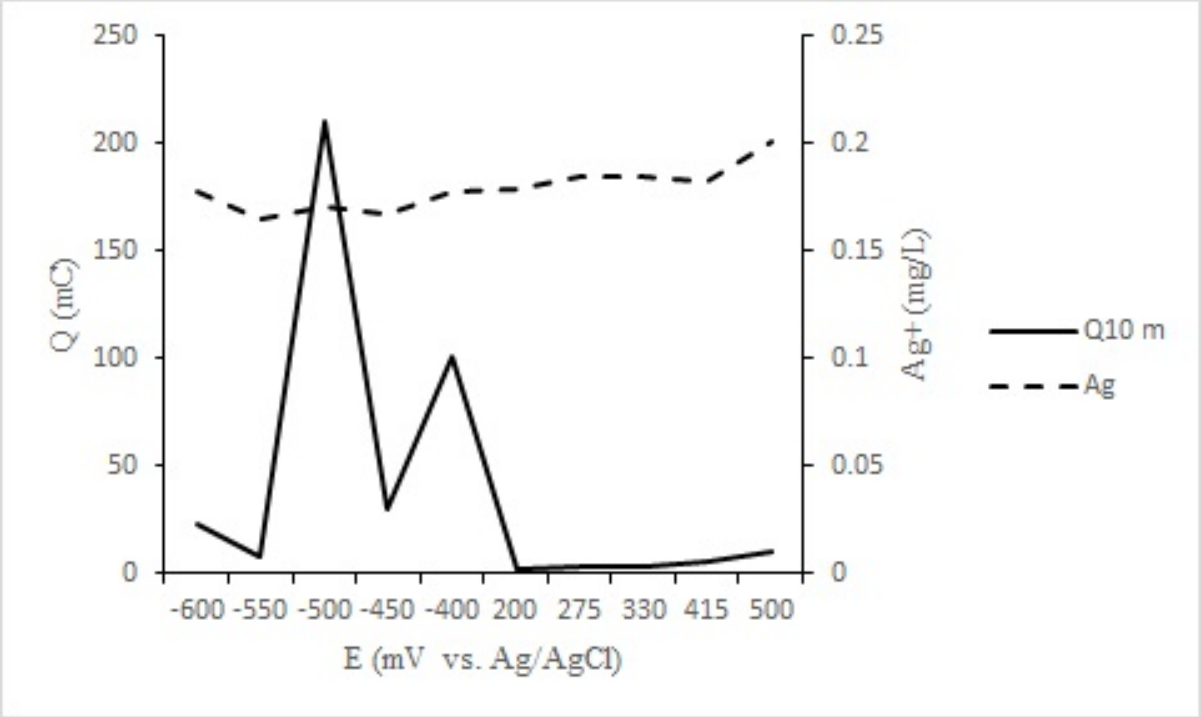

Figure 5. 19. The influence of the applied anodic potential with total anodic transferred charge (mC) and the dissolved silver ions from the silver sulfide-CPE at 600s.

CHAPTER 6: LEACHING

The main objective of this chapter is to investigate the leaching of different zinc minerals in the alkaline glycine solutions and simultaneous dissolution behaviour of copper, lead, and silver in different leaching systems through modelling and optimization.

6.1. Chapter objective

This chapter mainly consists of three sections according to the dissolution procedures used to investigate different objectives, namely:

- *Rotating disc experiments* to investigate the effect of pH, glycine, and sodium chloride on silver sulfide dissolution in the alkaline glycine process, modelling and optimization, and the effect of pH, glycine concentration, pH modifiers, and additives on zinc sulfide dissolution in the alkaline glycine process.
- *Agitated reactor experiments* to investigate the effects of cupric ions, dissolved oxygen, and temperature on the zinc sulfide leaching process. Furthermore, modelling and optimization of the sphalerite dissolution in the alkaline glycine solutions was investigated.
- *Bottle roll experiments* to investigate the effect of excessive glycine concentration and particle size on the zinc dissolution in the alkaline glycine solutions at extended leaching times.

6.2. Rotating disc experiments

6.2.1. The effects of parameters

Figure 6.1 and Table 6.1 show the main effects of the investigated parameters in the rotating disc dissolution experiments. To screen the most effective parameters and find the optimum working conditions, it is better to investigate the effects of each independent variable separately. As can be seen from Figure 6.1, the glycine concentration, pH modifier, and lead nitrate have negative effects on the sphalerite dissolution, while the impacts of sodium chloride, potassium permanganate, hydrogen peroxide, and pH on the sphalerite dissolution are positive.

Table 6. 1. Experimental design and outputs.

	Parameters							Zn Dissolution (ppm)				
test No.	Gly*(M)	Modifier	$Pb(NO_3)_2$	NaCl	$KMnO_4$	H_2O_2	pH	2hr	4hr	6hr	24hr	48hr
I	3	NaOH	0	0	0	0	9	41.07	43.8	55.6	112.8	132.2
II	3	NaOH	0	300	2	0.04	10.5	155.7	174.7	212.7	552.1	678.4
III	3	Ca(OH)2	200	0	0	0.04	10.5	85.2	103.2	115.5	276.5	444.4
IV	3	Ca(OH)2	200	300	2	0	9	156.3	265.0	321.5	606.3	836.0
V	4	NaOH	200	0	2	0	10.5	74.8	106.1	140.8	181.8	276.5
VI	4	NaOH	200	300	0	0.04	9	264.0	304.9	352.6	827.2	932.2
VII	4	Ca(OH)2	0	0	2	0.04	9	126.0	198.8	214.6	480.2	907.5
VIII	4	Ca(OH)2	0	300	0	0	10.5	105.4	144.6	193.5	504.0	667.8

*Glycine

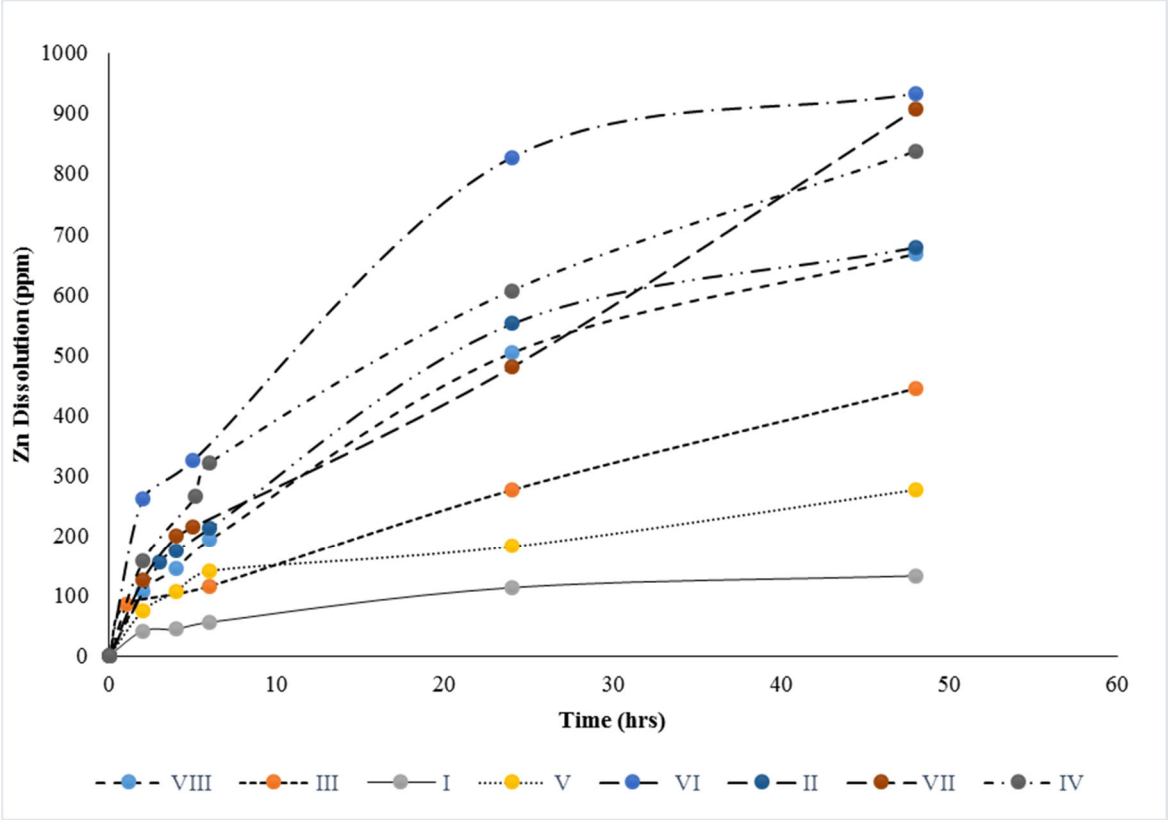

Figure 6. 1. Sphalerite dissolution curves for rotating disk dissolution experiments at a temperature of 35°C and stirring speed of 500 rpm.

With regard to the glycine concentration, as mentioned above, the variable range was between 3 and 4 moles. On the other hand, the solubility of glycine in the water at 25 °C is 3.33 moles, which can be increased to a higher amount in an alkaline medium and at higher temperature ("Pubchem," 2020). From Figure 6.1, it can be seen that increasing the glycine concentration from 3 to 4 moles leads to a decrease in sphalerite dissolution.

This behaviour can be related to either increasing the thickness of the diffusion layer on the sphalerite particles or the dissolution of more hydroxide following the rejection of Zn from the solution until it returned to homeostasis [Reaction (6.1)]:

$$ZnS + 8OH^- + 3Gly^- = Zn((gly)_3^- + SO_4^{2-} + 4H_2O + 8e^- \quad (6.1)$$

NaOH and $Ca(OH)_2$ were used to modify the solution pH in this study. Figure 6.13 shows that when using NaOH to modify the pH, the sphalerite dissolution can reach about 400 ppm, while in the same condition with $Ca(OH)_2$ the sphalerite dissolution dropped to under 200 ppm. The use of lead nitrate, as can be seen from Figure 6.13, has a negative effect on the sphalerite dissolution in alkaline glycine media. However, lead nitrate (at high concentration) can increase the sulfide minerals dissolution rate by reducing the inhibitory sulfide layer

formed on the particles (Deschênes et al., 2000; Senanayake, 2008) but can also decrease the dissolution rate of sulfide phases by galvanic interactions between zinc and lead (Morey, 1998).

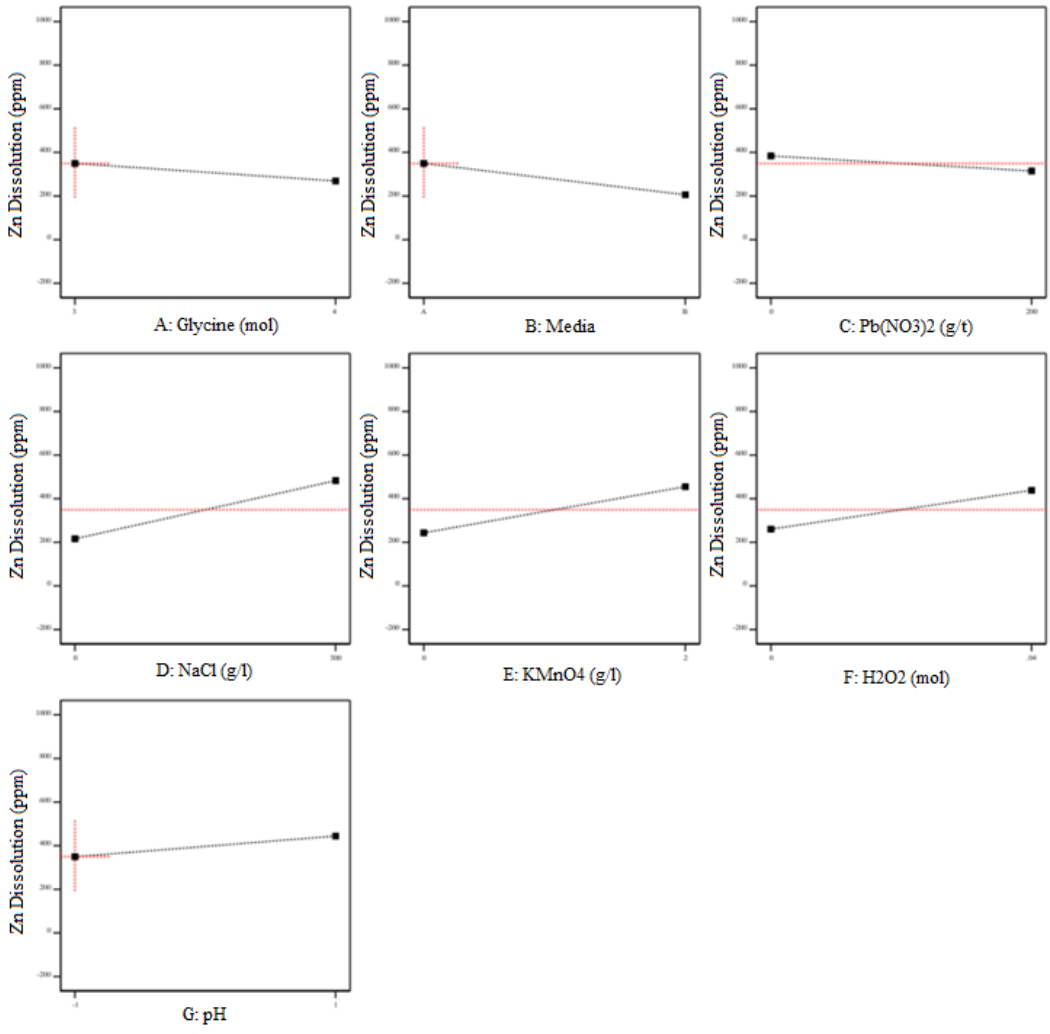

Figure 6. 2. The independent effects of parameters on the leaching process at glycine of 3 moles, pH 9, 35 °C, and 500 RPM.

This behaviour can be related to either increasing the thickness of the diffusion layer on the sphalerite particles or the dissolution of more hydroxide following the rejection of Zn from the solution until it returned to homeostasis [Reaction (6.1)]:

$$ZnS + 8OH^- + 3Gly^- = Zn((gly)_3^- + SO_4^{2-} + 4H_2O + 8e^- \quad (6.1)$$

NaOH and $Ca(OH)_2$ were used to modify the solution pH in this study. Figure 6.2 shows that when using NaOH to modify the pH, the sphalerite dissolution can reach about 400 ppm, while in the same condition with $Ca(OH)_2$ the sphalerite dissolution dropped to under 200 ppm. The fact that using $Ca(OH)_2$ causes precipitation of the gypsum formed from sulfates may be related to this. The use of lead nitrate, as can be seen from Figure 6.2, has a negative

effect on the sphalerite dissolution in alkaline glycine media. However, lead nitrate (at high concentration) can increase the sulfide minerals dissolution rate by reducing the inhibitory sulfide layer formed on the particles (Deschênes et al., 2000; Senanayake, 2008) but can also decrease the dissolution rate of sulfide phases by galvanic interactions between zinc and lead (Morey, 1998).

Sodium chloride, potassium permanganate, and hydrogen peroxide all have positive impacts on the sphalerite dissolution rate. Three factors were considered when choosing sodium chloride out of the three parameters for the rest of this study. Firstly, from a practical and economic point of view, using sodium chloride as the additive reagent in sphalerite dissolution is much cheaper and easier than using potassium permanganate and hydrogen peroxide. Secondly, the previous study has shown that using sodium chloride can facilitate the dissolution of silver and lead-bearing zinc resources. Finally, as can be seen from Figure 6.3, sodium chloride is the most effective parameter among the additives used for sphalerite dissolution in the rotating disc experiments.

Figure 6.3 shows that an increase in pH from 9 to 10.5 leads to an increase in the sphalerite dissolution. However, to confirm these results, a batch of tests under the same condition were performed in the pH range from 8 to 12 (Figure 6.4). In these experiments, for each pH value, one test was performed without sodium chloride and one was performed with 300 g/l of sodium chloride. Figure 6.4 illustrates that the same sphalerite dissolution can be achieved at pH 9 to 11 without using any additives; however when the sodium chloride was introduced to the medium, the maximum dissolution can be achieved at pH 10 compared to pH 9 and pH 11.

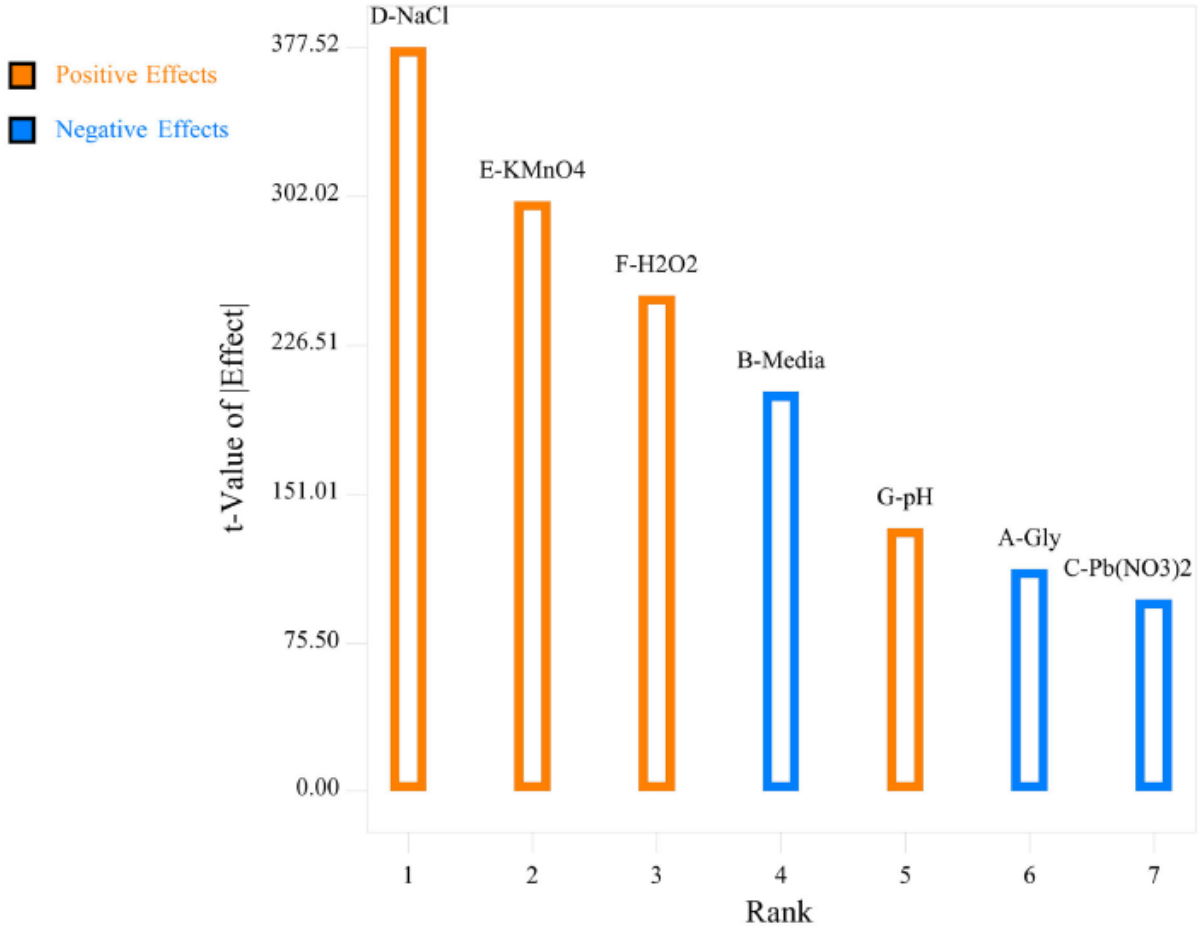

Figure 6. 3. The rank of investigated parameters in their design area.

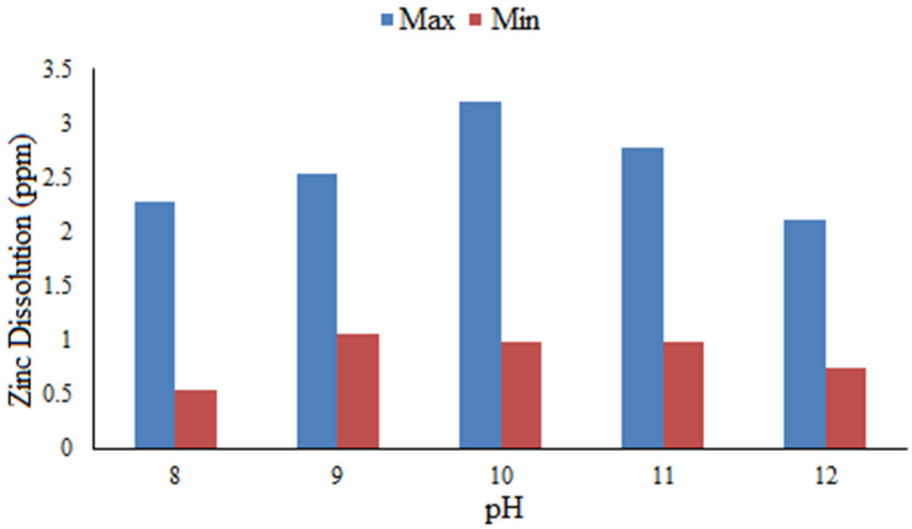

Figure 6. 4. Zinc dissolution as a function of pH without NaCl (in red) with 300 g/l NaCl (in blue) at a temperature of 35°C and stirring speed of 500 rpm, glycine concentration of 3 moles, pH was modified by NaOH.

6.2.2. Silver sulfide dissolution

For the modelling and optimization, RSM by I-Optimal experimental design was used. The I-Optimal algorithm was built to choose runs that minimize the integral of the prediction variance across the factor space. To determine the effects of the independent variables on the silver glycine leaching process, an I-Optimal design consisting of 25 runs was carried out (Table 6.2). The I-Optimal criteria are recommended to build response surface designs where the goal is to optimize the factor settings, requiring greater precision in the estimated model (Myers and Montgomery, 1995). This method can be more useful than conventional response surface methods such as the central composite design method since it is not necessary to conduct so many experiments and also it can tackle categorical factors included in the design of experiments (Azriel, 2014; Coetzer and Haines, 2017).

6.2.2.1. The effect of leaching parameters

Reproducibility

Figure 6.5 shows the results of the reproducibility of silver leaching in alkaline glycine solutions. As can be seen from Figure 6.5, the reproducibility of leaching under certain conditions was examined in some of the experiments which were repeated at least three times to ensure the data reproducibility. The experimental condition was 0.05 M glycine, 1 M NaCl, 25 °C, pH 10, and a rotation speed of 500 rpm. The precision was determined to be less than ± 5%.

Table 6. 2. Experimental design and outputs.

test No.	**Parameters**			**Ag dissolved (ppm)**	
	Glycine Conc. (Mole)	NaCl Conc. (Mole)	pH	experimental	Predicted
1	0	0	9	0	-0.041
2	1	0	9	0.04	0.06
3	2	0	9	0.05	0.034
4	0	2	9	0.15	0.14
5	1	2	9	0.41	0.38
6	1	2	9	0.41	0.38
7	0	3	9	0.32	0.32
8	2	3	9	0.61	0.71
9	0.5	1	10	0.2	0.21
10	0.5	1	10	0.2	0.21
11	0.5	1	10	0.21	0.21
12	2	1	10	0.26	0.28
13	2	1	10	0.27	0.28

14	0	3	10	0.38	0.4
15	1	3	10	0.74	0.71
16	2	3	10	0.86	0.79
17	1	0	11	0.16	0.16
18	1	0	11	0.15	0.16
19	0	1	11	0.11	0.13
20	0.5	0	11.5	0.12	0.13
21	0	1	11.5	0.1	0.12
22	2	1	11.5	0.33	0.3
23	0	3	11.5	0.44	0.42
24	1	3	11.5	0.79	0.72
25	1	3	11.5	0.64	0.72

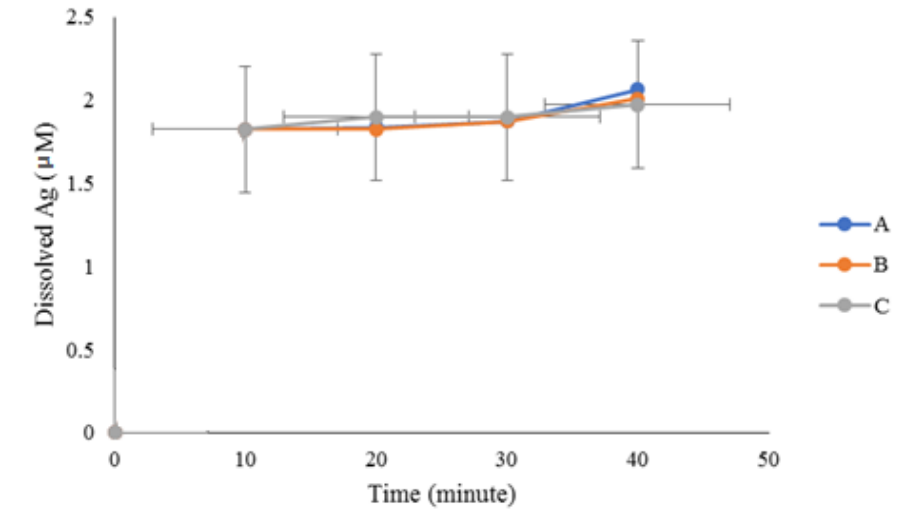

Figure 6. 5. Reproducibility of silver leaching at glycine of 0.05 mole, sodium chloride of 1 mole, pH 10, 25 °, and 500 RPM, N2.

Rotation speed

According to the Levich equation (6.2), the dissolution rate as a function of the square root of rotating speed should be linear under diffusion-controlled conditions. As can be seen from Figure 6.6, the leaching rate of silver sulfide disc versus the square root of rotation speed shows a nearly linear relationship; therefore, under the experimental conditions, it is indicated that the alkaline glycine leaching of silver sulfide is a diffusion-controlled process.

$$\frac{1}{A}\frac{dn}{dt} = J = 0.62 D_o^{2/3} \vartheta^{-1/6} \omega^{1/2} C_o \qquad (6.2)$$

where D_a (m^2/s) is the diffusivity, υ (m^2/s) is the viscosity, ω (rad/s) is angular velocity of the disk, and t C_a (mol/m^3) is the concentration.

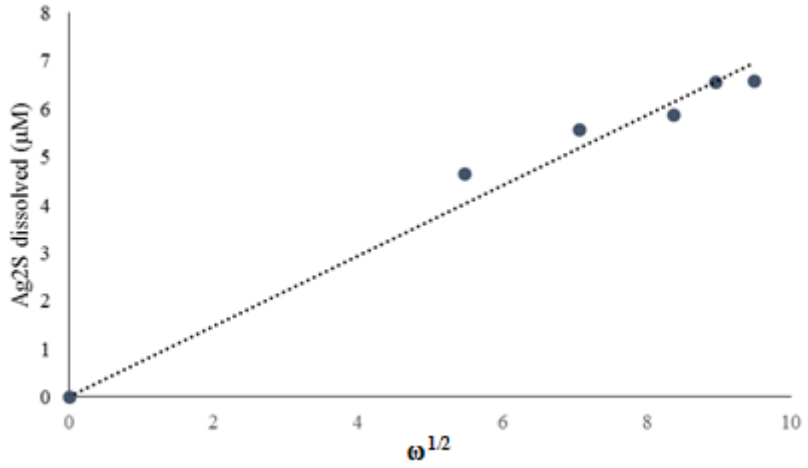

Figure 6. 6. Effect of rotating speed on the leaching rate of silver sulphide disc at glycine of 0.05 mole, sodium chloride of 1 mole, pH 10, 25 °C, N2.

Glycine concentration

Figure 6.7 illustrates the effect of changes in the glycine concentration on the silver extraction from Ag_2S leaching. This chart shows that by increasing the glycine concentration, the Ag_2S dissolution increases. It can be generally reported that the amount of silver dissolution increases in direct dependence on the concentration of glycine in the alkaline glycine solution.

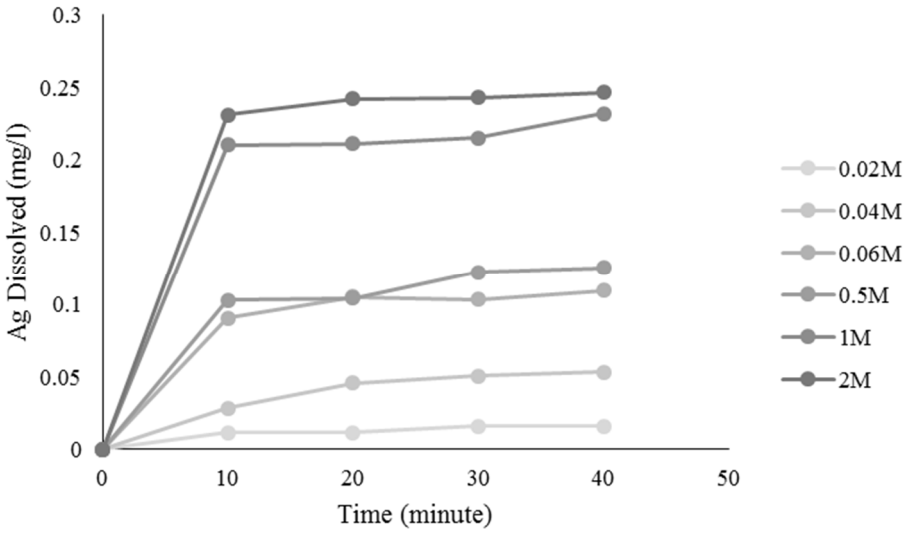

Figure 6. 7. The effect of glycine concentration on the leaching process in the absence of sodium chloride, pH 10, 25 °, and 500 RPM.

pH

The effect of the pH of the leaching solution on silver sulfide dissolution is shown in Figure 6.8. As can be seen from this figure, increasing the leaching pH increases the silver dissolution. However, it is clear that there are no significant differences between pH values of 10, 11, and 11.5 after 40 min of leaching.

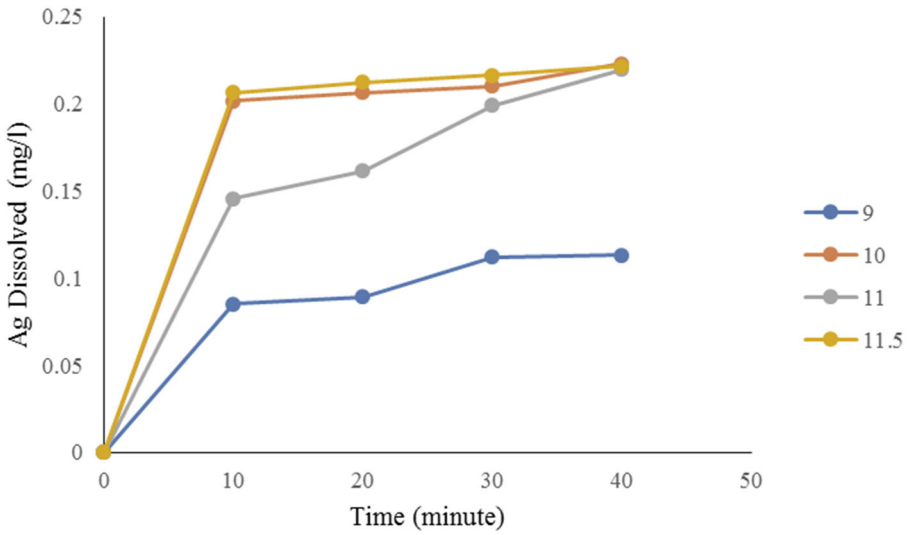

Figure 6. 8. The effect of pH on the leaching process at glycine of 0.5 moles, sodium chloride of 1 mole, 25 °, and 500 RPM, N2.

Sodium chloride concentration

Depending on the lixiviant system, most sulfide minerals require mild oxidation to convert the sulfide sulfur to either S^0, thiosulfate sulphite or sulfate while the metal ion is released to be complexed. However, by adding an external variable to the initial working factors, the obtained voltammogram should show new peaks and changes, and thus in this study, to increase the solution redox potential, the effect of chloride ions on the redox potential has been conducted.

In Figure 6.9, the dashed line shows the CV of the silver sulfide-CPE in 1 M glycine solution at pH 10 in the cathodic direction, the solid line shows the CV related to the anodic direction, and the blue line depicts the CV when 1 M sodium chloride was added to the dissolution medium.

It is clear from the data shown in Figure 6.9 that chloride ions have a significant effect on the electrochemical behaviour of the silver sulfide dissolution in alkaline glycine medium. In particular, the anodic peaks are more than 15 times as high in the presence of chloride ions. This factor, therefore, can accelerate the oxidation and reduction of silver sulfide in alkaline

glycine solutions. These results demonstrate that chloride ions improve the dissolution rate of silver sulfide in alkaline glycine medium and there is little need for more aggressive conditions such as high-pressure leaching. They also indicate that saline solutions like seawater may be used synergistically to enhance silver sulfide leaching, which is essential for deposits located in the proximity of the ocean or salt lakes.

Figure 6.10 shows the effect of adding sodium chloride on silver sulfide leaching in alkaline glycine medium. As can be seen from this figure, by adding sodium chloride to the leaching medium, the silver sulfide dissolution has been substantially increased. This kind of behaviour can be due to an interaction effect between the independent parameters, including sodium chloride and glycine, which is discussed further in the section on interactions.

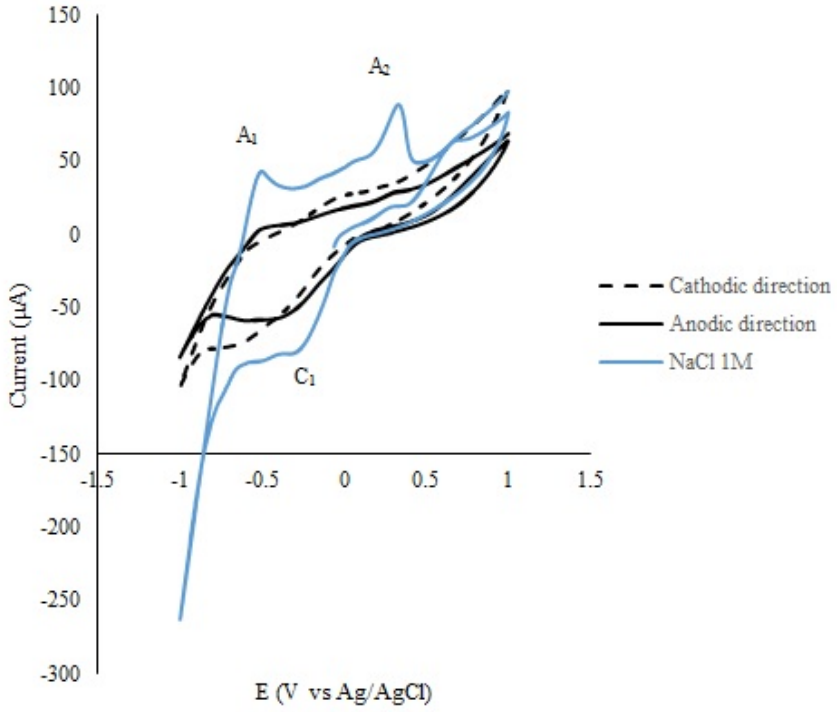

Figure 6. 9. The effect of sodium chloride on the silver sulphide-CPE dissolution in 1M glycine, pH 10, and a sweep rate of 20 mVs-1.

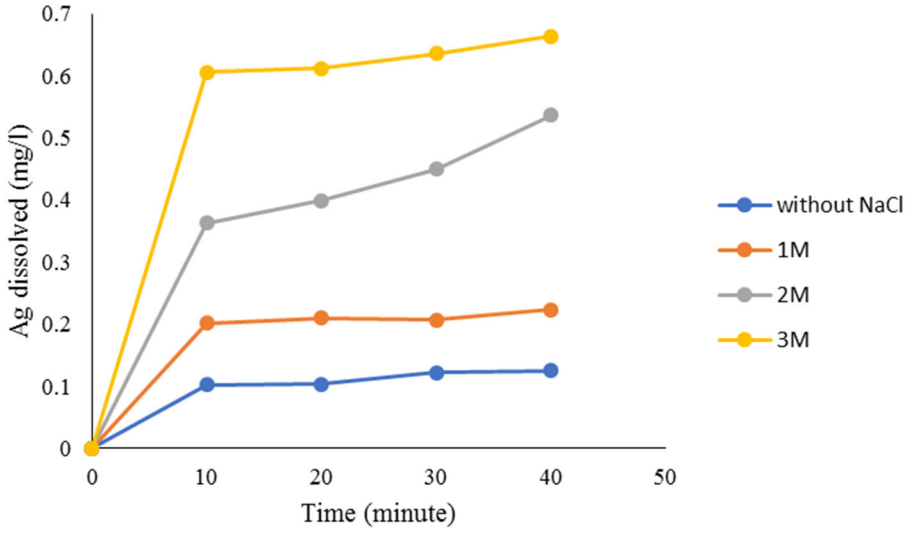

Figure 6. 10. The effect of sodium chloride concentration on the leaching process at glycine of 0.5 moles, pH 10, 25 °, and 500 RPM, N2.

Temperature

The effect of temperature on silver sulfide leaching in an alkaline glycine medium is shown in Figure 6.11. It was found that an increase in temperature from 25 to 35 °C increased the silver leaching, which then dropped gradually between 35 and 50 °C.

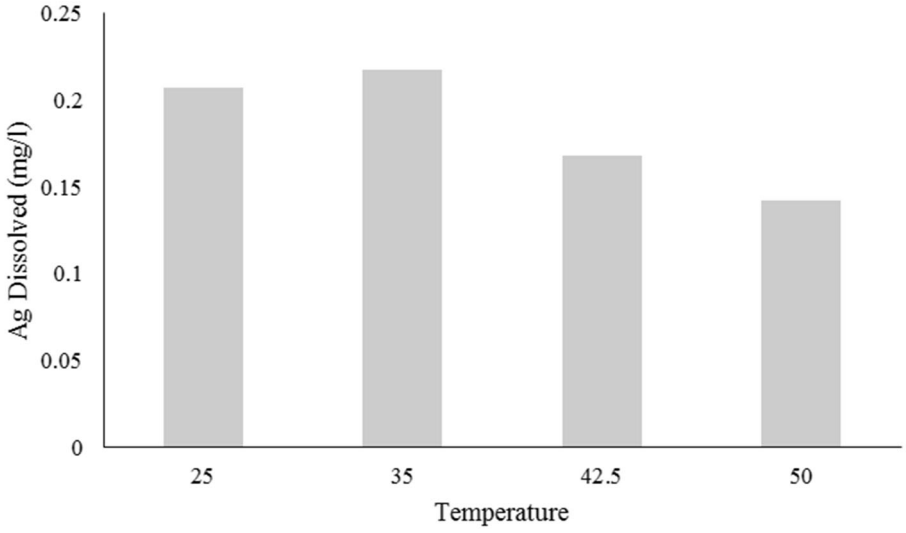

Figure 6. 11. The effect of temperature on the leaching process at glycine of 0.05 mole, sodium chloride of 1 mole, pH 10, and 500 RPM, N_2.

6.2.2.2. Modelling and optimization

Experimental design considerations

After investigating the effect of different parameters on silver leaching by the glycine process, the independent parameters were screened and the most effective parameters were selected for modelling and optimization. The temperature chosen for the rest of the experiments was 35 °C as the maximum silver recovery was achieved at this temperature.

Model fitting

The effects of the independent variables on the alkaline glycine process were investigated using the quadratic polynomial model, which was estimated based on the experimental results with the respective coefficients as given in Equation (6.3):

$$X = 0.34 + 0.12A + 0.26B + 0.047C + 0.078AB - 0.056A^2 + 0.064B^2 - 0.044C^2 \quad (6.3)$$

where X is the dissolution of silver in the alkaline glycine process.

Table 6. 3. Analysis of Variance of the model.

Source	SS	DF	MS	F-Value	p-Value	
Model	1.39	7	0.2	96.72	<0.0001	Significant
A-Gly Conc.	0.18	1	0.18	87.4	<0.0001	
B-NaCl Conc.	0.95	1	0.95	464.15	<0.0001	
C-pH	0.032	1	0.032	15.7	0.001	
AB	0.049	1	0.049	23.63	0.0001	
A^2	0.014	1	0.014	6.85	0.018	
B^2	0.018	1	0.018	8.64	0.0092	
C^2	8.62E-03	1	8.26E-03	4.2	5.63E-02	
Residual	0.035	17	2.06E-03			
Lack of Fit	0.024	11	2.14E-03	1.12	0.4661	not significant
Pure Error	0.011	6	1.90E-03			
Cor Total	1.43	24				
$F_{95\%}(7,17)$ = 2.61						

The analysis of variance based on ANOVA for this regression model is listed in Table 6.3. Glycine concentration, sodium chloride concentration, and pH were placed in the model. It can be seen from Table 5 that the model F-value of 96.72 implies that the model is significant (according to $F_{critical}$, a value higher than 2.61 is considered desirable). There is only a 0.01% chance that a model F-value could occur due to noise. Values of Prob > F less than 0.0500 indicate that model terms are significant. In this case, A, B, C, AB, A^2, B^2, and C^2 are

significant model terms. The regression coefficients of R^2 and R^2_{adj} for this model were found to be 0.9755 and 0.9654, respectively, indicating a good fit between the regression model and the experimental values. To check the adequacy of the model, plots of the actual and predicted silver dissolution are shown in Figure 6.12. The actual recovery is the measured value for a particular run, and the predicted value has been evaluated for that run from the model.

The Box-Cox power transformation plays a crucial role that may help normalize the data to determine the best model for describing the process. The Box-Cox plot is a tool to determine the most appropriate power transformation to apply to the data response. Most data transformations can be described by the following power function (Sakia, 1992; Mirazimi et al., 2013):

$$\delta=f(\mu\hat{}\omega) \qquad (6.4)$$

where δ is the standard deviation, μ is the mean, and ω is the power. If the standard deviation associated with observation is proportional to the mean raised to the power, then transforming the observation by the power λ (λ = 1 – α) gives a scale which satisfies the equal variance requirement of the statistical model. The Box-Cox plot for this model is shown in Figure 6.13. According to Figure 6.13, the recommended transformation power is a square root.

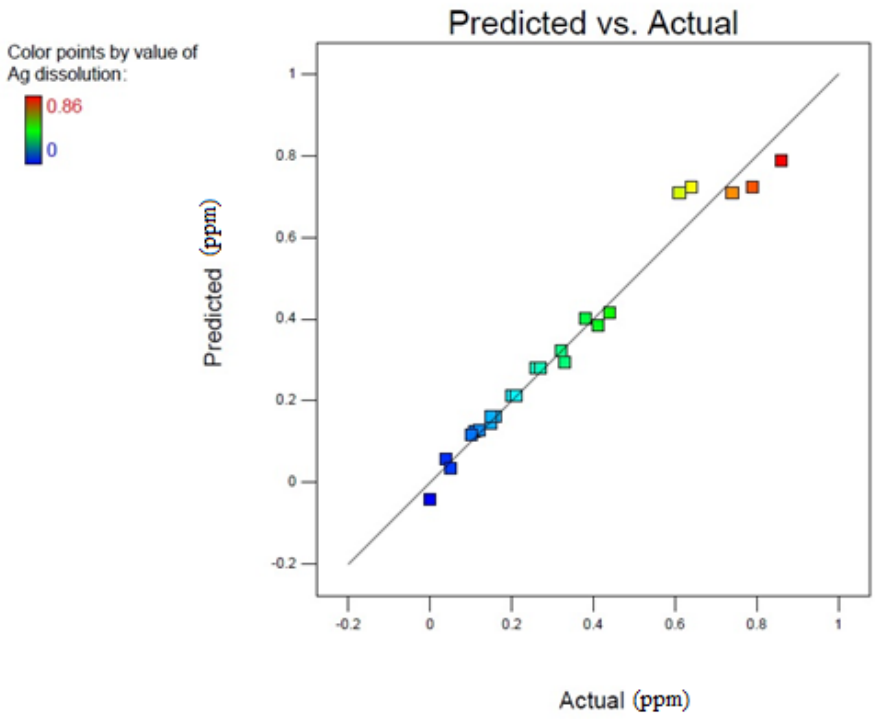

Figure 6. 12. Plot for predicted vs Actual responses (Actual from experiments and Predicted from the model).

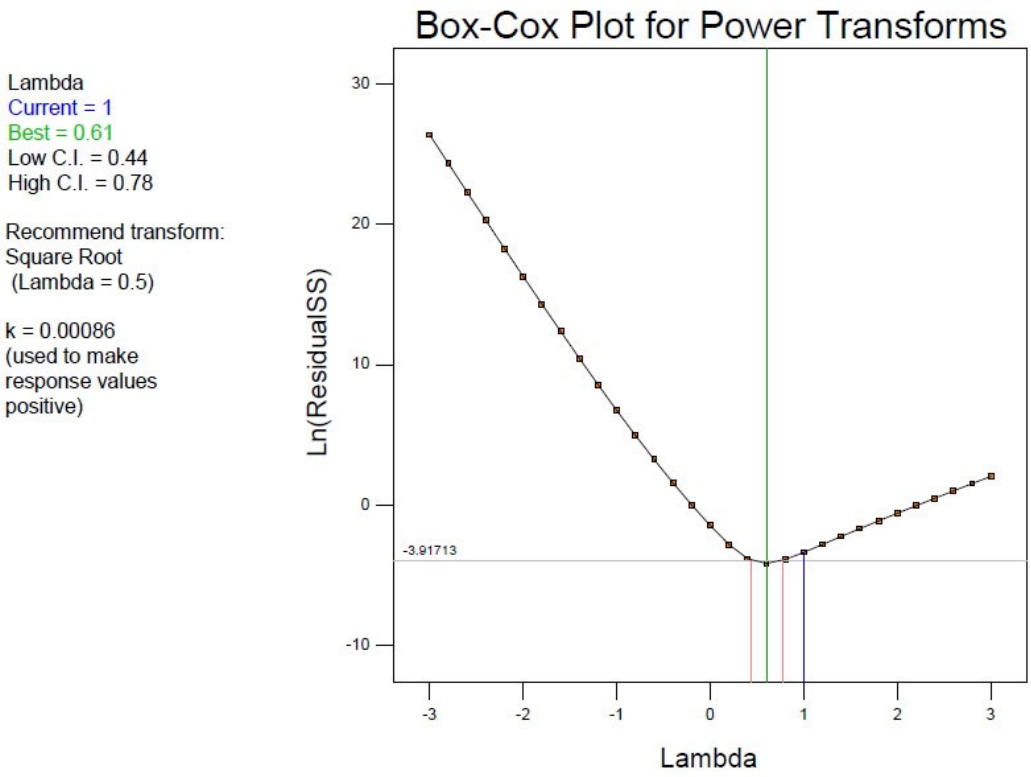

Figure 6. 13. The Box-Cox plot for power transform of the model.

The last modification of the model is to apply the k plot to make the response values positive. Finally, after applying the transformation, the response for the quadratic polynomials is described as follows:

$$X^{0.5}=+0.59+0.11*A+0.26*B+0.058*C-0.031*BC-0.082*A^2-0.046*C^2 \quad (6.5)$$

6.2.2.3. Interaction between glycine and sodium chloride

The interaction between glycine and sodium chloride is shown in Figure 6.14a and b. In Figure 6.14a, the least significant difference (LSD) bars with a confidence level of 95% have been considered for each parameter (dotted lines). As can be seen, in the absence of sodium chloride, increasing the glycine concentration increases the silver dissolution gradually, whereas in the presence of a high sodium chloride concentration in the solution, increasing the glycine concentration increases the silver dissolution significantly. Figure 6.14b shows the contour diagram for this interaction. The figure shows that the sodium chloride concentration has a substantial positive effect on the process to obtain a high silver dissolution rate.

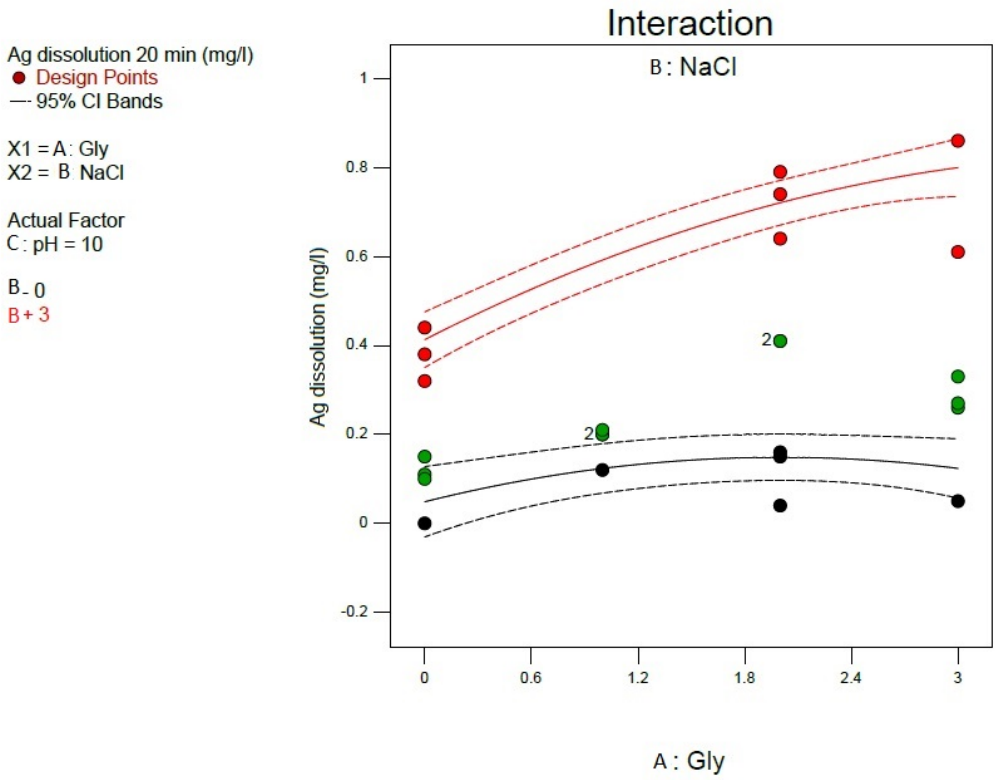

Figure 6. 14a. The 2D interaction plot for glycine and sodium concentration at, pH 10, and 500 RPM, N2.

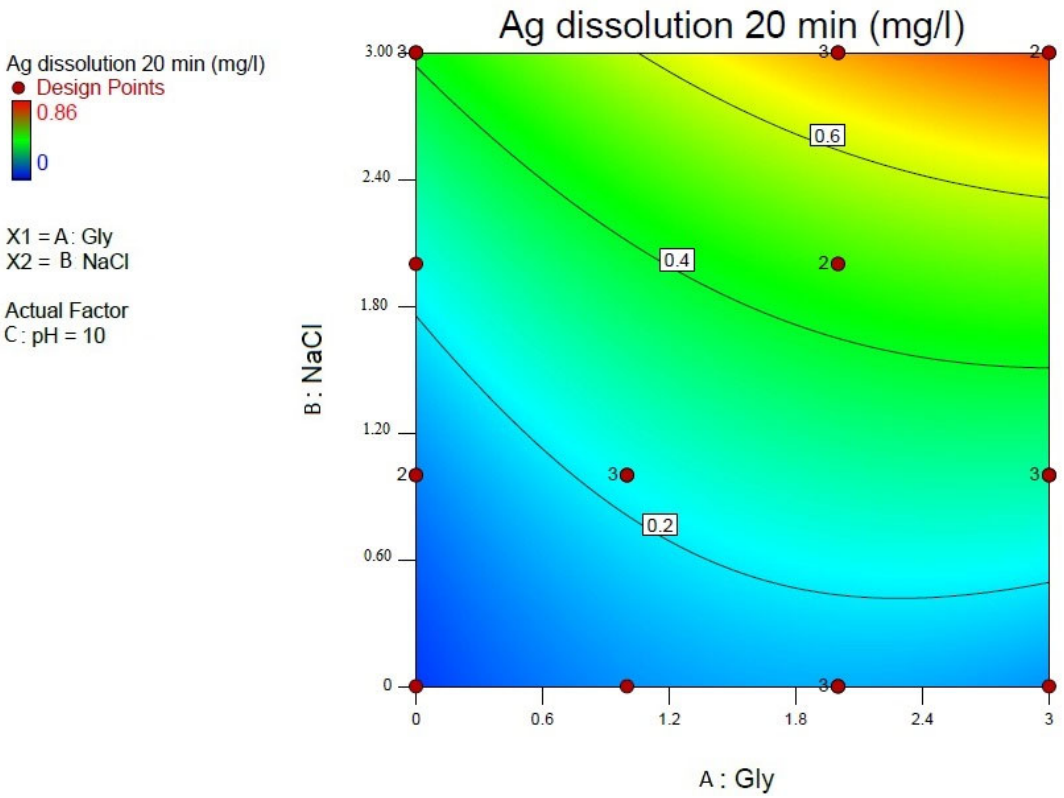

Figure 6. 14b. The contribution plot for glycine and sodium concentration at, pH 10, and 500 RPM, N2.

6.2.2.4. Optimization

According to the parameters of the model, the process was optimized using DX10 software, and 30 responses are presented as the best solution for the optimization model. An experiment was carried out using the parameters suggested to test the validity of the optimized conditions specified by the model. The conditions used in the confirmation experiment were as follows: a glycine concentration of 2 moles, a sodium chloride concentration of 3 moles, 35 °C, pH 10, and 500 rpm for a leaching period of 20 min. The predicted value was 0.78 mg/l of dissolved silver and the actual value obtained was 0.75 mg/l, which is reasonably acceptable. Figure 6.11 illustrates the application of the optimized conditions at different oxygen dosages. As shown in Figure 6.15, the amount of dissolved silver shows an increase on introducing oxygen into the leaching media. The atmospheric leaching trend shows that the process is oxygen-dependent since the amount of oxygen decreased during the leaching time. On the other hand, by purging the pure oxygen into the solution, the silver dissolution rises marginally.

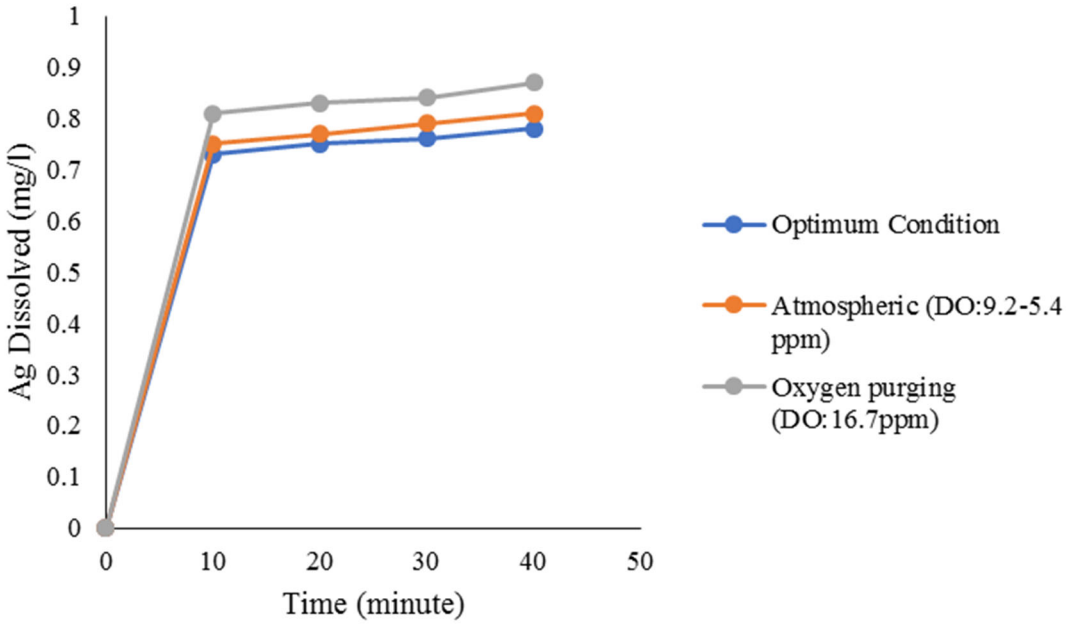

Figure 6. 15. Confirmation of optimum condition and effect of oxygen on the leaching process.

6.3. Agitated reactor tests

In these experiments, the sphalerite concentrate was used as the feeding material. The glycine concentration, pH, and Cu^{2+} ion concentration (as cupric sulfate) were chosen as the independent variables in these experiments (Table 3.5). In this section, the sphalerite

dissolution in the alkaline glycine medium was modelled and optimized. After that, the obtained optimum condition was used for the kinetics study at different temperatures and levels of dissolved oxygen. Table 6.4 shows the experimental design and outputs. In Table 6.5, the output for zinc is the dissolved zinc in ppm, while the outputs for copper and lead are their recovery percentages. Furthermore, the negative numbers shown for copper recovery represent the precipitated portions of copper used as the reagent for each test. In these experiments, the temperature was constant at 35 °C, the stirring speed was 500 rpm, the pH was adjusted by NaOH (±0.15), and sampling was done at 1, 2, 4, 6, and 24 h. Table 6.4 shows the sphalerite dissolution as a function of leaching time. As can be seen from Table 6.4, for most of the experiments, the dissolution trend fluctuated at an earlier dissolution time, and therefore the results at 24 h were chosen for modelling and optimization since they had a clearer trend and separation. Table 6. 4 shows the zinc leaching as a function of leaching time for the optimization experiments.

6.3.1. Model fitting

The effects of the independent variables on the dissolution of sphalerite in the alkaline glycine process were investigated using the quadratic polynomial model, which was estimated based on experimental results with the respective coefficients as given in Equation (6.6):

$$X = 142.69 + 33.79A + 32.47B + 10.13AB + 2.47B^2 \quad (6.6)$$

where X is the sphalerite dissolution in the alkaline glycine process.

.

Table 6. 4. Zinc recovery at temperature of 35°C.

No.	Zn Rec. 1 hr	Zn Rec. 2 hr	Zn Rec 4 hrs	Zn Rec. 6 hrs	Zn Rec. 24 hrs
	(%)	(%)	(%)	(%)	(%)
1	7.01	7.56	8.47	7.93	12.10
2	6.94	8.65	12.91	11.66	21.59
3	6.90	6.95	8.25	7.46	12.18
4	5.06	6.02	7.39	7.81	14.28
5	5.84	6.69	9.51	42.14	35.62
6	6.79	6.49	6.65	15.04	15.88
7	4.52	5.64	7.18	5.80	10.94
8	4.65	6.87	7.84	7.42	10.93
9	4.65	5.24	6.26	6.17	10.60
10	5.17	5.34	6.70	6.52	14.80
11	5.02	5.35	6.04	6.66	10.91
12	4.97	5.50	6.38	7.14	13.70
13	4.60	4.86	5.73	6.49	11.52
14	3.50	6.09	6.09	6.09	15.58
15	4.82	5.37	5.37	5.37	13.92
16	6.19	4.16	5.26	7.52	14.04
17	6.05	4.36	5.19	9.40	17.80
18	7.35	5.43	8.67	10.94	20.35
19	3.05	3.46	5.42	6.18	15.55
20	4.17	4.07	4.25	5.01	8.51
21	5.44	4.84	5.05	5.81	9.67
22	5.53	5.71	7.10	7.86	11.65
23	4.37	5.05	5.75	6.51	8.78
24	4.33	4.57	5.05	5.81	7.48

Table 6. 5. Experimental design and outputs.

Run	Parameters			Responses at 24hrs		
	pH	Glycine (g)	Cu^{2+}	Zn Diss. ppm	Cu Rec. %	Pb Rec. %
1	10	3.61	0.216	127.8	-31.83	2.08
2	11	5.25	0.393	228.0	-44.11	2.89
3	11	1.97	0.039	128.7	98.00	4.99
4	10.7	1.97	0.393	150.8	-46.21	0.68
5	10.6	5.25	0.039	237.1	63.13	6.56
6	11	3.67	0.209	167.7	-54.03	2.97
7	9	3.36	0.393	115.5	-99.16	5.99
8	10	3.56	0.223	115.4	-14.47	5.61
9	10.4	3.5	0.039	112.0	74.46	3.63
10	9.7	5.25	0.393	156.3	7.41	6.86
11	10	3.56	0.223	115.2	-15.17	6.42
12	9.7	5.25	0.393	144.6	-62.46	7.94
13	9	3.84	0.039	121.7	74.46	4.64
14	10	3.61	0.216	164.5	-3.96	2.78
15	9	5.25	0.192	147.0	-3.53	8.5
16	9	3.61	0.216	148.2	-7.06	6.29
17	10	3.56	0.223	188.0	18.35	4.55
18	10.6	5.25	0.039	214.9	79.40	2.97
19	10.9	1.99	0.218	164.2	3.18	0.99
20	9.7	1.97	0.039	89.8	74.81	2.64
21	9.6	1.97	0.393	102.1	-37.05	1.82
22	9.6	5.25	0.039	123.0	96.34	6.56
23	9	1.97	0.241	92.7	-64.93	1.41
24	9.7	1.97	0.039	79.0	73.05	2.25

Table 6. 6. Analysis of Variance of the model.

Source	SS	DF	MS	F-Value	p-Value	
Model	245.66	4	61.42	17.83	<0.0001	significant
A-pH	98.59	1	98.59	28.62	<0.0001	
B-Glycine Conc.	117.94	1	117.94	34.23	<0.0001	
AB	10.40	1	10.40	3.02	0.098	
B^2	39.10	1	39.10	11.35	0.0032	
Residual	65.46	19	3.45			
Lack of Fit	58.18	13	4.48	3.69	0.0594	not significant
Pure Error	7.29	6	1.21			
Cor Total	311.13	23				
$F_{critical}(4,19)=2.9$						

The analysis of variance based on ANOVA for this regression model is shown in Table 6. 6. Glycine concentration and pH were placed in the model. Sodium concentration was not placed in the model since it has an insignificant effect on the dissolution of zinc in the glycine medium. However sodium chloride has a strong positive effect on galena and silver dissolution. It is seen from Table 6. 6 that the model F-value of 17.83 implies that the model is significant (a value of $F_{critical}$ higher than 2.9 is considered desirable). There is only a 0.02% chance that such a model F-value could occur due to noise. Values of Prob > F less than 0.0500 indicate that the model terms are significant. In this case, A, B, and B^2 are significant model terms. The regression coefficients R^2 and R^2_{adj} for this model were found to be 0.8214 and 0.75.84, respectively, indicating a good fit between the regression model and the experimental values (StatEase, 2019).

6.3.2. The interaction between glycine and pH

The interaction between glycine and pH is shown in Figure 6.16. As can be seen from Figure 6.16, at the lower pH, increasing the glycine concentration increases the zinc dissolution gradually, whereas at the higher pH, increasing the glycine concentration increases the silver dissolution significantly. Figure 6.16 shows the 3D surface diagram for this interaction. The figure shows that to achieve a high zinc dissolution rate in the alkaline glycine process, the higher alkaline pH has a substantial positive effect on the process.

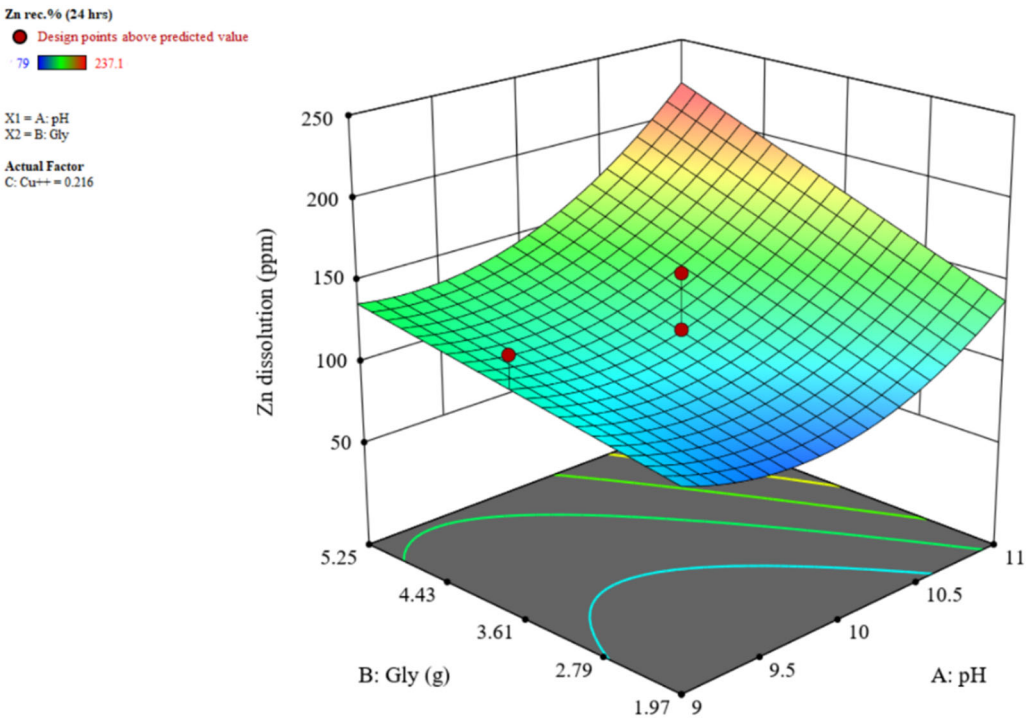

Figure 6. 16. The 3D surface diagram for interaction between glycine and pH 10 on zinc dissolution in the alkaline glycine media.

6.3.3. Optimization and effect of sodium chloride

According to the parameters of the model, the process was optimized using DX10 software, and 30 responses are presented as the best solution for the optimization model. An experiment was carried out using the parameters suggested to test the validity of the optimized condition specified by the model. The condition used in the confirmation experiment was as follows: a glycine concentration of 5.25 g, a cupric ion concentration of 10 mg/l, a sphalerite concentration of 1 g in 500 ml of solution at 35 °C, a pH of 10.7, and stirring speed of 500 rpm for a leaching period of 48 h. The predicted value was 204.44 mg/l of dissolved zinc and the actual value obtained was 210.29 mg/l, which is reasonably acceptable. Figure 6.17 illustrates the application of the optimized condition and compares the results for the dissolution of metals from the sphalerite concentrate in the presence of sodium chloride.

The effect of adding sodium chloride to the optimum condition on the sphalerite dissolution is shown in Figure 6.17a. As can be seen from this figure, adding 100 g/l sodium chloride to the solution has no significant effects on the sphalerite dissolution, whereas on increasing the amount of sodium chloride added to 200 g/l, the amount of dissolved zinc decreases in the

long run. In fact, at alkaline pH, the glycine is a glycinate anion. As the the chloride concentration is increased to high concentrations, the ionic strength of the solution becomes very high and the precipitation of zinc chloride hydroxide monohydrate becomes possible. [Zn5(OH)8Cl2.H2O]. This compound is insoluble in water, and is called *Simonkolleite* (Srivastava, 1967). However, the most important usage of sodium chloride is related to the dissolution of silver and galena, where, in the presence of excessive chloride ions, lead chloride and silver chloride can be redissolved again (Figures 6.18b and 6.18c).

With the addition of sodium chloride under the optimum condition, a high extraction rate of silver (above 92%) can be reached (Figure 6.17b). Figure 6.17b shows that there is no significant difference between the amounts of sodium chloride added. However, the extraction rate can reach more than 80 wt.% in 6 h shorter in case of using 100 g/l sodium chloride. It can be seen from Figure 6.17c that sodium chloride has a positive effect on galena dissolution, with a higher extraction rate being achieved when using 200 g/l sodium chloride and lower rates taking place under the optimum conditions without sodium chloride. The other striking feature of Figure 6.17c is that, in each case, the maximum recovery is obtained in the first hour of leaching and after that, the recovery decreases significantly. This can be related to the formation of a weak lead compound which can be easily broken and precipitated ($Pb(gly)_2$ log K=8.66) (Kiss et al., 1991). The copper dissolution response to the presence of sodium chloride is the same as the sphalerite response (Figure 6.17d). Therefore, the addition of 100 g/l of sodium chloride to the optimum condition was chosen for the rest of the experiments in

this study.

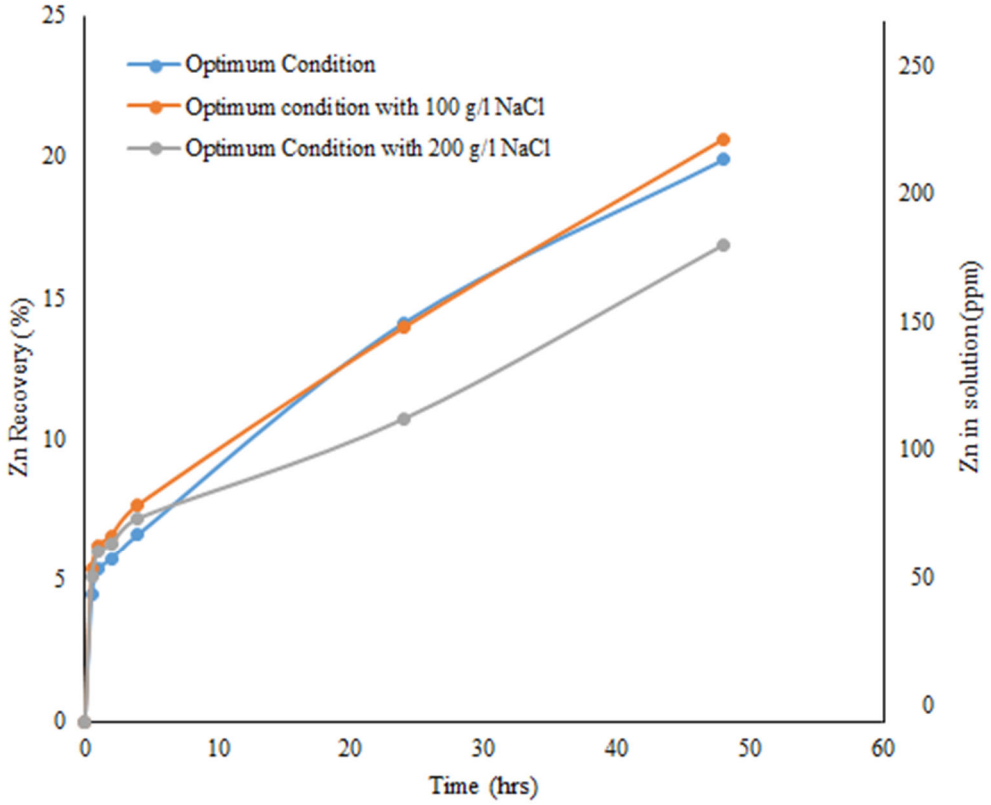

Figure 6. 17 a. Effect of adding sodium chloride to the optimum condition on the sphalerite dissolution in the alkaline glycine solution.

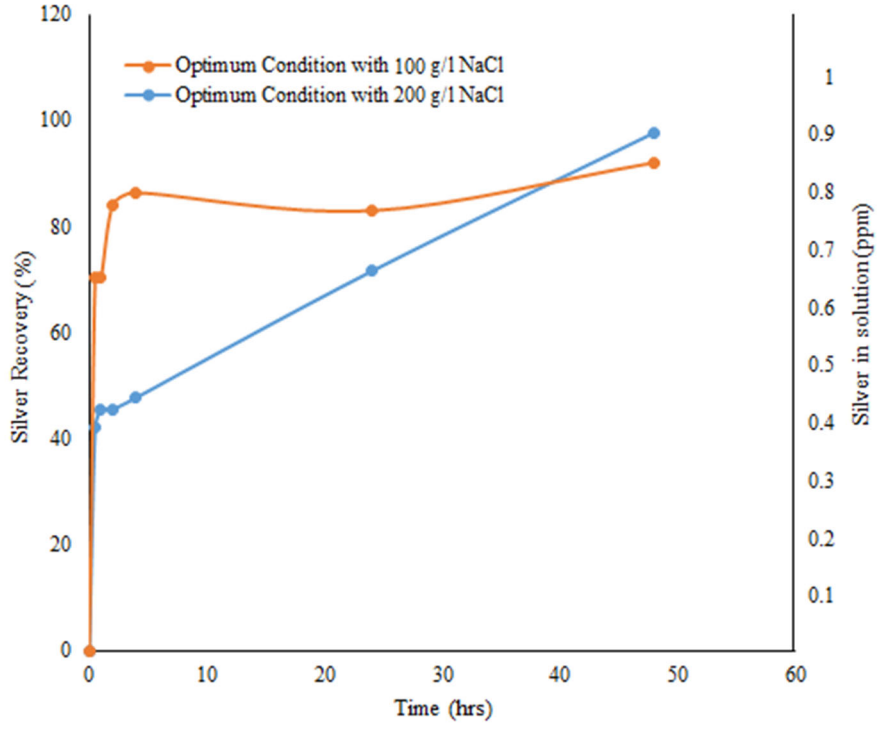

Figure 6. 17 b. Effect of adding sodium chloride on the silver dissolution in the alkaline glycine solution.

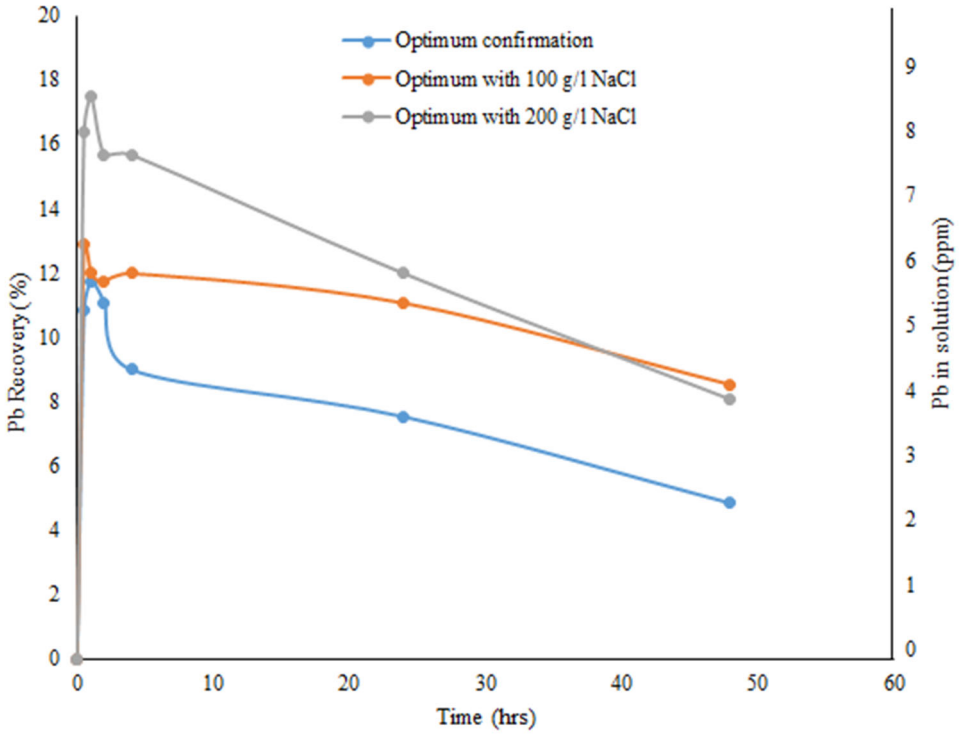

Figure 6. 17 c. Effect of adding sodium chloride on the galena dissolution in the alkaline glycine solution.

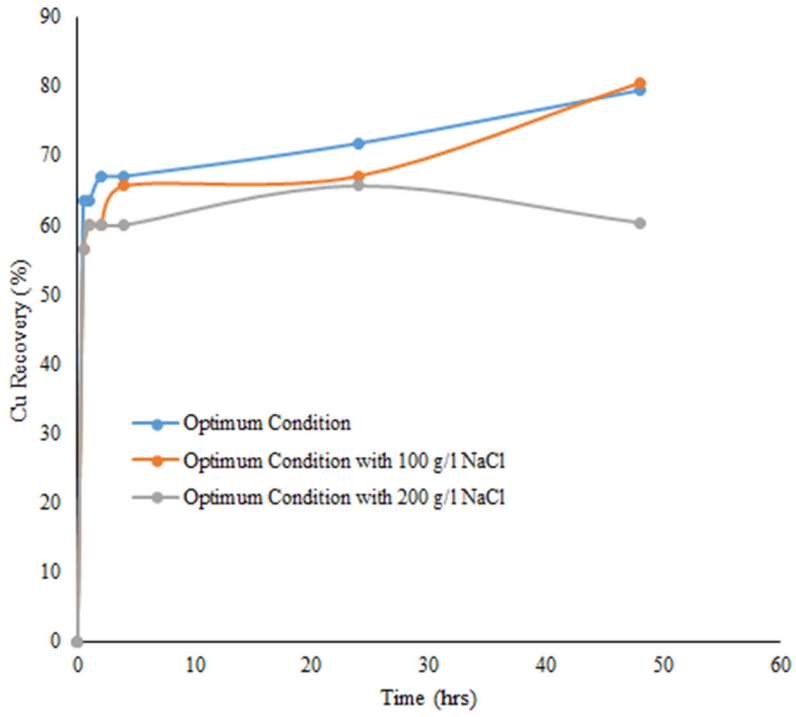

Figure 6. 17 d. Effect of adding sodium chloride to the optimum condition on the cupper dissolution in the alkaline glycine solution.

6.4. Bottle roll experiments

To investigate the condition and possibility of direct leaching of zinc in alkaline glycine media, bottle roll tests were carried out on two different materials, namely sphalerite concentrate and zinc oxide residues. All tests were carried out in a horizontal rotating incubator with a constant temperature of 35 °C and a solid/liquid ratio of 10 wt.%. The effects of excessive glycine concentration on the alkaline glycine process for direct leaching of sphalerite are shown in Figure 6.18. Figure 6.18 shows that by increasing the glycine/total metals concentration from 3 to 15 moles, the recovery of zinc increases by approximately 5 wt%, whereas decreasing the particle size results in a greater increase in the recovery of zinc (Figure 6.19). As can be seen from Figure 6.19, with the particle size distribution of >60 µm, only 14.81% of the zinc can be leached in 9 days, while at the same time for the particle size distribution of >10 µm, this value is 34 .24%.

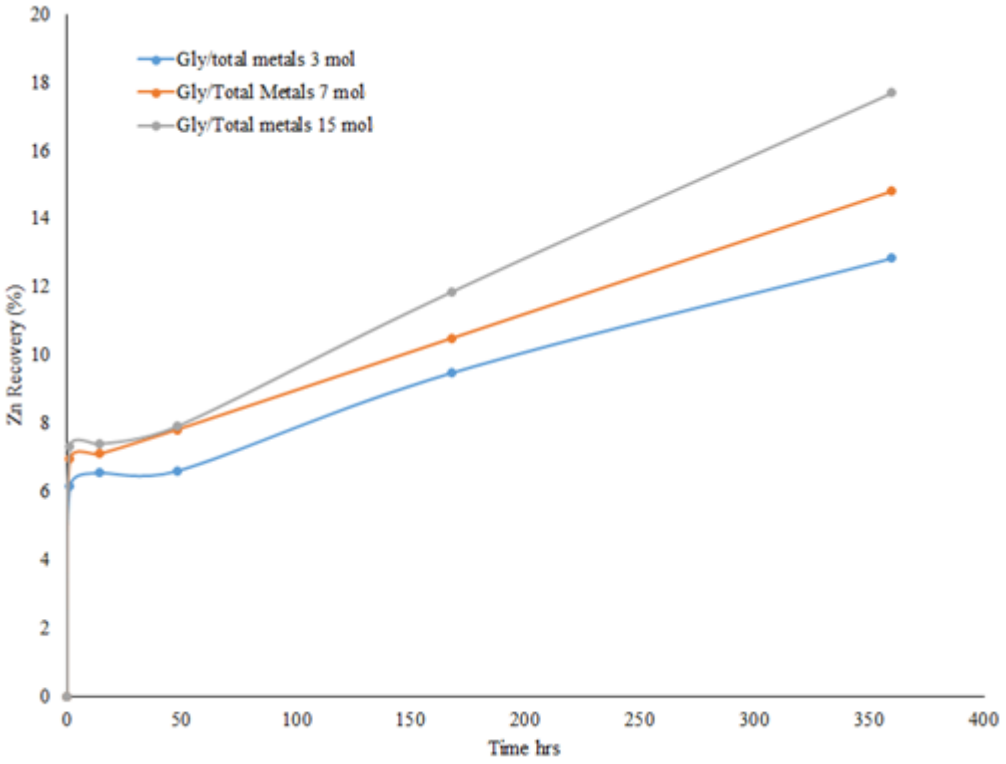

Figure 6. 18. The effect of excessive glycine concentration on the direct leaching of sphalerite in the alkaline glycine process at 35°C and 10 wt. % solid/liquid ratio.

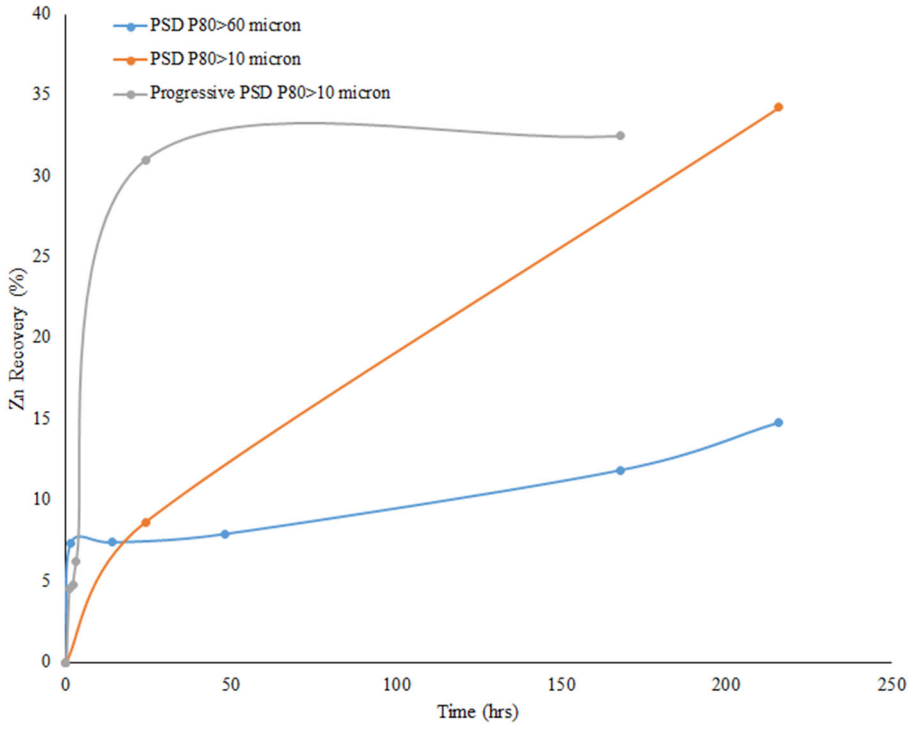

Figure 6. 19. The effect of particle size on the direct leaching of sphalerite in the alkaline glycine process at 35°C and 10 wt. % solid/liquid ratio.

6.4.1. ZnO dissolution

Compared with zinc sulfide, under the same working conditions, zinc extraction from zinc oxide can reach higher extraction rates (Figure 6.20). Figure 6.20 illustrates that under the same condition, a zinc oxide recovery of about 60% can be reached in 15 days. Furthermore, instead of adding the whole amount of glycine at the start of the reaction, it is shown that by introducing the glycine during the leaching time it is possible to increase the rate of the reaction and to reach a higher zinc recovery. The amount of glycine has been added proportionally to the leaching bottle for the first 6 h. Zinc dissolution behaviour in alkaline glycine solutions for znic sulphides and znic oxides is shown in Figure 6.19 and Figure 6.20 respectively.

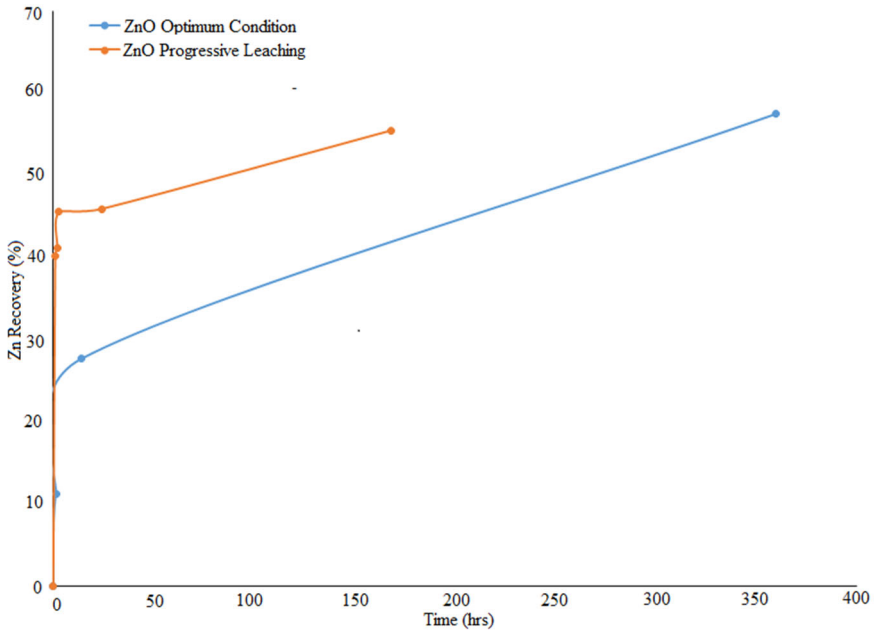

Figure 6. 20. The ZnO dissolution as a response to the obtained optimum condition in the alkaline glycine process at 35°C and 10 wt. % solid/liquid ratio.

CHAPTER 7: KINETICS STUDY

This chapter investigates the kinetics controlling step of the reaction of zinc, silver, and copper under the optimum conditions found in the previous chapter.

7.1. Chapter objective

This chapter covers the kinetics modelling of the dissolution of sphalerite along with silver and copper contained in the sphalerite concentrate. The complexity of galena dissolution means that no appropriate kinetics modelling is available and further studies are required. This chapter aims to identify the dissolution kinetics of the abovementioned metals under the optimum condition found in Chapter 6.

7.2. Dissolution kinetics in oxygenated alkaline glycine media

Figures 7.1a–d illustrate the kinetics trends for the dissolution of zinc, lead, silver, and copper under the optimum condition in the oxygenated alkaline glycine media, respectively. A constant solid/liquid ratio, 2 g/l of the fined-grained sphalerite concentrate (>10 μm), was used for each test while a specific amount of dissolved oxygen was maintained for each temperature to allow the results to be compared. At temperatures of 25 and 35 °C, the dissolved oxygen was maintained at 10 ppm while two different dissolved oxygen levels (10 and 20 ppm) were introduced in the experiments at 45 and 55 °C. As can be seen from Figure 7.1a, increases in temperature result in increases in dissolution. However, the temperatures higher than 35 °C are unsuitable for working with alkaline glycine media and the presence of sulfides since they cause deformation of the glycine and its complexes in the long run. Consequently, losing glycine leads to an increase in glycine consumption and operating cost.

As can be seen from Figure 7.1b, there is a substantial increase in the dissolution of galena. The dissolution of galena subsequently increases until approximately 20 min, followed by a sharp fall in the dissolution. Furthermore, increasing the temperature brings about increasing dissolution of galena in the alkaline glycine media. As shown in Figure 7.1c, the temperature has a negative impact on the dissolution of silver in the alkaline glycine media. The highest percentage of silver is extracted at 25 °C, whereas the recovery rates belong to 55 °C. Another striking feature of Figure 7.1c is that there is no noticeable difference between the dissolved oxygen levels of 20 and 10 ppm. Figure 7.1d shows the recovery of copper as a function of time in the alkaline glycine media. As in Figures 7.1a and b, the temperature has a positive effect on the recovery of the copper in this process. However, it can be seen from Figure 7.1d that increasing the dissolved oxygen level from 10 to 20 ppm decreased the copper recovery at 55 °C, which can be related to an interaction between the temperature and dissolved oxygen in this process which results in the deformation of glycine and produced glycine.

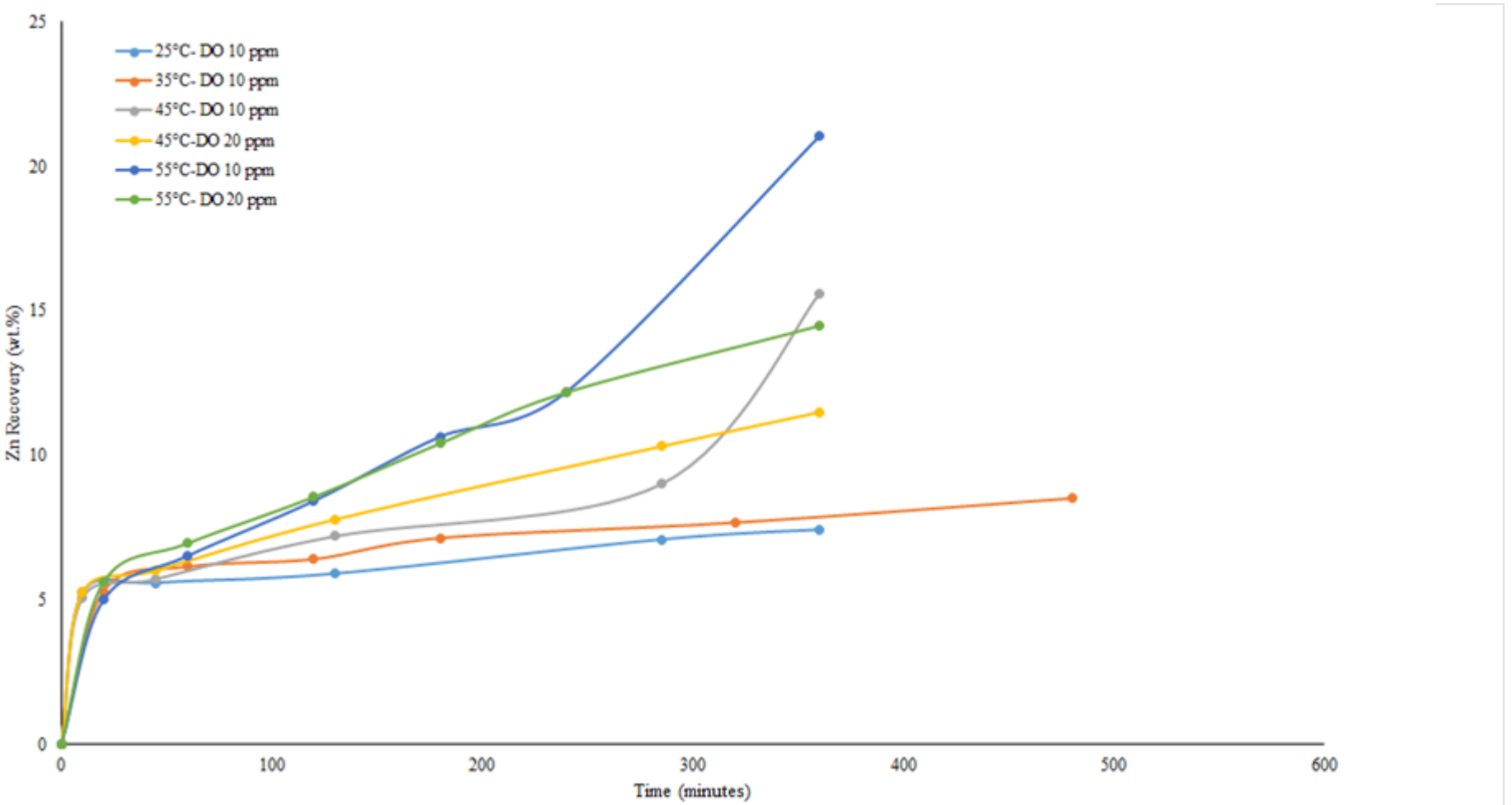

Figure 7. 1 a. The kinetics trends for sphalerite dissolution as a function of time.

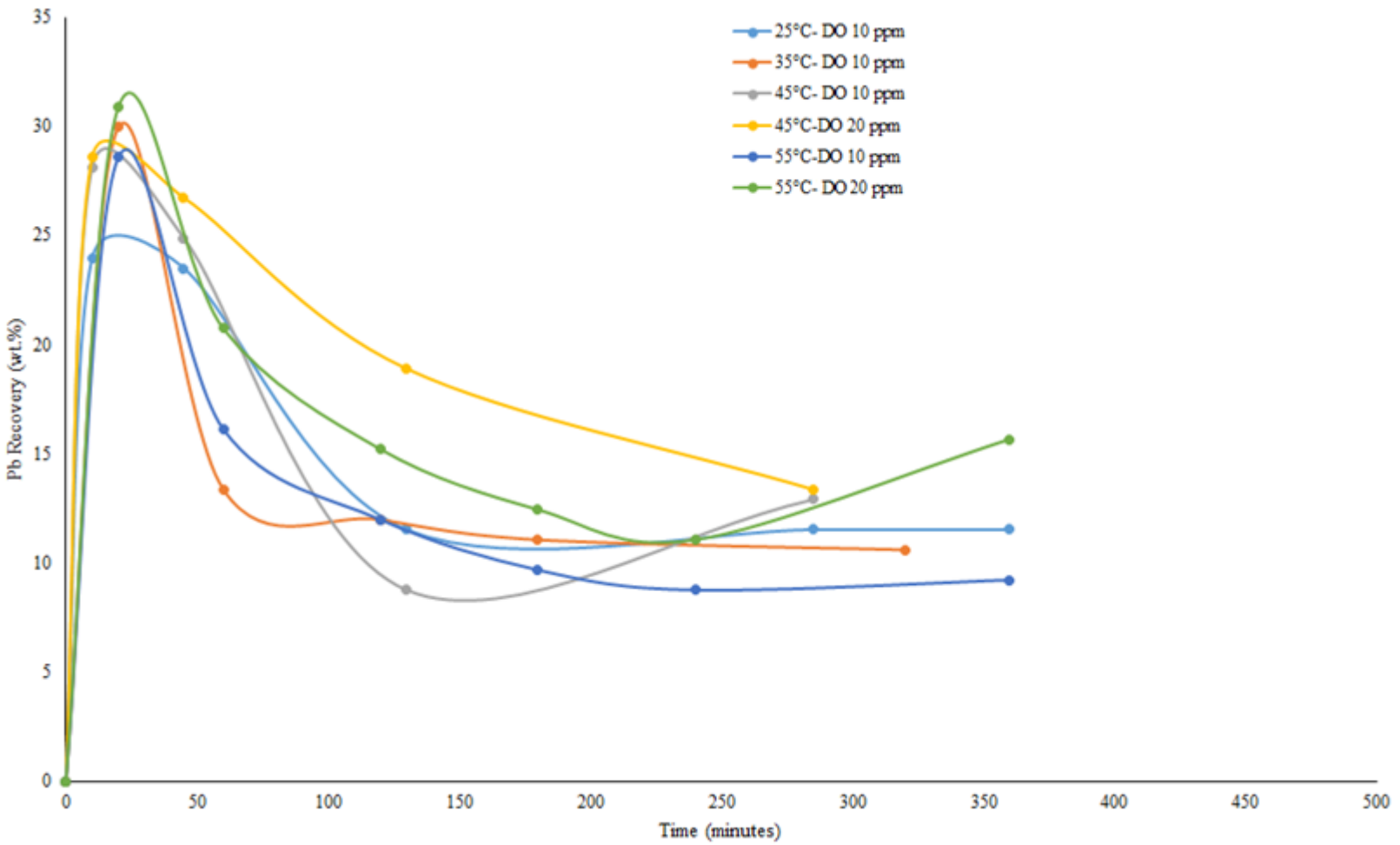

Figure 7. 1 b. The kinetics trends for galena dissolution as a function of time.

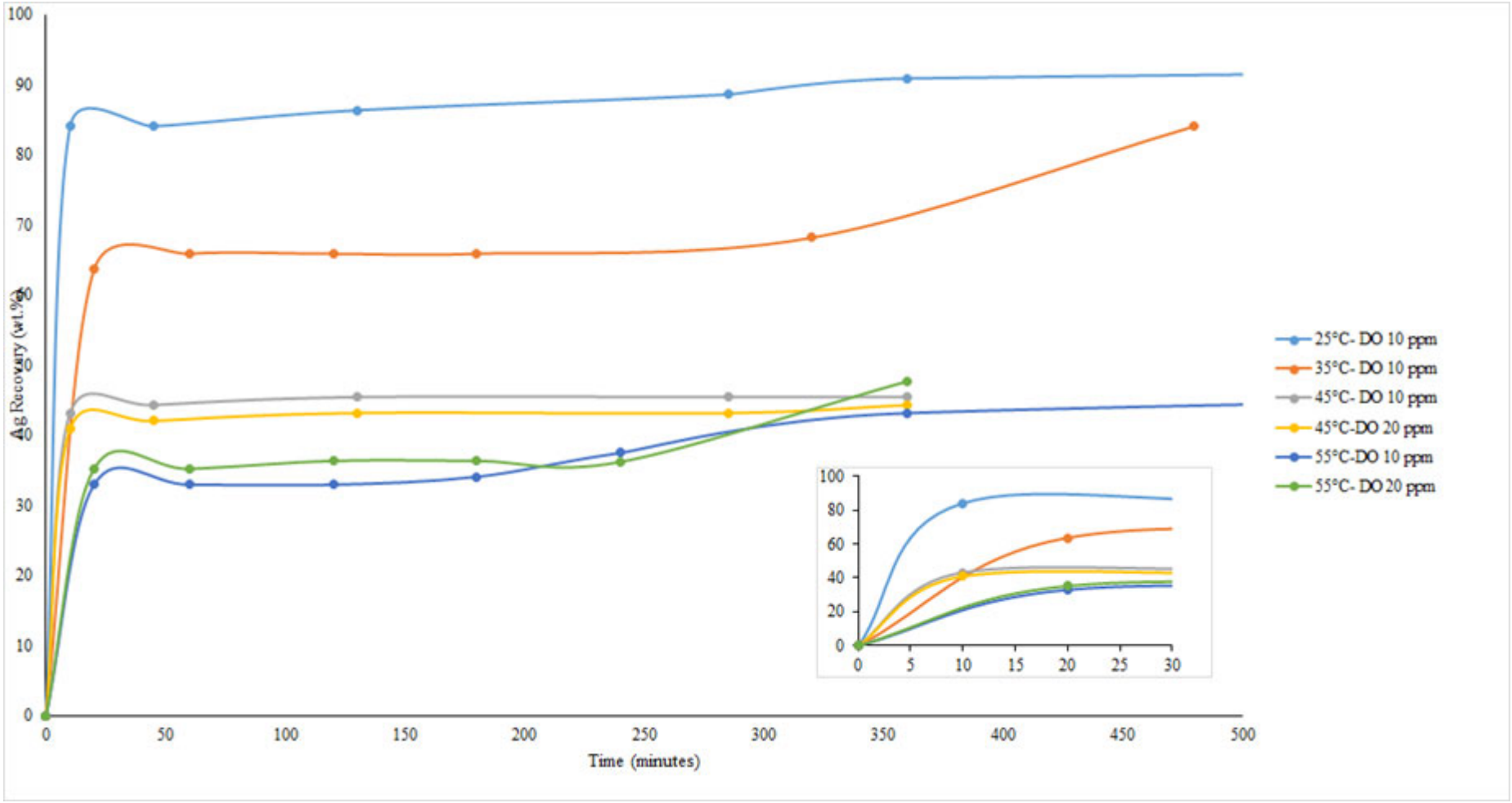

Figure 7. 1 c. The kinetics trends for silver dissolution as a function of time.

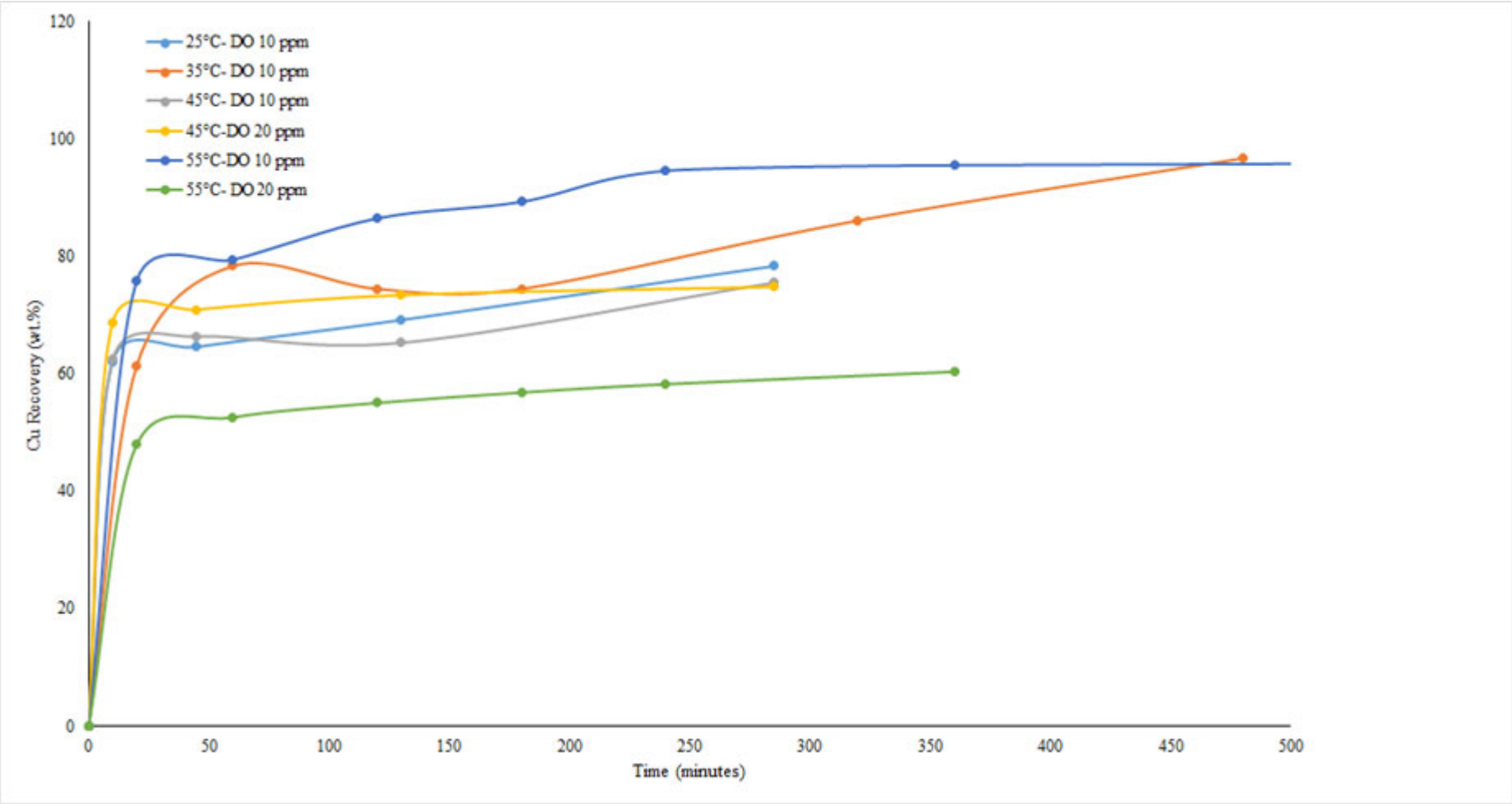

Figure 7. 1 d. The kinetics trends for copper dissolution as a function of time.

Table 7.1 represents the calculation results using the experimental data obtained from kinetics tests for zinc, silver, and copper. For zinc, the controlling mechanism in the whole range of temperature used in this work is diffusion through the product layer. However, there is some mixture of diffusion through the liquid film that can be expected for very fine particles. In the same way as for the dissolution of zinc, the rate-controlling step for copper dissolution in the alkaline glycine medium in this study is diffusion through the product layer which comply with copper kinetics studies in the alkaline glycine media by Tanda (2017). However, the kinetics of silver are more complex than for the other metals. As can be seen from Table 7.1, the results for silver do not have an acceptable R^2, which means the modelling is not accurate. To overcome this issue, the kinetics trends for dissolution of silver at different temperatures were divided into two sections, one with sharp slopes (t = 0–20 min) and the other with moderate slopes (t_1 = 20 min).

The data extracted from Equations (3.2) and (3.5) for silver dissolution are shown in Table 7.2. According to Table 7.2, at the temperature of 25 °C, a mixed kinetics model governing the dissolution rate of the process includes reaction control and film diffusion in the first stage followed by a reaction-controlling mechanism in the second stage. This behaviour can be expected from low-temperature leaching and fine particles in the same way as the mechanism at 35 °C. The kinetics at higher temperatures (45 and 55 °C) include a mixed controlling mechanism with all three mechanisms, which can be related to the formation of new complexes at temperatures higher than 35 °C.

Table 7. 1. Calculated data from Equation 3.2.

Metal	Temperature (◦C)	Coefficient	Film Diffusion	Ash Diffusion	Reaction Control	R^2
Zn	25	1.00E+05	0	1.38	0	0.8699
	35	1.00E+05	0	1.35	0	0.8911
	45	1.00E+04	0.13	2.13	0	0.9076
	55	1.00E+03	1.29	6.25	0	0.9698
Cu	25	1.00E+00	0	547.00	0	0.8228
	35	1.00E+00	0	559.86	0	0.9523
	45	1.00E+00	0	801.29	0	0.8593
	55	1.00E+00	0	349.49	0	0.8909
Ag	25	1.00E+00	0	361.46	0	0.657
	35	1.00E+00	0	800.39	0	0.5793
	45	1.00E+03	0	2.02	0	0.7555
	55	1.00E+03	0	3.45	0	0.8432

Table 7. 2. Calculated data From Equations 3.2 and 3.5.

Temperature (◦C)	t	X	Coefficient	Film Diffusion	Ash Diffusion	Reaction Control	R^2
25	0	0		2.08	0	39.14	0.9975
35	0	0		0	67.72	0	0.9253
45	0	0		0	156.96	0	0.8997
55	0	0		0.00	92.29	127.56	0.9987
Calculated data Equation 3.5							
35	20	0.841	1000	0	0	5.97	0.8997
25	20	0.634	1000	0	0	3.05	0.9871
45	20	0.421	1.00E-06	0.96	0.17	0.75	0.9534
55	20	0.322	1.00E-06	0.06	0.04	0.12	0.9397

CHAPTER 8: CONCLUSIONS

This chapter summarizes all the findings that have been discussed in the previous chapters. A retrospective of the research conducted is also provided. The next section outlines the achievements and enumerates the conclusions drawn from the results of the different sections covered in this thesis. Furthermore, this chapter proposes possible flowsheets for zinc ores. Finally, it provides some recommendations for further investigations considered worthy towards this research.

8.1. Retrospective and Discussion

The main objective of this research was to investigate the dissolution behaviour of zinc in alkaline glycine solutions and the application of glycine as a leachant for zinc resources. Conventional processing of zinc sulfide concentrate (as its main resources) by the roasting–leaching–electrowinning (RLE) procedure as fully described in Chapter 1 poses challenges to metallurgists at all unit stages of the process. From the literature review, one of these processes that can be considered to have a promising future in the zinc leaching industry is the use of glycine as a reagent in alkaline medium. Glycine as the simplest amino acid has been found as a promising alternative reagent for many conventional metal extraction processes. It has been successfully tested for the extraction of copper from primary and secondary resources and used as a complexing agent in gold cyanidation that can reduce the cyanide consumption by a factor of approximately five (Eksteen and Oraby, 2014; Eksteen and Oraby 2016; Eksteen et al., 201; Tannda, 2017) Because of its novelty, there were no reliable data available in the literature on direct leaching of zinc using the alkaline glycine procedure.

Therefore, fundamental studies such as thermodynamics and electrochemistry play a vital role in investigating the behaviour of zinc leaching using such media. Figure 8.1 illustrates all of the objectives of the research study performed in this thesis based on the different zinc species. Thus, the first objective was to propose a mechanism for the dissolution of zinc, silver, and lead in the alkaline glycine media, and thermodynamic and electrochemical studies were the tools used to reach this target.

As lead and silver are common by-products from zinc processing, they were investigated but to a lesser degree than zinc. Thus investigating silver and zinc is useful, but secondary to the understanding of zinc leaching, which is the predominant mineralisation.

This research aimed to gain insight into the fundamental aspects of zinc sulfide dissolution behaviour in alkaline glycine media. In addition, the potential application of this new medium (alkaline glycine medium) to simultaneous leaching of zinc, silver, lead, and copper has been introduced. Moreover, the effects of independent parameters and different dissolution procedures such as rotating disc dissolution, agitated reactor leaching, and bottle roll tests have been investigated. This investigation aimed to deal with the development of a new eco-friendly procedure for direct leaching of sphalerite without any pre-treatments (e.g. roasting).

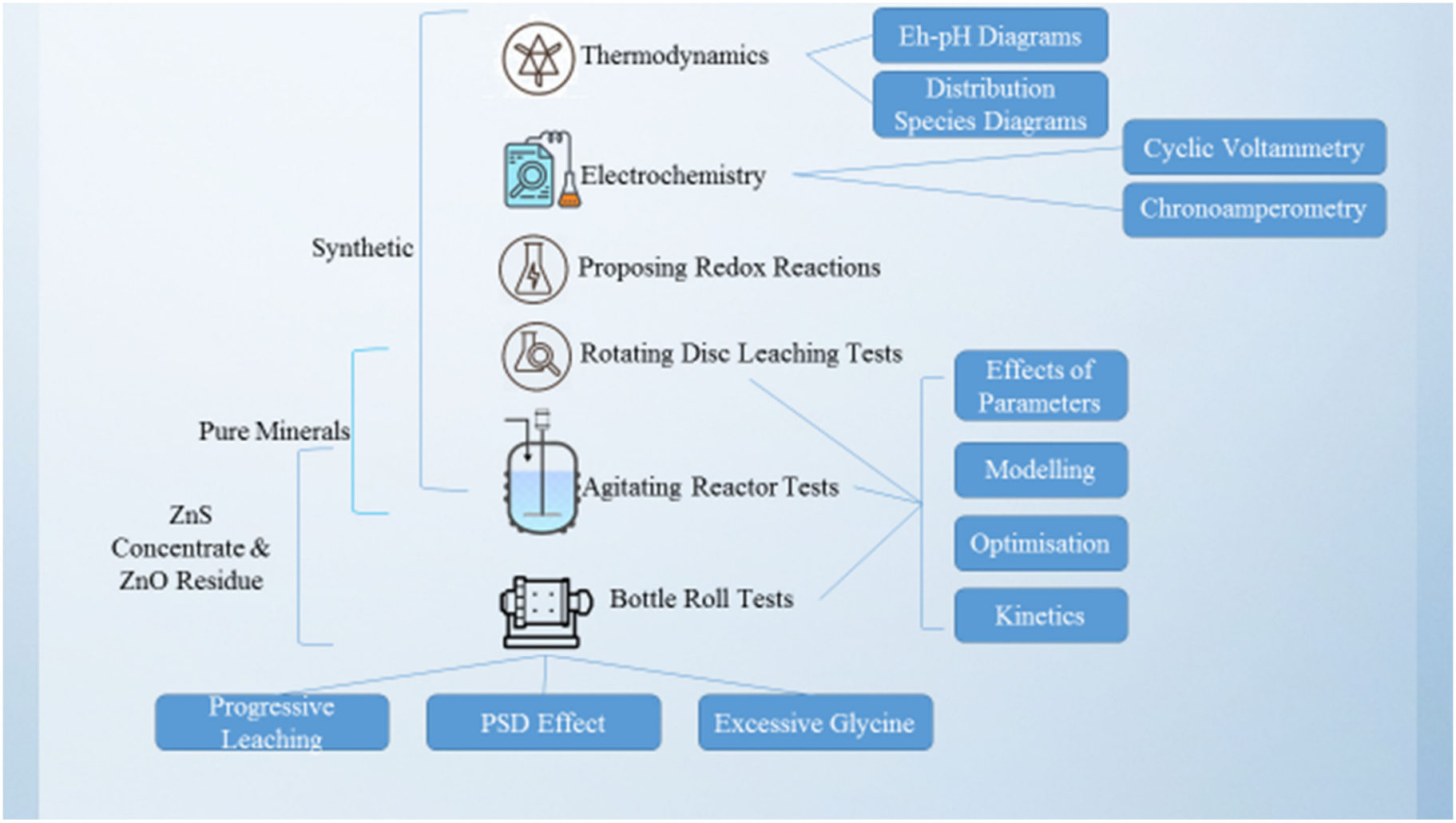

Figure 8. 1. Schematic of the thesis experiments.

8.2. Thermodynamics of the specimen-glycine-sulfur systems

This section offers an insight into the thermodynamic study of three different dissolution systems, namely zinc-glycine-sulfur, silver-glycine-sulfur, and lead-glycine-sulfur. The thermodynamic information for these systems presented in this section is either collected from textbooks or predicted by sophisticated thermodynamic software (HSC Chemistry 10). This section details Pourbaix diagrams as well as the species-distribution diagrams for these three dissolution systems separately. The information presented in this section was the fundamental resource for the following sections. In summary:

- Equilibrium potential–pH diagrams for the zinc-sulfur-glycine-water system were derived at different total zinc and glycine concentrations. The diagrams illustrate that to optimally make use of the zinc-glycine complex formation area in alkaline media, a high concentration of glycine is needed. Under such conditions, the predominant zinc-glycine species is $ZnGly_3^-$.
- Equilibrium potential–pH diagrams for the silver-sulfur-glycine-water and lead-sulfur-glycine-water systems were derived from thermodynamic data. The diagrams illustrate that the predominant metal-glycine species at pH 10 are $AgGly_2^-$ and $PbGly_2$.

8.3. Electrochemistry of the specimen-glycine-sulfur systems

In this section, the electrochemical oxidation of zinc sulfide, lead sulfide, and silver sulfide in alkaline glycine solution was investigated. In summary:

- CV experiments revealed that the resulting voltammograms have three anodic peaks, namely: (1) zinc sulfide oxidation to soluble and insoluble species; (2) formation of $ZnGly_3^-$ from the produced $ZnGly_2$; and (3) oxidation of the produced zinc hydroxide at high negative potentials from the prior peaks. The cathodic peak includes the reduction of the produced zinc hydroxide.
- The galena-CPE has four anodic peaks, namely (1) direct oxidation of galena to lead (IV) hydroxide (as an oxidant product), (2) direct oxidation of galena to lead (II) hydroxide (as an oxidant product), (3) formation of $PbGly_2$ from lead produced from the prior peaks, and (4) oxidation of galena to lead ions and elemental sulfur, and two cathodic peaks, namely (1) reduction of oxidation products [lead (IV) hydroxide] to galena, and (2) reduction of galena oxidation to elemental lead.

- The silver-sulfide-CPE has two anodic peaks, namely (1) direct oxidation of silver sulfide to silver ions and elemental sulfur, and (2) the formation of $AgGly_2^-$ from silver produced from the prior peaks.
- Chronoamperometry experiments were carried out to confirm the proposed mechanism in CV. These experiments confirmed that the oxidation of zinc sulfide has three different mechanisms which can be varied by changing the working potential. Moreover, it was confirmed that the oxidation of silver sulfide has two different mechanisms which vary on changing the working potential, while the oxidation of galena has four different mechanisms.

8.4. Leaching of zinc, silver, and lead in alkaline glycine solutions

In this section, the direct dissolution of zinc from different resources, namely pure sphalerite, synthetic silver sulfide, a zinc sulfide concentrate, and a zinc oxide residue, in alkaline glycine solutions was investigated. For silver leaching in alkaline glycine solutions, the most effective parameters were found to be the glycine and sodium chloride concentrations. Based on the results, sodium chloride has a complex effect on silver sulfide leaching. In this regard, the interaction of sodium chloride with glycine was proposed. Furthermore, a quadratic numerical model was successfully applied to the results to model and find the optimum working conditions. Under the optimum conditions obtained at a temperature of 35 °C, a glycine concentration of 2 moles, a sodium chloride concentration of 3 moles, a pH of 10, and a leaching time of 40 min, a leaching rate of silver sulfide of ca. 8.53 μmol m^{-2} s^{-1} was achieved. The confirmation tests for the obtained numerical model were carried out. The predicted value of dissolved silver was 0.78 mg/l at 20 min while the actual value obtained was 0.75 mg/l.

In galena leaching, it was shown that the extraction of lead could reach more than 30 %. in less than an hour and after that it faced a significant drop during the rest of the leaching time. This could be related to the weakness of the lead-glycine complex, which did not have sufficient stability in the leaching solutions and deformed to elemental lead as mentioned in the section on thermodynamics (Chapter 4).

For zinc leaching, the effects of additives, namely potassium permanganate, cupric ions, sodium chloride, hydrogen peroxide, and lead nitrite, were investigated. The experiments showed that not only sodium chloride is the most effective additive in the process but also it has a positive impact on the dissolution of galena and silver in the process (in which above 90 wt.% silver extraction can be reached). With regard to modifying the pH, better results were obtained by using NaOH than by using $Ca(OH)_2$.

However an increase in glycine concentration can increase the rate of sphalerite dissolution. Glycine concentration, cupric ions, and pH were modelled via the two-factor interaction

model and optimized for the process. The optimum condition was a glycine concentration of 5.25 g/l, cupric ion concentration of 10 mg/l, sphalerite concentration of 1 g in 500 ml of solution at a temperature of 35 °C, pH of 10.7, and stirring speed of 500 rpm. In the optimum condition, about 30 % of sphalerite was dissolved in 48 h, and the extraction rates for silver and copper were found to be above 92 wt.%. It was shown that increasing the dissolved oxygen from 10 to 20 ppm did not have a significant effect on the dissolution, even at higher temperatures. In another words, increasing the temperature results in a decrease in the dissolution rate. Kinetics studies showed that the dissolution mechanisms of silver, copper, and zinc could be considered through the SCMs. However it was shown that a mixed mechanism governed the higher temperatures while at lower temperatures diffusion through the product layer was the main controlling mechanism in this process. Decreasing the particle size was shown to have a positive effect on the process and significantly increased the dissolution of the sphalerite. The application of the obtained optimum condition to a zinc oxide residue was also investigated. The results showed that under this condition, in the bottle roll test, a zinc recovery of more than 60 % can be reached in 7 days.

8.5. Proposed process flowsheets for different silver and zinc ores

The results obtained in this thesis can lead to the development of conceptual flowsheets for the industrial production of zinc and silver depending on their nature.

8.5.1. Deposits of low-grade zinc oxide/silver

Considering large deposits containing low-grade zinc oxide resources such as ores, tailings, or residues,

- Appropriately stacking solid materials (e.g. crushing, agglomerating) on a prepared heap leaching pad
- Making up the reagent by using sodium hydroxide, glycine, and the pre-calculated water volume as:
  $NaOH_{(aq)} + NH_2CH_2COOH_{(aq)} \rightarrow Na^+_{(aq)} + NH_2CH_2COO^-_{(aq)}$ (8.1)
- Adding 0.5 M NaCl to the made-up solution (in favour of silver extraction)
- Performing leaching by spreading the leaching solution on top of the heap.
- Collecting the PLS at the bottom of the heap and clarifying it to remove any solids (to prevent crud formation during solvent extraction)
- Zinc recovery from the solution through an appropriate solvent extraction step followed by glycine regeneration

- Readjusting the pH and precipitating the sulfite/sulfate species or dissolved silicates, phosphates, or aluminates through the addition of lime

$$Ca(OH)_{2(aq)} + SO_4^{-2} \rightarrow CaSO_4.2H_2O_{(s)} \quad (8.2)$$

The proposed flowsheets for possible industrial processes are given in Figures 8.2 .

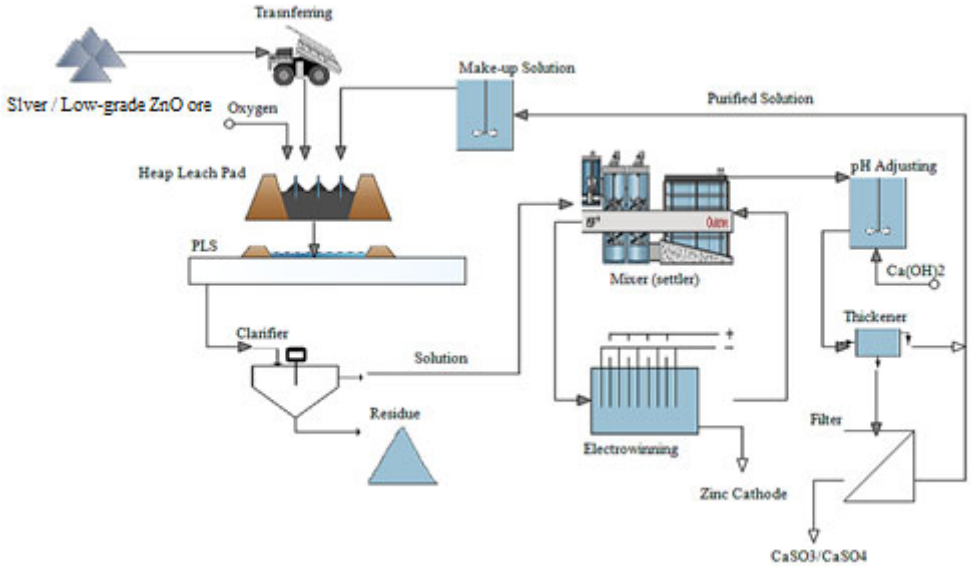

Figure 8. 2. Conceptual flowsheet for leaching of silver / low-grade zinc oxide resources in alkaline glycine solutions.

8.5.2. Deposits of zinc sulfide ore/residue

The major difference between the processing of zinc oxide and zinc sulfide is that zinc sulfide requires a pre-oxidation stage before the leaching stage. This pre-oxidation can be achieved by alkaline oxidation of solid in an oxygenated solution as follows:

$$ZnS + Ca(OH)_2 \rightarrow ZnO + CaS + H2O \quad (8.3)$$

The proposed condition for such pre-oxidation is a pH higher than 10.5 with more than 10 ppm of dissolved oxygen for 48 h. By introducing the pre-oxidation stage before the leaching stage, selective extraction of zinc from lead is achievable (about 70% of zinc and 1% lead). Figure 8.3 illustrates the modified flowsheet for zinc sulfide resources.

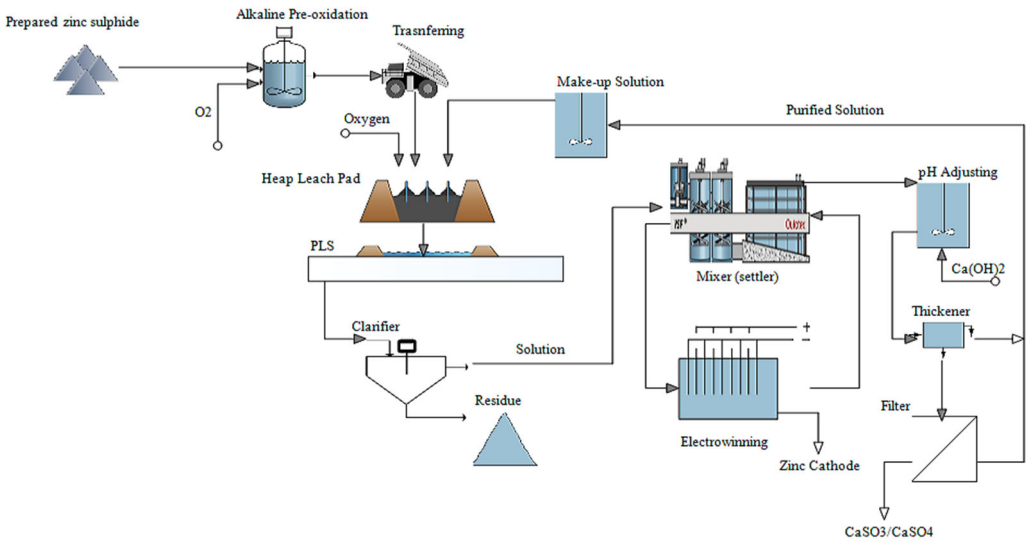

Figure 8. 3. Conceptual Flowsheet for leaching of low-grade zinc sulphide resources in alkaline glycine solutions.

8.6. Recommendations

To develop this research more robustly with regard to the scientific and practical aspects and to overcome the barriers to leaching, the following issues are required to be addressed in future works:

1. Locked cycle testing and the impact of recycling streams
2. Finding the life cycle of reagents during the recycling
3. Separation methods for separating metal species from the barren liquor including zinc, copper, lead, and silver through separation processes
4. Heap leaching tests on low-grade materials for long leaching time
5. Material balancing and techno-economic modelling of the leaching porcess

Bibliography

Abdel-Aal, E. A., 2000. Kinetics of Sulfuric Acid Leaching of Low-Grade Zinc Silicate Ore. Hydrometallurgy 55 (3): 247–54.

Abkhoshk, E., Jorjani, E., Al-Harahsheh, M. S., Rashchi, F., and Naazeri, M., 2014. Review of the Hydrometallurgical Processing of Non-Sulfide Zinc Ores. Hydrometallurgy 149 : 153–67.

Ahlberg, E., Ásbjörnsson, J., 1994. Carbon paste electrodes in mineral processing: an electrochemical study of sphalerite, Hydrometallurgy, vol. 36, no. 1, pp. 19–37.

Aksu, S., Doyle, F.M., 2001. Electrochemistry of Copper in Aqueous Glycine Solutions, J. Electrochem. Soc., vol. 148, no. 1, pp. B51–B57.

Alberts, E., and Dorfling, C., 2013. Stripping Conditions to Prevent the Accumulation of Rare Earth Elements and Iron on the Organic Phase in the Solvent Extraction Circuit at Skorpion Zinc. Minerals Engineering 40: 48–55.

Alguacil, F. J., Cobo, A., and Caravaca, C., 1992. Study of the Extraction of zinc(II) in Aqueous Chloride Media by Cyanex 302. Hydrometallurgy 31 (3): 163–74.

Al-Harahsheh, M., and Kingman, S. W., 2004. Microwave-Assisted Leaching—a Review. Hydrometallurgy 73 (3–4): 189–203.

Ali, A. M. I., Ahmad, I. M., and Daoud, J. A., 2006. CYANEX 272 for the Extraction and Recovery of Zinc from Aqueous Waste Solution Using a Mixer-Settler Unit. Separation and Purification Technology 47 (3): 135–40.

Allen, C, Kondos, P., Payant, S., Van Weert, G., and Van Sandwijk, A., 2002. Production of zinc oxide from complex sulfide concentrates using chloride processing. US Patent 6,395,242, filed May 28, and issued 2002.

Al-Merey, R, Al-Masri, M. S, and Bozou, R., 2002. Cold Ultrasonic Acid Extraction of Copper, Lead and Zinc from Soil Samples. Analytica Chimica Acta 452 (1): 143–48.

Almeida, C.M.V.B., Giannetti, B.F., 2002. A new and practical carbon paste electrode for insoluble and ground samples, Electrochem. Commun., vol. 4, no. 12, pp. 985–988.

Amer, S., Figueiredo, J. M., and Luis, A., 1995. The Recovery of Zinc from the Leach Liquors of the CENIM-LNETI Process by Solvent Extraction with Di(-2-Ethylhexyl)phosphoric Acid. Hydrometallurgy 37 (3): 323–37.

Aparajith, B., Mohanty, D.B., Gupta, M.L., 2010. Recovery of enriched lead–silver residue from silver-rich concentrate of hydrometallurgical zinc smelter. Hydrometallurgy, 105, 127-133.

Aarabi-Karsagani, M., Rashchi, F., Mostoufi, N., Vahidi, E., 2010. Leaching of vanadium from LD converter slag using sulfuric acid. Hydrometallurgy 102: 14-25.

Asianmetal 2020, Zinc, viewed 08 Feb 2020, <http://metalpedia.asianmetal.com/metal/zinc/extraction.shtml>

Ashtari, P., and Pourghahramani, P., 2015. Selective Mechanochemical Alkaline Leaching of Zinc from Zinc Plant Residue. Hydrometallurgy 156 (July): 165–72.

Aydogan, S., 2006. Dissolution Kinetics of Sphalerite with Hydrogen Peroxide in Sulphuric Acid Medium. Chemical Engineering Journal 123 (3): 65–70.

Aydogan, S., Aras, A., and Canbazoglu, M., 2005. Dissolution Kinetics of Sphalerite in Acidic Ferric Chloride Leaching. Chemical Engineering Journal 114 (1–3): 67–72.

Azizkarimi, M., Tabaian, S.H., Rezai, B., 2014. Electrochemical investigation of chalcopyrite oxidation in alkaline solution, Separation Science and Technology, vol. 49, p.p. 2595-2601.

Azriel, D., 2014. Optimal sequential designs in phase I studies. Computational statics & data analysis, 71, pp: 288-297.

Baba, A. A., and Adekola, F. A., 2010. Hydrometallurgical Processing of a Nigerian Sphalerite in Hydrochloric Acid: Characterization and Dissolution Kinetics. Hydrometallurgy 101 (1–2): 69–75.

Balarini, J. C., Polli L. D. O., Miranda, T. L. S., de Castro. R. M. Z., and Salum A., 2008. Importance of Roasted Sulphide Concentrates Characterization in the Hydrometallurgical Extraction of Zinc. Minerals Engineering, Selected papers from Bio and Hydrometallurgy '07, Falmouth, UK, May 2007, 21 (1): 100–110.

Balaz, P., Ficeriova, J., Leon, C.V., 2003. Silver leaching from a mechanochemically pretreated complex sulfide concentrate. Hydrometallurgy, 70, 113-119.

Baláž, P., 2003. Mechanical Activation in Hydrometallurgy. International Journal of Mineral Processing, Special Issue To Honor Professor Douglas W. Fuerstenau, 72 (1–4): 341–54.

Baláž, P., and Ebert, I., 1991. Oxidative Leaching of Mechanically Activated Sphalerite. Hydrometallurgy 27 (2): 141–50.

Baláž, P., and Achimovičová, M., 2006. Mechano-Chemical Leaching in Hydrometallurgy of Complex Sulphides. Hydrometallurgy 84 (1–2): 60–68.

Ballesteros, J.C., Chaînet, E., Ozil, P., Trejo, G., Meas, Y., 2011. Electrochemical studies of Zn underpotential/overpotential deposition on a nickel electrode from non-cyanide alkaline solution containing glycine, Electrochimica Acta, vol. 56, no. 16, pp. 5443–5451.

Ballesteros, J.C., Chaînet, E., Ozil, P., Trejo, G., Meas, Y., 2010. Initial stages of the electrocrystallization of copper from non-cyanide alkaline bath containing glycine, J. Electroanal. Chem., vol. 645, no. 2, pp. 94–102.

Behnajady, B., Balesini, A. A., and Moghaddam, J., 2014. A New Approach to the Optimisation of Zinc Electrolyte Cold Purification Process by Taguchi's Method. Canadian Metallurgical Quarterly 53 (3): 333–39.

Behnajady, B., and Moghaddam, J., 2015. Statistical Evaluation and Optimization of Zinc Electrolyte Hot Purification Process by Taguchi Method. Journal of Central South University 22 (6): 2066–72.

Bodas, M. G., 1996. Hydrometallurgical Treatment of Zinc Silicate Ore from Thailand. Hydrometallurgy 40 (1): 37–49.

Brownson, D.A.C., Banks, C.E., 2014. Interpreting Electrochemistry, in The Handbook of Graphene Electrochemistry, Springer London, pp. 23–77.

Buban, K. R., Collins, M. J., Masters, I. M., and Trytten, L. C., 2000. Comparison of Direct Pressure Leaching with Atmospheric Leaching of Zinc Concentrates. In Lead-Zinc 2000, edited by Dutrizac, J. E., John Wiley & Sons, Inc., 727–38.

Buckett, G.A., Fountain, C.R., and Sinclair, R.J., 1998. Refining Zinc Sulphide Ores. WO patent 1998036102 A1, Feb 17

Buttinelli, D., Lavecchia, R., Pochetti, F., Geveci, A., Guresin, N., and Topkaya, Y., 1992. Leaching by Ferric Sulphate of Raw and Concentrated Copper-Zinc Complex Sulphide Ores. International Journal of Mineral Processing 36 (3): 245–57.

Canterford, J. H., Davey, P. T., and Tsambourakis, G., 1985. Gangue Mineral Dissolution and Jarosite Formation in Copper Solution Mining. Hydrometallurgy 13 (3): 327–43.

Carranza, F., and Iglesias, N., 1998. Application of IBES Process to a Zn Sulphide Concentrate: Effect of Cu2+ Ion. Minerals Engineering 11 (4): 385–90.

Casaroli, S. J. G., Cohen, B., Tong, A. R., Linkson, P., and Petrie, J. G., 2005. Cementation for Metal Removal in Zinc Electrowinning Circuits. Minerals Engineering, Selected papers from Bio and Hydrometallurgy ’05, Cape Town, South Africa, 18 (13–14): 1282–88.

Chang, L., Bo, Y., Tao, C., Xiao-Liang, W., Xian-Ming, X., 2018. Silver leaching and recovery of valuable metals from magnetic tailings using chloride leaching. Journal of cleaner production, 181, 408-415.

Chen, L., Uchida, T., Chang, H., Osawa, M., 2013. Adsorption and oxidation of glycine on Au electrode: An in situ surface-enhanced infrared study, Electrochemistry Communications, Vol. 34, pp. 56-59.

Chen, A., Zhao, Z. W., Jia, X., Long, S., Huo, H., and Chen, X., 2009. Alkaline Leaching Zn and Its Concomitant Metals from Refractory Hemimorphite Zinc Oxide Ore. Hydrometallurgy 97 (3–4): 228–32.

Chen, Q., Yin, Z., Zhang, P., Hu, H., and Ye, L., 2002. The Oxidation Behavior of Unactivated and Mechanically Activated Sphalerite. Metallurgical and Materials Transactions B 33 (6): 897–900.

Chenglong, Z., Youcai, Z., Cuixiang, G., Xi, H., and Hongjiang, L., 2008. Leaching of Zinc Sulfide in Alkaline Solution via Chemical Conversion with Lead Carbonate. Hydrometallurgy 90 (1): 19–25.

Cisneros-gonzalez, I., Oropeza-guzman, M.T.,Gonzalez, I., 1999. Cyclic voltammetry applied to the characterisation of galena. Hydrometallurgy, 53, pp: 133-144.

Cisneros-gonzalez, I., Oropeza-guzman, M.T.,Gonzalez, I., 2000. Electrochemical study of galena concentrate in perchlorate medium at pH 2.0: The influence of chloride ions. Electrochimica Acta, 45, pp: 2729-2741.

Claassen, J. O, Meyer, E. H. O., Rennie, J., and Sandenbergh, R. F., 2002. Iron Precipitation from Zinc-Rich Solutions: Defining the Zincor Process. Hydrometallurgy 67 (1–3): 87–108.

Coetzer, R., Haines, L.M., 2017. The construction of D- and I-optimal designs for mixture experiments with linear constraints on the components. Chemometrics and Intelligent Laboratory Systems, 171, pp:112-124.

Cole, P. M., and Sole, K. C., 2003. Zinc Solvent Extraction in the Process Industries. Mineral Processing and Extractive Metallurgy Review 24 (2): 91–137.

Cole, P.M., and Sole, K.C., 2002. Solvent Extraction in the Primary and Secondary Processing of Zinc. The Journal of the South African Institute of Mining and Metallurgy 102 (8): 451-456.

Constantineau, J. P., Bouffard, S. C., Grace, J. R., Richards, G. G., and Lim, C. J., 2011. Demonstration of the Conditions Conducive to Agglomeration of Zinc Calcine in Fluidized Bed Roasters. Minerals Engineering 24 (13): 1409–20.

Cooper, W. C., Dreisinger, D. B., Dalton, R. F., Burgess, A., and Quan, P. M., 1992a. Hydrometallurgy, Theory and Practice Proceedings of the Ernest Peters International Symposium. Part BACORGA ZNX50—a New Selective Reagent for the Solvent Extraction of Zinc from Chloride Leach Solutions. Hydrometallurgy 30 (1): 385–400.

Cooper, W. C., Dreisinger, D. B., andDutrizac, J. E., 1992b. Hydrometallurgy, Theory and Practice Proceedings of the Ernest Peters International Symposium. Part A The Leaching of Sulphide Minerals in Chloride Media. Hydrometallurgy 29 (1): 1–45.

Corriou, J. P., Gély, R., and Viers, P., 1988. Thermodynamic and Kinetic Study of the Pressure Leaching of Zinc Sulfide in Aqueous Sulfuric Acid. Hydrometallurgy 21 (1): 85–102.

Covadonga, M. S. M., and Hourn, M. M., 2008. Recovery of zinc from sulphide concentrates by atmospheric leaching with sulphuric acid at a controlled acidity. EP1939310 A1, filed December 28, 2006, and issued July 2, 2008.

Crundwell, F. K. 1988. The Influence of the Electronic Structure of Solids on the Anodic Dissolution and Leaching of Semiconducting Sulphide Minerals. Hydrometallurgy 21 (2): 155–90.

Da Silva, G., 2004. Relative Importance of Diffusion and Reaction Control during the Bacterial and Ferric Sulphate Leaching of Zinc Sulphide. Hydrometallurgy 73 (3–4): 313–24.

Darvishi, D., Haghshenas, D. F., Keshavarz Alamdari, E., and Sadrnezhaad, S. K., 2011. Extraction of zn, mn and co from Zn-Mn-Co-Cd-Ni containing solution using d2ehpa, cyanex® 272 and cyanex® 302. International Journal of Engineering - Transactions B: Applications 24 (2): 181.

De Souza, A. D., Pina, P. S., and Leão, V. A., 2007. Bioleaching and Chemical Leaching as an Integrated Process in the Zinc Industry. Minerals Engineering 20 (6): 591–99.

De Wet, J.R., and Singleton, J. D., 2008. Development of a Viable Process for the Recovery of Zinc from Oxide Ores. The Journal of the Southern African Institute of Mining and Metallurgy 108 (5): 253-259.

Deep, A., and de Carvalho, J. M. R., 2008. Review on the Recent Developments in the Solvent Extraction of Zinc. Solvent Extraction and Ion Exchange 26 (4): 375–404.

Dehghan, R., Noaparast, M., and Kolahdoozan, M., 2009. Leaching and Kinetic Modelling of Low-Grade Calcareous Sphalerite in Acidic Ferric Chloride Solution. Hydrometallurgy 96 (4): 275–82.

Dehghan, R., Noaparast, M., Kolahdoozan, M., and Mousavi, S. M., 2008. Statistical Evaluation and Optimization of Factors Affecting the Leaching Performance of a Sphalerite Concentrate. International Journal of Mineral Processing 89 (1–4): 9–16.

Demarthe, J.M., Gandon, L., and Georgeaux, A., 1979. Method of Selectively Bringing into Solution the Non-Ferrous Metals Contained in Sulphurized Ores and Concentrates. CA1061572 A. Sep. 4. (Assigned to Penarroya Miniere Metall)

Demopoulos, G. P. 1977. M.Sc. Thesis. McGill University, Montreal, Canada.

Demopoulos, G. P., 1999. Leaching Fundamentals and Industrial Practice. In Short Course. San Diego.

Deschênes, G., Lastra, R., Brown, J.R., Jin, S., May, O., Ghali, E., 2000. Effect of lead nitrate on cyanidation of gold ores: progress on the study of the mechanism. Miner. Eng. 13 (12), 1263–1279.

Deutsch, J.L., and Dreisinger, D. B., 2013a. Silver sulfide leaching with thiosulfate in the presence of additives Part I: Copper–ammonia leaching. Hydrometallurgy, 137, 156-164.

Deutsch, J.L., Dreisinger, D.B., 2013b. Silver sulfide leaching with thiosulfate in the presence of additives Part II: Ferric complexes and the application to silver sulfide ore. Hydrometallurgy, 137, 165-172.

Devi, N.B., Nathsarma, K.C., and Chakravortty, V., 1997. Extraction and Separation of Mn(II) and Zn(II) from Sulphate Solutions by Sodium Salt of Cyanex 272. Hydrometallurgy 45 (1–2): 169–79.

Díaz, G., and Martín, D., 1994. Recycling of Materials in Industry Modified Zincex Process: The Clean, Safe and Profitable Solution to the Zinc Secondaries Treatment. Resources, Conservation and Recycling 10 (1): 43–57.

Doche, M. L., Hihn, J. Y., Mandroyan, A., Viennet, R., and Touyeras, F., 2003. Influence of Ultrasound Power and Frequency upon Corrosion Kinetics of Zinc in Saline Media. Ultrasonics Sonochemistry 10 (6): 357–62.

Doyle, B.N., MASTERS, I. M., Webster, I.C., and Veltman, H., 1978. Acid Pressure Leaching of Zinc Concentrates with Elemental Sulfur as a Byproduct. In Proceedings of the XIth Commonwealth Mining and Metallurgical Congress. Hong Kong.

Dreisinger, D. B., and Peters, E., 1989. The Oxidation of Ferrous Sulphate by Molecular Oxygen under Zinc Pressure-Leach Conditions. Hydrometallurgy 22 (1): 101–19.

Dutrizac, J. E., 2006. The Dissolution of Sphalerite in Ferric SulfateSulphate Media. Metallurgical and Materials Transactions B 37 (2): 161–71.

Dutrizac, J. E., and Dinardo, O., 1983. The Co-Precipitation of Copper and Zinc with Lead Jarosite. Hydrometallurgy 11 (1): 61–78.

Dutrizac, J. E., Dinardo, O., and Kaiman, S., 1980. Factors Affecting Lead Jarosite Formation. Hydrometallurgy 5 (4): 305–24.

Ejtemaei, M., Gharabaghi, M., and Irannajad, M., 2014. A Review of Zinc Oxide Mineral Beneficiation Using Flotation Method. Advances in Colloid and Interface Science, Manuel G. Velarde, 206 (April): 68–78.

Ekinci, Z., Colak, S., Cakici, A., and Sarac, H., 1998. Leaching Kinetics of Sphalerite with Pyrite in Chlorine Saturated Water. Minerals Engineering 11 (3): 279–83.

Eksteen, J.J., and Oraby, E.A., A process for precious metals recovery, PCT/AU2014/000877

Eksteen, J. J., Oraby, E. A, and Tanda, B. C.. 2015. Alkaline Glacine Systems as Alternatives Reagents for Copper Deposits of Complex Mineralogy. ALTA nickel-cobalt-copper conference, In Perth, Australia.

Eksteen, J.J. and Oraby, E.A., Process for selective recovery of chalcophile group elements. PCT/AU2016/050171

Espiari, S., Rashchi, F., and Sadrnezhaad, S. K., 2006. Hydrometallurgical Treatment of Tailings with High Zinc Content. Hydrometallurgy 82 (1–2): 54–62.

EstatEase. 2019. Design expert 10. [Software]. [2019]

Ferella, F., De Michelis, I., Beolchini, F., Innocenzi, V., Vegliò, F., 2010. Extraction of Zinc and Manganese from Alkaline and Zinc-Carbon Spent Batteries by Citric-Sulphuric Acid Solution. International Journal of Chemical Engineering, 2010.

Filippou, D., 2004. Innovative Hydrometallurgical Processes for the Primary Processing of Zinc. Mineral Processing and Extractive Metallurgy Review 25 (3): 205–52.

Frenay, J., 1985. Leaching of Oxidized Zinc Ores in Various Media. Hydrometallurgy 15 (2): 243–53.

Friedrich, B., Kruger, J., Bernal, G.M., 2001. Alternative solution purification in the hydrometallurgical zinc production. Proceedings of EMC, september 2001. Friedrichshafen, Germany.

Fugleberg, S., and Jarvinen, A. E., 1992. Hydrometallurgic method for processing raw materials containing zinc sulphide. US Patent 5,120,353, issued 1992.

Fugleberg, S., and Jarvinen, A. E., 1994. Hydrometallurgic method for processing raw materials containing zinc sulphide. European Patent 0451456, issued 1994.

Fugleberg, S., and Jarvinen, A. E., 1996. Method for leaching material containing zinc oxide and zinc silicate. US Patent 5,585,079, issued 1996.

Fugleberg, S., and Jarvinen, A. E., 1998. Method for leaching zinc concentrate in atmospheric conditions. PCT World Patent WO98/06879, issued 1998.

Fugleberg, S., Pekkala, P., Talonen, P., and Riekkola-Vanhanen, M., 2009. Method for the precipation of silica conection with zinc ore leaching. US 7,615,100 B2, filed November 10, 2009, and issued 2009.

Ghassa, S., Boroumand, Z., Moradian, M., Abdollahi, H., Akcil, A., 2014. Microbial Dissolution of Zn-Pb Sulfide Minerals Using Mesophilic Iron and Sulfur-Oxidizing Acidophiles. Mineral processing and extraction metallurgy 36 (2):112-122.

Ghosh, A., and Ghosh, S., 2014. A textbook of metallurgical kinetics. PHI Learning Pvt. Ltd.

Ghosh, M. K, Das, R. P., and Biswas. A. K., 2002. Oxidative Ammonia Leaching of Sphalerite: Part I: Noncatalytic Kinetics. International Journal of Mineral Processing 66 (1–4): 241–54.

Ghosh, M. K, Das, R. P., and Biswas. A. K., 2003. Oxidative Ammonia Leaching of Sphalerite: Part II: Cu(II)-Catalyzed Kinetics. International Journal of Mineral Processing 70 (1–4): 221–34.

Ghosh, M. K., Sukla, L. B., and Misra, V. N., 2004. Cobalt and zinc extraction from sikkim complex sulphide concentrate. Trans. Indian Inst. Met 57 (6): 617–21.

Giaveno, A., Lavalle, L., Chiacchiarini, P., and Donati. E., 2007. Bioleaching of Zinc from Low-Grade Complex Sulfide Ores in an Airlift by Isolated Leptospirillum Ferrooxidans. Hydrometallurgy 89 (1–2): 117–26.

Gilg, H. A., Struck, U., Vennemann, T., and Boni, M., 2003. Phosphoric Acid Fractionation Factors for Smithsonite and Cerussite between 25 and 72°C1. Geochimica et Cosmochimica Acta 67 (21): 4049–55.

Grzeszczyk, A., and Regel-Rosocka, M., 2007. Extraction of zinc(II), iron(II) and iron(III) from Chloride Media with Dibutylbutylphosphonate. Hydrometallurgy 86 (1–2): 72–79.

Gu, Y., Zhang, T., Liu, Y., Mu, W., Zhang, W., Dou, Z., and Jiang, X., 2010. Pressure Acid Leaching of Zinc Sulfide Concentrate. Transactions of Nonferrous Metals Society of China 20 (May): s136–40.

Guler, E., 2016. Pressure acid leaching of sphalerite concentrate. Modeling and optimization by response surface methodology. Physicochemical Problems of Mineral Processing 52 (1): 479–96.

Gupta, C.K., 2003. Chemical Metallurgy: Principles and Practice. Wiley-VCH Verlag GmbH & Co. KGaA.

Gupta, C.K., and Mukherjee, T.K., 1990. Hydrometallurgy in Extraction Processes. Vol. 1. CRC Press.

Haakana, T., Lahtinen, M., Takala, H., Ruonala, M., and Turunen, I., 2007. Development and Modelling of a Novel Reactor for Direct Leaching of Zinc Sulphide Concentrates. Chemical Engineering Science, 19th International Symposium on Chemical Reaction Engineering - From Science to Innovative EngineeringISCRE-19, 62 (18–20): 5648–54.

Haakana, T., Saxen, B., Lehtinen, L., Takala, H., Lahtinen, M., Svens, K., Ruonala, M., and Xiao, G., 2008. Outotec direct leaching application in china. In The Southern African Institute of Mining and Metallurgy lead and zinc.

Habashi, F., 1997. Handbook of Extractive Metallurgy. Vol. 2. Heidelberg, Germany: WILEY-VCH.

Habashi, F., 1999. Nitric Acid in the Hydrometallurgy of Sulfides. In TMS – AIME. San Diego.

Harlamovs, J. S., Ashman, D. W., Gonzalez-Dominguez, J. A., Lizama, H. M., Makwana, D., and Strandling, A. W., 2003. Heap bioleching process for the extraction of zinc. Canadian Patent Application CA 2353002, filed January 13, and issued 2003.

Harvey, T. G., 2006. The Hydrometallurgical Extraction of Zinc by Ammonium Carbonate: A Review of the Schnabel Process. Mineral Processing and Extractive Metallurgy Review 27 (4): 231–79.

Harvey, T. J, Van Der Merwe, W., and Afewu, K., 2002. The Application of the GeoBiotics GEOCOAT® Biooxidation Technology for the Treatment of Sphalerite at Kumba Resources' Rosh Pinah Mine. Minerals Engineering 15 (11): 823–29.

He, S., Wang, J., and Yan, J., 2010. Pressure Leaching of High Silica Pb–Zn Oxide Ore in Sulfuric Acid Medium. Hydrometallurgy 104 (2): 235–40.

He, S., Wang, J., and Yan, J., 2011. Pressure Leaching of Synthetic Zinc Silicate in Sulfuric Acid Medium. Hydrometallurgy 108 (3–4): 171–76.

Hourn, M. M, Turner, D. W., and Holzberger, I. R., 1999. Atmospheric mineral leaching process. US Patent 5,993,635, issued 1999. (Assigned to MIM Hpldings, Ltd.).

Hourn, M. M, Turner, D. W., and Holzberger, I. R., 1996. Atmospheric mineral leaching process. PCT World Patent WO 96/29439. (Assigned to MIM Hpldings, Ltd.).

Hua, Y., Lin, Z., and Yan, Z., 2002. Application of Microwave Irradiation to Quick Leach of Zinc Silicate Ore. Minerals Engineering 15 (6): 451–56.

Hurşit, M., Laçin, O., and Saraç, H., 2009. Dissolution Kinetics of Smithsonite Ore as an Alternative Zinc Source with an Organic Leach Reagent. Journal of the Taiwan Institute of Chemical Engineers 40 (1): 6–12.

Jadhav, U., Hocheng, H., 2013. Extraction of silver from spent silver oxide–zinc button cells by using Acidithiobacillus ferrooxidans culture supernatant. Journal of cleaner production, 44, 39-44.

Jiang, H., Xie, F., Dreisinger, D. B., 2015. Comparative study of auxiliary oxidants in cyanidation of silver sulfide . Hydrometallurgy, 158, 149-156.

Jakubiak, A., and Szymanowski, J., 1998. Zinc(II) Extraction from Chloride Solutions by Kelex 100. Physicochemical Problems of Mineral Processing 32: 255–64.

Jankola, W. A. , 1995. Zinc Pressure Leaching at Cominco. Hydrometallurgy 39 (1): 63–70.

Jansz, J.J.C., 1984. Chloride Hydrometallurgy for Pyritic Zinc-Lead Sulfide Ores: The Non-Oxidative Leaching Route. Dissertatie Drukkery Wibro.

Jia, Q., Bi, L., and Shang, Q., 2003. Extraction Equilibrium of Zinc(II) and Cadmium(II) by Mixtures of Primary Amine N1923 and 2-Ethylhexyl Phosphonic Acid Di-2-Ethylhexyl Ester. Industrial & Engineering Chemistry Research 42 (18): 4223–27.

Jiang, H., Xie, F., Dreisinger, D. B., 2015. Comparative study of auxiliary oxidants in cyanidation of silver sulfide. Hydrometallurgy, 158, 149-156.

Jin, Z., Warren, G. W., and Henein, H., 1983. Reaction Kinetics of the Ferric Chloride Leaching of Sphalerite—an Experimental Study. Metallurgical Transactions B 15 (1): 5–12.

Ju, S., Motang, T., Shenghai, Y., and Yingnian, L., 2005. Dissolution Kinetics of Smithsonite Ore in Ammonium Chloride Solution. Hydrometallurgy 80 (1–2): 67–74.

Kai, T., Suenaga, Y., Migita, A., and Takahashi, T., 2000. Kinetic Model for Simultaneous Leaching of Zinc Sulfide and Manganese Dioxide in the Presence of Iron-Oxidizing Bacteria. Chemical Engineering Science 55 (17): 3429–36.

Kanno, M., Watanabe, Y., Saruta, K., and Narumi, A., 2002. Method and apparatus for leaching zinc concentrates. European Patent Application EP 1245686 A2, filed January 29, and issued 2002.

Karimi, S., Rashchi, F., Moghaddam, J., 2017. Parameters optimization and kinetics of direct atmospheric leaching of Angouran sphalerite. International Journal of mineral processing, 162: 58-68.

Kaskiala, T., 2005. Determination of Mass Transfer between Gas and Liquid in Atmospheric Leaching of Sulphidic Zinc Concentrates. Minerals Engineering, JKMRC International Student Conference, September 2004JKMRC, 18 (12): 1200–1207.

Kawulka, P., Haffenden, W. J., and Mackiw, V. N., 1973. Recovery of zinc from zinc sulphides by direct pressure leaching. 3867268, filed August 21, 1973, and issued 1973.

Kiss, T., SOVAGO, I., Gergely, A., 1991. Critical survey of stability constants of complexes of glycine, Pure and Allied Chemistry, Vol. 63, No. 4, pp. 597-638.

Kuzminkh, I.N., and Yakhontova, E.L., 1950. Wet Extraction of Zinc from Mixture of Sulfides. Z. Priklad. Khim 23: 1121–26.

Lahtinen, M., Svens, K., Haakana, T., and Lehtinen, L., 2008. Zinc plant expansion by outotec direct leaching process. In , 167–178. Winnipeg, Manitoba Canada,: Outotec Oyj,.

Lampinen, M., Laari, A., and Turunen, I., 2015. Kinetic Model for Direct Leaching of Zinc Sulfide Concentrates at High Slurry and Solute Concentration. Hydrometallurgy 153 (March): 160–69. doi:10.1016/j.hydromet.2015.02.012.

Leclerc, N., Meux, E., and Lecuire, J., 2003. Hydrometallurgical Extraction of Zinc from Zinc Ferrites. Hydrometallurgy 70 (1–3): 175–83.

Levenspiel, O., 1999. Chemical Reaction Engineering, (2nd ed.), John Wiley and Sons, New York, USA.

Lewis, A., 1982. Thiourea: a potential alternative for Au/Ag leaching. Eng. Min. J., 59–63.

Li, C., Xu, H., Deng, Z., Li, X., Li, M., and Wei, C., 2010. Pressure Leaching of Zinc Silicate Ore in Sulfuric Acid Medium. Transactions of Nonferrous Metals Society of China 20 (5): 918–23.

Li, H., Yao, X., Wang, M., Wu, S., Ma, W., Wei, W., and Li, L., 2014. Recovery of Elemental Sulfur from Zinc Concentrate Direct Leaching Residue Using Atmospheric Distillation: A Pilot-Scale Experimental Study. Journal of the Air & Waste Management Association 64 (1): 95–103.

Liao, M. X., and Deng, T. L., 2004. Zinc and Lead Extraction from Complex Raw Sulfides by Sequential Bioleaching and Acidic Brine Leach. Minerals Engineering 17 (1): 17–22.

Limpo, J. L., Figueiredo, J. M., Amer, S., and Luis, A., 1992. The CENIM-LNETI Process: A New Process for the Hydrometallurgical Treatment of Complex Sulphides in Ammonium Chloride Solutions. Hydrometallurgy 28 (2): 149–61.

Lloyd, T. B. and Showak, W., 1984, ‘‘Zinc and zinc alloys,’’ In; Kirk Othmer Encyclopedia of Chemical Technology, Vol. 24, 3rd Ed., New York: Wiley-Interscience, pp. 807–851.

Lochmann, J., and Pedĺik, M., 1995. Kinetic Anomalies of Dissolution of Sphalerite in Ferric Sulfate Solution. Hydrometallurgy 37 (1): 89–96.

Lorenzo-Tallafigo, J., Iglesias-González, N., Mazuelos, A., Romero, R., 2019. An alternative approach to recover lead, silver and gold from black gossan (polymetallic ore). Study of biological oxidation and lead recovery stages. Journal of cleaner production, 207, 510-521

Luna, R.M., Lapidus, G.T., 2000. Cyanidation kinetics of silver sulfide. Hydrometallurgy, 56, 171-188.

Luo, W., Li, D., Mu, D., Bai, J., and Xiao B., 2016. Preliminary Study on Zinc Smelting Relics from the Linjiangerdui Site in Zhongxian County, Chongqing City, Southwest China. Microchemical Journal 127 (July): 133–41.

Mackiw, V. N., and Veltman, H., 1967. Recovery of Zinc and Lead from Complex Low-Grade Sulphide Concentrates by Acid Pressure Leaching. Can Mining Met Bull 60 (657): 80–85.

Madhuchhanda, M., Devi, N. B., Rath, P. C., Rao, K. S., and Paramguru, R. K., 2003. Leaching of Manganese Nodule in Hydrochloric Acid in Presence of Sphalerite. Canadian Metallurgical Quarterly 42 (1): 49–59.

Madhuchhanda, M., Devi, N. B., Rao, K. S., Rath, P. C., and Paramguru, R. K., 2000a. Galvanic Interaction between Sulfide Minerals and Pyrolusite. Journal of Solid State Electrochemistry 4 (4): 189–98.

Madhuchhanda, M., Devi, N. B., Rao, K. S., Rath, P. C., and Paramguru, R. K., 2000b. Oxidation of Sphalerite in Hydrochloric Acid Medium in the Presence of Manganese Dioxide. Mineral Processing and Extractive Metallurgy 109 (3): 150–55.

Mandre, N. R., and 0Sharma, T., 1993. Preferential Leaching of Lead Zinc Complex Sulphide Ore Using Ferric Chloride. International Journal of Mineral Processing 39 (1): 75–85.

Markus, H., Fugleberg, S., Valtakari, D., Salmi, T., Murzin, D. Y., and Lahtinen, M., 2004. Kinetic Modelling of a Solid–liquid Reaction: Reduction of Ferric Iron to Ferrous Iron with Zinc Sulphide. Chemical Engineering Science 59 (4): 919–30.

Marsden, J., House, I., 2006. The chemistry of gold extraction, SME, 2nd ed., 2006.

Miceli, J.A., Stuehr, J. E., 1972. Kinetics of zinc-glycine interactions in aqueous solution, Inorg. Chem., vol. 11, no. 11, pp. 2763–2767.

Miceli, J.A., Stuehr, J. E., 1972. Kinetics of zinc-glycine interactions in aqueous solution, Inorg. Chem., vol. 11, no. 11, pp. 2763–2767.

Mellah, A., and Benachour, D., 2006. The Solvent Extraction of Zinc and Cadmium from Phosphoric Acid Solution by Di-2-Ethyl Hexyl Phosphoric Acid in Kerosene Diluent. Chemical Engineering and Processing: Process Intensification 45 (8): 684–90.

Mirazimi, S.M.J., Rashchi, F., Saba, M., 2015. A new approach for direct leaching of vanadium from LD converter slag. Chemical engineering research and design, 94,131-140.

Mirazimi, S.M.J., Rashchi, F., Saba, M., 2013. Vanadium removal from roasted LD converter slag: Optimization of parameters by response surface methodology (RSM). Separation and purification Technology, 116, 175-183.

Mizoguchi, T., and Habashi, 1981. The Aqueous Oxidation of Complex Sulfide Concentrates in Hydrochloric Acid. International Journal of Mineral Processing 8 (2): 177–93.

Mohamed, M. S., Shoukry, A. A., and Ali, A. G., 2012. Synthesis and structural characterization of ternary Cu (II) complexes of glycine with 2,2′-bipyridine and 2,2′-

dipyridylamine. The DNA-binding studies and biological activity, Spectrochim. Acta. A. Mol. Biomol. Spectrosc., vol. 86, pp. 562–570.

Molleman, E., Van Sandwijk, T., and Van, W., 1998. Acid Dissolution of Iron-Bearing Zinc Concentrates - A First Step towards Residue-Free Zinc Refining? Minerals and Metallurgical Processing 15 (3): 38–42.

Morey, M.S., 1998, PhD Thesis, University of South Australia, Adelaide, Australia.

Mu, W., Zhang, T., Liu, Y., Gu, Y., Dou, Z., Lü, G., Bao, L., and Zhang, W., 2010. E-pH Diagram of ZnS-H2O System during High Pressure Leaching of Zinc Sulfide. Transactions of Nonferrous Metals Society of China 20 (10): 2012–19.

Muir, D. M., Gale, D. C., Parker, A. J., and Giles, D. E., 1976. Leaching of the McArthur River Zinc-Lead Sulfide Concentrate in Aqueous Chloride and Chlorine Systems. Proc. Australas. Inst. Min. Met. 259 (23).

Myers, R. H., and Montgomery, D. C., Response Surface Methodology: Process and Product Optimization Using Designed Experiments, Wiley, New York, 1995.

Nava, J.L., Oropeza, M.T., González, I., 2004. Oxidation of Mineral Species as a Function of the Anodic Potential of Zinc Concentrate in Sulfuric Acid, J. Electrochem. Soc., vol. 151, no. 7, pp. B387–B393.

Nava, J., Oropeza, M., Gonza, I., 2002. Electrochemical characterisation of sulfur species formed during anodic dissolution of galena concentrate in perchlorate medium at pH 0, Electrochimica Acta, Vol. 47, pp. 1513-1525.

Navidi Kashani, A. H., and Rashchi, F., 2008. Separation of Oxidized Zinc Minerals from Tailings: Influence of Flotation Reagents. Minerals Engineering, xxxxSelected Papers from Flotation ’07, 21 (12–14): 967–72.

Nazemi, M. K., Rashchi, F., Mostoufi, N., 2011. A new approach for identifying the rate controlling step applied to the leaching of nickel from spent catalyst. International Journal of Mineral Processing 100 (1-2): 21-26.

Nilsson, L., Pettersson, S., and Sandström, Å., 1996. New Process for Zinc Recovery from Bacterial Leach Solutions. Scandinavian Journal of Metallurgy 25 (4): 161–71.

Nogueira, E. D., Regife, J. M., and Viegas, M. P., 1979. Winning Zinc through Solvent Extraction and Electrowinning. Engineering and Mining Journal 180 (10): 92–94.

Nogueira, E. D., Regife, J. M., and Viegas, M. P., 1982. Design Features and Operating Experience of the Quimigal ZINCEX Plant.

O'Brien, R.N., 1996. Hydrometallurgical recovery of copper and zinc from complex sulfide ores. US Patent 5,484,579, issued 1996.

O'Brien, R.N., and Peters, E., 1998. Preferential hydrometallurgical conversion of zinc sulfide to sulfate from zinc sulfide containing ores and concentrates. US Patent 5,711,922, filed January 27, and issued 1998.

Ogura, K., Kobayashi, M., Nakayama, M., Miho, Y., 1998. Electrochemical and in situ FTIR studies on the adsorption and oxidation of glycine and lysine in alkaline medium, Journal of Electroanalytical Chemistry, Vol. 449, pp. 101-109.

Oraby, E.A., and Eksteen, J. J., 2014. The selective leaching of copper from a gold–copper concentrate in glycine solutions, Hydrometallurgy, vol. 150, pp. 14–19.

Oraby E. A., and Eksteen, J. J., 2015. The leaching of gold, silver and their alloys in alkaline glycine–peroxide solutions and their adsorption on carbon, Hydrometallurgy, vol. 152, pp. 199–203.

Ortiz-Aparicio, J. L., Meas, Y., Trejo, G., Ortega, R., Chapman, T.W., Chainet, E., Ozil, P., 2007. Electrodeposition of zinc–cobalt alloy from a complexing alkaline glycinate bath, Electrochimica Acta, vol. 52, no. 14, pp. 4742–4751.

Owusu, G., 1993. The role of surfactants in the leaching of zinc sulphide minerals at temperatures above the melting point of sulphur. Doctor of Philosophy, Vancuver, Canada: The University of British Columbia.

Owusu, G., Peters, E., and Dreisinger, D. B., 1992. Surface Tensions and Contact Angles due to Lignin Sulphonates in the System: Liquid Sulphur, Aqueous Zinc Sulphate and Zinc Sulphide. The Canadian Journal of Chemical Engineering 70 (1): 173–80.

Ozberk, E., Ckalkley, M. E., Collins, M. J., and Masters, I. M., 1995. Commercial Applications of the Sherritt Zinc Pressure Leach Process and Iron Disposal. Mineral Processing and Extractive Metallurgy Review 15 (1–4): 115–33

Palencia, I., Romero, R., and Carranza, F., 1998. Silver Catalyzed IBES Process: Application to a Spanish Copper–zinc Sulphide Concentrate. Part 2. Biooxidation of the Ferrous Iron and Catalyst Recovery. Hydrometallurgy 48 (1): 101–12.

Palencia, I., Romero, R., Mazuelos, A., and Carranza, F., 2002. Treatment of Secondary Copper Sulphides (Chalcocite and Covellite) by the BRISA Process. Hydrometallurgy 66 (1–3): 85–93.

Pande, A. M., Gupta, K. N., and Altekar, V. A., 1982. Single Cell Extraction of Zinc and Manganese Dioxide from Zinc Sulphide Concentrate and Manganese Ores. Hydrometallurgy 9 (1): 57–68.

Pawlek, F. E., 1969. Research in Pressure Leaching. Journal of the South Africa Institute of Mining and Metallurgy 69 (12): 632–54.

Pecina, T., Franco, T., Castillo, P., and Orrantia, E., 2008. Leaching of a Zinc Concentrate in H2SO4 Solutions Containing H2O2 and Complexing Agents. Minerals Engineering, Selected papers from Bio and Hydrometallurgy 107, Falmouth, UK, May 2007, 21 (1): 23–30.

Peng, J., and Liu, C., 1997. Kinetics of Leaching of Sphalerite with Pyrolusite Simultaneously by Microwave Irradiation. Transactions of Nonferrous Metals Society of China 7 (3): 152–54.

Peng, P., Xie, H., and Lu, L., 2005a. Coupling Leaching of Sphalerite Concentrate. Minerals Engineering 18 (5): 553–55.

Peng, P., Xie, H., and Lu, L., 2005b. Leaching of a Sphalerite Concentrate with H2SO4–HNO3 Solutions in the Presence of C2Cl4. Hydrometallurgy 80 (4): 265–71.

Peters, E., 1976. Direct Leaching of Sulfides: Chemistry and Applications. Metallurgical Transactions B 7 (4): 505–17.

Petersen, J., and Dixon, D. G., 2007. Modelling Zinc Heap Bioleaching. Hydrometallurgy 85 (2–4): 127–43. doi:10.1016/j.hydromet.2006.09.001.

Pistorio, M., Curutchet, G., Donati, E., and Tedesco, P., 1995. Direct zinc sulphide bioleaching by thioemcillus eerrooxidans and thioracillus thiooxidans. Biotechnology Letters 16 (4): 419–24.

Pubchem 2020, Glycine, viewed 02 Feb 2020, <https://pubchem.ncbi.nlm.nih.gov/compound/Glycine>.

Puente-Siller, D.M., Fuentes-Aceituno, J.C., Nava-Alonso, F. , 2013. A kinetic–thermodynamic study of silver leaching in thiosulfate–copper–ammonia–EDTA solutions. Hydrometallurgy, 134-135, 124-131.

Raghavan, R, Mohanan, P. K., and Patnaik, S. C., 1998. Innovative Processing Technique to Produce Zinc Concentrate from Zinc Leach Residue with Simultaneous Recovery of Lead and Silver. Hydrometallurgy 48 (2): 225–37.

Raghavan, R, Mohanan, P. K., and Verma, S. K., 1999. Modified Zinc Sulphate Solution Purification Technique to Obtain Low Levels of Cobalt for the Zinc Electrowinning Process. Hydrometallurgy 51 (2): 187–206.

Rao, S., Yang, T., Zhang, D., Liu, W., Chen, L., Hao, Z., Xiao, Q., and Wen, J., 2015. Leaching of Low Grade Zinc Oxide Ores in NH4Cl–NH3 Solutions with Nitrilotriacetic Acid as Complexing Agents. Hydrometallurgy 158 (December): 101–6.

Rice, N. M., and Smith, M. R. 1975. Recovery of Zinc, Cadmium and Mercury (II) from Chloride and Sulphate Media by Solvent Extraction. Journal of Applied Chemistry and Biotechnology 25 (5): 379–402.

Riveros, P. A., and Dutrizac, J. E., 1997. Regeneration of Spent Phosphoric Acid Leaching Solutions by Solvent Extraction. Mineral Processing and Extractive Metallurgy Review 17 (1–4): 1–22.

Rodriguez-Torres, I., Valentin, G., Chanel, S., and Lapicque, F., 2000. Recovery of zinc and nickel from electrogalvanisation sludges using glycine solutions, Electrochimica Acta, vol. 46, no. 2–3, pp. 279–287.

Rojas-Hernández, A., Teresa Ramírez, M., González, I., 1993. Equilibria among Condensed Phases and a Multi-Component Solution Using the Concept of Generalized Species, Analytica Chimica Acta, vol. 278, no. 2, p.p 321–33.

Romero, R., Palencia, I., and Carranza, F., 1998. Silver Catalyzed IBES Process: Application to a Spanish Copper–zinc Sulphide Concentrate: Part 3. Selection of the Operational Parameters for a Continuous Pilot Plant. Hydrometallurgy 49 (1–2): 75–86.

Chaudhury, R.G., and Das, R. P., 1987. Bacterial Leaching — Complex Sulphides of Copper, Lead and Zinc. International Journal of Mineral Processing 21 (1): 57–64.

Safari, V., Arzpeyma, G., Rashchi, F., and Mostoufi, N., 2009. A Shrinking Particle—shrinking Core Model for Leaching of a Zinc Ore Containing Silica. International Journal of Mineral Processing 93 (1): 79–83.

Sakia, R.M. 1992. The Box–Cox transformation technique: a review. Journal of the Royal Statistical Society. Series D (The Statistician), 41, 169-178.

Sandström, Å., and Petersson, S., 1997. Bioleaching of a Complex Sulphide Ore with Moderate Thermophilic and Extreme Thermophilic Microorganisms. Hydrometallurgy 46 (1): 181–90.

Santos, F. M. F., Pina, P. S., Porcaro, R., Oliveira, V. A., Silva, C. A., and Leão, V. A., 2010. The Kinetics of Zinc Silicate Leaching in Sodium Hydroxide. Hydrometallurgy 102 (1–4): 43–49.

Santos, S. M. C., Rosinda, M., Ismael, C., Joana, M., Correia, N. , Teresa, M., Reis, A., Deep, A., and de Carvalho, J. M. R., 2007. Hydrometallurgical Treatment of a Zinc Concentrate by Atmospheric Direct Leach Process. In Proceedings of European Congress of Chemical Engineering. Copenhagen.

Santos, S. M. C., Machado, R. M., Joana, M., Correia, N., Teresa, M., Reis, A., Rosinda, M., Ismael, C., and de Carvalho, J. M. R., 2010. Ferric Sulphate/chloride Leaching of Zinc and Minor Elements from a Sphalerite Concentrate. Minerals Engineering 23 (8): 606–15.

Saxén, B., 2008. Zinc Direct Leaching. Outotec.

Senanayake, G., 2008. A review of effects of silver, lead, sulfide and carbonaceous matter on gold cyanidation and mechanistic interpretation. Hydrometallurgy, vol. 90, pp. 46-73.

Srinivasan, G.N., Venkatakrishna Iyer, S., 2000. Cyclic voltammetric studies on sphalerite electrodes, Bull. Electrochem., vol. 16, no. 1, pp. 5–9.

Shi, S., Fang, Z., and Ni, J., 2006. Comparative Study on the Bioleaching of Zinc Sulphides. Process Biochemistry 41 (2): 438–46.

Shibayama, A., Kagaya, S., Miyazaki, T., Kuzuno, E., Fujita, T., and Masuda, H., 2001. Studies of the Direct Leaching of Zinc Concentrates and the Recovery of Elemental Sulfur from the Leach Residue. Resources Processing 48 (1): 37–43.

Sinclair, R. J., 2005. The Extractive Metallurgy of Zinc [Electronic Resource] / Roderick J. Sinclair. A Spectrum Series (Australasian Institute of Mining and Metallurgy) ; No. 13. Carlton South, Vic: AusIMM.

Sinclair, R. J., 2009. The Extractive Metallurgy of Lead [Electronic Resource] / Roderick J. Sinclair. Spectrum Series (Carlton, Vic. (CD-ROM)) ; No. 15. Carlton South, Vic: AusIMM.

Srivastava, O. K.; Secco, E. A. "Studies on metal hydroxy compounds. I. Thermal analyses of zinc derivatives e-Zn(OH)2, Zn5(OH)8Cl2•(H2O), beta-ZnOHCl, and ZnOHF." Can. J. Chem.1967, 45, 579.

Smale, D., 2015. Review and Outlook for Copper, Nickel, Lead and Zinc. J-SUMIT 2. Tokyo, Japan: International lead and zinc study group.

Smyres, G. A., and Garnahan, T. G., 1985. Chlorine-Oxygen Leaching of a Low-Grade Zinc Sulfide Flotation Concentrate. Pittsburgh, Pa: U.S. Dept. of the Interior, Bureau of Mines Pgh.

Sokić, M., Marković, B., Matković, V., Živković, D., Štrbac, N., and Stojanović, J., 2012. Kinetics and mechanism of sphalerite leaching by sodium nitrate in sulphuric acid solution. Journal of Mining and Metallurgy Section B: Metallurgy 48 (2): 185–95.

Soleimani, M., Petersen J., Roostaazad, R., Hosseini, S., Mousavi, S. M., Najafi, A., and Kazemi Vasiri, A., 2011. Leaching of a Zinc Ore and Concentrate Using the GeocoatTM Technology. Minerals Engineering 24 (1): 64–69.

Souza, A. D., Pina, P. S., Leão, V. A., Silva, C. A., and Siqueira, P. F., 2007. The Leaching Kinetics of a Zinc Sulphide Concentrate in Acid Ferric Sulphate. Hydrometallurgy 89 (1–2): 72–81.

Souza, A. D., Pina, P. S., Santos, F. M. F., da Silva, C. A., and Leão, V. A.. 2009. Effect of Iron in Zinc Silicate Concentrate on Leaching with Sulphuric Acid. Hydrometallurgy 95 (3–4): 207–14.

Steemson, M. L., Sheehan, G. J, Winborne, D. A., and Wong, F. S., 1994. An integrated bioleach/solvent extraction process for zinc metal production from zinc concentrates. PCT World Patent WO 94/28184, filed December 8, 1994, and issued 1994.

Steemson, M. L., Wong, F. S., and Goebel, B., 1997. The Integration of Zinc Bioleaching with Solvent Extraction for the Production of Zinc Metal from Zinc Concentrates. In: Proc. Int. Biohydrometallurgy Symp. IBS97_BIOMINE97 'Biotechnology Comes of Age.' Glenside, Australia: Australian Mineral Foundation. Pp. M1.4.1_M1.4.10.

Silva, G, 2004. Kinetics and mechanism of the bacterial and ferric sulphate oxidation of galena. Hydrometallurgy, 75, pp:99-110.

Tanda, B.C., Eksteen, J.J., and Oraby, E.A, 2017. An investigation into the leaching behaviour of copper oxide minerals in aqueous alkaline glycine solutions. Hydrometallurgy, 167, pp:153-162.

Tanda, B.C., 2017, PhD Thesis, Curtin University, Perth, Australia.

Thompson, W.T., Kaye, M.H., Bale, C.W., Pelton, A.D., 2011. Pourbaix Diagrams for Multielement Systems, in Uhlig's Corrosion Handbook, R. W. Revie, Ed. John Wiley & Sons, Inc., pp. 103–9.

Tian, M., Mu, F., Jia, Q., Quan, X., and Liao, W., 2011. Solvent Extraction Studies of Zinc(II) and Cadmium(II) from a Chloride Medium with Mixtures of Neutral Organophosphorus

Extractants and Amine Extractants. Journal of Chemical & Engineering Data 56 (5): 2225–29.

Tiechui, Y., Qinyuan, C., and Jie, Li., 2010. Effects of Mechanical Activation on Physicochemical Properties and Alkaline Leaching of Hemimorphite. Hydrometallurgy 104 (2): 136–41.

Tkáčová, K., Baláž, P., Mišura, B., Vigdergauz, V. E., and Chanturiya, V. A., 1993. Selective Leaching of Zinc from Mechanically Activated Complex Cu-Pb-Zn Concentrate. Hydrometallurgy 33 (3): 291–300.

Tromans, D., 2000. Oxygen Solubility Modelling in Ammoniacal Leaching Solutions: Leaching of Sulphide Concentrates. Minerals Engineering 13 (5): 497–515.

Uçar, G., 2009. Kinetics of Sphalerite Dissolution by Sodium Chlorate in Hydrochloric Acid. Hydrometallurgy 95 (1–2): 39–43.

Urzúa-Abarcaa, D.A., Fuentes-Aceitunoa, J.C., Uribe-Salasa, A., Lee, J.C., 2018. An electrochemical study of silver recovery in thiosulfate solutions. A window towards the development of a simultaneous electroleaching- electrodeposition process. Hydrometallurgy, 177. 104-117.

Vazarlis, H. G., 1987. Hydrochloric Acid-Hydrogen Peroxide Leaching and Metal Recovery from a Greek Zinc-Lead Bulk Sulphide Concentrate. Hydrometallurgy 19 (2): 243–51.

Verink, E.D., 2011. Simplified Procedure for Constructing Pourbaix Diagrams, in Uhlig's Corrosion Handbook, R. W. Revie, Ed. John Wiley & Sons, Inc., pp. 93–101.

Vignes, A., 2011. Extractive Metallurgy: Processing Operation and Routes. Vol. 3. John Wiley & Sons.

Vignes, A., 2013. Extractive Metallurgy 2: Metallurgical Reaction Processes. 1 edition. Wiley-ISTE.

Walkiewicz, J. W., Kazonich, G., and McGill, S. L., 1988. Microwave Heating Characteristics of Selected Minerals and Compound. Minerals and Metallurgical Processing 5 (1): 39–42.

Wang, R., Tang, M., Yang, S., Zhagn, W., Tang, C., He, J., and Yang, J., 2008. Leaching Kinetics of Low Grade Zinc Oxide Ore in NH3-NH4Cl-H2O System. Journal of Central South University of Technology 15 (5): 679–83.

Wassink, B., Dreisinger, D., and Howard, J., 2000. Solvent Extraction Separation of Zinc and Cadmium from Nickel and Cobalt Using Aliquat 336, a Strong Base Anion Exchanger, in the Chloride and Thiocyanate Forms. Hydrometallurgy 57 (3): 235–52.

Weert, G. V., and van Sandwijk, T., 1999. Routes to Residue-Free Zinc Refining. JOM 51 (12): 26–28. doi:10.1007/s11837-999-0167-7.

Weisener, C. G., Smart, R. S. t. C., and Gerson, A. R., 2003. Kinetics and Mechanisms of the Leaching of Low Fe Sphalerite. Geochimica et Cosmochimica Acta, Advances in Oxide and Sulfide Mineral Surface Chemistry, 67 (5): 823–30.

Weisener, C. G., Smart, R. St. C., and Gerson, A. R., 2004. A Comparison of the Kinetics and Mechanism of Acid Leaching of Sphalerite Containing Low and High Concentrations of Iron. International Journal of Mineral Processing 74 (1–4): 239–49.

Weiss, H. V., Lai, M. G., and Gillespie, A., 1961. Co-Crystallization of Ultramicro Quantities of Various Elements with α-Nitroso-β-Naphthol Determination of Uranium in Seawater. Analytica Chimica Acta 25 (6): 550–56.

West-sells, P.G., 1992. Fundamental Study of the Deposition of Cobalt from Electrolytes Containing Zinc. BSc, Vancuver, Canada: University of British Columbia.

Xia, D. K., and Picklesi, C. A., 2000. Microwave Caustic Leaching of Electric Arc Furnace Dust. Minerals Engineering 13 (1): 79–94.

Xiao, L., Wang, Y.L., Yu, Y., Fu, G.Y., Han, P.W., Sun, Z.H.I., Ye, S.F., 2018. An environmentally friendly process to selectively recover silver from copper anode slime. Journal of cleaner production, 187, 708-716.

Xie, K., Wen, J., Hua, Y., and Ruan, R., 2008. Selective Separation of Cu(II), Zn(II), and Cd(II) by Solvent Extraction. Rare Metals 27 (3): 228–32.

Xie, F., Dreisinger, D. B., 2007. Leaching of silver sulfide with ferricyanide–cyanide solution. Hydrometallurgy, 88, 98-108.

Xie, F., Dreisinger, D. B., 2009. Use of ferricyanide for gold and silver cyanidation. Transactions of Nonferrous Metals Society of China, 19, 714-718.

Xu, H., Wei, C., Li, C., Fan, G., Deng, Z., Zhou, X., and Qiu, S., 2012. Leaching of a Complex Sulfidic, Silicate-Containing Zinc Ore in Sulfuric Acid Solution under Oxygen Pressure. Separation and Purification Technology 85 (February): 206–12.

Xu, Z., Jiang, Q., and Wang, C., 2013. Atmospheric Oxygen-Rich Direct Leaching Behavior of Zinc Sulphide Concentrate. Transactions of Nonferrous Metals Society of China 23 (12): 3780–87.

Yin, Z., Ding, Z., Hu, H., Liu, K., and Chen, Q., 2010. Dissolution of Zinc Silicate (Hemimorphite) with Ammonia–ammonium Chloride Solution. Hydrometallurgy 103 (1–4): 215–20.

Zárate-Gutiérrez, R., Lapidus, G. T., and Morales, R. D., 2010. Pressure Leaching of a Lead–zinc–silver Concentrate with Nitric Acid at Moderate Temperatures between 130 and 170 °C. Hydrometallurgy 104 (1): 8–13.

Zhao, Z., Long, S., Chen, A., Huo, G., Li, H., Jia, X., and Chen, X., 2009. Mechanochemical Leaching of Refractory Zinc Silicate (Hemimorphite) in Alkaline Solution. Hydrometallurgy 99 (3–4): 255–58.

Appendices

Appendix A: Experimental Data

Appendix A 1 Additives screening dissolution data

Constants:

Pure sphalerite mineral
P80 < 65 micro
12mm Cold pressed disc
Nitrogen atmosphere
500 ml DI water
500 rpm
Temperature 35

Run			1	2	3	4
Factor 1	A:Gly	M	3	4	4	4
Factor 2	B:Media		NaOH	Ca(OH)2	Ca(OH)2	NaOH
Factor 3	C:Pb(NO3)2	g/t	0	0	0	200
Factor 4	D:NaCl	g/l	300	300	0	300
Factor 5	E:KMnO4	g/l	2	0	2	0
Factor 5	F:H2O2	M	.04	0	.04	.04
Factor 7	G:pH		10.5	10.5	9	9
Zn Dissolution	2hrs	ppm	**2.5**	**105.4**	**126**	**262**
Zn Dissolution	4hrs	ppm	**148.9**	**144.6**	**198.8**	**291**
Zn Dissolution	6hrs	ppm	**807.1**	**193.5**	**221.7**	**351**
Zn Dissolution	24hrs	ppm	**4544**	**504**	**6416**	**1456**
Zn Dissolution	48hrs	ppm	**8000**	**667.8**	**8107.2**	**2144**

Run			5	6	7	8
Factor 1	A:Gly	M	3	3	3	4
Factor 2	B:Media		Ca(OH)2	NaOH	Ca(OH)2	NaOH
Factor 3	C:Pb(NO3)2	g/t	200	0	200	200
Factor 4	D:NaCl	g/l	0	0	300	0
Factor 5	E:KMnO4	g/l	0	0	2	2
Factor 6	F:H2O2	M	.04	0	0	0
Factor 7	G:pH		10.5	9	9	10.5

Zn Dissolution	2hrs	ppm	ND	41.1	156.3	136
Zn Dissolution	4hrs	ppm	ND	43.8	265	175
Zn Dissolution	6hrs	ppm	115.5	55.6	321.5	213
Zn Dissolution	24hrs ppm	ppm	276.5	112.8	606.2	6480
Zn Dissolution	48hrs ppm	ppm	444.4	132.2	836	6784

Appendix A 2 Silver sulphide leaching data

Constants:

Synthetic silver sulphide
12mm cold pressed disc
500 ml DI Water
Nitrogen Atmosphere
500 rpm
±0.1 Tolerance

Run			1	2	3	4
Factor 1	A:Temperature		25	50	25	42.5
Factor 2	B:Glycine	M	2	2	2	2
Factor 3	C:NaCl	g/l	300	300	300	300
Factor 4	D:pH		11.5	11.5	11.5	10

Ag Dissolution	10 min		0.11	0.42	0.49	0.18
Ag Dissolution	20 min		0.111	0.42	0.5	0.18
Ag Dissolution	30 min		0.116	0.43	0.5	0.19
Ag Dissolution	40 min		0.123	0.46	0.61	0.2

Run			5	6	7	8
Factor 1	A:Temperature		25	25	25	50
Factor 2	B:Glycine	M	1	3	1.605	0
Factor 3	C:NaCl	g/l	0	100	117	100
Factor 4	D:pH		11.5	11.5	10.5	11.5

Ag Dissolution	10 min		0.035	0.115	0.145	0.096
Ag Dissolution	20 min		0.035	0.117	0.145	0.098

Ag Dissolution	30 min		**0.036**	**0.117**	**0.235**	**0.099**
Ag Dissolution	40 min		**0.037**	**0.127**	**0.315**	**0.102**

Run			9	10	11	12
Factor 1	A:Temperature		50	25	25	35
Factor 2	B:Glycine	M	2	3	1	2
Factor 3	C:NaCl	g/l	0	300	100	200
Factor 4	D:pH		9	10	10	9

Ag Dissolution	10 min		**0.021**	**0.47**	**0.103**	**0.106**
Ag Dissolution	20 min		**0.022**	**0.49**	**0.104**	**0.187**
Ag Dissolution	30 min		**0.023**	**0.5**	**0.108**	**0.229**
Ag Dissolution	40 min		**0.023**	**0.53**	**0.134**	**ND**

Run			13	14	15	16
Factor 1	A:Temperature		50	25	35	25
Factor 2	B:Glycine	M	0	1	0	3
Factor 3	C:NaCl	g/l	300	100	300	0
Factor 4	D:pH		10	10	11.5	9

Ag Dissolution	10 min		**0.37**	**ND**	**0.44**	**0.44**
Ag Dissolution	20 min		**0.38**	**ND**	**0.015**	**0.015**
Ag Dissolution	30 min		**0.39**	**ND**	**0.099**	**0.107**
Ag Dissolution	40 min		**0.42**	**ND**	**0.104**	**0.105**

Run			17	18	19	20
Factor 1	A:Temperature		25	42.5	35	25
Factor 2	B:Glycine	M	1	3	0	0
Factor 3	C:NaCl	g/l	100	100	0	300
Factor 4	D:pH		10	10	9	9

Ag Dissolution	10 min		**0.44**	**0.44**	**0**	**0.3**
Ag Dissolution	20 min		**0.015**	**0.015**	**0**	**0.32**
Ag Dissolution	30 min		**0.107**	**0.115**	**0**	**0.33**
Ag Dissolution	40 min		**0.109**	**0.112**	**0**	**0.35**

Run			21	22	23	24
Factor 1	A:Temperature		35	50	35	42.5

Factor 2	B:Glycine	M	2	3	2	3
Factor 3	C:NaCl	g/l	0	300	200	100
Factor 4	D:pH		11	9	9	10
Ag Dissolution	10 min		**0.033**	**0.41**	**0.3**	**0.112**
Ag Dissolution	20 min		**0.034**	**0.42**	**0.695**	**0.114**
Ag Dissolution	30 min		**0.036**	**0.42**	**0.845**	**0.115**
Ag Dissolution	40 min		**0.039**	**0.48**	**0.87**	**0.116**

Run			25
Factor 1	A:Temperature		35
Factor 2	B:Glycine	M	2
Factor 3	C:NaCl	g/l	0
Factor 4	D:pH		11
Ag Dissolution	10 min		**0.025**
Ag Dissolution	20 min		**0.026**
Ag Dissolution	30 min		**0.027**
Ag Dissolution	40 min		**0.031**

Appendix A 3 Sphalerite leaching optimisation data

Constants:

500 rpm
500 g DI water
1 Sphalerite concentrate
PSD < 10 micron
Temperature 35
Dissolved oxygen 8 ppm

Run			1	2	3	4
Factor 1	A:pH		10	11	11	10.7
Factor 2	B:Gly	g/l	3.61	5.25	1.97	1.97
Factor 3	C:Cu++	g	0.216	0.393	0.039	0.393
Zn Rec.%		24 hrs	**12.1**	**21.59**	**12.18**	**14.28**
Cu Rec.		%+%	**-31.8**	**-44.1**	**98**	**-146.2**

Pb Rec. %		1 hr	**13.59**	**20.14**	**3.02**	**10.12**
Pb Rec. %		24 hrs	**4.72**	**6.66**	**11.5**	**1.57**

Run			5	6	7	8
Factor 1	A:pH		10.62	11	9	10.07
Factor 2	B:Gly	g/l	5.25	3.667196	3.364	3.5608
Factor 3	C:Cu++	g	0.039	0.20892	0.393	0.22308

Zn rec.%		24 hrs	**20.78**	**15.88**	**10.94**	**10.93**
Cu Rec.		%+%	**63.1**	**-54**	**-99.2**	**-14.5**
Pb Rec. %		1 hr	**23.39**	**16.2**	**22.03**	**18.11**
Pb Rec. %		24 hrs	**15.12**	**6.84**	**13.8**	**12.93**

Run			9	10	11	12
Factor 1	A:pH		10.42	9.68	10.07	9.68
Factor 2	B:Gly	g/l	3.4952	5.25	3.5608	5.25
Factor 3	C:Cu++	g	0.039	0.393	0.22308	0.393

Zn Rec.%		24 hrs	**10.6**	**14.8**	**10.91**	**13.7**
Cu Rec.		%+%	**74.5**	**7.4**	**-15.1**	**-62.5**
Pb Rec. %		1 hr	**14.49**	**27.56**	**17.21**	**25.48**
Pb Rec. %		24 hrs	**8.36**	**15.81**	**14.79**	**18.29**

Run			13	14	15	16
Factor 1	A:pH		9	10	9	9
Factor 2	B:Gly	g/l	3.8396	3.61	5.25	3.61
Factor 3	C:Cu++	g	0.039	0.216	0.192392	0.216

Zn Rec.%		24 hrs	**11.5**	**15.58**	**13.92**	**14.04**
Cu Rec.		%+%	**74.5**	**-4**	**-3.5**	**-7.1**
Pb Rec. %		1 hr	**23.39**	**16.2**	**28.87**	**23.8**
Pb Rec. %		24 hrs	**0**	**0**	**0**	**14.49**

Run			17	18	19	20
Factor 1	A:pH		10.07	10.62	10.91585	9.68
Factor 2	B:Gly	g/l	3.5608	5.25	1.9864	1.97
Factor 3	C:Cu++	g	0.22308	0.039	0.21777	0.039

Zn Rec.%		24 hrs	**10.98**	**20.35**	**15.55**	**8.51**
Cu Rec.		%+%	**18.4**	**79.4**	**3.2**	**74.8**
Pb Rec. %		1 hr	**17.6**	**12.03**	**10.35**	**11.36**
Pb Rec. %		24 hrs	**10.48**	**6.84**	**2.28**	**6.08**

Run			21	22	23	24
Factor 1	A:pH		9.636193	9.56	9	9.68
Factor 2	B:Gly	g/l	1.97	5.25	1.97	1.97
Factor 3	C:Cu++	g	0.392557	0.039	0.24078	0.039

Zn Rec.%		24 hrs	**9.67**	**11.65**	**10.58**	**7.48**
Cu Rec.		%+%	**-37.1**	**96.3**	**-64.9**	**73.1**
Pb Rec. %		1 hr	**13.87**	**25.92**	**5.97**	**15.46**
Pb Rec. %		24 hrs	**4.19**	**15.12**	**3.25**	**5.18**

Appendix A 4 Bottle roll leaching data

Constants:

500 g DI water
10 g/l zinc sulphide concentrate
0.00875 M Total metal for 1 g solid
PSD >75 micron
Temperature 30

Run			1	2	3	4
Factor 1	A:pH		8.5	10	10	11
Factor 2	B:Gly/Total Metal	M	7	15	3	15
Factor 3	C:Cu++	ppm	10	0	10	10
Factor 4	D:NaCl	M	0.5	0.5	1	0

Zinc Recovery@1:30 hr	%	**6.38**	**6.98**	**6.23**	**6.77**
Zinc Recovery@24 hr	%	**6.49**	**7.06**	**6.6**	**6.92**
Zinc Recovery@48 hr	%	**7.21**	**7.32**	**6.81**	**7.72**
Zinc Recovery@168 hr	%	**9.81**	**11.2**	**9.31**	**11.9**
Zinc Recovery@360 hr	%	**13.8**	**16**	**12.6**	**18.5**
Lead Recovery@1:30 hr	%	**43.6**	**44.7**	**28.1**	**28.6**

Copper Recovery@168 hr		%	**47.3**	**29.6**	**39.3**	**37.5**
Silver Recovery@48 hr		%	**35.9**	**91.8**	**78.2**	**94.4**

Run			5	6	7	8
Factor 1	A:pH		10	8.5	11	11
Factor 2	B:Gly/Total Metal	M	7	3	3	7
Factor 3	C:Cu++	ppm	20	0	20	0
Factor 4	D:NaCl	M	0	0	0.5	1

Zinc Recovery@1:30 hr		%	**6.52**	**4.93**	**5.79**	**6.46**
Zinc Recovery@24 hr		%	**6.67**	**5.3**	**6.34**	**6.66**
Zinc Recovery@48 hr		%	**8.73**	**5.41**	**7.27**	**7.23**
Zinc Recovery@168 hr		%	**10.1**	**6.98**	**11.4**	**10.8**
Zinc Recovery@360 hr		%	**13.9**	**8.8**	**15.4**	**15.1**
Lead Recovery@1:30 hr		%	**45.2**	**33**	**16.6**	**12.9**
Copper Recovery@168 hr		%	**73.6**	**21.9**	**88**	**18.7**
Silver Recovery@48 hr		%	**43.9**	**3.64**	**65.7**	**98.1**

Run			9
Factor 1	A:pH		8.5
Factor 2	B:Gly/Total Metal	M	15
Factor 3	C:Cu++	ppm	20
Factor 4	D:NaCl	M	1

Zinc Recovery@1:30 hr		%	**6.7**
Zinc Recovery@24 hr		%	**6.8**
Zinc Recovery@48 hr		%	**8.4**
Zinc Recovery@168 hr		%	**11.7**
Zinc Recovery@360 hr		%	**16.9**
Lead Recovery@1:30 hr		%	**42.6**
Copper Recovery@168 hr		%	**69.5**
Silver Recovery@48 hr		%	**56.6**

Appendix A 5 Kinetics data

Constants:

Sphalerite concentrate 2 g/l
PSD < 75 micron
10 ppm Cupric ion
500 gr DI water
100 g/l NaCl
500 rpm

25 Degree								
		0	10	45	130	285	360	1430
Do 10	Pb	0	23.96313	23.5023	11.52074	11.52074	11.52074	
	Zn	0	5.253692	5.588792	5.911587	7.092957	7.432791	
	Ag	0	84.09091	84.09091	86.36364	88.63636	90.90909	94.2
	Cu	0	62.11019	64.58048	69.16817	78.34354	-7.05798	-7.05798

35 Degree	500cc							
		0	20	60	120	180	320	480
Do 10	Pb	0	29.95392	13.36406	11.98157	11.05991	10.59908	
	Zn	0	5.289663	6.147293	6.405718	7.138395	7.672283	8.510034
	Ag	0	63.63636	65.90909	65.90909	65.90909	68.18182	84.09091
	Cu	0	61.40439	78.34354	74.46165	74.46165	86.10731	96.69427

45 Degree	1 litre	22032019						
		0	10	45	130	285	360	1262
Do 10	Pb	0	28.1106	24.88479	8.75576	12.90323	0	
	Zn	0	5.06437	5.717531	7.198031	9.002272	15.57412	
	Ag	0	43.18182	44.31818	45.45455	45.45455	45.45455	53.40909
	Cu	0	62.46309	66.34498	65.28628	75.52035	81.1	
Do 20	Pb	0	28.57143	26.72811	18.89401	13.36406	0	
	Zn	0	5.251799	6.012874	7.778304	10.3086	11.48713	
	Ag	0	40.90909	42.04545	43.18182	43.18182	44.31818	45.45455
	Cu	0	68.81527	70.93266	73.40295	74.81455	-7.05798	

55 Degree

		0	20	60	120	180	240	360
Do 10	Pb	0	28.57143	16.12903	11.98157	9.677419	8.75576	9.21659
	Zn	0	4.990534	6.520257	8.423892	10.64701	12.19945	21.03133
	Ag	0	32.95455	32.95455	32.95455	34.09091	37.5	43.18182
	Cu	0	75.87324	79.40223	86.46021	89.2834	94.57688	95.51
Do 20	Pb	0	30.87558	20.73733	15.20737	12.4424	11.05991	15.6682
	Zn	0	5.604885	6.952859	8.558311	10.41272	12.17815	14.47842
	Ag	0	35.22727	35.22727	36.36364	36.36364	36.23	47.72727
	Cu	0	47.99424	52.58192	55.05221	56.81671	58.2283	60.3457

Appendix A 6 Condition of cyclic voltammetry tests

Run		**#1**	**#2**	**#3**	**#4**	**#5**	**#6**	**#7**
Number of Segment		3	3	3	3	3	3	3
Initial Potential	mV	-188.8	-188.8	-188.8	-188.8	-188.8	-188.8	-188.8
Initial direction		falling	rising	rising	rising	rising	rising	rising
Upper potential	mV	1000	1000	-50	150	350	-188	-188
Lower potential	mV	-1000	-1000	-650	-650	-650	-650	-650
Final potential	mV	-1000	-1000	0	170	400	0	-150
Sweep rate	mV/s	100	100	20	20	20	20	20
Induction period	mV	-188.8	-188.8	-188.8	-188.8	-188.8	-188.8	-188.8
Duration	s	3	3	3	3	3	3	3
Relaxaion period	V	-1	-1	0	170	400	0	-150
Duration	s	1	1	1	1	1	1	1
Run		**#8**	**#9**	**#10**	**#11**	**#12**	**#13**	**#14**
Number of Segment		3	3	2	3	3	3	3
Initial Potential	mV	-188.8	-188.8	0	0	-188.8	-188.8	-188.8
Initial direction		rising	falling		rising	falling	rising	falling
Upper potential	mV	1000	1000	1000	1000	100	100	100
Lower potential	mV	-1000	-1000		-1000	-400	-400	-500
Final potential	mV	1000	-1000	-1000	0	-188.8	-188.8	-188.8
Sweep rate	mV/s	20	20	20	20	20	20	20
Induction period	mV	-188.8	-188.8	0	0	-188.8	-188.8	-188.8
Duration	s	3	3	3	3	3	3	3
Relaxaion period	V	1	-1	-1	-1	-188.8	-188.8	-188.8
Duration	s	1	1	1	1	1	1	1
Run		**#15**	**#16**	**#17**	**#18**	**#19**	**#20**	**#21**
Number of Segment		3	3	3	3	3	3	3

Initial Potential	mV	-188.8	-188.8	-188.8	-188.8	-188.8	-188.8	-188.8
Initial direction		rising	falling	rising	rising	rising	rising	falling
Upper potential	mV	100	100	100	350	350	500	100
Lower potential	mV	-500	-600	-600	-650	-650	-650	-300
Final potential	mV	-188.8	-188.8	-188.8	-188.8	350	500	-188.8
Sweep rate	mV/s	20	20	20	20	20	20	20
Induction period	mV	-188.8	-188.8	-188.8	-188.8	-188.8	-188.8	-188.8
Duration	s	3	3	3	3	3	3	3
Relaxaion period	V	-188.8	-188.8	-188.8	-188.8	350	500	-188.8
Duration	s	1	1	1	1	1	1	1
Run		#22	#23	#24	#25	#26	#27	#28
Number of Segment		3	3	10	3	3	3	9
Initial Potential	mV	-188.8	-188.8	-188.8	61	61	61	61
Initial direction		falling	rising	rising	falling	rising	rising	rising
Upper potential	mV	100	650	1000	1000	1000	1000	1000
Lower potential	mV	-250	-650	-1000	-1000	-1000	-1000	-1000
Final potential	mV	-188.8	650	-188.8	61	1000	1000	1000
Sweep rate	mV/s	20	20	20	20	20	20	20
Induction period	mV	-188.8	-188.8	-188.8	61	61	61	61
Duration	s	3	3	3	3	3	3	3
Relaxaion period	V	-188.8	650	-188.8	61	1	1	1
Duration	s	1	1	1	1	1	1	1
Run		#29	#30	#31				
Number of Segment		9	3	3				
Initial Potential	mV	-75	-75	-75				
Initial direction		rising	rising	falling				
Upper potential	mV	1000	1000	1000				
Lower potential	mV	-1000	-1000	-1000				
Final potential	mV	1000	0	-75				
Sweep rate	mV/s	20	20	20				
Induction period	mV	-75	-75	-75				
Duration	s	3	3	3				
Relaxaion period	V	1	0	-75				
Duration	s	1	1	1				

Appendix A 7 Chronoamperometry data of silver sulphide

Silver Sulphide							
-600	mV	-550	mV	-450	mV	200	mV
Time (s)	Current (A)	Time (s)	Current (A)	Time (s)	Current (A)	Time (s)	Current (A)
0	-1.0533E-05	0	-1.0533E-05	0	-1.0533E-05	0	1.6346E-05
6	-5.6589E-05	6	-2.1803E-05	6	-6.3851E-05	6	5.5387E-06
12	-4.4314E-05	12	-2.0526E-05	12	-4.8498E-05	12	4.9637E-06
18	-3.9222E-05	18	-1.9185E-05	18	-3.7447E-05	18	4.6716E-06
24	-3.676E-05	24	-1.7909E-05	24	-3.1507E-05	24	4.4525E-06
30	-3.4979E-05	30	-1.6672E-05	30	-2.7892E-05	30	4.3085E-06
36	-3.3955E-05	36	-1.5616E-05	36	-2.5929E-05	36	4.2554E-06
42	-3.3547E-05	42	-1.4845E-05	42	-2.4964E-05	42	4.2167E-06
48	-3.3184E-05	48	-1.4236E-05	48	-2.4225E-05	48	4.1191E-06
54	-3.2964E-05	54	-1.3763E-05	54	-2.3992E-05	54	4.0763E-06
60	-3.2984E-05	60	-1.3446E-05	60	-2.3629E-05	60	4.0553E-06
66	-3.2932E-05	66	-1.3245E-05	66	-2.3565E-05	66	4.0299E-06
72	-3.3949E-05	72	-1.3031E-05	72	-2.3467E-05	72	4.0292E-06
78	-3.3327E-05	78	-1.2999E-05	78	-2.3545E-05	78	3.9152E-06
84	-3.3068E-05	84	-1.3096E-05	84	-2.3558E-05	84	3.8308E-06
90	-3.3074E-05	90	-1.3057E-05	90	-2.3701E-05	90	3.8933E-06
96	-3.3307E-05	96	-1.3051E-05	96	-2.3817E-05	96	3.7383E-06
102	-3.3392E-05	102	-1.2973E-05	102	-2.3999E-05	102	3.8376E-06
108	-3.3495E-05	108	-1.2973E-05	108	-2.4277E-05	108	3.7119E-06
114	-3.3845E-05	114	-1.2992E-05	114	-2.418E-05	114	3.6298E-06
120	-3.3942E-05	120	-1.3096E-05	120	-2.4478E-05	120	3.6713E-06
126	-3.4201E-05	126	-1.3206E-05	126	-2.4536E-05	126	3.5486E-06
132	-3.4584E-05	132	-1.3187E-05	132	-2.4789E-05	132	3.5161E-06
138	-3.4726E-05	138	-1.3232E-05	138	-2.4854E-05	138	3.5096E-06
144	-3.5082E-05	144	-1.3362E-05	144	-2.497E-05	144	3.4884E-06
150	-3.5393E-05	150	-1.3459E-05	150	-2.499E-05	150	3.4513E-06
156	-3.5549E-05	156	-1.3582E-05	156	-2.5191E-05	156	3.3705E-06
162	-3.5789E-05	162	-1.3595E-05	162	-2.5527E-05	162	3.3853E-06
168	-3.6041E-05	168	-1.3692E-05	168	-2.5527E-05	168	3.2935E-06
174	-3.6372E-05	174	-1.3744E-05	174	-2.591E-05	174	3.2036E-06
180	-3.6469E-05	180	-1.3841E-05	180	-2.5897E-05	180	3.2436E-06
186	-3.6754E-05	186	-1.3945E-05	186	-2.6201E-05	186	3.2226E-06
192	-3.7E-05	192	-1.4016E-05	192	-2.6376E-05	192	3.1108E-06
198	-3.735E-05	198	-1.4113E-05	198	-2.659E-05	198	3.1395E-06
204	-3.7538E-05	204	-1.4184E-05	204	-2.6849E-05	204	3.1318E-06
210	-3.7732E-05	210	-1.434E-05	210	-2.6914E-05	210	3.1695E-06
216	-3.8036E-05	216	-1.4392E-05	216	-2.7017E-05	216	3.0831E-06
222	-3.8198E-05	222	-1.4489E-05	222	-2.716E-05	222	2.9833E-06
228	-3.849E-05	228	-1.4515E-05	228	-2.7302E-05	228	3.0364E-06
234	-3.8976E-05	234	-1.4567E-05	234	-2.7393E-05	234	3.0574E-06
240	-3.9196E-05	240	-1.4742E-05	240	-2.76E-05	240	3.0071E-06
246	-3.941E-05	246	-1.4858E-05	246	-2.7762E-05	246	2.9865E-06
252	-3.9377E-05	252	-1.4942E-05	252	-2.7872E-05	252	2.9852E-06
258	-3.9967E-05	258	-1.502E-05	258	-2.8151E-05	258	2.9984E-06
264	-3.9954E-05	264	-1.5124E-05	264	-2.8183E-05	264	2.8963E-06
270	-4.0213E-05	270	-1.5156E-05	270	-2.83E-05	270	2.8322E-06
276	-4.0258E-05	276	-1.524E-05	276	-2.8468E-05	276	2.8834E-06
282	-4.0543E-05	282	-1.5331E-05	282	-2.8656E-05	282	2.8944E-06
288	-4.0867E-05	288	-1.5525E-05	288	-2.8689E-05	288	2.78E-06
294	-4.1049E-05	294	-1.5616E-05	294	-2.9006E-05	294	2.8148E-06
300	-4.1224E-05	300	-1.5765E-05	300	-2.9097E-05	300	2.8219E-06
306	-4.1282E-05	306	-1.5752E-05	306	-2.9207E-05	306	2.8109E-06
312	-4.1476E-05	312	-1.5823E-05	312	-2.9233E-05	312	2.7736E-06
318	-4.1515E-05	318	-1.5933E-05	318	-2.9434E-05	318	2.7961E-06
324	-4.1807E-05	324	-1.6005E-05	324	-2.968E-05	324	2.7932E-06

330	-4.1884E-05	330	-1.6141E-05	330	-3.012E-05	330	2.7207E-06
336	-4.228E-05	336	-1.6309E-05	336	-2.9842E-05	336	2.7043E-06
342	-4.2461E-05	342	-1.6316E-05	342	-3.003E-05	342	2.6608E-06
348	-4.2636E-05	348	-1.6309E-05	348	-3.0243E-05	348	2.6386E-06
354	-4.2727E-05	354	-1.6478E-05	354	-3.0237E-05	354	2.645E-06
360	-4.2921E-05	360	-1.6549E-05	360	-3.0574E-05	360	2.6392E-06
366	-4.3141E-05	366	-1.6581E-05	366	-3.0917E-05	366	2.5771E-06
372	-4.3361E-05	372	-1.6769E-05	372	-3.1111E-05	372	2.6621E-06
378	-4.3452E-05	378	-1.6886E-05	378	-3.1073E-05	378	2.5951E-06
384	-4.3705E-05	384	-1.6957E-05	384	-3.1358E-05	384	2.511E-06
390	-4.388E-05	390	-1.6983E-05	390	-3.1584E-05	390	2.5668E-06
396	-4.397E-05	396	-1.7074E-05	396	-3.1656E-05	396	2.5996E-06
402	-4.4003E-05	402	-1.7229E-05	402	-3.1779E-05	402	2.5355E-06
408	-4.421E-05	408	-1.7294E-05	408	-3.1928E-05	408	2.4617E-06
414	-4.4385E-05	414	-1.7359E-05	414	-3.1876E-05	414	2.4637E-06
420	-4.467E-05	420	-1.7339E-05	420	-3.2193E-05	420	2.4695E-06
426	-4.4683E-05	426	-1.7501E-05	426	-3.1973E-05	426	2.4766E-06
432	-4.4871E-05	432	-1.7637E-05	432	-3.2303E-05	432	2.4724E-06
438	-4.5033E-05	438	-1.7663E-05	438	-3.2485E-05	438	2.5265E-06
444	-4.5227E-05	444	-1.7663E-05	444	-3.2647E-05	444	2.484E-06
450	-4.5415E-05	450	-1.7825E-05	450	-3.2362E-05	450	2.4898E-06
456	-4.5493E-05	456	-1.7961E-05	456	-3.2375E-05	456	2.5043E-06
462	-4.5577E-05	462	-1.7968E-05	462	-3.2861E-05	462	2.4998E-06
468	-4.5713E-05	468	-1.7929E-05	468	-3.2886E-05	468	2.4189E-06
474	-4.5927E-05	474	-1.8091E-05	474	-3.3165E-05	474	2.3603E-06
480	-4.6024E-05	480	-1.8162E-05	480	-3.3197E-05	480	2.35E-06
486	-4.6179E-05	486	-1.8291E-05	486	-3.3385E-05	486	2.3384E-06
492	-4.6251E-05	492	-1.8298E-05	492	-3.3625E-05	492	2.3954E-06
498	-4.6393E-05	498	-1.8376E-05	498	-3.3418E-05	498	2.3976E-06
504	-4.6581E-05	504	-1.846E-05	504	-3.3094E-05	504	2.3857E-06
510	-4.6736E-05	510	-1.8525E-05	510	-3.3333E-05	510	2.3206E-06
516	-4.684E-05	516	-1.8855E-05	516	-3.3405E-05	516	2.3503E-06
522	-4.7034E-05	522	-1.8862E-05	522	-3.391E-05	522	2.4305E-06
528	-4.708E-05	528	-1.8842E-05	528	-3.4001E-05	528	2.3628E-06
534	-4.7294E-05	534	-1.8816E-05	534	-3.3975E-05	534	2.3158E-06
540	-4.7319E-05	540	-1.8933E-05	540	-3.4014E-05	540	2.3387E-06
546	-4.7546E-05	546	-1.9088E-05	546	-3.3858E-05	546	2.3973E-06
552	-4.7617E-05	552	-1.9121E-05	552	-3.4279E-05	552	2.3464E-06
558	-4.7715E-05	558	-1.916E-05	558	-3.4156E-05	558	2.3313E-06
564	-4.7838E-05	564	-1.9172E-05	564	-3.4512E-05	564	2.3232E-06
570	-4.798E-05	570	-1.9237E-05	570	-3.448E-05	570	2.3335E-06
576	-4.8071E-05	576	-1.9341E-05	576	-3.4402E-05	576	2.3651E-06
582	-4.8181E-05	582	-1.9464E-05	582	-3.4681E-05	582	2.2862E-06
588	-4.8285E-05	588	-1.9574E-05	588	-3.4694E-05	588	2.2401E-06
594	-4.8421E-05	594	-1.9639E-05	594	-3.4577E-05	594	2.302E-06
599	-4.8401E-05	599	-1.9652E-05	599	-3.4959E-05	599	2.3213E-06

Silver Sulphide

275	mV	330	mV	415	mV
Time (s)	Current (A)	Time (s)	Current (A)	Time (s)	Current (A)
0	3.6001E-05	0	4.5122E-05	0	4.6404E-05
6	1.1844E-05	6	9.538E-06	6	1.0328E-05
12	1.0056E-05	12	7.9979E-06	12	8.7919E-06
18	9.1704E-06	18	7.3166E-06	18	7.9689E-06
24	8.5445E-06	24	6.9455E-06	24	7.5434E-06
30	8.177E-06	30	6.7435E-06	30	7.3333E-06
36	7.6522E-06	36	6.4678E-06	36	7.2067E-06
42	7.5157E-06	42	6.3244E-06	42	6.9841E-06
48	7.2895E-06	48	6.269E-06	48	6.9088E-06
54	7.0518E-06	54	6.0999E-06	54	6.9787E-06
60	6.6111E-06	60	5.9327E-06	60	7.0399E-06
66	6.6353E-06	66	5.9205E-06	66	6.864E-06

72	6.1266E-06	72	5.8657E-06	72	6.9922E-06
78	6.0799E-06	78	5.8013E-06	78	7.0176E-06
84	6.0184E-06	84	5.6689E-06	84	7.0692E-06
90	5.9102E-06	90	5.6434E-06	90	7.1475E-06
96	5.7327E-06	96	5.6457E-06	96	7.1378E-06
102	5.6489E-06	102	5.6006E-06	102	7.1326E-06
108	5.6067E-06	108	5.5577E-06	108	7.198E-06
114	5.542E-06	114	5.4917E-06	114	7.3488E-06
120	5.5114E-06	120	5.4424E-06	120	7.2866E-06
126	5.5217E-06	126	5.446E-06	126	7.4483E-06
132	5.4311E-06	132	5.4595E-06	132	7.4696E-06
138	5.3045E-06	138	5.4518E-06	138	7.4184E-06
144	5.31E-06	144	5.4163E-06	144	7.5949E-06
150	5.2127E-06	150	5.3606E-06	150	7.5897E-06
156	5.3219E-06	156	5.3287E-06	156	7.61E-06
162	5.0977E-06	162	5.3358E-06	162	7.7695E-06
168	5.0704E-06	168	5.3281E-06	168	7.7498E-06
174	4.9802E-06	174	5.3993E-06	174	7.7022E-06
180	4.8967E-06	180	5.3223E-06	180	7.8365E-06
186	4.8603E-06	186	5.2337E-06	186	7.9376E-06
192	4.7985E-06	192	5.2939E-06	192	7.9447E-06
198	4.8065E-06	198	5.3516E-06	198	8.0237E-06
204	4.7502E-06	204	5.2971E-06	204	8.1966E-06
210	4.8139E-06	210	5.2843E-06	210	8.0807E-06
216	4.7856E-06	216	5.3519E-06	216	8.0514E-06
222	4.6706E-06	222	5.3461E-06	222	8.0923E-06
228	4.7189E-06	228	5.3107E-06	228	8.1589E-06
234	4.641E-06	234	5.2788E-06	234	8.1741E-06
240	4.61E-06	240	5.3171E-06	240	8.2057E-06
246	4.5975E-06	246	5.3116E-06	246	8.2997E-06
252	4.5028E-06	252	5.3686E-06	252	8.2962E-06
258	4.4564E-06	258	5.3886E-06	258	8.349E-06
264	4.4734E-06	264	5.3957E-06	264	8.3857E-06
270	4.4838E-06	270	5.3435E-06	270	8.4418E-06
276	4.4776E-06	276	5.3184E-06	276	8.5046E-06
282	4.37E-06	282	5.2984E-06	282	8.5568E-06
288	4.3182E-06	288	5.3622E-06	288	8.6299E-06
294	4.255E-06	294	5.3699E-06	294	8.5958E-06
300	4.3166E-06	300	5.3641E-06	300	8.5912E-06
306	4.3246E-06	306	5.3068E-06	306	8.6025E-06
312	4.2534E-06	312	5.3065E-06	312	8.6702E-06
318	4.2467E-06	318	5.3094E-06	318	8.6544E-06
324	4.1784E-06	324	5.3364E-06	324	8.6792E-06
330	4.2966E-06	330	5.3306E-06	330	8.7468E-06
336	4.248E-06	336	5.3538E-06	336	8.7253E-06
342	4.208E-06	342	5.3281E-06	342	8.7433E-06
348	4.2686E-06	348	5.3274E-06	348	8.8055E-06
354	4.1864E-06	354	5.3194E-06	354	8.6628E-06
360	4.1665E-06	360	5.3107E-06	360	8.6673E-06
366	4.1684E-06	366	5.3667E-06	366	8.7227E-06
372	4.0669E-06	372	5.4192E-06	372	8.7443E-06
378	4.1036E-06	378	5.4166E-06	378	8.7552E-06
384	4.1272E-06	384	5.4179E-06	384	8.7562E-06
390	4.0756E-06	390	5.3432E-06	390	8.7391E-06
396	4.0331E-06	396	5.378E-06	396	8.7201E-06
402	4.0344E-06	402	5.4501E-06	402	8.8032E-06
408	4.0998E-06	408	5.3648E-06	408	8.8467E-06
414	4.0621E-06	414	5.3786E-06	414	8.7649E-06
420	4.0476E-06	420	5.4315E-06	420	8.8235E-06
426	4.0505E-06	426	5.4324E-06	426	8.8921E-06
432	4.0373E-06	432	5.4147E-06	432	8.9056E-06
438	4.0746E-06	438	5.4108E-06	438	8.8857E-06
444	4.1114E-06	444	5.4018E-06	444	8.8705E-06

450	4.0856E-06	450	5.4131E-06	450	8.9224E-06
456	4.0257E-06	456	5.454E-06	456	8.8754E-06
462	4.0489E-06	462	5.4634E-06	462	8.8328E-06
468	4.0112E-06	468	5.5358E-06	468	8.9189E-06
474	4.0035E-06	474	5.5242E-06	474	8.8796E-06
480	3.9564E-06	480	5.4762E-06	480	8.9311E-06
486	3.8923E-06	486	5.4975E-06	486	8.9691E-06
492	3.8463E-06	492	5.6022E-06	492	9.1279E-06
498	3.8817E-06	498	5.5777E-06	498	8.9404E-06
504	3.8398E-06	504	5.5394E-06	504	8.9295E-06
510	3.9068E-06	510	5.5104E-06	510	9.0165E-06
516	3.9758E-06	516	5.5329E-06	516	8.963E-06
522	3.9345E-06	522	5.5513E-06	522	8.9282E-06
528	3.8804E-06	528	5.6019E-06	528	9.0264E-06
534	3.8575E-06	534	5.6666E-06	534	9.0252E-06
540	3.8427E-06	540	5.6547E-06	540	9.0542E-06
546	3.8852E-06	546	5.616E-06	546	9.0171E-06
552	3.8614E-06	552	5.6676E-06	552	9.0142E-06
558	3.8595E-06	558	5.7597E-06	558	9.0809E-06
564	3.8955E-06	564	5.7346E-06	564	9.115E-06
570	3.8417E-06	570	5.7053E-06	570	9.0509E-06
576	3.9178E-06	576	5.6847E-06	576	9.0361E-06
582	3.8401E-06	582	5.6866E-06	582	9.0835E-06
588	3.9616E-06	588	5.7555E-06	588	9.1192E-06
594	3.8901E-06	594	5.8277E-06	594	9.0255E-06
599	3.872E-06	599	5.7636E-06	599	9.0809E-06

Appendix A8 Chronoamperometry data of lead sulphide

Lead Sulphide							
562.5	mV	625	mV	678.5	mV	100	mV
Time (s)	Current (A)	Time (s)	Current (A)	Time (s)	Current (A)	Time (s)	Current (A)
0	0.000167107	0	0.00021314	0	0.00028089	0	9.8462E-05
10	0.0004118	10	0.00019502	10	0.0003752	10	7.1759E-05
20	0.000356332	20	0.00014972	20	0.00030747	20	7.1422E-05
30	0.000342165	30	0.00013325	30	0.00029293	30	7.1468E-05
40	0.000336115	40	0.00012305	40	0.00028536	40	7.1176E-05
50	0.000333795	50	0.00011652	50	0.00027936	50	7.0995E-05
60	0.000333076	60	0.00011061	60	0.0002753	60	7.0716E-05
70	0.000334171	70	0.00010544	70	0.00027259	70	7.0276E-05
80	0.00033526	80	0.00010004	80	0.00027052	80	6.9777E-05
90	0.000336438	90	9.4983E-05	90	0.00026886	90	6.9324E-05
100	0.000337812	100	9.0571E-05	100	0.00026737	100	6.8766E-05
110	0.000339373	110	8.6393E-05	110	0.00026628	110	6.8235E-05
120	0.000341401	120	8.3212E-05	120	0.00026533	120	6.7413E-05
130	0.000343053	130	8.009E-05	130	0.00026428	130	6.659E-05
140	0.000344484	140	7.6644E-05	140	0.00026343	140	6.58E-05
150	0.000346661	150	7.3716E-05	150	0.00026298	150	6.5048E-05
160	0.000349122	160	7.0749E-05	160	0.00026242	160	6.4258E-05
170	0.000351059	170	6.8177E-05	170	0.00026177	170	6.3467E-05
180	0.000353346	180	6.5385E-05	180	0.00026128	180	6.258E-05
190	0.000354668	190	6.293E-05	190	0.00026091	190	6.1854E-05
200	0.000356501	200	6.0293E-05	200	0.00026055	200	6.109E-05
210	0.000357971	210	5.7585E-05	210	0.0002602	210	6.0125E-05
220	0.000359124	220	5.5299E-05	220	0.00025975	220	5.9471E-05
230	0.000360634	230	5.3407E-05	230	0.0002596	230	5.8693E-05
240	0.000362694	240	5.1755E-05	240	0.00025919	240	5.8045E-05
250	0.000363834	250	5.0207E-05	250	0.00025896	250	5.7184E-05
260	0.000365473	260	4.7732E-05	260	0.00025874	260	5.6607E-05

270	0.000366451	270	4.6068E-05	270	0.00025853	270	5.5966E-05
280	0.000367578	280	4.4636E-05	280	0.00025819	280	5.5221E-05
290	0.000367805	290	4.369E-05	290	0.00025805	290	5.456E-05
300	0.000369308	300	4.2848E-05	300	0.00025774	300	5.3958E-05
310	0.000370435	310	4.2006E-05	310	0.00025764	310	5.3401E-05
320	0.000371413	320	4.1371E-05	320	0.00025751	320	5.285E-05
330	0.000371608	330	4.073E-05	330	0.00025731	330	5.2176E-05
340	0.000372741	340	4.0244E-05	340	0.00025722	340	5.1632E-05
350	0.00037346	350	3.9758E-05	350	0.00025711	350	5.1043E-05
360	0.000373182	360	3.9227E-05	360	0.00025691	360	5.0544E-05
370	0.000373713	370	3.8773E-05	370	0.00025679	370	4.9974E-05
380	0.000374704	380	3.8242E-05	380	0.00025668	380	4.9417E-05
390	0.000375468	390	3.7912E-05	390	0.00025668	390	4.8918E-05
400	0.000374626	400	3.7303E-05	400	0.00025662	400	4.8426E-05
410	0.000375028	410	3.6895E-05	410	0.00025656	410	4.7927E-05
420	0.000374516	420	3.6597E-05	420	0.00025639	420	4.7467E-05
430	0.000375093	430	3.6163E-05	430	0.00025631	430	4.7052E-05
440	0.000375307	440	3.6027E-05	440	0.00025613	440	4.6625E-05
450	0.000375177	450	3.5767E-05	450	0.00025603	450	4.6229E-05
460	0.000374516	460	3.5819E-05	460	0.00025599	460	4.5789E-05
470	0.000373979	470	3.6001E-05	470	0.00025591	470	4.5348E-05
480	0.000373855	480	3.5301E-05	480	0.00025588	480	4.4966E-05
490	0.000374121	490	3.4997E-05	490	0.00025573	490	4.4591E-05
500	0.000372204	500	3.4971E-05	500	0.00025567	500	4.4208E-05
510	0.000373156	510	3.5068E-05	510	0.00025569	510	4.3826E-05
520	0.000372897	520	3.4828E-05	520	0.00025564	520	4.3548E-05
530	0.000371795	530	3.4763E-05	530	0.00025559	530	4.3152E-05
540	0.000371672	540	3.4498E-05	540	0.00025563	540	4.2777E-05
550	0.000371621	550	3.4407E-05	550	0.00025559	550	4.2485E-05
560	0.000370357	560	3.4731E-05	560	0.00025553	560	4.2122E-05
570	0.000370247	570	3.4485E-05	570	0.00025554	570	4.1818E-05
580	0.000369787	580	3.4167E-05	580	0.00025555	580	4.1572E-05
590	0.00036776	590	3.4167E-05	590	0.00025546	590	4.1183E-05
600	0.000366898	600	3.4012E-05	600	0.00025536	600	4.0989E-05

Lead Sulphide

-160	mV	-450	mV	-387.5	mV	-325	mV
Time (s)	Current (A)	Time (s)	Current (A)	Time (s)	Current (A)	Time (s)	Current (A)
0	-1.0533E-05	0	-1.0533E-05	0	-1.0533E-05	0	-1.0533E-05
6	4.8655E-08	6	-3.6184E-05	6	-1.9451E-05	6	-1.1664E-05
12	6.9916E-08	12	-3.7389E-05	12	-2.0572E-05	12	-1.2273E-05
18	1.22745E-07	18	-3.882E-05	18	-2.1168E-05	18	-1.2785E-05
24	1.33054E-07	24	-4.0096E-05	24	-2.2243E-05	24	-1.3077E-05
30	1.22101E-07	30	-4.1774E-05	30	-2.2664E-05	30	-1.3614E-05
36	8.6345E-08	36	-4.3148E-05	36	-2.3804E-05	36	-1.4081E-05
42	7.2171E-08	42	-4.3867E-05	42	-2.4484E-05	42	-1.4301E-05
48	1.09216E-07	48	-4.4936E-05	48	-2.4899E-05	48	-1.4819E-05
54	1.22745E-07	54	-4.7747E-05	54	-2.5353E-05	54	-1.5104E-05
60	1.0535E-07	60	-4.8537E-05	60	-2.6136E-05	60	-1.5499E-05
66	1.14048E-07	66	-4.9496E-05	66	-2.7497E-05	66	-1.5797E-05
72	1.0374E-07	72	-5.0008E-05	72	-2.7555E-05	72	-1.6089E-05
78	9.6653E-08	78	-5.0727E-05	78	-2.7821E-05	78	-1.6219E-05
84	4.7689E-08	84	-5.3337E-05	84	-2.7037E-05	84	-1.6322E-05
90	3.3515E-08	90	-5.5145E-05	90	-2.8598E-05	90	-1.6484E-05
96	4.0924E-08	96	-5.5747E-05	96	-2.9077E-05	96	-1.6549E-05
102	3.8025E-08	102	-5.5307E-05	102	-2.9388E-05	102	-1.6905E-05
108	8.9244E-08	108	-5.644E-05	108	-2.9375E-05	108	-1.7119E-05
114	8.4412E-08	114	-5.828E-05	114	-2.9531E-05	114	-1.7138E-05
120	2.0952E-08	120	-5.9232E-05	120	-3.0276E-05	120	-1.7074E-05
126	9.033E-09	126	-6.0982E-05	126	-3.0438E-05	126	-1.719E-05
132	1.1288E-08	132	-5.9757E-05	132	-3.0503E-05	132	-1.7611E-05
138	6.58E-10	138	-6.1273E-05	138	-2.9706E-05	138	-1.7864E-05
144	1.8375E-08	144	-6.3463E-05	144	-3.0833E-05	144	-1.7728E-05

150	2.224E-08	150	-6.5166E-05	150	-3.1545E-05	150	-1.811E-05
156	5.1232E-08	156	-6.549E-05	156	-3.1403E-05	156	-1.7922E-05
162	6.7339E-08	162	-6.5944E-05	162	-3.1507E-05	162	-1.7935E-05
168	5.993E-08	168	-6.5769E-05	168	-3.1235E-05	168	-1.7961E-05
174	6.7983E-08	174	-6.6358E-05	174	-3.1973E-05	174	-1.8201E-05
180	5.091E-08	180	-6.8917E-05	180	-3.2511E-05	180	-1.813E-05
186	5.8319E-08	186	-7.0848E-05	186	-3.2323E-05	186	-1.8356E-05
192	5.7675E-08	192	-7.0977E-05	192	-3.2323E-05	192	-1.8285E-05
198	4.6078E-08	198	-6.9746E-05	198	-3.2083E-05	198	-1.8674E-05
204	-1.919E-09	204	-7.0886E-05	204	-3.2984E-05	204	-1.8732E-05
210	-8.362E-09	210	-7.3419E-05	210	-3.3288E-05	210	-1.8538E-05
216	-6.751E-09	216	-7.4346E-05	216	-3.3061E-05	216	-1.8771E-05
222	-8.362E-09	222	-7.4048E-05	222	-3.2239E-05	222	-1.879E-05
228	-1.2872E-08	228	-7.316E-05	228	-3.3333E-05	228	-1.8816E-05
234	-8.684E-09	234	-7.4061E-05	234	-3.378E-05	234	-1.8751E-05
240	-1.1905E-08	240	-7.6483E-05	240	-3.3314E-05	240	-1.8874E-05
246	-9.973E-09	246	-7.8051E-05	246	-3.3547E-05	246	-1.879E-05
252	-4.174E-09	252	-7.888E-05	252	-3.3495E-05	252	-1.8693E-05
258	-1.2228E-08	258	-7.6334E-05	258	-3.4137E-05	258	-1.8894E-05
264	2.913E-09	264	-7.6911E-05	264	-3.4234E-05	264	-1.8706E-05
270	3.235E-09	270	-7.9405E-05	270	-3.3722E-05	270	-1.8862E-05
276	2.268E-09	276	-8.2255E-05	276	-3.3256E-05	276	-1.8894E-05
282	-8.684E-09	282	-8.2501E-05	282	-3.4441E-05	282	-1.9153E-05
288	-4.174E-09	288	-7.9211E-05	288	-3.4448E-05	288	-1.9062E-05
294	-3.852E-09	294	-8.0241E-05	294	-3.4765E-05	294	-1.9121E-05
300	8.711E-09	300	-8.346E-05	300	-3.4299E-05	300	-1.9088E-05
306	2.268E-09	306	-8.4523E-05	306	-3.4499E-05	306	-1.9341E-05
312	-5.463E-09	312	-8.4827E-05	312	-3.5277E-05	312	-1.9321E-05
318	5.4131E-08	318	-8.2314E-05	318	-3.5011E-05	318	-1.9406E-05
324	6.9594E-08	324	-8.3136E-05	324	-3.5011E-05	324	-1.9432E-05
330	5.0588E-08	330	-8.5235E-05	330	-3.38E-05	330	-1.9114E-05
336	4.845E-09	336	-8.6531E-05	336	-3.5244E-05	336	-1.9367E-05
342	-5.463E-09	342	-8.8656E-05	342	-3.5743E-05	342	-1.9347E-05
348	4.5756E-08	348	-8.5656E-05	348	-3.5413E-05	348	-1.9458E-05
354	5.7031E-08	354	-8.5488E-05	354	-3.4979E-05	354	-1.9412E-05
360	6.0574E-08	360	-8.8235E-05	360	-3.5329E-05	360	-1.9419E-05
366	7.3781E-08	366	-9.0884E-05	366	-3.5925E-05	366	-1.9632E-05
372	6.456E-09	372	-9.135E-05	372	-3.5912E-05	372	-1.9756E-05
378	3.235E-09	378	-8.9763E-05	378	-3.6242E-05	378	-1.9697E-05
384	2.8039E-08	384	-8.8805E-05	384	-3.4584E-05	384	-1.96E-05
390	6.2507E-08	390	-8.964E-05	390	-3.573E-05	390	-1.9684E-05
396	5.9608E-08	396	-9.1687E-05	396	-3.6158E-05	396	-1.949E-05
402	6.2829E-08	402	-9.1325E-05	402	-3.6307E-05	402	-1.9548E-05
408	4.5756E-08	408	-9.2659E-05	408	-3.5756E-05	408	-1.9529E-05
414	9.355E-09	414	-9.102E-05	414	-3.6054E-05	414	-1.9568E-05
420	2.3851E-08	420	-9.2439E-05	420	-3.6184E-05	420	-1.9613E-05
426	8.0868E-08	426	-9.5516E-05	426	-3.6417E-05	426	-1.9205E-05
432	6.444E-08	432	-9.3559E-05	432	-3.6521E-05	432	-1.903E-05
438	1.6764E-08	438	-9.5483E-05	438	-3.5076E-05	438	-1.9153E-05
444	1.7408E-08	444	-9.3229E-05	444	-3.6333E-05	444	-1.9296E-05
450	2.4817E-08	450	-9.411E-05	450	-3.6929E-05	450	-1.9283E-05
456	2.2563E-08	456	-9.5924E-05	456	-3.6981E-05	456	-1.9315E-05
462	7.4426E-08	462	-9.652E-05	462	-3.6883E-05	462	-1.914E-05
468	6.9594E-08	468	-9.8528E-05	468	-3.5866E-05	468	-1.9153E-05
474	8.6345E-08	474	-9.5393E-05	474	-3.6922E-05	474	-1.9134E-05
480	9.8263E-08	480	-9.6449E-05	480	-3.7227E-05	480	-1.9211E-05
486	7.4748E-08	486	-9.9752E-05	486	-3.744E-05	486	-1.8952E-05
492	4.0924E-08	492	-0.0001006	492	-3.6184E-05	492	-1.8894E-05
498	3.0294E-08	498	-0.00010109	498	-3.6534E-05	498	-1.9147E-05
504	5.5098E-08	504	-9.8638E-05	504	-3.7168E-05	504	-1.9198E-05
510	9.2465E-08	510	-9.9273E-05	510	-3.7389E-05	510	-1.8913E-05
516	1.01807E-07	516	-0.00010149	516	-3.7317E-05	516	-1.9011E-05
522	9.8263E-08	522	-0.00010277	522	-3.6598E-05	522	-1.8972E-05

528	9.4398E-08	528	-0.00010087	528	-3.711E-05	528	-1.8946E-05
534	5.8963E-08	534	-0.00010219	534	-3.7829E-05	534	-1.8913E-05
540	3.9313E-08	540	-0.00010228	540	-3.7881E-05	540	-1.8829E-05
546	4.5434E-08	546	-0.00010357	546	-3.7641E-05	546	-1.8946E-05
552	1.13404E-07	552	-0.00010426	552	-3.5918E-05	552	-1.8894E-05
558	1.07283E-07	558	-0.00010395	558	-3.7512E-05	558	-1.8855E-05
564	5.0588E-08	564	-0.00010395	564	-3.8108E-05	564	-1.8849E-05
570	5.7031E-08	570	-0.0001047	570	-3.8049E-05	570	-1.8777E-05
576	1.15336E-07	576	-0.00010562	576	-3.6935E-05	576	-1.8751E-05
582	1.0986E-07	582	-0.00010616	582	-3.7162E-05	582	-1.8667E-05
588	4.8011E-08	588	-0.00010552	588	-3.8101E-05	588	-1.8719E-05
594	6.3795E-08	594	-0.00010633	594	-3.8127E-05	594	-1.8641E-05
599	5.8963E-08	599	-0.00010653	599	-3.8237E-05	599	-1.8654E-05

Lead Sulphide

137.5	mV	175	mV	250	mV
Time (s)	Current (A)	Time (s)	Current (A)	Time (s)	Current (A)
0	0.0001593	0	0.00018103	0	0.000213135
10	0.00010448	10	0.00013167	10	0.000330304
20	0.00010532	20	0.00013427	20	0.000258748
30	0.0001039	30	0.00014017	30	0.000214984
40	0.00010362	40	0.00013861	40	0.000192477
50	0.00010397	50	0.0001359	50	0.0001768
60	0.00010387	60	0.00013908	60	0.000165807
70	0.00010074	70	0.00014038	70	0.000157651
80	0.00010074	80	0.00013776	80	0.000151536
90	9.6887E-05	90	0.00013735	90	0.000145855
100	9.714E-05	100	0.00014085	100	0.000141223
110	9.6544E-05	110	0.00013823	110	0.000137563
120	9.4964E-05	120	0.00013697	120	0.000133436
130	9.0992E-05	130	0.00013825	130	0.000130029
140	8.9425E-05	140	0.00013317	140	0.000126006
150	8.8706E-05	150	0.00013315	150	0.000122055
160	8.6322E-05	160	0.00013368	160	0.000118686
170	8.5415E-05	170	0.00013232	170	0.000115078
180	8.5214E-05	180	0.00012736	180	0.000111767
190	8.3964E-05	190	0.00012823	190	0.000108975
200	8.3951E-05	200	0.00012805	200	0.000106287
210	8.283E-05	210	0.00012208	210	0.000103534
220	8.1949E-05	220	0.00012362	220	0.000100923
230	7.9656E-05	230	0.00012463	230	9.87855E-05
240	7.8425E-05	240	0.00012388	240	9.63239E-05
250	7.6436E-05	250	0.00012275	250	9.4387E-05
260	7.4836E-05	260	0.00012343	260	9.25926E-05
270	7.3359E-05	270	0.00012346	270	9.08305E-05
280	7.2971E-05	280	0.00012282	280	8.9088E-05
290	7.2491E-05	290	0.00012189	290	8.73454E-05
300	7.126E-05	300	0.00012189	300	8.58684E-05
310	7.0516E-05	310	0.00012067	310	8.44303E-05
320	6.9149E-05	320	0.00011771	320	8.3044E-05
330	6.8196E-05	330	0.0001168	330	8.16965E-05
340	6.7289E-05	340	0.00011734	340	8.06277E-05
350	6.6655E-05	350	0.0001132	350	7.95199E-05
360	6.5806E-05	360	0.00011318	360	7.84316E-05
370	6.4834E-05	370	0.00011411	370	7.73304E-05
380	6.4232E-05	380	0.00011353	380	7.65141E-05
390	6.3377E-05	390	0.00011198	390	7.5685E-05
400	6.2884E-05	400	0.00011164	400	7.47716E-05
410	6.2029E-05	410	0.00011259	410	7.41238E-05
420	6.1543E-05	420	0.00011051	420	7.3612E-05
430	6.0928E-05	430	0.00011122	430	7.28994E-05
440	6.0766E-05	440	0.00011233	440	7.242E-05
450	6.0403E-05	450	0.00011162	450	7.185E-05

460	6.0105E-05	460	0.00011094	460	7.14289E-05
470	5.973E-05	470	0.00011037	470	7.09884E-05
480	5.9036E-05	480	0.00011089	480	7.07682E-05
490	5.868E-05	490	0.0001089	490	7.03924E-05
500	5.7773E-05	500	0.00010904	500	7.00167E-05
510	5.7721E-05	510	0.00010916	510	6.98094E-05
520	5.7132E-05	520	0.00010914	520	6.96475E-05
530	5.6756E-05	530	0.00010739	530	6.94596E-05
540	5.651E-05	540	0.00010747	540	6.92717E-05
550	5.6173E-05	550	0.00010824	550	6.91875E-05
560	5.5512E-05	560	0.00010681	560	6.91227E-05
570	5.5247E-05	570	0.00010557	570	6.9181E-05
580	5.4683E-05	580	0.00010629	580	6.90774E-05
590	5.4508E-05	590	0.00010654	590	6.90774E-05
600	5.4256E-05	600	0.00010536	600	6.90644E-05

Appendix A 9 Chronoamperometry data of zinc sulphide

Zinc Sulphide							
-550	mV	-500	mV	-450	mV	-175	mV
Time (s)	Current (A)	Time (s)	Current (A)	Time (s)	Current (A)	Time (s)	Current (A)
0	-10.5327053	0	-10.5327	0	-10.5327053	0	-10.5327053
6	-50.7851546	0.1	-49.1462	6	-31.007803	0.1	-1.82646966
12	-41.4309143	0.2	-47.7211	12	-25.8642649	0.2	-1.54879262
18	-41.1782712	0.3	-46.121	18	-24.4779712	0.3	-1.4653607
24	-37.6348034	0.4	-47.164	24	-23.47388	0.4	-1.49080904
30	-37.2461218	0.5	-48.4077	30	-23.4414911	0.5	-1.53816234
36	-36.5724081	0.6	-49.0231	36	-23.5969619	0.6	-1.57778447
42	-37.0841699	0.7	-49.5867	42	-23.9143847	0.7	-1.64059998
48	-36.818572	0.8	-51.3164	48	-24.1605485	0.8	-1.6892418
54	-38.0429155	0.9	-53.2986	54	-25.2618102	0.9	-1.76333197
60	-38.1465652	1	-53.9205	60	-25.6893582	1	-1.83677776
66	-38.91097	1.1	-55.0542	66	-26.2659014	1.1	-1.94887934
72	-39.8049342	1.2	-56.7125	72	-27.1015633	1.2	-2.00976228
78	-40.5887731	1.3	-58.1312	78	-28.6627637	1.3	-2.1511778
84	-41.9038079	1.4	-59.4333	84	-29.4919482	1.4	-2.25619237
90	-43.06337	1.5	-60.9232	90	-30.4053465	1.5	-2.33124888
96	-42.5386534	1.6	-61.9597	96	-31.4159151	1.6	-2.40759391
102	-44.8124338	1.7	-63.5792	102	-32.4329631	1.7	-2.55223085
108	-44.5597907	1.8	-64.1104	108	-34.0135957	1.8	-2.63856191
114	-46.5938829	1.9	-65.2829	114	-34.9593865	1.9	-2.74035528
120	-46.5355806	2	-67.33	120	-36.6760578	2	-2.85310125
126	-49.2563449	2.1	-68.2628	126	-37.3109033	2.1	-2.92493655
132	-50.6620709	2.2	-68.9236	132	-38.7619766	2.2	-2.99612748
138	-51.0960999	2.3	-69.7333	138	-40.1223551	2.3	-3.09598795
144	-51.8151573	2.4	-71.1326	144	-41.2819209	2.4	-3.18489629
150	-52.9423305	2.5	-73.1667	150	-42.6746919	2.5	-3.26414056
156	-54.9440338	2.6	-73.7886	156	-43.8148199	2.6	-3.32856666
162	-55.2549791	2.7	-75.8421	162	-45.0326843	2.7	-3.42810517
168	-56.0064291	2.8	-76.7101	168	-46.3606775	2.8	-3.46482807
174	-57.230769	2.9	-77.643	174	-47.6627538	2.9	-3.53601899
180	-58.2542962	3	-77.915	180	-47.1704261	3	-3.602378
186	-58.7401446	3.1	-79.5151	186	-50.1697432	3.1	-3.66970335
192	-59.5822858	3.2	-80.3508	192	-51.1220096	3.2	-3.70674843
198	-61.3183947	3.3	-81.8861	198	-52.8322053	3.3	-3.77632887
204	-62.1346189	3.4	-82.6764	204	-53.4800056	3.4	-3.79340167
210	-63.294181	3.5	-83.2659	210	-54.8598218	3.5	-3.83592305
216	-64.5962646	3.6	-84.4708	216	-56.4145412	3.6	-3.88102126
222	-65.704	3.7	-86.1097	222	-57.3149846	3.7	-3.96219866

228	-66.844128	3.8	-87.5284	228	-58.3579422	3.8	-3.98088196
234	-67.8935685	3.9	-86.7187	234	-60.0875719	3.9	-4.03564445
240	-69.4353366	4	-88.7268	240	-61.3443044	4	-4.03403374
246	-70.0183518	4.1	-89.9512	246	-62.5103421	4.1	-4.06334766
252	-70.88641	4.2	-90.6962	252	-64.0845028	4.2	-4.07365587
258	-72.1560937	4.3	-91.2597	258	-65.0108559	4.3	-4.08396409
264	-73.2508779	4.4	-92.1472	264	-66.0149453	4.4	-4.12777399
270	-74.3910059	4.5	-92.795	270	-67.1680318	4.5	-4.09298354
276	-74.9286846	4.6	-93.9222	276	-68.1203019	4.6	-4.10039274
282	-75.8420792	4.7	-94.6672	282	-69.5713752	4.7	-4.12712961
288	-76.9044782	4.8	-95.1595	288	-70.6208084	4.8	-4.17544925
294	-77.8502654	4.9	-96.9086	294	-71.475908	4.9	-4.20476317
300	-79.1976927	5	-97.822	300	-73.0111933	5	-4.21893674
306	-80.3572548	5.1	-97.9774	306	-74.2808843	5.1	-4.2340771
312	-81.555685	5.2	-98.9491	312	-74.792646	5.2	-4.22086987
318	-82.4885137	5.3	-99.4868	318	-75.4404464	5.3	-4.20572951
324	-83.7258121	5.4	-100.115	324	-76.8137834	5.4	-4.23214442
330	-84.3088346	5.5	-101.203	330	-78.238947	5.5	-4.25115013
336	-85.3064485	5.6	-101.754	336	-78.238947	5.6	-4.23665415
342	-86.1226799	5.7	-102.978	342	-80.1240458	5.7	-4.19187791
348	-87.2109813	5.8	-103.114	348	-80.9532285	5.8	-4.2079846
354	-88.2409877	5.9	-104.125	354	-82.3783921	5.9	-4.20605147
360	-88.739791	6	-105.226	360	-83.583298	6	-4.22344692
366	-89.7892314	6.1	-105.168	366	-84.1080182	6.1	-4.2340771
372	-91.1496099	6.2	-106.263	372	-85.0343713	6.2	-4.22344692
378	-91.4540797	6.3	-107.118	378	-86.2522356	6.3	-4.20734023
384	-92.1796163	6.4	-108.588	384	-87.2304154	6.4	-4.2079846
390	-93.4169148	6.5	-108.323	390	-88.0207372	6.5	-4.23890879
396	-94.019364	6.6	-109.113	396	-88.9600415	6.6	-4.2353654
402	-95.0882386	6.7	-109.78	402	-90.2167812	6.7	-4.22602398
408	-95.9368554	6.8	-110.078	408	-90.9423179	6.8	-4.2079846
414	-96.7142187	6.9	-111.523	414	-91.9464073	6.9	-4.23762049
420	-97.7247837	7	-111.601	420	-92.5229469	7	-4.20701781
426	-98.1523335	7.1	-111.206	426	-93.1189279	7.1	-4.19155594
432	-99.771838	7.2	-111.957	432	-94.045281	7.2	-4.23504343
438	-100.225298	7.3	-113.836	438	-94.9133318	7.3	-4.23697611
444	-101.125741	7.4	-114.347	444	-95.9822064	7.4	-4.24889504
450	-101.799451	7.5	-115.326	450	-97.0964174	7.5	-4.26274664
456	-102.589773	7.6	-114.218	456	-97.6859155	7.6	-4.27402119
462	-103.470775	7.7	-116.271	462	-98.7742242	7.7	-4.29882539
468	-104.144492	7.8	-117.262	468	-99.6293238	7.8	-4.2704778
474	-104.98015	7.9	-116.375	474	-100.25769	7.9	-4.29946977
480	-105.640909	8	-117.088	480	-100.996178	8	-4.27981968
486	-106.515443	8.1	-118.707	486	-101.287689	8.1	-4.28175235
492	-107.091982	8.2	-119.672	492	-102.764672	8.2	-4.26886709
498	-108.01186	8.3	-119.549	498	-102.589773	8.3	-4.25501548
504	-108.419976	8.4	-118.927	504	-103.140403	8.4	-4.26951146
510	-109.676708	8.5	-120.08	510	-104.442479	8.5	-4.28819521
516	-110.512374	8.6	-120.994	516	-105.660343	8.6	-4.2640354
522	-110.661364	8.7	-122.309	522	-106.515443	8.7	-4.27466557
528	-111.633068	8.8	-121.991	528	-106.904125	8.8	-4.25888129
534	-112.578855	8.9	-121.726	534	-107.603744	8.9	-4.295282
540	-113.233131	9	-123.151	540	-108.4135	9	-4.29238298
546	-113.99106	9.1	-124.667	546	-109.346329	9.1	-4.28916155
552	-114.606468	9.2	-124.719	552	-109.825705	9.2	-4.27981968
558	-115.163581	9.3	-124.79	558	-110.628978	9.3	-4.28400745
564	-116.025156	9.4	-124.984	564	-111.082438	9.4	-4.29818101
570	-116.323143	9.5	-125.742	570	-112.177222	9.5	-4.2704778
576	-116.925599	9.6	-127.012	576	-112.747286	9.6	-4.27949772
582	-117.599309	9.7	-127.167	582	-112.941627	9.7	-4.2965703
588	-118.37019	9.8	-127.783	588	-113.984584	9.8	-4.32330717
594	-119.037424	9.9	-127.86	594	-114.677729	9.9	-4.30784485
599	-119.348369	9.983333	-128.126	599	-114.813767	9.98333333	-4.29109423

Zinc Sulphide

-137.5	mV	-100	mV	500	mV	700	mV
Time (s)	Current (A)	Time (s)	Current (A)	Time (s)	Current (A)	Time (s)	Current (A)
0	-10.5327	0	-10.5327053	0	10.5781528	0	10.5781528
6	-2.61505	6	-1.74497052	6	116.166018	6	261.303707
12	-2.30773	12	-1.42960414	12	103.689381	12	212.108993
18	-2.22398	18	-1.26982718	18	97.1206828	18	190.706109
24	-2.09416	24	-1.19573701	24	93.7974619	24	178.458533
30	-2.08965	30	-1.12003625	30	91.3487747	30	168.521263
36	-2.07612	36	-1.03048376	36	89.6450656	36	160.993819
42	-2.01395	42	-0.94576336	42	87.8376959	42	154.768451
48	-2.00622	48	-0.90614122	48	88.8223585	48	149.819258
54	-1.97368	54	-0.85556667	54	88.0385196	54	145.1227
60	-1.93857	60	-0.79693882	60	86.8983843	60	141.229422
66	-1.87865	66	-0.75828308	66	86.3866226	66	137.653566
72	-1.82454	72	-0.73122408	72	86.3931054	72	134.33682
78	-1.80328	78	-0.73025768	78	86.1015942	78	131.110777
84	-1.79458	84	-0.68387078	84	84.6181283	84	128.299318
90	-1.75947	90	-0.64489296	90	83.970328	90	125.850638
96	-1.71791	96	-0.57402411	96	84.7023402	96	123.583333
102	-1.71791	102	-0.54954216	102	84.4302704	102	121.225341
108	-1.69633	108	-0.5366569	108	84.1517103	108	119.03578
114	-1.67829	114	-0.54052248	114	83.1281868	114	117.034069
120	-1.65703	120	-0.53472411	120	84.307183	120	115.012932
126	-1.64672	126	-0.52924793	126	84.3914022	126	113.043621
132	-1.61161	132	-0.50637658	132	83.6917752	132	111.52777
138	-1.56297	138	-0.48092824	138	82.4609524	138	110.886445
144	-1.54364	144	-0.46031187	144	82.7978074	144	108.781096
150	-1.52141	150	-0.46772087	150	83.0569334	150	107.278196
156	-1.5504	156	-0.43937334	156	81.5410749	156	105.729952
162	-1.52592	162	-0.42230039	162	80.9127087	162	104.214101
168	-1.49951	168	-0.43099794	168	81.223654	168	102.879632
174	-1.45086	174	-0.45225858	174	81.3273	174	101.681195
180	-1.47502	180	-0.40136189	180	80.9515768	180	100.385594
186	-1.4528	186	-0.42294465	186	80.420381	186	99.1353445
192	-1.40834	192	-0.37752417	192	80.5305099	192	97.8721291
198	-1.42509	198	-0.38815452	198	80.1288697	198	96.7320011
204	-1.43218	204	-0.37301436	204	79.0535196	204	95.7926895
210	-1.41382	210	-0.38106762	210	78.3215073	210	94.7043882
216	-1.3932	216	-0.37816844	216	78.5028897	216	93.9594174
222	-1.35809	222	-0.35948483	222	78.1595591	222	92.9877133
228	-1.37001	228	-0.36592746	228	77.9263501	228	91.9641898
234	-1.36292	234	-0.38010123	234	77.3562861	234	90.9212322
240	-1.36969	240	-0.36624959	240	77.6672314	240	90.03374
246	-1.3655	246	-0.35046517	246	78.1789931	246	89.2110329
252	-1.32652	252	-0.40361681	252	77.5311928	252	88.3559405
258	-1.34649	258	-0.37720204	258	76.8380414	258	87.6627892
264	-1.36582	264	-0.35497501	264	76.4558426	264	86.6586997
270	-1.38032	270	-0.3578742	270	76.4688011	270	85.810083
276	-1.34521	276	-0.33757993	276	76.1643314	276	85.110456
282	-1.33071	282	-0.34724386	282	74.693824	282	84.4108363
288	-1.32588	288	-0.3569078	288	75.1861517	288	83.6917752
294	-1.33296	294	-0.35722994	294	75.4064022	294	82.9144119
300	-1.33103	300	-0.36592746	300	74.8557723	300	82.260136
306	-1.32201	306	-0.35594141	306	73.994197	306	81.5151652
312	-1.3117	312	-0.35819633	312	73.9877214	312	80.9127087
318	-1.31557	318	-0.30665535	318	73.890551	318	80.290818
324	-1.33747	324	-0.34015699	324	73.3075285	324	79.6365421
330	-1.33683	330	-0.34756599	330	72.1674005	330	78.962832
336	-1.33039	336	-0.36109549	336	72.2645709	336	78.3668511
342	-1.32846	342	-0.3578742	342	72.7633815	342	77.8421381
348	-1.33715	348	-0.32147338	348	71.5714268	348	77.3562861

354	-1.33844	354	-0.33081517	354	72.0702301	354	76.7473539
360	-1.32749	360	-0.34176765	360	70.9560118	360	76.196724
366	-1.30268	366	-0.33886846	366	71.1892208	366	75.5813089
372	-1.35712	372	-0.34273404	372	70.8912339	372	75.0630716
378	-1.35584	378	-0.32533896	378	70.1009194	378	74.5189172
384	-1.32008	384	-0.34724386	384	69.7575815	384	74.0395481
390	-1.3014	390	-0.32856028	390	69.9907905	390	73.5277863
396	-1.32395	396	-0.32533896	396	69.2458198	396	73.0225001
402	-1.31106	402	-0.32340617	402	68.8960063	402	72.5690406
408	-1.32942	408	-0.34176765	408	68.3065082	408	72.0637545
414	-1.33554	414	-0.34949878	414	68.7275824	414	71.5519927
420	-1.33876	420	-0.34627746	420	68.0214798	420	71.1762696
426	-1.34392	426	-0.3507873	426	67.5421034	426	70.6968931
432	-1.36131	432	-0.35658567	432	67.0173904	432	70.3535625
438	-1.36292	438	-0.35272009	438	67.4514158	438	69.8288422
444	-1.34875	444	-0.34724386	444	66.8619177	444	69.5178969
450	-1.36937	450	-0.35368649	450	65.7865676	450	69.1033056
456	-1.38418	456	-0.34627746	456	65.9614743	456	68.6239291
462	-1.39063	462	-0.32920454	462	66.0845544	462	68.2546888
468	-1.36904	468	-0.32340617	468	65.4302785	468	67.9113509
474	-1.35584	474	-0.32211764	474	64.7306515	474	67.5032352
480	-1.37516	480	-0.34047912	480	64.7889538	480	67.0886438
486	-1.35133	486	-0.35529715	486	65.1711525	486	66.7388304
492	-1.36099	492	-0.35819633	492	64.510401	492	66.3890169
498	-1.35068	498	-0.3382242	498	64.2124069	498	66.0327278
504	-1.35648	504	-0.33886846	504	63.9856808	504	65.6699631
510	-1.37549	510	-0.37655778	510	63.9986392	510	65.2812814
516	-1.37001	516	-0.35948483	516	63.4609605	516	64.8990826
522	-1.37903	522	-0.37075944	522	62.3856104	522	64.5622204
528	-1.38902	528	-0.36914878	528	62.7289483	528	64.4002721
534	-1.36937	534	-0.37752417	534	62.5475659	534	64.0375074
540	-1.3903	540	-0.37784631	540	62.3726592	540	63.7654302
546	-1.37355	546	-0.35561928	546	61.9256753	546	63.4091411
552	-1.38193	552	-0.34595533	552	61.9515849	552	63.0722789
558	-1.38354	558	-0.36657173	558	61.6082543	558	62.8066846
564	-1.3829	564	-0.34692172	564	61.1612704	564	62.3597007
570	-1.40641	570	-0.36463894	570	60.7401998	570	62.100582
576	-1.38032	576	-0.35207583	576	60.9993185	576	61.8285048
582	-1.37098	582	-0.34853238	582	60.8503251	582	61.6082543
588	-1.3597	588	-0.35239796	588	60.4357338	588	61.271392
594	-1.38	594	-0.34982091	594	59.9887499	594	60.9928429
599	-1.38257	599	-0.34788812	599	59.5288111	599	60.7272414

Appendix A 10 Anodic transferred charge data of zinc sulphide

	Zinc Sulphide			
	Potential	Q (200S)	Q (10min)	Conc. (ppm)
Peak I	-600	28.59	65.19	0.2007
	-550	30.5	73.33	0.23
	-500	27.32	64.25	0.2006
	-450	32.85	77.99	0.1832
	-400	10.73	20.93	0.1871

Peak II	-250	6.33	15.62	0.1918
	-212.5	0.9972	2.234	0.2141
	-175	3.434	9.771	0.1964
	-137.5	3.581	11.06	0.1893
	-100	3.754	11.56	0.188
Peak III	300	3.77	14.55	0.2086
	500	16.92	44.75	0.2569
	700	26	55.98	0.3182

Appendix A 11 Anodic transferred charge data of silver sulphide

	Silver Sulphide			
	Potential	Q (200S)	Q (10min)	Conc (ppm)
Peak I	-600	8.852	23.42	0.178
	-550	3.098	8.3	0.165
	-500	3.33	210.1	0.171
	-450	10.48	30.04	0.167
	-400	32.68	101.2	0.178
Peak II	200	0.7982	1.845	0.179
	275	1.35	3.02	0.184
	330	1.295	3.48	0.185
	415	1.605	5.108	0.182
	500	3.525	9.798	0.201

Appendix A 12 Anodic transferred charge data of lead sulphide

	Lead Sulphide			
	Potential	Q (200S)	Q (10min)	Conc (ppm)
Peak I	500	10.12	54.33*	2.26
	562.5	35.05	184.8*	3.13
	625	20.23	50.01*	2.08
	678.5	7.887	22.64*	1.83
	750	52.04	85.91*	2.28

Peak II	100	9.707	28.15*	1.36
	137.5	19.44	64.66*	1.31
	175	17.32	61.11*	1.28
	212.5	8.941	53.48*	1.27
	250	31.99	92.59*	1.2
Peak III	-160	2.951	8.982	1.36
	-140	2.951	9.027	1.31
	-120	2.986	9.251	1.28
	-100	3.049	9.485	1.27
	-80	3.124	9.968	1.2
Peak VI	-450	28.85	72.72	1.32
	-387.5	4.413	10.16	1.12
	-325	0.7631	1.123	1.03
	-262.5	2.297	6.347	0.9
	-200	1.276	4.356	0.42

Appendix B: Particle Size Distribution

Appendix B 1 Particle size distribution pure sphalerite mineral

Dispersant:	Water	**RI/ABS:**	2.74 / 1
Additives:	10 ml Calgon	**Analysis Model:**	General purpose Volum
Sonication:	20 minutes in Ultrasonic bath	**Result units:**	e

Concentration:	0.012 % vol	**Vol. Weighted Mean D[4,3]:**	39.254	µm	**d(0.1):**	3.024	µm
Obscuration:	15.14 %	**Surface Weighted Mean D[3,2]:**	6.293	µm	**d(0.5):**	20.42	µm
Weighted Residual:	0.911 %	**Specific Surface Area:**	0.953	m^2/cc	**P80:**	60.01	µm
					d(0.9):	89.71	µm

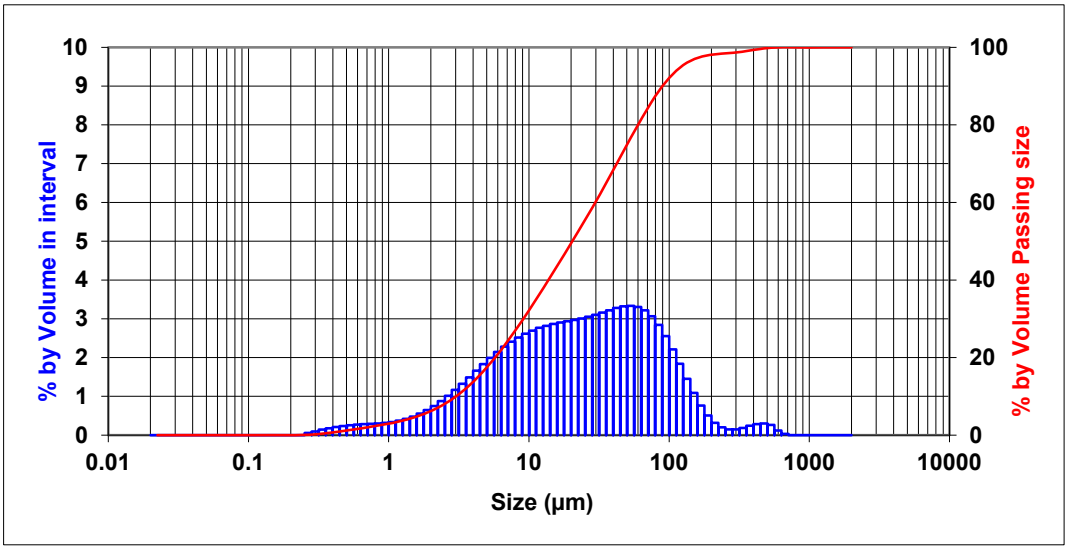

Appendix B 2 Particle size distribution ultrafine sphalerite concentrate

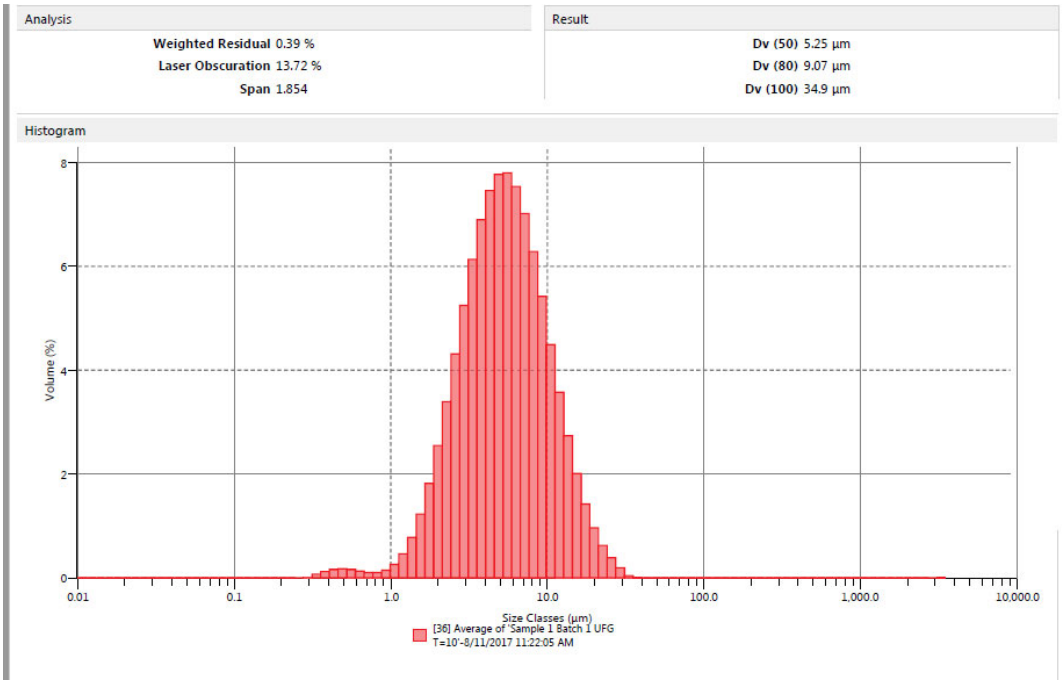

Appendix C: XRD Analysis

Appendix C 1 Pure galena and pure sphalerite

Table 1 – Quantitative XRD results

Please take into consideration the following notes when viewing the data. The data should be treated as indicative only and further work would be required for a more accurate classification;

- A number of 'minor' peaks are k-beta and tungsten lines
- Due to a limitation with the SIROQUANT software, galena could not be quantified and qualitative results have been reported for Samples 2 and 4.

	Formula	3 - Sph	4 - Gal
Pyrrhotite[1]	Fe_7S_8		
Pyrite	FeS_2		
Sphalerite[2]	(Zn,Fe)S	100	A
Galena[3]	PbS		D
Quartz	SiO_2		
Mica[4]	$X_2Y_{4-6}Z8O20(OH,F)_4$		
Chlorite[5]	$(X_5Al)(AlSi_3O_{10}(OH)_8$		
Calcite	$CaCO_3$		
Dolomite[6]	$CaMg(CO_3)_2$		
Ankerite	$Ca(Fe^{2+},Mg,Mn)(CO_3)_2$		
Gypsum[6]	$CaSO_4(H_2O)_2$		
Rutile[6]	TiO_2		
Unassigned Peak[7]	2.63A / 39.6 degrees two-theta		
TOTAL		100	0

1. To model pyrrhotite in SIROQUANT Pyrrhotite-4C was used.
2. There may be elemental substitution in sphalerite. HighScore Plus Search match software also identified an iron-rich sphalerite.
3. Due to a limitation with the SIROQUANT software, galena could not be quantified.
4. Mica group in which X is K, Na, Ca or less commonly Ba, Rb, or Cs; Y is Al, Mg, Fe or less commonly Mn, Cr, Ti, Li, etc.; Z is chiefly Si or Al but also may include Fe^{3+} or Ti. Muscovite was used in the SIROQUANT Rietveld refinement, as it gave the best agreement between the calculated and observed patterns. Further investigation would be required for more accurate classification of the mica mineral.

5. Where X = Mg,Fe,Ni and Mn. Chlorite may be under/over-estimated.
6. Dolomite, gypsum and rutile were identified through peak intensity and not directly by HighScore Plus search match software. Further investigation would be required to determine if these phases are present.
7. Due to the lack of other identifying peaks, unidentified peaks/phases were observed. Identification of these peaks will require further investigations by other techniques.

Tr = Trace. i.e. the mineral that gives rise to this peak is assumed to be present in trace amounts.

A = Accessory. Components judged to be present between the levels of roughly 5 and 20%.

D = Dominant. Used for the component apparently most abundant, regardless of its probable percentage level.

Appendix C 2 Sphalerite concentrate

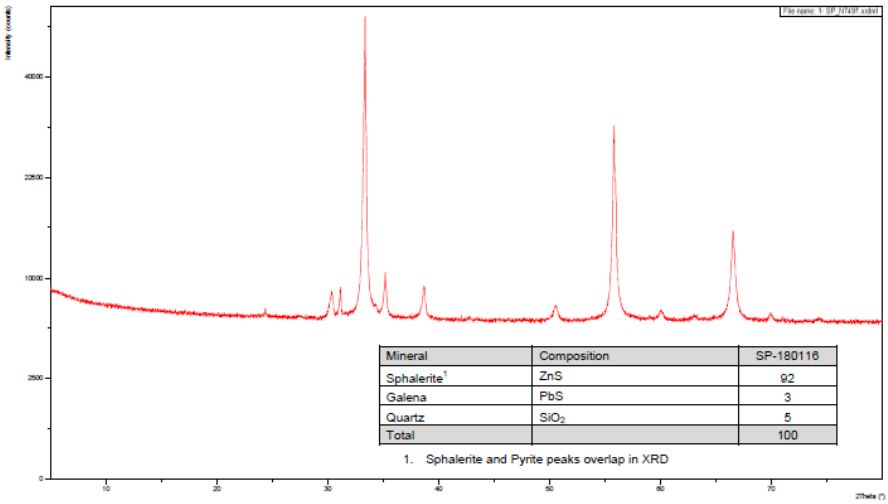

Mineral	Composition	SP-180116
Sphalerite[1]	ZnS	92
Galena	PbS	3
Quartz	SiO_2	5
Total		100

1. Sphalerite and Pyrite peaks overlap in XRD

Appendix D: SEM Images

Appendix D 1 SEM image of sphalerite concentrate residue

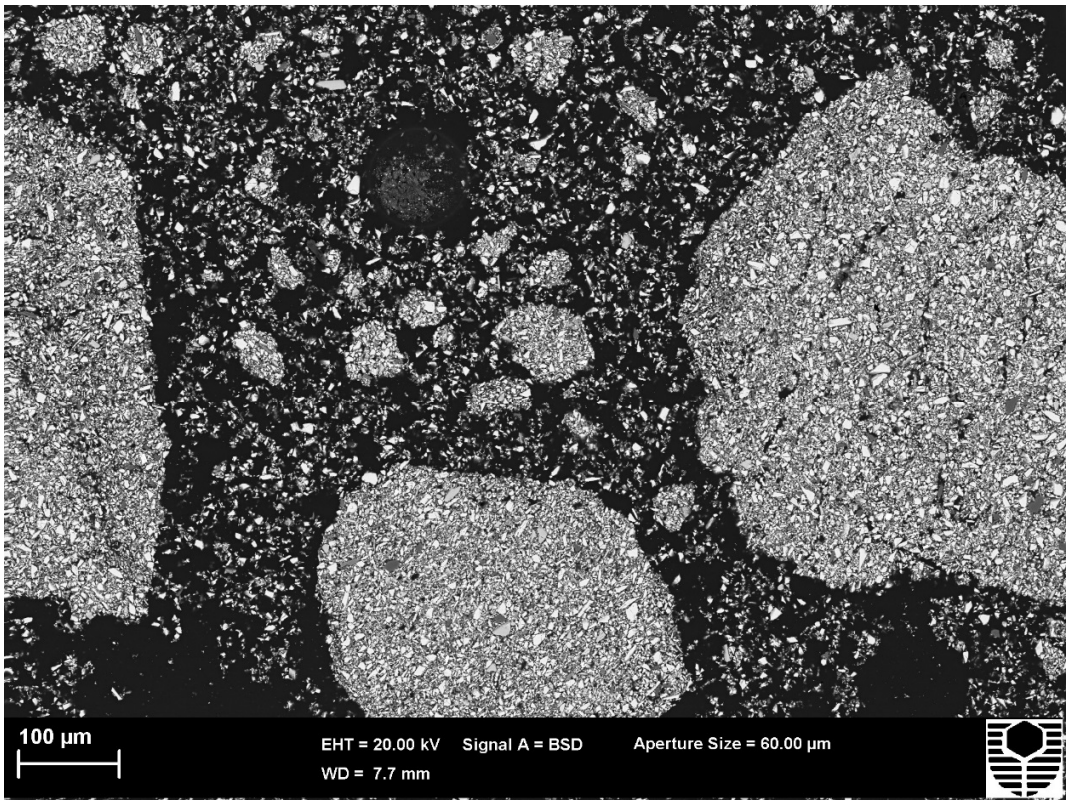

Appendix D 2 SEM image of ZnO residue

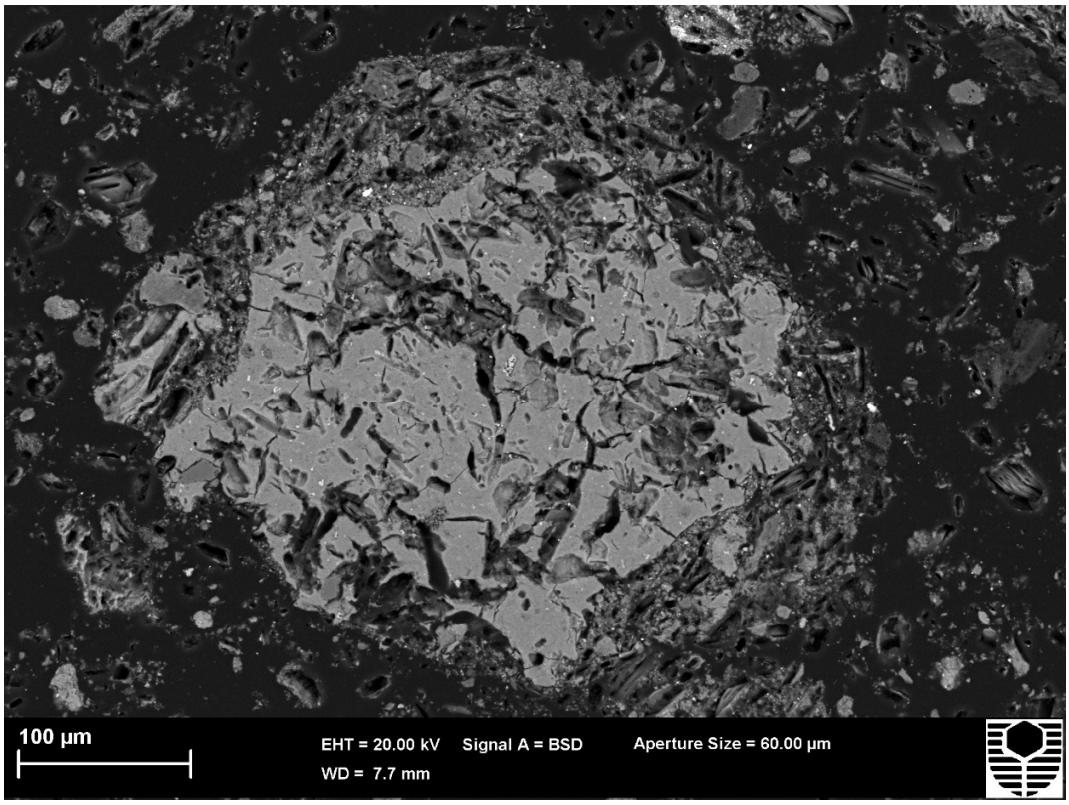

Appendix E: Properties of Reagents

Appendix E 1 Properties of glycine (Chemicalland21, 2019)

GLYCINE	
PRODUCT IDENTIFICATION	
CAS NO.	56-40-6
EINECS NO.	200-272-2
FORMULA	H_2NCH_2COOH

MOL WT.	75.07
H.S. CODE	2922.49
TOXICITY	Oral rat LD50 7930 mg/kg

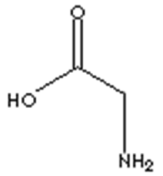

SYNONYMS Aminoacetic Acid; Glycocoll; Athenon; Gly; G salt; Iconyl; Monazol; glycosthene; p-Hydroxyphenylaminoacetic Acid; Aminoethanoic Acid; p-Hydroxyanilinoacetic Acid; para-Oxyphenyl Glycocoll; Sucre De Gelatine;

SMILES

CLASSIFICATION

PHYSICAL AND CHEMICAL PROPERTIES

PHYSICAL STATE	White crystals, Odorless
MELTING POINT	245 C (Decompose)
BOILING POINT	
SPECIFIC GRAVITY	1.6
SOLUBILITY IN WATER	25g/100 ml
pH	5.97 (Isoelectric point)
VAPOR DENSITY	
REFRACTIVE INDEX	
AUTOIGNITION	
NFPA RATINGS	Health: 0 Flammability: 1 Reactivity: 0
FLASH POINT	145 C
STABILITY	Stable under ordinary conditions

APPLICATIONS

Flavor enhancers and maskers, pH buffers and stabilizers, an ingredient in pharmaceutical products, food and personal care products and as a chemical intermediate.

SALES SPECIFICATION

TECHNICAL GRADE	
APPEARANCE	white to off-white crystalline powder
ASSAY (DRY BASIS)	98.5% min
LOSS ON DRYING	0.5% max
CHLORIDE	0.5% max
Fe	0.003% max
FEED GRADE	
APPEARANCE	white to off-white crystalline powder
ASSAY (DRY BASIS)	98.5% min
CHLORIDE	0.5% max
HEAVY METALS	20ppm max
ARSENIC	3ppm max
LOSS ON DRYING	0.2% max
FOOD GRADE	

BIBLIOGRAPHY	FCC IV
APPEARANCE	white, odorless, crystalline powder
ASSAY (DRY BASIS)	99.0% min
IDENTIFICATION	passes test
LOSS ON DRYING	0.2% max
CHLORIDE	0.002% max
HEAVY METALS	20ppm max
SULPHATE	50ppm max
pH	5.5 - 7.0
RESIDUE ON IGNITION	0.05% max
As	3ppm max
Pb	5ppm max
USP/BP GRADE	
BIBLIOGRAPHY	USP 24 / BP 93
APPEARANCE	white, odorless, crystalline powder
ASSAY (DRY BASIS)	99.0 -101.0%
IDENTIFICATION	passes test
LOSS ON DRYING	0.2% max
CHLORIDE	70ppm max
HEAVY METALS	20ppm max
SULPHATE	65 ppm
pH	5.5 - 6.5
RESIDUE ON IGNITION	0.1% max
As	3ppm max
Pb	5ppm max
HYDROLYZABLE SUBSTANCES	passes test
PYROGEN CONTENT	meets the requirements
ALUMINUM	meets the requirements
ORGANIC VOLATILES	meets the requirements
TRANSPORTATION	
PACKING	25kgs in Fiber Drum
HAZARD CLASS	Not regulated
UN NO.	

GENERAL PROPERTIES OF GLYCINE

Glycine is a white, crystalline amino acid; dissolve in water and. As also known as aminoacetic acid, it is the simplest amino acid. It has acid group as well as amino group which both groups act as a base. It is not optically active, i.e., it does not have d- and l-stereoisomers as two hydrogens are bonded to the central carbon atom. It is nonessential amino acids for mammals; i.e., they can synthesize it from amino acids serine and threonine and from other sources and do not require dietary sources. It is commercially synthesis from ammonia. It is also prepared from bromoethanoic acid by reaction with potassium phthalimide. It helps to improve glycogen storage utilized in the synthesis of hemoglobin, collagen, and glutathione, and facilitates the amelioration of high blood fat and uric acid levels.

Appendix F: The thermodynamic information

Appendix F 1 Thermodynamic information for lead-sulphur-glycine and silver-sulphur-glycine systems.

Reaction	Log K	Reaction	Log K
$2\ H^+ + 2\ e^- = H_{2(aq)}$	-3.15	$4\ H^+ + 2\ e^- + SO_4^{2-} = SO_2(g)$	5.26
$2\ H_2O = 2\ H^+ + 2\ e^- + H_2O_{2(aq)}$	-59.601	$H^+ + Gly^- = H(Gly)$	9.778
$9\ H^+ + 8\ e^- + SO_4^{2-} = HS^-$	33.692	$HGly + H^+ = H_2(Gly)^+$	2.35
$H^+ + SO_4^{2-} = HSO_4^-$	1.98	$2\ H^+ + Gly^- = H_2(Gly)^+$	12.128
$2\ H_2O = 4\ H^+ + 4\ e^- + O_{2(aq)}$	-86.08	$8\ H^+ + 6\ e^- + SO_4^{2-} = S_{(cr)} + 4\ H_2O$	35.837
$2\ H_2O = 4\ H^+ + 4\ e^- + O_{2(g)}$	-83.12	$10\ H^+ + 8\ e^- + SO_4^{2-} = H_2S_{(aq)} + 4\ H_2O$	40.686
$3\ H_2O = 6\ H^+ + 6\ e^- + O_{3(aq)}$	-156.05	$10\ H^+ + 8\ e^- + SO_4^{2-} = H_2S_{(g)} + 4\ H_2O$	41.683
$3\ H_2O = 6\ H^+ + 6\ e^- + O_{3(g)}$	-153.25	$10\ H^+ + 8\ e^- + 2\ SO_4^{2-} = H_2S_2O_3 + 4\ H_2O$	40.863
$H_2O = H^+ + OH^-$	-14	$11\ H^+ + 8\ e^- + 2\ SO_4^{2-} = HS_2O_3^- + 5\ H_2O$	40.276
$10\ H^+ + 8\ e^- + 2\ SO_4^{2-} = S_2O_3^{2-}$	38.591	$3\ H^+ + 2\ e^- + SO_4^{2-} = HSO_3^- + H_2O$	3.74
$2\ SO_4^{2-} = 2\ e^- + S_2O_8^{2-}$	-66.261	$8\ H^+ + 8\ e^- + SO_4^{2-} = S^{2-} + 4\ H_2O$	14.692
$2\ H^+ + 2\ e^- + SO_4^{2-} = SO_3^{2-}$	-3.48	$4\ H^+ + 2\ e^- + SO_4^{2-} = SO_{2(g)}$	5.58
Lead Species			
$Pb^{2+} = 2\ e^- + Pb^{4+}$	-57.13	$4\ Pb^{2+} + 4\ H_2O = 4\ H^+ + Pb_4(OH)_4^{4+}$	-20.88
$Pb^{2+} + H_2O = H^+ + PbOH^+$	-7.71	$6\ Pb^{2+} + 8\ H_2O = 8\ H^+ + Pb_6(OH)_8^{4+}$	-43.61
$Pb^{2+} + 2\ H_2O = 2\ H^+ + Pb(OH)_{2(aq)}$	-17.12	$Pb^{2+} + 3\ H_2O = 6\ H^+ + 2\ e^- + PbO_3^{2-}$	-81.22
$Pb^{2+} + 3\ H_2O = 3\ H^+ + Pb(OH)_3^-$	-28.06	$Pb^{2+} + SO_4^{2-} = PbSO_{4(aq)}$	2.75
$Pb^{2+} + 3\ H_2O = 3\ H^+ + 2\ e^- + Pb(OH)_3^+$	-53.93	$Pb^{2+} + 2\ e^- = Pb_{(cr)}$	-4.27
$Pb^{2+} + 4\ H_2O = 4\ H^+ + 2\ e^- + Pb(OH)_4$	-53.13	$Pb^{2+} + Gly^- = Pb(Gly)^+$	5
$Pb^{2+} + 4\ H_2O = 4\ H^+ + Pb(OH)_4^{2-}$	-39.7	$Pb^{2+} + 2\ Gly^- = Pb(Gly)_2$	8.66

$Pb^{2+} + 4\ H_2O = 6\ H^+ + 2\ e^- + Pb(OH)_6^{2-}$	-81.63	$H^+ + Pb^{2+} + Gly^- = Pb(HGly)^{2+}$	10.8
$2\ Pb^{2+} + SO_4^{2-} + H_2O = 2\ H^+ + PbO{:}PbSO_{4(cr)}$	0.280	$Pb^{2+} + Gly^- = H^+ + Pb(Gly)OH$	-2.64
$Pb^{2+} + Gly^- = Pb(Gly)^+$	5	$Pb^{2+} + 2\ H_2O = 2\ H^+ + Pb(OH)_{2(cr)}$	-8.15
$Pb^{2+} + 2\ Gly^- = Pb(Gly)_2$	8.66	$Pb^{2+} + H_2O = 2\ H^+ + PbO_{(cr)}$	-12.91
$H^+ + Pb^{2+} + Gly^- = Pb(HGly)^{2+}$	10.8	$Pb^{2+} + SO_4^{2-} = PbSO_{4(cr)}$	7.79
$Pb^{2+} + Gly^- = H^+ + Pb(Gly)OH$	-2.64	$8\ H^+ + 8\ e^- + Pb^{2+} + SO_4^{2-} = PbS_{(cr)}$	46.472
$2\ e^- + Pb^{2+} = Pb_{(cr)}$	-4.27	$2\ Pb^{2+} + 3\ H_2O = 6\ H^+ + 2\ e^- + Pb_2O_{3(cr)}$	-61.04
$Pb^{2+} + 2\ SO_4^{2-} = Pb(SO_4)_2^{2-}$	3.47	$3\ Pb^{2+} + 4\ H_2O = 8\ H^+ + 2\ e^- + Pb_3O_{4(cr)}$	-73.69
$2\ Pb^{2+} + H_2O = H^+ + Pb_2(OH)^{3+}$	-6.36	$2\ Pb^{2+} + 3\ H_2O = 4\ H^+ + PbO{:}Pb(OH)_{2(cr)}$	-26.2
$3\ Pb^{2+} + 4\ H_2O = 4\ H^+ + Pb_3(OH)_4^{2+}$	-23.88	$Pb^{2+} + 2H_2O = 4\ H^+ + 2\ e^- + PbO_{2(cr)}$	-49.13
$H^+ + Pb^{2+} + 2\ Gly^- = Pb(HGly)(Gly)^+$	15.66	$2\ H^+ + Pb^{2+} + 2\ Gly^- = Pb(HGly)_2^{2+}$	21.1
$4\ Pb^{2+} + SO_4^{2-} + 6\ H_2O = 6\ H^+ + Pb_4(OH)_6SO_{4(cr)}$			-21.1
$27\ H^+ + 24\ e^- + Pb^{2+} + 3\ SO_4^{2-} = Pb(HS)_3^- + 12\ H_2O$			117.646
$18\ H^+ + 1\ 6\ e^- + Pb^{2+} + 2\ SO_4^{2-} = Pb(HS)_{2(aq)} + 8\ H_2O$			82.654
$3\ Pb^{2+} + SO_4^{2-} + 2\ H_2O = 4\ H^+ + PbSO_4{:}2PbO_{(cr)}$			-10.4
$4\ Pb^{2+} + SO_4^{2-} + 3\ H_2O = 6\ H^+ + PbSO_4{:}3PbO_{(cr)}$			-22.1
Silver Species			
$Ag^+ = e^- + Ag^{2+}$	-33.470	$Ag^+ + Gly^- = Ag(Gly)$	3.51
$Ag^+ + H_2O = H^+ + AgOH_{(aq)}$	-12	$Ag^+ + 2\ Gly^- = Ag(Gly)_2^-$	6.890
$Ag^+ + 2\ H_2O = 2\ H^+ + Ag(OH)_2^-$	-24	$H^+ + Ag^+ + Gly^- = Ag(HGly)^+$	9.88
$8\ H^+ + 8\ e^- + Ag^+ + SO_4^{2-} = AgS^- + 4\ H_2O$	38.992	$Ag^+ + e^- = Ag_{(cr)}$	13.51
$2\ H^+ + 2\ e^- + Ag^+ + SO_4^{2-} = AgSO_3^- + H_2O$	2.120	$Ag^+ + H_2O = 2\ H^+ + 2\ e^- + AgO_{(cr)}$	-29.95
$2\ H^+ + 2\ e^- + 2\ Ag^+ + SO_4^{2-} = Ag_2SO_{3(cr)} + H_2O$	10.340	$2\ Ag^+ + H_2O = 2\ H^+ + Ag_2O_{(cr)}$	-12.58
$Ag^+ + SO_4^{2-} = AgSO_{4(aq)}$	1.29	$8\ H^+ + 8\ e^- + 2Ag^+ + SO_4^{2-} = Ag_2S_{(cr)}$	69.742
$2\ Ag^+ + SO_4^{2-} = Ag_2SO_{4(cr)}$	4.920	$2\ Ag^+ + 3\ H_2O = 6\ H^+ + 4\ e^- + Ag_2O_{3(cr)}$	-112.920
$9\ H^+ + 8\ e^- + Ag^+ + SO_4^{2-} = AgHS + 4\ H_2O$			47.742
$4\ H^+ + 4\ e^- + Ag^+ + 2\ SO_4^{2-} = Ag(SO_3)_2^{3-} + 2\ H_2O$			90.882
$6\ H^+ + 6\ e^- + Ag^+ + 2\ SO_4^{2-} = Ag(SO_3)_3^{5-} + 3\ H_2O$			129.976
$17\ H^+ + 16\ e^- + Ag^+ + 2\ SO_4^{2-} = AgHS_2^{2-} + 8\ H_2O$			75.584
$18\ H^+ + 1\ 6\ e^- + Ag^+ + 2\ SO_4^{2-} = Ag(HS)_2^- + 8\ H_2O$			85.834
$10\ H^+ + 8\ e^- + Ag^+ + 2\ SO_4^{2-} = AgS_2O_3^- + 5\ H_2O$			47.391
$20\ H^+ + 1\ 6\ e^- + Ag^+ + 4\ SO_4^{2-} = Ag(S_2O_3)_2^{3-} + 10\ H_2O$			90.882
$30\ H^+ + 24\ e^- + Ag^+ + 6\ SO_4^{2-} = Ag(S_2O_3)_3^{5-} + 10\ H_2O$			129.976
$64\ H^+ + 52\ e^- + Ag^+ + 8\ SO_4^{2-} = Ag(S_4)_2^{3-} + 32\ H_2O$			283.397
$72\ H^+ + 58\ e^- + Ag^+ + 9\ SO_4^{2-} = Ag(S_4)S_5^{3-} + 36\ H_2O$			318.923
$41\ H^+ + 34\ e^- + Ag^+ + 5\ SO_4^{2-} = AgHS(S_4)^{2-} + 20\ H_2O$			185.325

Appendix F 2 Thermodynamic information for Zinc-Sulfur-Glycine-System.

Reaction	Log k	Reaction	Log k
$2\ H^+ + 2\ e^- = H_{2(aq)}$	-3.15	$4\ H^+ + 2\ e^- + SO_4^{2-} = SO_2(g)$	5.26
$2\ H_2O = 2\ H^+ + 2\ e^- + H_2O_{2(aq)}$	-59.601	$18\ H^+ + 16\ e^- + Zn^{2+} + 2\ SO_4^{2-} = Zn(HS)_{2(aq)} + 8\ H_2O$	80.204
$9\ H^+ + 8\ e^- + SO_4^{2-} = HS^-$	33.692	$27\ H^+ + 24\ e^- + Zn^{2+} + 3\ SO_4^{2-} = Zn(HS)_3^- + 12\ H_2O$	117.176
$H^+ + SO_4^{2-} = HSO_4^-$	1.98	$36\ H^+ + 32\ e^- + Zn^{2+} + 4\ SO_4^{2-} = Zn(HS)_4^{2-} + 16\ H_2O$	149.408
$2\ H_2O = 4\ H^+ + 4\ e^- + O_{2(aq)}$	-86.08	$17\ H^+ + 16\ e^- + Zn^{2+} + 2\ SO_4^{2-} = ZnS(HS)^-$	74.225
$2\ H_2O = 4\ H^+ + 4\ e^- + O_{2(g)}$	-83.12	$26\ H^+ + 24\ e^- + Zn^{2+} + 3\ SO_4^{2-} = ZnS(HS)_2^{2-}$	107.227
$3\ H_2O = 6\ H^+ + 6\ e^- + O_{3(aq)}$	-156.05	$10\ H^+ + 8\ e^- + Zn^{2+} + 2\ SO_4^{2-} = ZnS_2O_{3(aq)}$	40.891
$3\ H_2O = 6\ H^+ + 6\ e^- + O_{3(g)}$	-153.25	$H^+ + Gly^- = H(Gly)$	9.778
$H_2O = H^+ + OH^-$	-14	$HGly + H^+ = H_2(Gly)^+$	2.35
$10\ H^+ + 8\ e^- + 2\ SO_4^{2-} = S_2O_3^{2-}$	38.591	$2\ H^+ + Gly^- = H_2(Gly)^+$	12.128
$2\ SO_4^{2-} = 2\ e^- + S_2O_8^{2-}$	-66.261	$Zn^{2+} + Gly^- = Zn(Gly)^+$	5.38
$2\ H^+ + 2\ e^- + SO_4^{2-} = SO_3^{2-}$	-3.48	$Zn^{2+} + 2\ Gly^- = Zn(Gly)_2$	9.81
$Zn^{2+} + H_2O = H^+ + Zn(OH)^+$	-7.5	$Zn^{2+} + 3\ Gly^- = Zn(Gly)_3^-$	12.3
$Zn^{2+} + 2\ H_2O = 2\ H^+ + Zn(OH)_{2(aq)}$	16.4	$Zn^{2+} + Gly^- = H^+ + Zn(Gly)OH$	-3.52
$Zn^{2+} + 3\ H_2O = 3\ H^+ + Zn(OH)_3^-$	-28.2	$Zn^{2+} + 2\ H_2O = 2\ H^+ + Zn(OH)_{2(cr)}$	-12.45
$Zn^{2+} + 4\ H_2O = 4\ H^+ + Zn(OH)_4^{2-}$	-41.3	$2\ e^- + Zn^{2+} = Zn_{(cr)}$	-25.757
$Zn^{2+} + 2\ SO_4^{2-} = Zn(SO_4)_2^{2-}$	3.28	$2\ Zn^{2+} + SO_4^{2-} + H_2O = 2\ H^+ + Zn_2(OH)_2SO_{4(cr)}$	-7500
$Zn^{2+} + 3\ SO_4^{2-} = Zn(SO_4)_3^{4-}$	1.7	$Zn^{2+} + H_2O = 2\ H^+ + ZnO_{(cr)}$	-11.2
$2\ Zn^{2+} + 6\ H_2O = 6\ H^+ + Zn_2(OH)_6^{2-}$	-54.3	$Zn^{2+} + SO_4^{2-} = ZnSO_{4(cr)}$	-3.01
$2\ Zn^{2+} + H_2O = H^+ + Zn_2(OH)^{3+}$	9	$8\ H^+ + 6\ e^- + SO_4^{2-} = S_{(cr)} + 4\ H_2O$	35.837
$4\ Zn^{2+} + 4\ H_2O = 4\ H^+ + Zn_4(OH)_4^{4+}$	-27	$8\ H^+ + 8\ e^- + Zn^{2+} + SO_4^{2-} = ZnS_{(cr)}$	42.744
$Zn^{2+} + SO_4^{2-} = ZnSO_{4(aq)}$	2.37	$3\ H^+ + 2\ e^- + SO_4^{2-} = HSO_3^- + H_2O$	3.74
$10\ H^+ + 8\ e^- + SO_4^{2-} = H_2S_{(aq)} + 4\ H_2O$	40.686	$8\ H^+ + 8\ e^- + SO_4^{2-} = S^{2-} + 4\ H_2O$	14.692
$10\ H^+ + 8\ e^- + SO_4^{2-} = H_2S_{(g)} + 4\ H_2O$	41.683	$4\ H^+ + 2\ e^- + SO_4^{2-} = SO_{2(g)}$	5.58
$10\ H^+ + 8\ e^- + 2\ SO_4^{2-} = H_2S_2O_3 + 4\ H_2O$	40.863	$11\ H^+ + 8\ e^- + 2\ SO_4^{2-} = HS_2O_3^- + 5\ H_2O$	40.276